ERDC/CHL TR-14-13

Coastal and Hydraulics Laboratory

US Army Corps of Engineers®
Engineer Research and Development Center

ERDC
INNOVATIVE SOLUTIONS for a safer, better world

Coastal Inlets Research Program

Comprehensive Condition Survey and Storm Waves, Circulation, and Sediment Study, Dana Point Harbor, California

Chia-Chi Lu, Arthur T. Shak, Honghai Li, and Lihwa Lin

December 2014

The U.S. Army Engineer Research and Development Center (ERDC) solves the nation's toughest engineering and environmental challenges. ERDC develops innovative solutions in civil and military engineering, geospatial sciences, water resources, and environmental sciences for the Army, the Department of Defense, civilian agencies, and our nation's public good. Find out more at www.erdc.usace.army.mil.

To search for other technical reports published by ERDC, visit the ERDC online library at http://acwc.sdp.sirsi.net/client/default.

ERDC/CHL TR-14-13
December 2014

Comprehensive Condition Survey and Storm Waves, Circulation, and Sedimentation Study, Dana Point Harbor, California

Chia-Chi Lu

Noble Consultants Inc.
2201 Dupont Drive, Suite 620
Irvine, CA 92612

Arthur T. Shak

U.S. Army Engineer District, Los Angeles District
915 Wilshire Blvd
Los Angeles, CA 90017

Honghai Li and Lihwa Lin

Coastal and Hydraulics Laboratory
U.S. Army Engineer Research and Development Center
3909 Halls Ferry Road
Vicksburg, MS 39180-6199

Final report

Prepared for U.S. Army Engineer District, Los Angeles
915 Wilshire Blvd
Los Angeles, CA 90017

Abstract

The U.S. Army Engineer District, Los Angeles (SPL), and the Coastal Inlets Research Program (CIRP) have conducted a comprehensive study to investigate wave, flow, sediment transport, and permeable breakwaters with rocky outcrop bottom at Dana Point Harbor, as a part of the harbor revitalization project, on the southern Orange County coast, CA. The 5,500 ft shore-parallel West Breakwater and 2,250 ft shore-normal East Breakwater to protect the harbor are the main interest in the study of the structural integrity and functionality. The field data collection includes 2009 survey of breakwaters, marinas, harbor entrance and surroundings at the harbor, and installation of a pair of Acoustic Doppler Current Profilers (ADCP) to measure water levels, waves, and currents inside and outside West Breakwater. The numerical models were used to calculate wave transmission, current and sediment seepage through permeable breakwaters, and circulation in the harbor under combined wave, tide, and flow conditions. Permeable breakwater functions with hydraulic conductivity and void for sediment passage through structures were developed within the Coastal Modeling System (CMS), and were subject to sensitivity tests on wind forcing, tides, bottom friction, and wave reflection. The oceanographic design criteria established previously for Dana Point Harbor were updated based on historical storm waves and the present model simulations for 50-year and 100-year return periods. The data analysis and model results together provide information to ascertain the action to repair breakwaters and structural alternatives to improve the navigation channel maintenance and tidal flushing in the harbor.

Contents

Figures and Tables

Figures

Tables

Preface

The field data collection and numerical modeling study presented in this report was authorized by the U.S. Army Corps of Engineers (USACE) District, Los Angeles (SPL), to investigate the channel shoaling, flow circulation, and permeable breakwaters at Dana Point Harbor. This study was a part of the harbor revitalization project for Dana Point Harbor, located on the southern Orange County coast, CA. Arthur Shak was the project study manager. The technical work was performed by Dr. Chia-Chi at Noble Consultants Inc., Irvine, CA, and Drs. Honghai Li and Lihwa Lin at the U.S. Army Engineer Research and Development Center (ERDC), Coastal and Hydraulics Laboratory (CHL). This study was supported by the SPL and City of Dana Point, CA.

This work was performed at the SPL and CHL during the period October 2009 to December 2011. The report was prepared under the direction of Tanya M. Beck, Chief of the Coastal Engineering Branch; Dr. Jackie S. Pettway, Chief of the Navigation Division; Dr. Kevin Barry, Deputy Director; and José E. Sánchez, Director of CHL.

COL Jeffrey R. Eckstein was Commander and Executive Director, and Dr. Jeffery P. Holland was Director of ERDC.

Unit Conversion Factors

Multiply	By	To Obtain
cubic yards	0.7646	cubic meters
feet	0.3048	meters
inches	0.3937	centimeters
miles (U.S. statute)	1,609.3470	meters

1 Introduction

Dana Point Harbor is located in the City of Dana Point, midway between Los Angeles and San Diego, along the southern Orange County Coast of California, as depicted in Figure 1. The harbor consists of dual protective breakwaters (East and West Breakwater), two recreational marina basins, a turning basin, two anchorage basins, a boat launch ramp area, a bathing beach, and several shallow-draft navigation channels. The development of Dana Point Harbor was initiated in 1949, and an optimal design plan was later selected after various design alternatives were formulated and evaluated. Construction of the dual breakwaters at Dana Point Harbor commenced in 1963 and was completed in 1968. The harbor operation for boat occupation and recreational purposes began after the completion of channel and basin dredging in 1970. The harbor project maintains the entrance channel depth from 4.6 to 6 meters (m) (15 to 20 feet (ft)) and inside channels from 3 to 4.6 m (10 to 15 ft) relative to the Mean Lower Low Water (MLLW). Table 1 presents the physical dimension of the dual protective breakwaters and various depths in the channels and basins.

At the time of construction, both East and West Breakwater were designed as a semipermeable structure as comprised of multiple layers of riprap stones without an impermeable core layer. The weight of riprap stones in the outer layers range from 6 tons at the landward end to as heavy as 20 tons in the structure head area. Small voids were left intentionally during stone placement to allow currents partially flowing through the breakwaters, thereby promoting better water circulation within the harbor.

Sediment began to seep through West Breakwater in the 1980s, and as a consequence, three maintenance dredging activities have been conducted by the County of Orange to remove sand material that has accumulated on the lee of West Breakwater in the last 2 decades. The increased rate of shoaling in recent years necessitates a better understanding of the water and sediment exchange throughout the harbor and permeable breakwaters with specific interest on the physical processes that occur across West Breakwater.

Dana Point Harbor was designed and described to be self-cleaning, defined as receiving sufficient circulation to prevent stagnation of the water within the harbor. However, since its construction, water quality issues have been

Figure 1. Location map.

Table 1. Physical dimensions of breakwaters and project depths.

Parameter	Dimension, m (ft)
East Breakwater	
Length	686 m (2,250 ft)
Crest Width	4.3 m (14 ft)
Crest Elevation	+4.3 m (+14 ft) MLLW
West Breakwater	
Length	1,676 m (5,500 ft)
Crest Width	4.9 m (16 ft)
Crest Elevation	+5.5 m (+18 ft) MLLW
Project Depth	
Entrance Channel	4.6 to 6 m (15 to 20 ft) MLLW
Main Channel	4.6 m (15 ft) MLLW
West Channel and Turning Basin	3 m (10 ft) MLLW
East Channel	3.6 to 4.6 m (12 to 15 ft) MLLW
Boat Anchorage Areas	3.6 to 4.6 m (12 to 15 ft) MLLW

regularly observed at Baby Beach located on the northwest corner of the harbor (Figure 1). Several studies and field data collection have been performed to characterize the water circulation pattern and explore mitigation measures to improve the water quality, particularly at Baby Beach (SAIC 2002, 2003). Various mitigation measures (e.g., diversion of storm drains, installation of bird exclusion fencing, and bird-proof trash cans) to limit sources of bacterial contamination, have been implemented that proved to be effective in significantly reducing the number of posted beach-closure days at Baby Beach. Nevertheless, a better understanding of water circulation within the harbor will allow for the formulation of a permanent measure to enhance the water quality in the Baby Beach area.

1.1 Purpose and scope

The purpose of this study is 1) to conduct a comprehensive condition survey of the two breakwaters and assess the present-day structure conditions and 2) to investigate the permeability of the breakwaters via field data collection and numerical simulations. The investigation includes an assessment of the wave transmission, flow, and sediment seepage through West Breakwater, which results in a sand shoal formed on the lee side of West Breakwater, as well as an evaluation of the water circulation pattern within the harbor, particularly in the Baby Beach area.

To support this study, the Coastal Inlets Research Program (CIRP), USACE, funded the implementation of numerical schemes that depict the physical process of wave transmission, flow, and sediment seepage through the semipermeable breakwater configuration in the existing Coastal Modeling System (CMS). This model development advances the state of engineering technology for furthering the CIRP's goals. Using the CMS, the study also assessed the water circulation pattern within the harbor, particularly at Baby Beach. In addition, the study applies the present-day engineering standards to characterize the oceanographic conditions at the breakwaters, based on historical storm events, and subsequently updates the previously-established design criteria.

Specific tasks that were performed in this study include the following:

- A hydrographic survey using a multibeam sonar to collect bathymetric data and to examine the underwater portion of the breakwater conditions, a LiDAR (light detection and ranging) survey using a laser system for the breakwater conditions above the water level, and a visual inspection of the existing breakwater.
- An 8-week field data collection to measure currents and waves using Acoustic Doppler Current Profilers (ADCP) instruments.
- Improvement of the CMS to enhance the model capability in characterizing the permeability and functionality of breakwaters.
- Updating of oceanographic conditions for Dana Point Harbor, including estimates of the extreme design wave heights (e.g., 50- and 100-year (yr) return periods) at various locations along the breakwaters.
- Numerical modeling to identify the water circulation pattern within the harbor and characterize sediment seepage through the existing semi-permeable breakwaters.

1.2 Prior studies

Comprehensive Condition Survey, Dana Point Harbor (USACE LAD 1991)

A comprehensive condition survey report was prepared by the U.S. Army Engineer District, Los Angeles (USACE LAD), in 1991. The findings from that study concluded the following:

- East Breakwater remained in excellent design condition.

- West Breakwater had two areas showing displaced armor stones that did not warrant immediate corrective actions at that time as both areas appeared to be functioning as designed.
- A recommendation of annual monitoring and a repeated comprehensive condition survey in 5 to 10 yr was made.

Evaluation Studies of Bacteriological Data and Water Circulation at Baby Beach, Dana Point Harbor (prepared by SAIC 2002–2003)

Between 2002 and 2003, a series of five reports was prepared by Science Applications International Corporation (SAIC) for or in conjunction with the County of Orange Public Facilities and Resources Department (PFRD). These reports, as listed below, sought to understand the water circulation issues and related beach closures that were observed at Baby Beach.

Baby Beach Circulation Study Sampling and Analysis Plan (September 2002)

Data Mining Task for State of the Beach Report: Evaluation of Bacteriological Data and Associated Parameters for Baby Beach (SAIC 2003a)

Baby Beach Circulation Study Final Report (SAIC 2003b)

Baby Beach Bacteriological Special Studies Report (SAIC 2003c)

State of the Beach Report, Baby Beach Region (SAIC 2003d)

The general findings from the abovementioned reports included the following items:

- Sources of the bacteria are limited to (a) contaminated discharges from storm drains, (b) bacteria resident (regrowth) in beach sediments, (c) weak near-beach water circulation, and (d) bacterial contamination from birds residing in the harbor area.
- Water circulation in the Baby Beach area is limited. Periodic sand replenishment efforts may be required at approximately 5 yr intervals to replace the contaminated sediment.
- Storm drains are a significant source of contaminants. High bacteria levels occur inside and just outside of the storm drains, decreasing

significantly within a short distance away from the pipe mouth. A practice on storm drain plugging during the summer months showed a decrease in total coliform and fecal coliform but an increase in enterococcus. Measurable quantities of bacteria are able to enter the beachfront waters via leaks in the drain plugs and may be responsible for beach-closure postings.

- Groundwater can potentially provide a transport mechanism for bacteria from various source locations into receiving waters.
- During low water levels, prevailing wind patterns appear to *pen* water within the beach area and create eddy currents near Baby Beach that may tend to restrict water flow.
- Bacteria concentrations in water vary widely at different times of the day.
- Boating activities do not contribute to a measurable quantity of bacteria. The number of beach users and turbidity does not correlate with the bacteria concentrations in the water. There is no known correlation with the tidal fluctuation; however, this could be due to field tests being conducted only once a week.
- A field study showed that large waves and swells along the outer breakwater can cause substantial disturbance and resuspension of sediments in the Baby Beach vicinity. During this disturbance, sharp increases in bacterial concentrations were observed.
- An increase in water circulation can improve water quality near Baby Beach as a result of greater dilution and mixing. A recommendation to conduct a demonstration project using mechanical means to improve water circulation in the Baby Beach area was made.

Circulation Improvement Pilot Project at Baby Beach, Dana Point, Final Report (Everest International Consultants 2006)

A circulation-improvement pilot project was conducted in 2005 by the collaborative efforts of the County of Orange and the City of Dana Point. The pilot project consisted of installing six circulation enhancing devices, called oloids, in the immediate water zone at Baby Beach in June 2005. The layout of the oloid deployment was chosen to enhance the existing flow conditions at Baby Beach. During this time, the adjacent storm drains were plugged to prevent various discharges onto the beach.

The pilot project was designed to provide field data to determine 1) the capability of the oloids to improve water circulation, 2) the change in

bacteria levels due to water circulation improvement, and 3) the impact of the potential decrease in the bacteria levels to reduce the occurrence of the Assembly Bill (AB) 411 violation. It is noted that AB 411 refers to California Assembly Bill No. 411 requiring the State Department of Health Service to adopt regulations to test all beaches for total coliform, fecal coliform, enterococci, and streptococci bacteria, to establish minimum standards for these indicators, and to require posting at subject beaches whenever the established standards are violated. Specific findings and recommendations from this pilot project study are presented as follows:

- The current configuration of the oloids improved water circulation in the alongshore direction from the west end towards the east but was not effective in moving the water at the east end toward the deeper water region. Improvements in circulation were found at the west end, buoy line, and swim sampling locations. Only a slight improvement in water circulation occurred at the east end near the Youth Dock.
- Under low-wind conditions (less than 6 mph), the oloids can contribute more to water circulation at Baby Beach than the wind-induced drag.
- Bacteria levels at Baby Beach were low throughout the pilot project period. While there was a reduction in bacteria level at some sampling locations, but not all of them during which the oloids were operating, it is inconclusive that the reduction was due to the direct impact of the oloids or a natural fluctuation in bacteria level.
- The limited data of bacteria sampling did not conclusively show that the improvement of water quality was due to the employment of the oloids, even though the data did show some reduction in bacteria level at some locations where the oloids were in operation.
- Winds may play a major role in water circulation at Baby Beach. It was suggested that wind data at Baby Beach be analyzed to understand the role of wind-induced circulation and mixing at Baby Beach.
- Investigation of the sources that contribute to high bacteria levels at Baby Beach should be continued and other control measures considered to prevent contaminated sources entering the harbor should be pursued.
- The oloid design should be reviewed for compatibility in the marine environment.

Baby Beach in Dana Point Harbor, Orange County, Final Report, CBI Grant Nos. 19 and 260 (Orange County Resources and Development Management Department (OC RDMD) 2006)

The report summarized a two-phase project for monitoring and improving the water quality at Baby Beach. Phase I consisted of the previously mentioned efforts by SAIC and the PFRD as described above. Also included in Phase I was the installation of a structural storm-water treatment (Stormceptor®) in the site drainage system at Ocean Institute. Due to some constraints such as low hydraulic profile of the system and absence of a flap gate, the system's effectiveness was compromised approximately 45% of the days during the wet season.

Phase II of the project included the installation of sewer diversion for the Baby Beach storm drain system, bird exclusion fencing under the Baby Beach pier, and bird-proof trash cans on Baby Beach to discourage bird activity that could result in waste becoming a contaminated source. Six regular sampling locations in the Baby Beach area were monitored and compared against AB411 bacteria standards. The following results were obtained from the Phase II study:

- Despite postings for various brief periods when the diversion was operational in the summer of 2005, available data demonstrate that Baby Beach was much cleaner in 2005 than in 2004. However, a direct impact associated with the diversion of the drainage water into the sanitary sewer system cannot be assessed due to the concurrent implementation of the oloid circulation device during the pilot project period in the summer of 2005 and the extremely wet 2004–05 winter season.
- Installation of a new chain-link fence under the fishing pier proved to be effective in excluding pigeons' or gulls' staging underneath the pier. The bird-proof trash cans also reduced the bird gathering in the Baby Beach area.

Regional Harbor Monitoring Program Pilot Project 2005-06 Final Report (Weston Solutions, Inc. 2006)

The Regional Harbor Monitoring Program (RHMP) was a comprehensive effort to survey the general water quality and condition of aquatic life in San Diego Bay, Mission Bay, Oceanside Harbor, and Dana Point Harbor.

The Pilot Program for the RHMP is a scaled-down version of the proposed RHMP that focused on a limited number of indicator measurements and samples in marinas and freshwater influenced waters. Three sampling stations were located near boat slips within Dana Point Harbor. An additional station was located adjacent to a storm drain. Based on the data collected during the first year (i.e., 2005), the following general findings were established for all sampled areas:

- The copper concentration in the water column of the marinas is higher than those found in freshwater-influenced areas; the proportion of marina samples with elevated concentrations is higher than the historical measurements throughout the harbors.
- Concentrations of other metals and polyaromatic hydrocarbons in the water column were below water quality objectives.
- All bacterial indicators were below the AB411 levels.
- Measurements of sediment quality were mixed as compared to the historical measurements.
- Biological indicators for benthic infauna show poor habitat quality in the marinas and freshwater-influenced areas than was found historically throughout the harbors.
- Sediment toxicity test indicates healthier conditions than found historically.

2 Physical Conditions

Dana Point Harbor is located in the City of Dana Point, Orange County, approximately midway between Los Angeles and San Diego (Figure 1). The harbor is situated on an arc-shaped shoreline section of Capistrano Bay bound by the Dana Headlands on the northwest and Doheny State Beach to the south. The onshore features include the 55 m (180 ft) high coastal bluffs that are landward of the harbor and the promontory at the base of West Breakwater. The facilities located within the harbor are protected from ocean swells and storm wave attack by a pair of rubble mound breakwaters.

2.1 Physiographic setting

East Breakwater starting at Doheny Beach extends seawards for a total length of 686 m (2,250 ft) while West Breakwater originating from the Dana Cove Park stretches for 1,676 m (5,500 ft) to the southwest toward the harbor entrance. The bedrock layers that make up the foundation of the breakwaters are part of a wave-cut, submarine terrace as created by a combination of a rising sea level and an eroding shoreline. The foundation of the breakwaters consists of the hard bedrock overlaid with a thin lens of marine sands.

The harbor consists of two marina basins (East and West Basins) containing a total of 2,500 slips for vessels of various sizes. Also included in the harbor are fifty guest slips for boats, a ten-lane launch ramp, a dry boat storage hoist, a fishing pier, a shipyard, a marine fuel dock, three yacht clubs, and a commercial sports fishing operation that offers whale watching trips throughout the year (County of Orange Parks 2011). Recreational activities in the harbor also include an educational experience at the Orange County Ocean Institute, bathing and swimming at Baby Beach, and water-related recreation for youth at the County's Dana Point Harbor Youth and Group Facility.

2.2 Bathymetric and LiDAR survey

A bathymetric and LiDAR survey was conducted during October 20–24, 2009 (Fugro 2010), to collect basic physical data so that numerical modeling tasks can be performed to characterize the wave environment at

breakwaters and water circulation within the harbor. The collected LiDAR and sonar data of the breakwaters allow for assessment of the present-day protective structure conditions. The previous condition survey and an evaluation of the dual breakwaters were performed in 1991 (USACE LAD 1991).

The bathymetric and side-scan sonar data below the water surface and the LiDAR data above the water level were acquired along both sloping faces of East and West Breakwater extending out approximately 46 m (150 ft) offshore on the ocean side and in the main navigation channels on the harbor side (Figure 2). In addition to these areas, Baby Beach and the primary access channels within the marina basins were also surveyed.

Figure 2. Bathymetric survey area.

The survey utilized the swath bathymetry system for the underwater portion and the laser scanning system for elevations above the water line, as illustrated in Figure 3. The Kongsberg GeoSwath Plus system (http://www.km.kongsberg.com/geoacoustics), mounted to the port side of a survey vessel, was used to provide swath bathymetry coverage of the seabed. The system employed interferometric sonar, which generates short pulses of

Figure 3. Integration of LiDAR scanner and swath bathymetry systems.

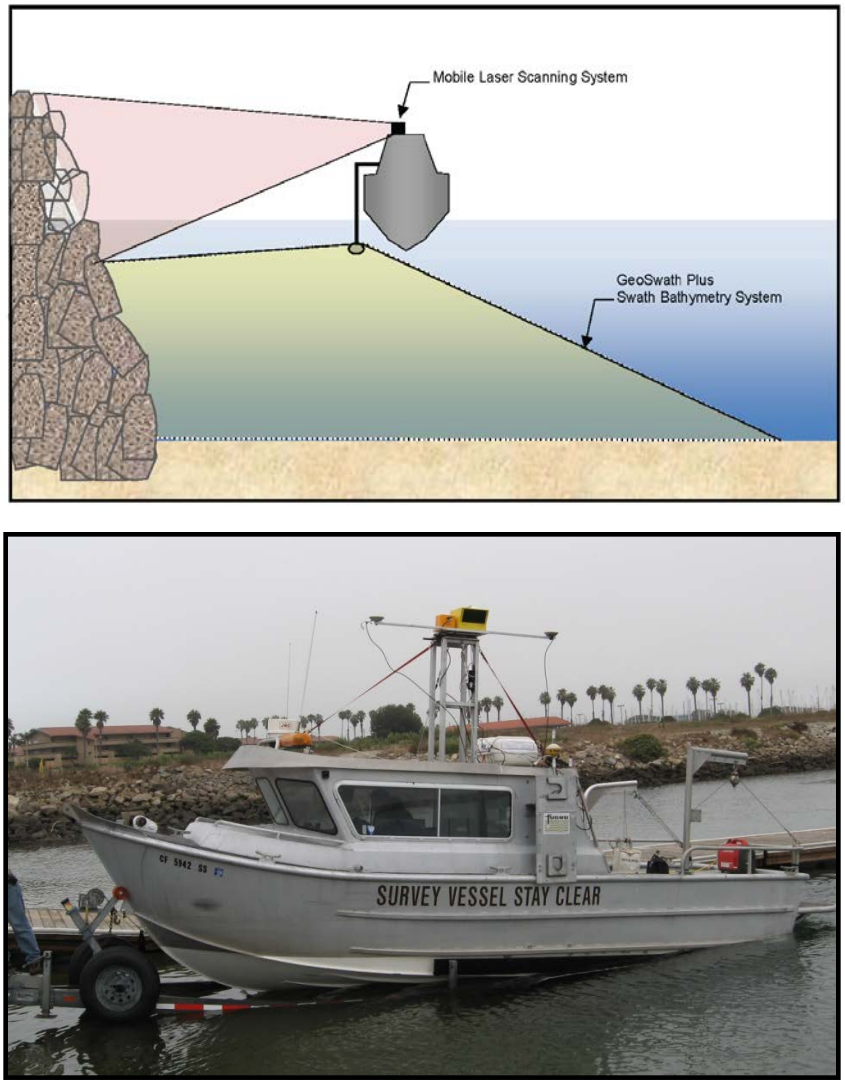

acoustic energy that propagate out from the transducers at the speed of sound in water, insonifying a narrow strip of seabed perpendicular to the vessel track (Fugro 2010). A base station used for the survey control was set up on land to improve horizontal and vertical positioning. The survey control at the project site was logged based on the NAD83 coordinate system, California State Plane Zone 6 (i.e., the horizontal coordinates) and MLLW elevations (i.e., the vertical datum). The accuracy for the Swath bathymetry system is 0.5 m (1.5 ft) horizontally and 0.2 m (0.7 ft) vertically. An ILRIS (Intelligent Laser Ranging and Imaging System) 3D LiDAR Scanner system mounted on top of the vessel was used for collecting above-water data. The LiDAR system is an optical remote sensing technology that measures properties of scattered light to find range and/or other information of a distant target. The horizontal and vertical accuracies of the LiDAR

data are 0.15 m (0.5 ft) and 0.07 m (0.25 ft), respectively. Figure 3 provides a systematic sketch of the data integration that was obtained by these two measurement systems. A detailed description and survey operation of these two survey systems was presented in Fugro's survey report (Fugro 2010).

The swath bathymetry and LiDAR data were integrated in the compilation of longitudinal profiles and cross sections along the breakwaters and bathymetric contour maps adjacent to the breakwaters and within the harbor. Topographic maps above the water line of the breakwaters and revetment along the island mole inside the harbor were also deduced from the collected data. Figure 4 shows the contour plot of the breakwaters, main navigation channel, and various areas within the harbor. Figure 5 illustrates the 3D images generated from the LiDAR data at the head of the West Breakwater, the entrance area, and in the areas of Baby Beach and Ocean Institute. A complete set of bathymetric plots including the side-scan sonar data is presented in a report by Fugro (2010). The 2009 bathymetry combined with available bathymetric data in the nearshore region was then used to generate the modeling grid for numerical simulations to characterize the wave environment adjacent to the breakwaters and water circulation in the harbor.

2.3 Present-day breakwater condition

Since the completion of the harbor construction in 1970, the harbor had only suffered damages once during the 1983 El Nino winter season when a cluster of major storms resulted in some damage to West Breakwater from Sta 0+61 to Sta 3+51 (referenced to the meter unit) and from Sta 3+51 to Sta 7+01 as identified in Figure 4. The damaged areas located on the ocean side were subsequently repaired in 1984. Another extreme storm event that occurred in January 1988 did not render any recorded damages to the protective breakwaters. A comprehensive condition survey consisting of side-scan sonar, image sonar profiling, and topographic surveys and visual inspection was conducted in 1991. The field study indicated that East Breakwater remained stable in excellent condition while some armor stones were displaced on the seaward slope of West Breakwater.

The present structure conditions of both breakwaters were examined via the processed 3D LiDAR images with a visual confirmation in sections above the water line. At West Breakwater, dislodged stones on the harbor side near Sta 00+97 and Sta 02+13 were detected below the water surface (Figure 6). This may be attributed to a slumping effect as a consequence of maintenance dredging in the past. In addition, some isolated armor stones above the water surface are also displaced from their original placement.

Figure 4. Bathymetric contour map.

Figure 5. 3D images of LiDAR survey.

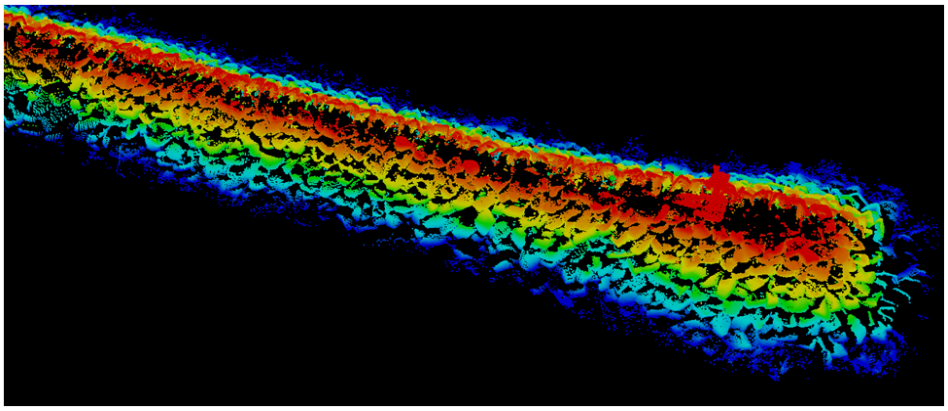

Head of West Breakwater

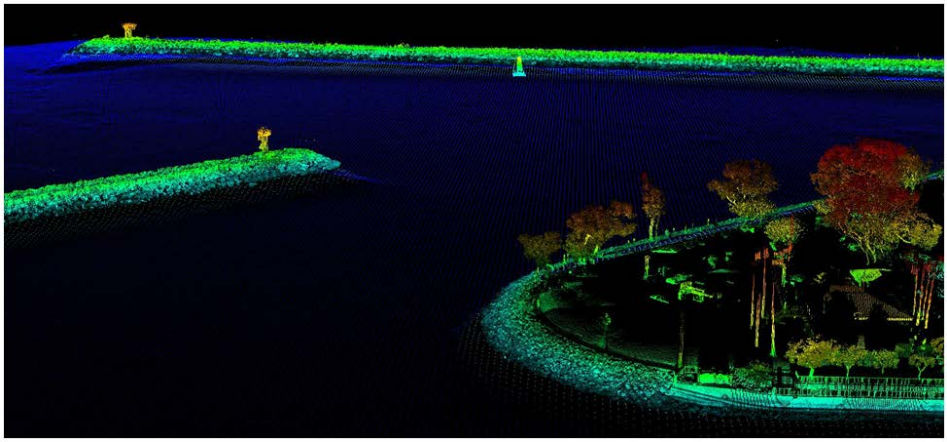

Harbor Entrance

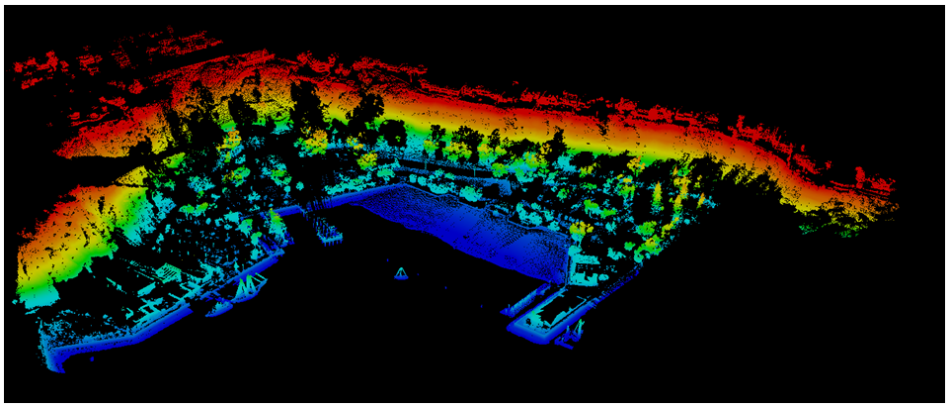

Baby Beach and Ocean Institute

Figure 6. Dislodged stones at West Breakwater.

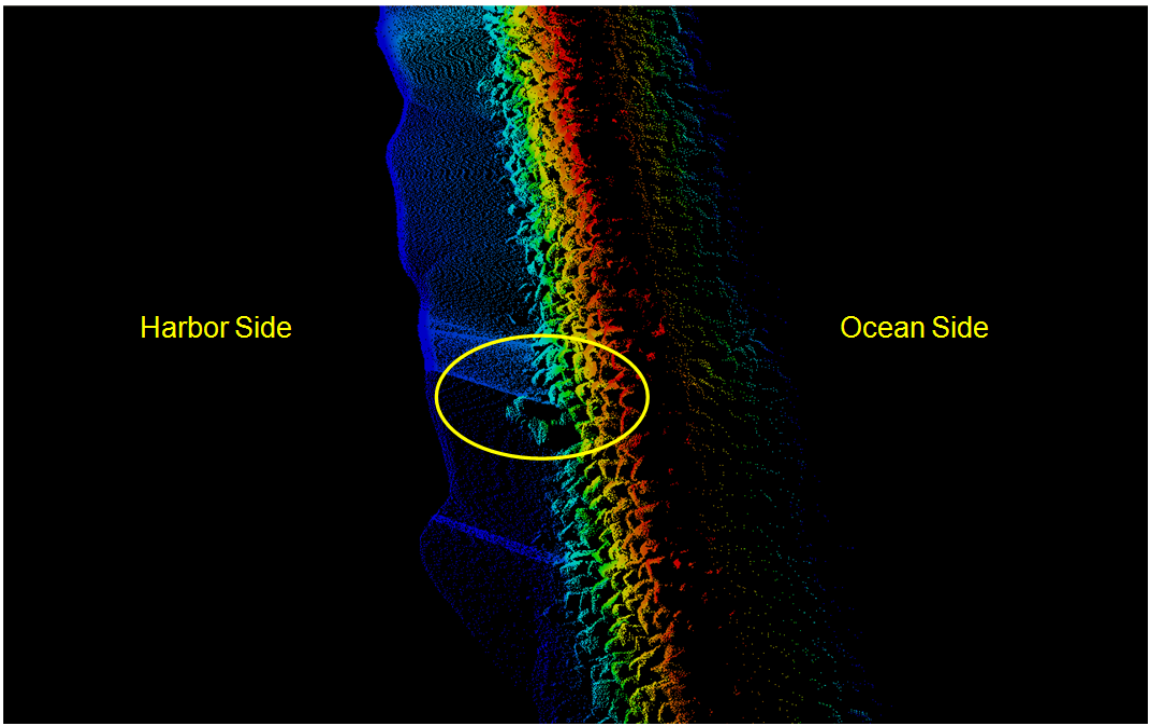

Dislodged stones near Sta 00+97

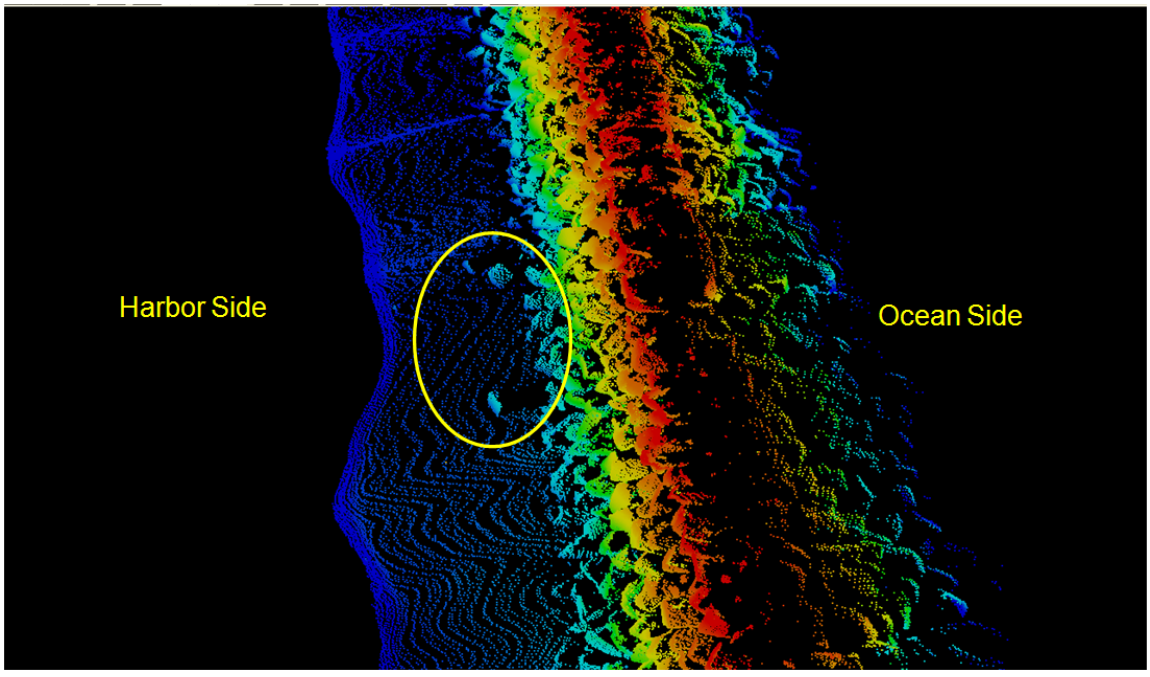

Dislodged stones near Sta 02+13

Figures 7 and 8 show displaced stones at Sta 15+54 and around the head of West Breakwater, respectively. The structure appears to function as originally designed to shelter the harbor facilities from west to northwest winter storm waves. At East Breakwater, the structure remains intact and functions as a protective device for the harbor operation (Figure 9). However, some armor stones below the water surface on the harbor side appear to be dislodged from their original positions. Figures 10 and 11 illustrate the processed 3D images indicating the dislodged stones from Sta 3+30 to 4+08 and near the head structure, respectively.

Figure 7. Displaced stone near Sta 15+54.

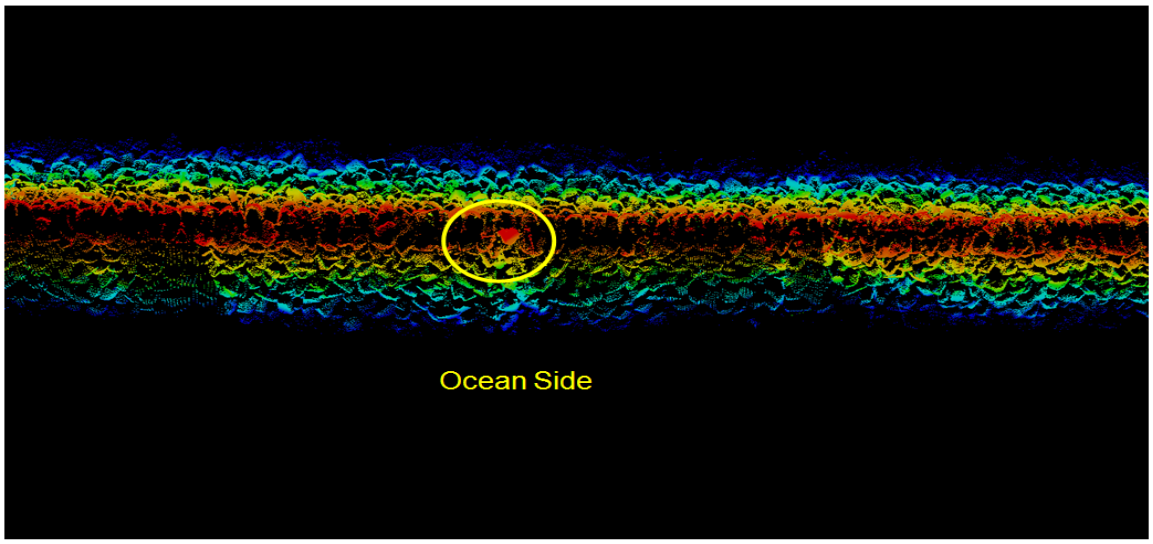

3D LiDAR Image

Photo taken on 1/15/2010

Figure 8. Displaced stone at structure head of West Breakwater.

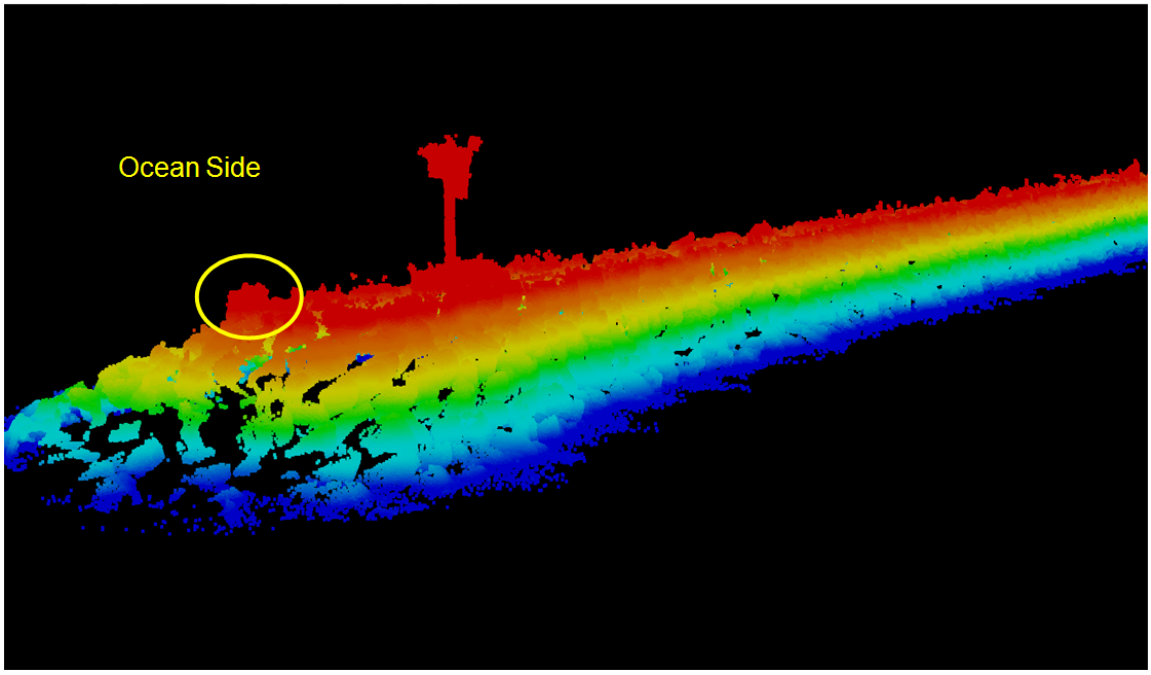

3D LiDAR Image

Photo taken 1/15/2010

Figure 9. East Breakwater.

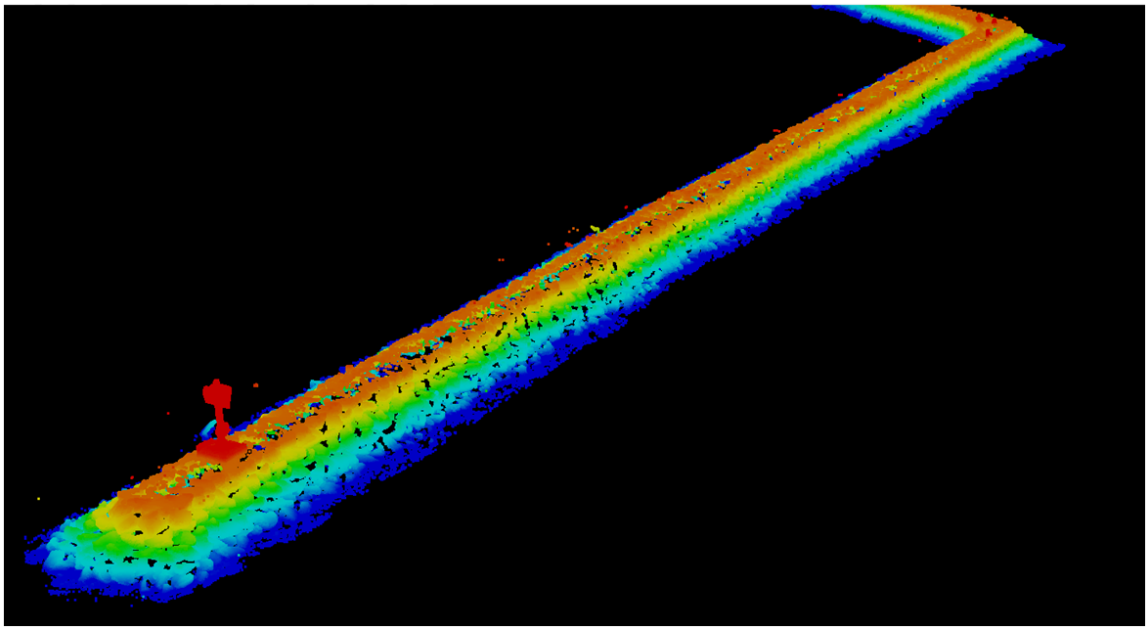

3D LiDAR Image

Photo taken 1/15/2010

Figure 10. Dislodged stones at East Breakwater.

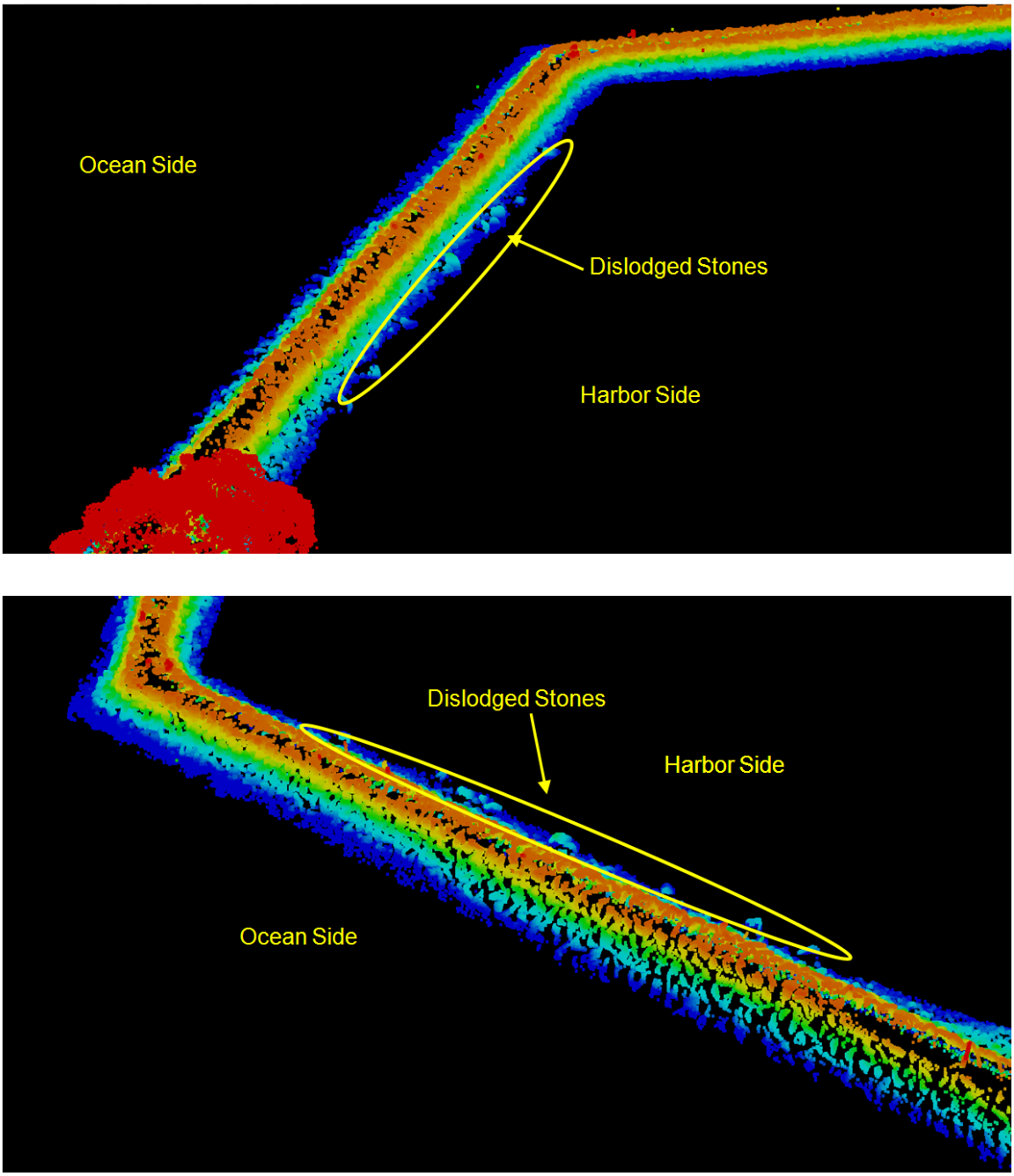

Figure 11. Displaced stone near structure head of East Breakwater.

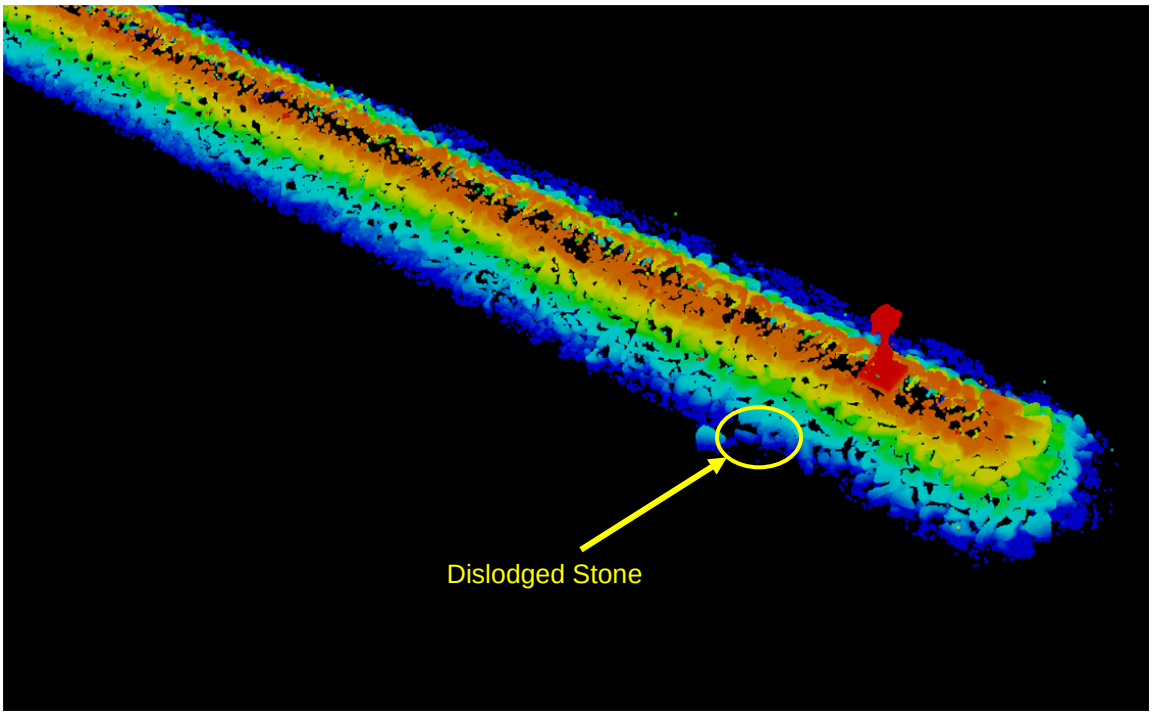

3D LiDAR Image

Photo taken on 1/15/2010

2.4 ADCP current measurements

Temporal currents were measured in the areas on both the harbor (inside) and ocean (outside) sides of West Breakwater to provide the flow field information for the calibration of the CMS models. Directional wave data were also collected on the ocean side of West Breakwater by a bottom-mount Acoustic Doppler Current Profiler (ADCP). Figure 12 shows the location map of two ADCPs that were deployed in Dana Point Harbor. Table 2 presents the coordinates of the deployed ADCPs and their respective depths.

Figure 12. ADCP gauge locations.

Table 2. ADCP locations and depths.

Instrument ID	Coordinates	Depth, m (ft) MLLW
Inside ADCP	N33°27'28.66",W117o42'12.28"	7.8 (25.6)
Outside ADCP	N33°27'25.46",W117o42'12.95"	8.4 (27.6)

2.4.1 Field work

Two self-contained RDI Workhorse Sentinel (http://www.rdinstruments.com/monitor.aspx) 1200 kHz (RD-WHS 1200) ADCPs that have a typical depth range up to 13 to 16 m (40 to 50 ft) for a vertical cell size of 0.5 m (1.6 ft) were deployed on 20 November 2009 for approximately 8 weeks till 15 January 2010. A vessel named *Early Bird* was equipped with an A-frame to carry and lower the ADCPs onto the sea floor. Prior to the deployment, divers

were dispatched to inspect and identify the appropriate location where the sea floor was flat for ADCP deployment. Each ADCP was mounted to a tripod as illustrated in Figure 13. The tripod was anchored by a chain-link section weighing about 400 kilograms (880 lbs). The tripod was further secured on the bottom by three 10 m (33 ft) ropes tied with metal rods that were nailed into the sea floor. Table 3 presents the measurement setup of the ADCP. The two ADCPs were retrieved on 15 January 2010 using the same A-frame on the *Early Bird* (Figure 14).

Figure 13. Deployment of ADCP instruments.

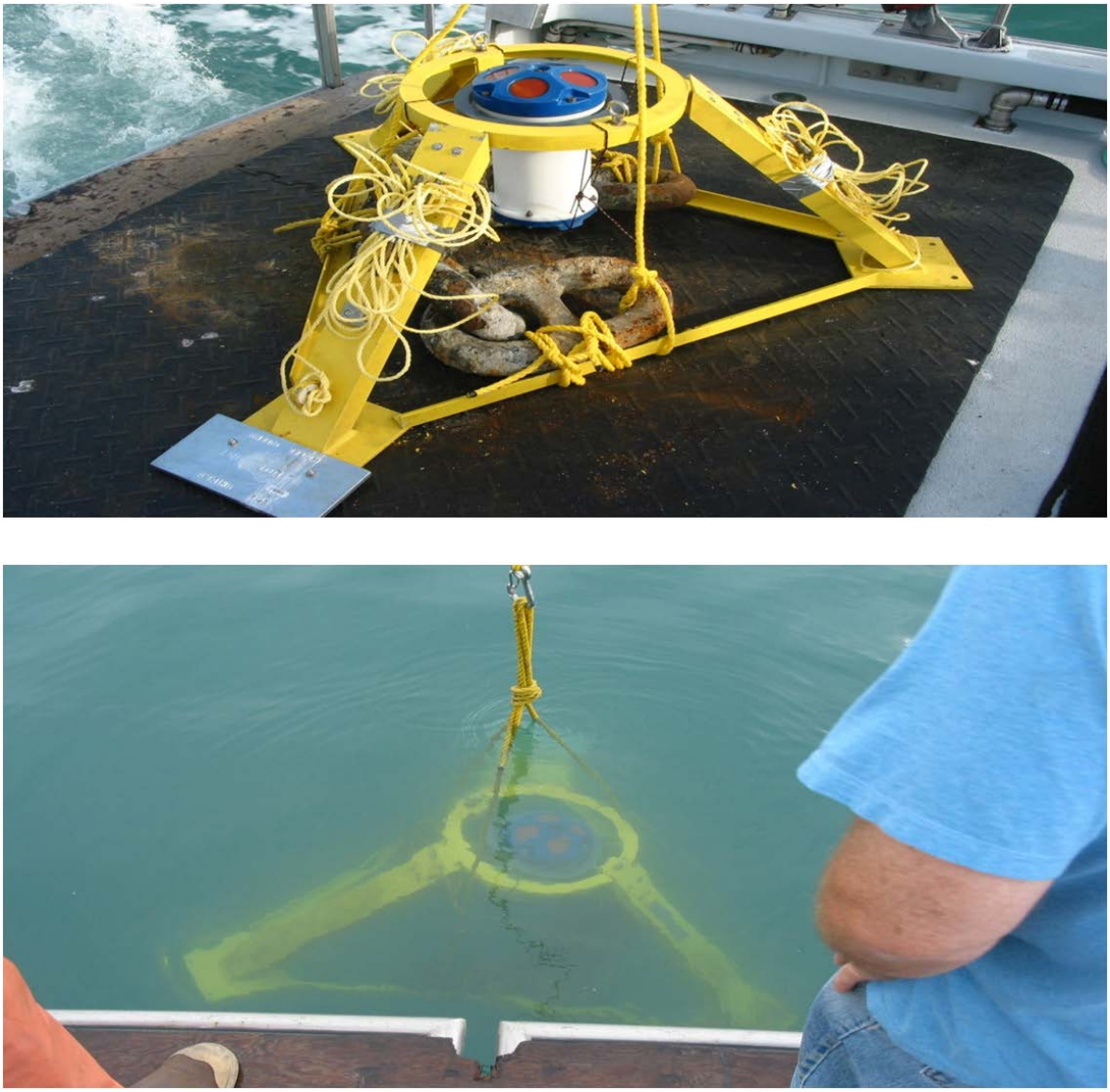

Table 3. ADCP measurement setup.

Instrument setting	Inside ADCP	Outside ADCP
Current Sampling	1 min.	1 min.
Vertical Bin Width	1.5 m	1 m
Wave Sampling	-	2 hours with a burst duration of 20 min.
Expected S.D.	0.52 cm/sec	1.12 cm/sec

Figure 14. Retrieval of ADCP instruments.

2.4.2 Data process and results

As described in Section 2.4.1, two ADCPs were deployed for 8 weeks from 20 November 2009 to 5 January 2010. However, the outside 2-5 ADCP collected only about one week of current and wave data as the instrument malfunctioned and failed to operate after 26 November 2009. Because the echo from the sea surface is much stronger than the echo from scatters in the water, the fault echo from the surface can overwhelm the side lobe suppression of the transducer to contaminate the data near the surface (Teledyne 2006). Figure 15 shows the anomaly of current speeds measured in the upper cells that are inconsistent with the lower cells at the inside ADCP for some measurements (e.g., 11/22/09, 3:25 and 11/25/09, 15:20). It is important to note that the predominant tidal-driven currents at the inside ADCP should not reach such a high velocity when compared to the measured tidal ranges and wave conditions outside the harbor during the measurement period. A similar data contamination near the ocean surface is identified for the outside ADCP (Figure 16).

It is suggested that the current data close to the surface not be considered representative. A personal communication with Teledyne's engineer confirmed the potential data contamination near the surface based on previous experience with the instrument hardware and processing. Consequently, current measurements that were at the upper two to three bins were rejected as the data collected are not consistent with the vertical cells below. The applicable current data from the inside ACDP are limited to Bins 1 through 4 while the outside ADCP is restricted to Bins 1 through 7. Figures 17 and 18 show the filtered current measurements during the same time period of data shown in Figures 15 and 16, respectively, with the contaminated data being removed from the upper bins.

Figures 19 to 29 show the time series of measured current velocity and direction at different applicable bins from two ADCPs and wave measurements from the Coastal Data Information Program (CDIP) at Dana Point (Buoy 096) with predicted tides at Newport Beach, CA (Station 9410580), in 20–26 November 2009 (Week 1). Figures 30–33 show current roses for selected periods at the two ADCPs. Appendix A presents the figures for the remaining data collected at the inside ADCP (i.e., Weeks 2–8). Note that water levels at low tides were occasionally above the measurement elevations at Bin 4 (inside) and Bin 7 (outside) during the deployment period. The mid depths of Bins 4 and 7 are 6.6 m (21.5 ft) and 8.2 m (26.7 ft) above the sea floor, respectively. Therefore, current data collected at Bins 4 (inside) and 7 (outside) may be contaminated during some neap ebb tides (Figures A40 and A42).

Figure 15. Unfiltered current profiles collected at Inside Gauge.

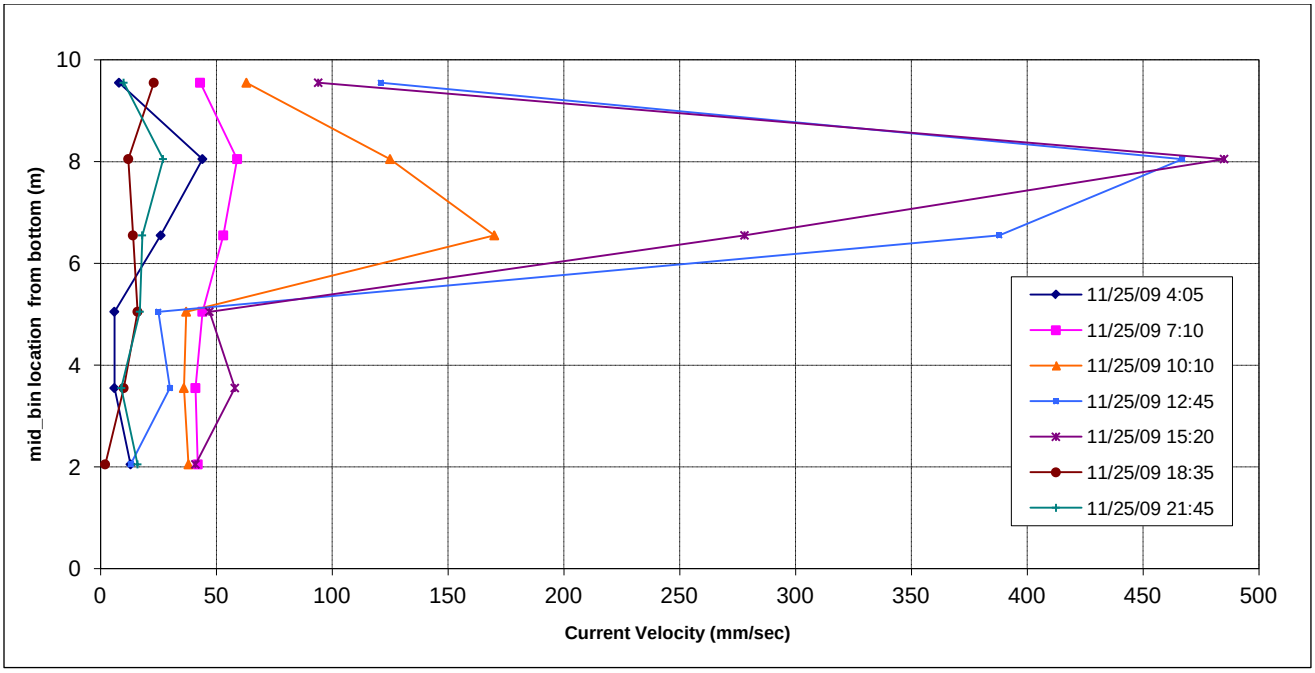

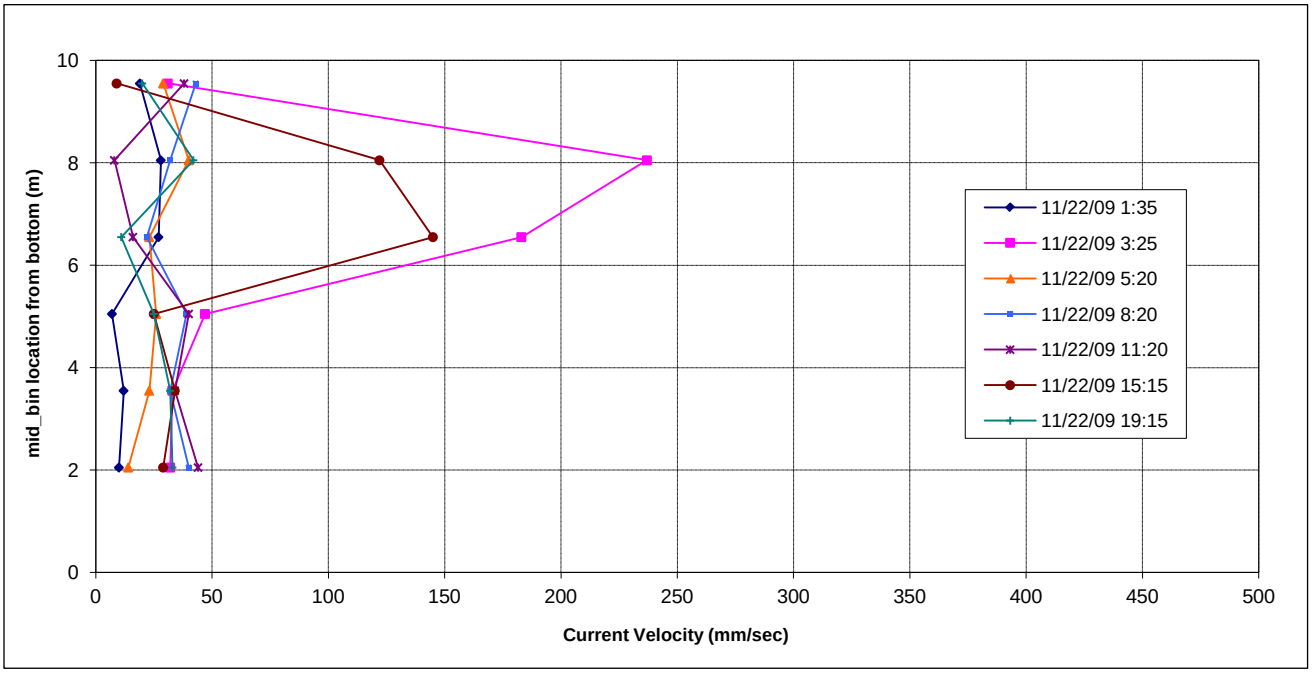

Figure 16. Unfiltered current profiles collected at Outside Gauge.

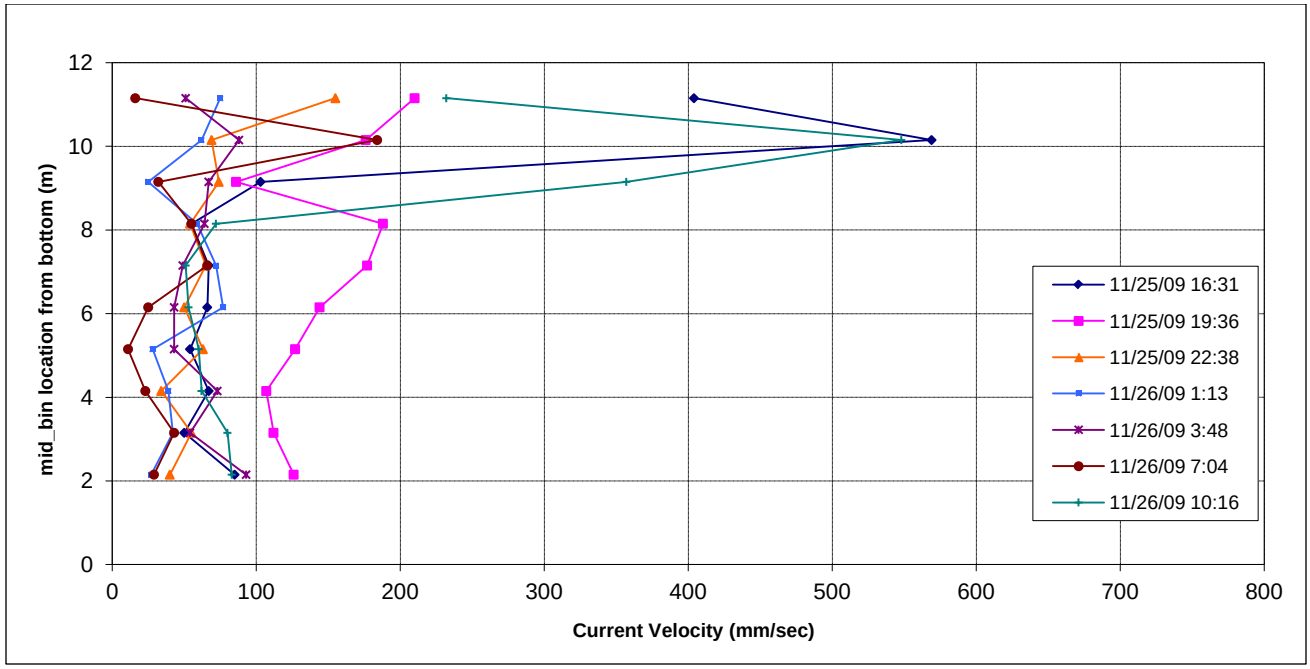

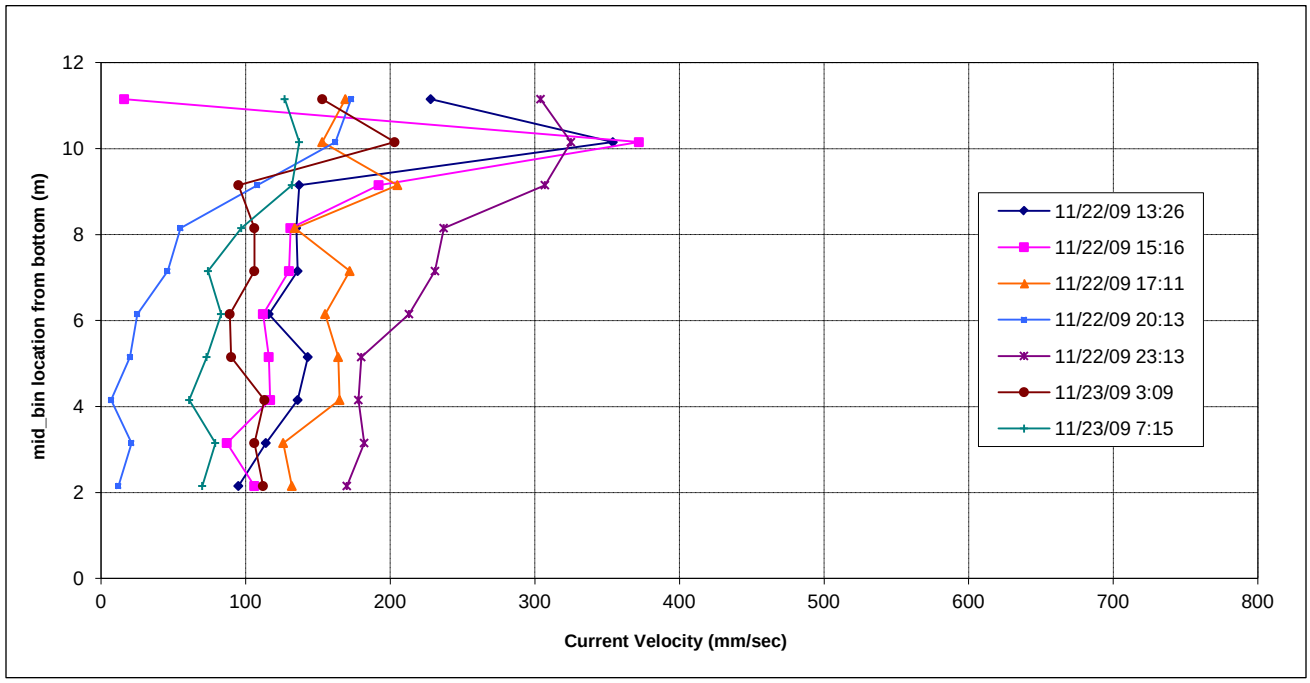

Figure 17. Filtered current profiles at Inside Gauge (continued).

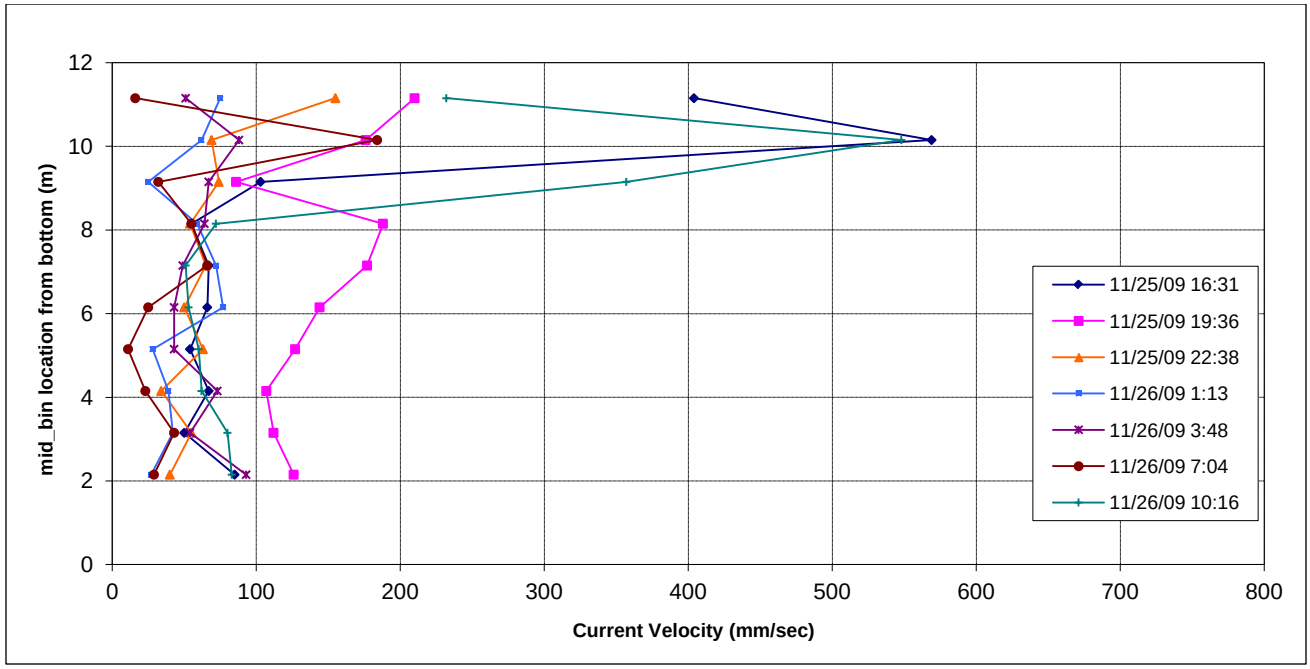

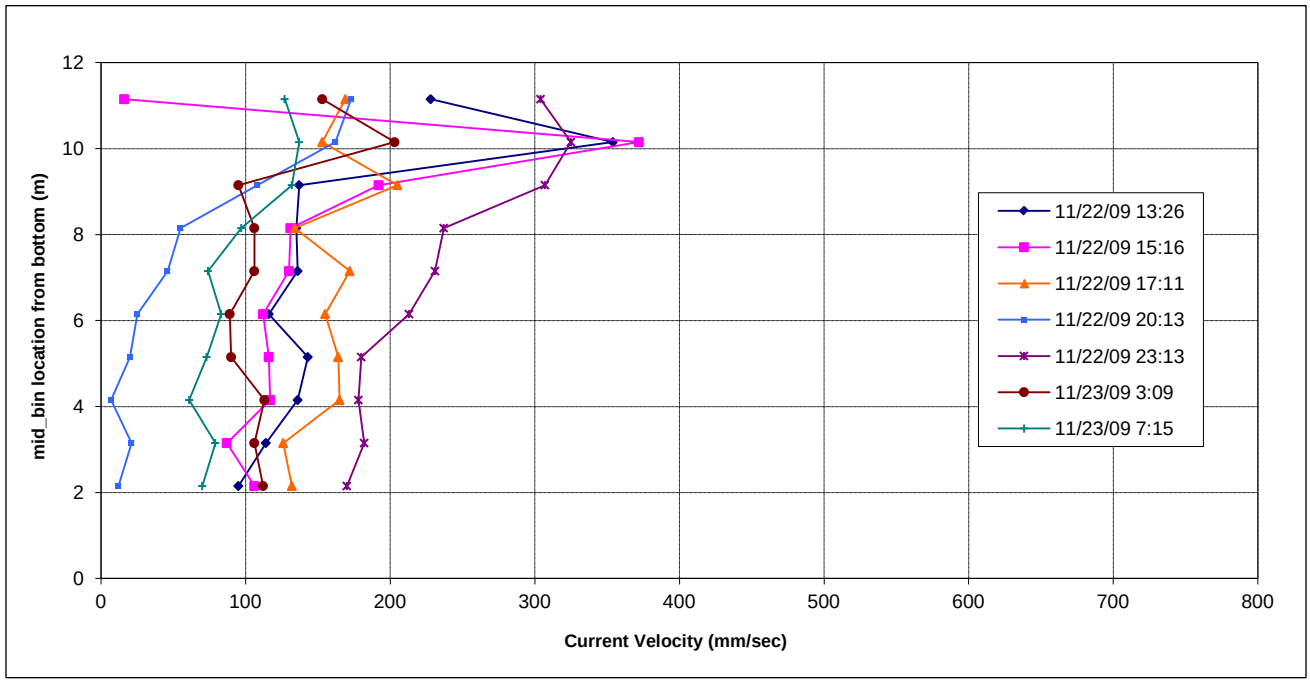

Figure 17. Concluded.

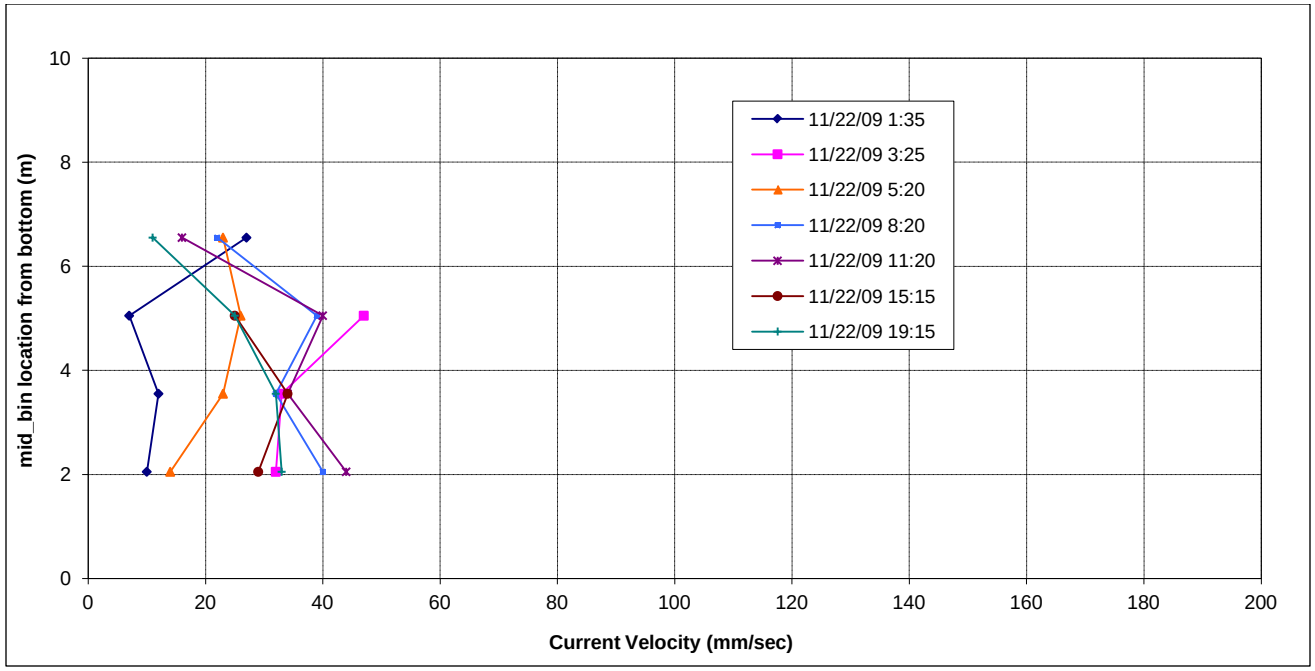

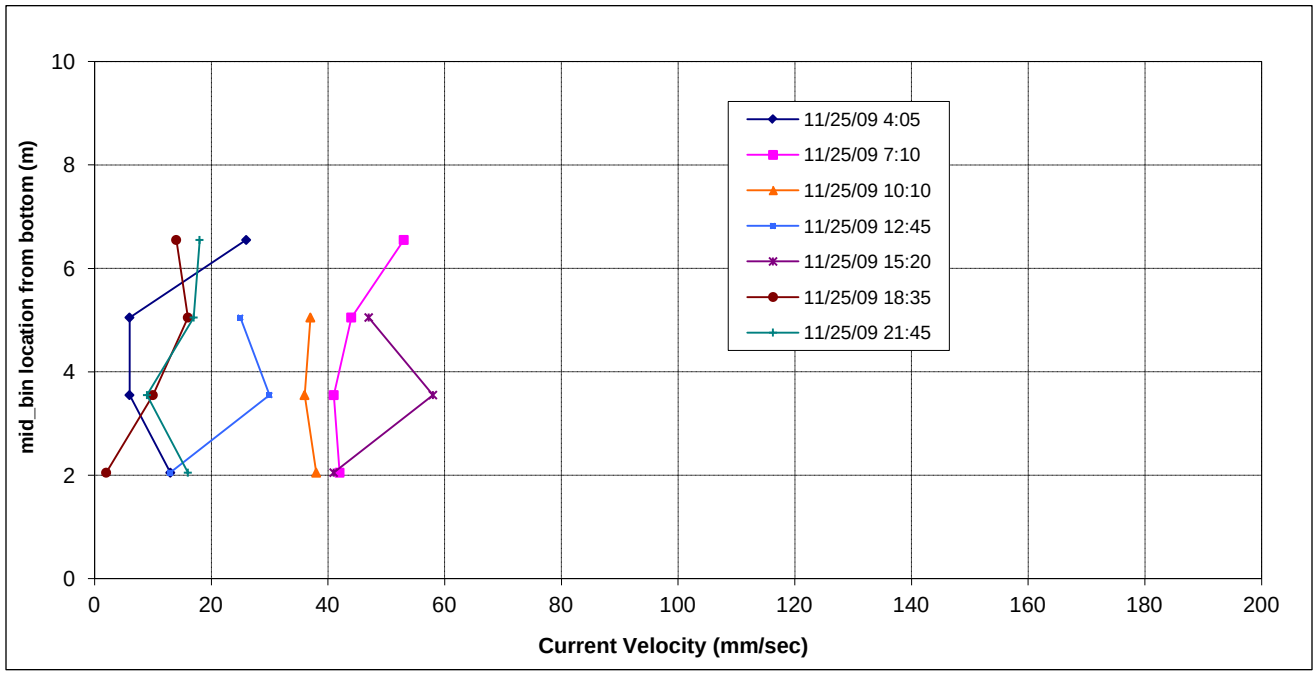

Figure 18. Filtered current profiles at Outside Gauge.

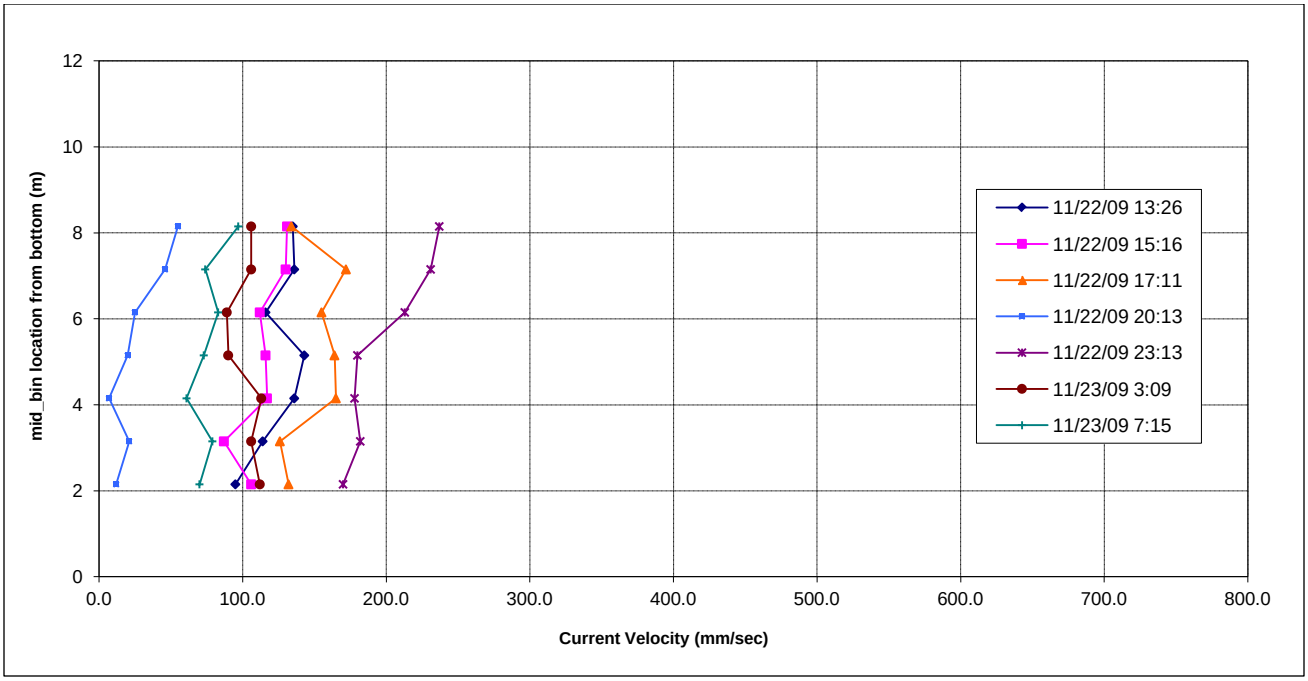

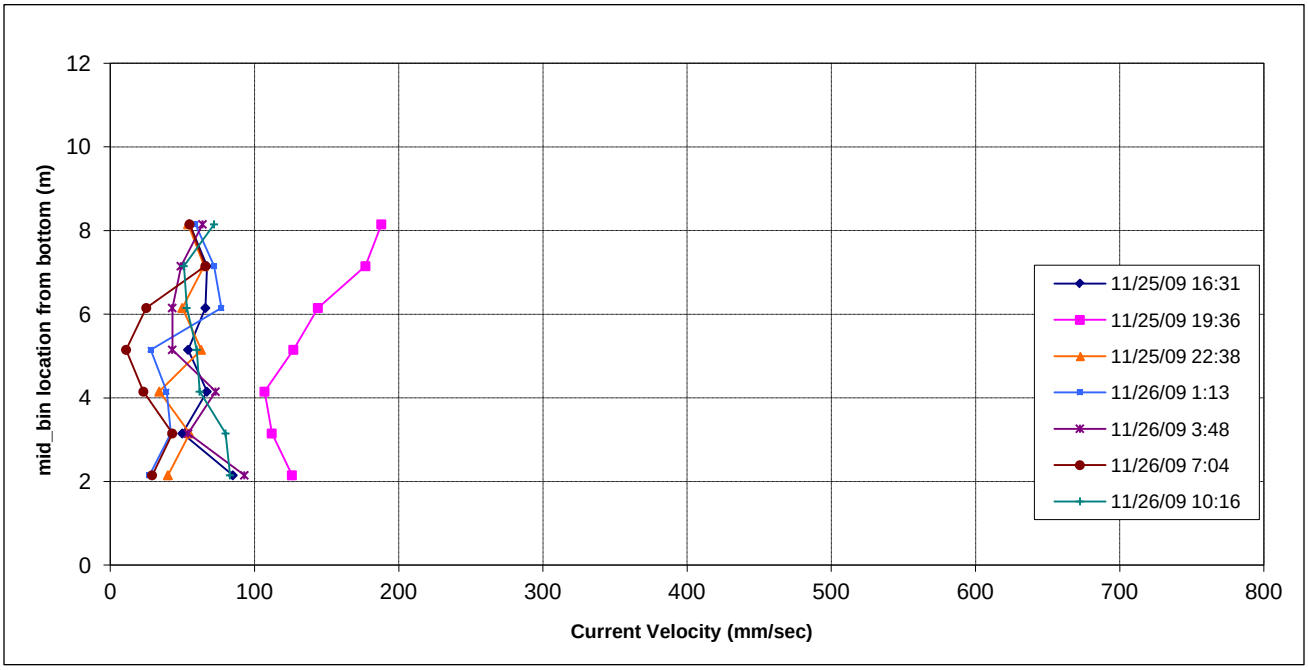

Figure 19. Week 1 - Bin 1 current measurements at Inside Gauge.

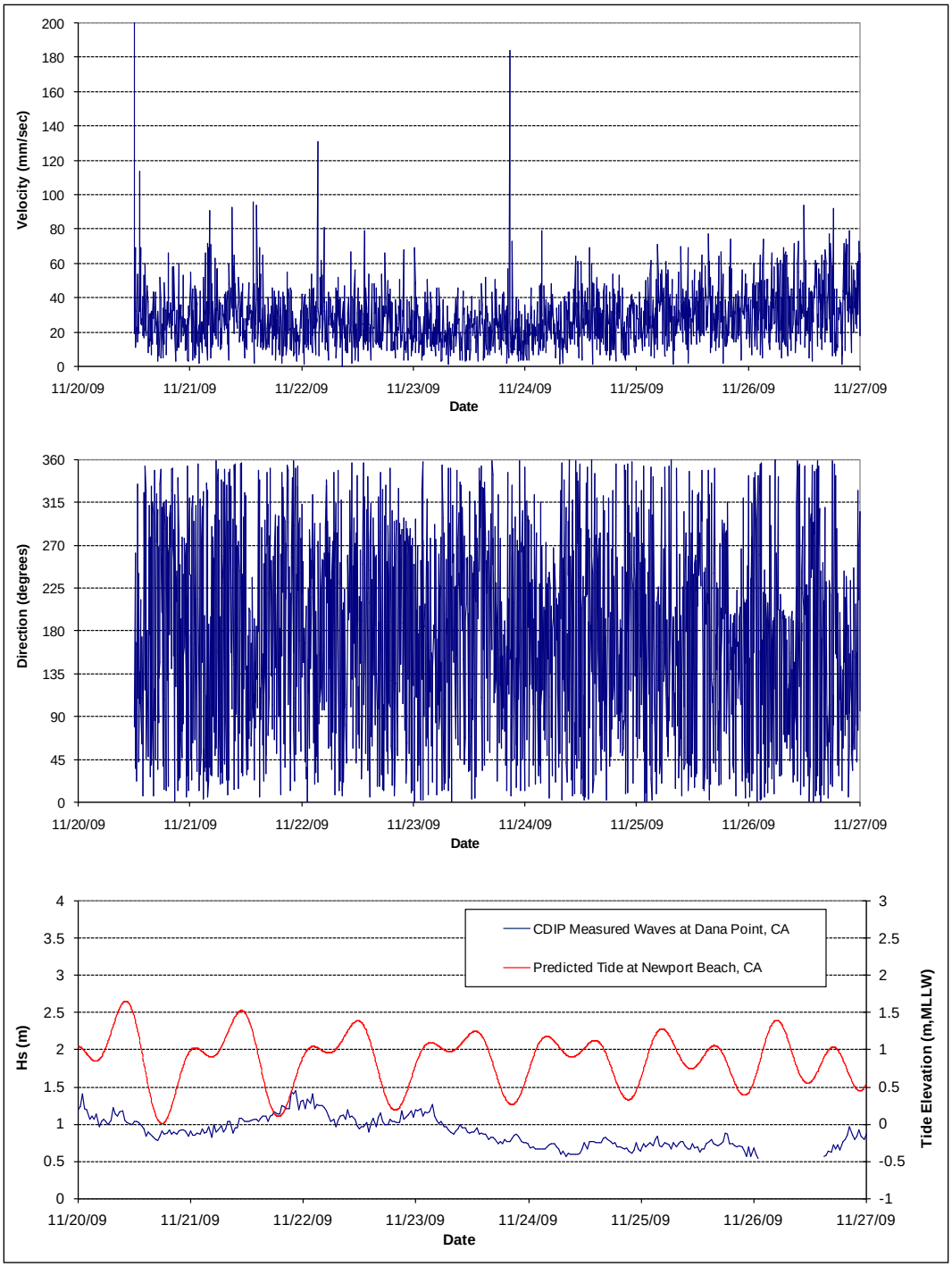

Figure 20. Week 1 – Bin 2 current measurements at Inside Gauge.

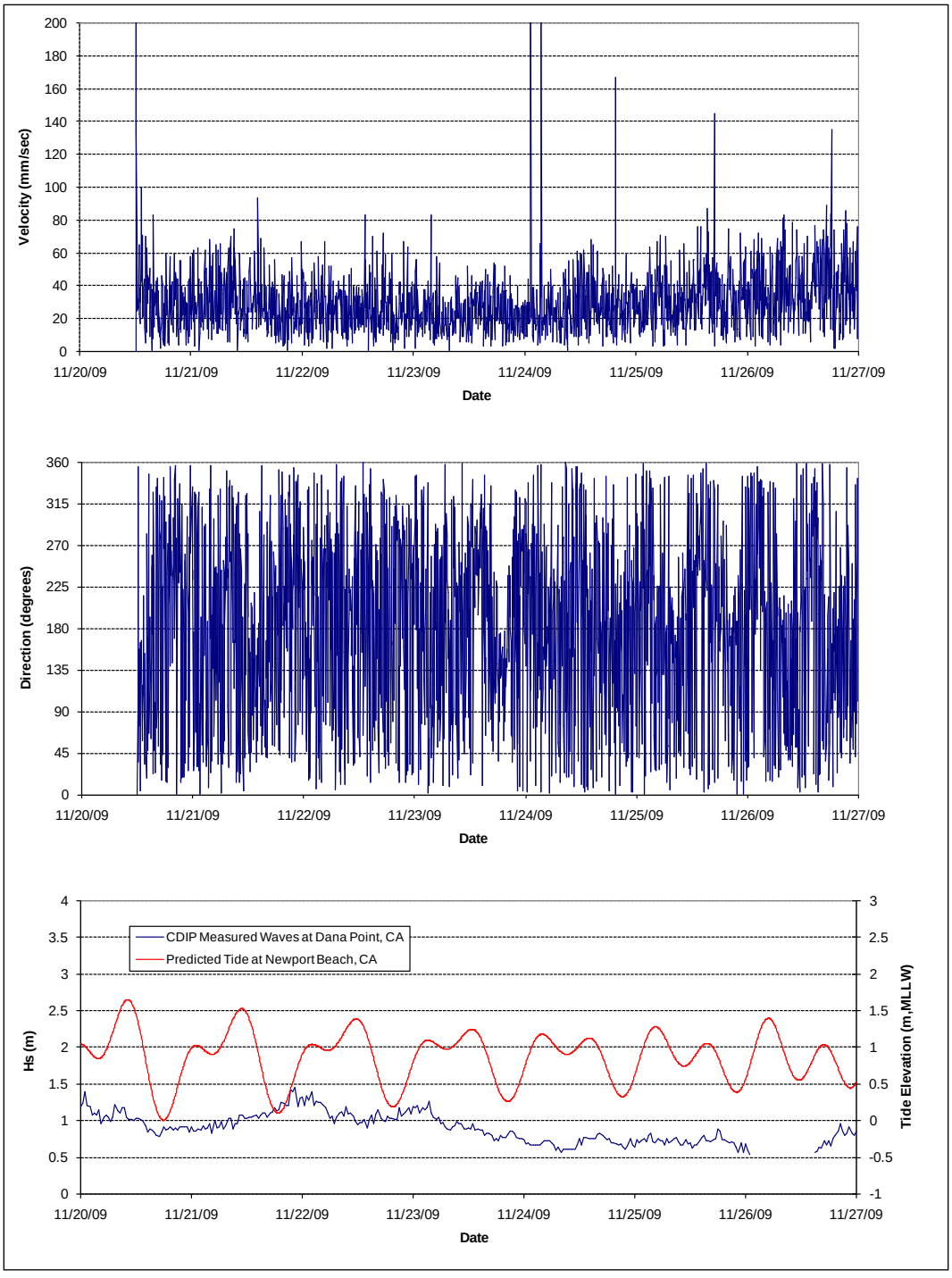

Figure 21. Week 1 – Bin 3 current measurements at Inside Gauge.

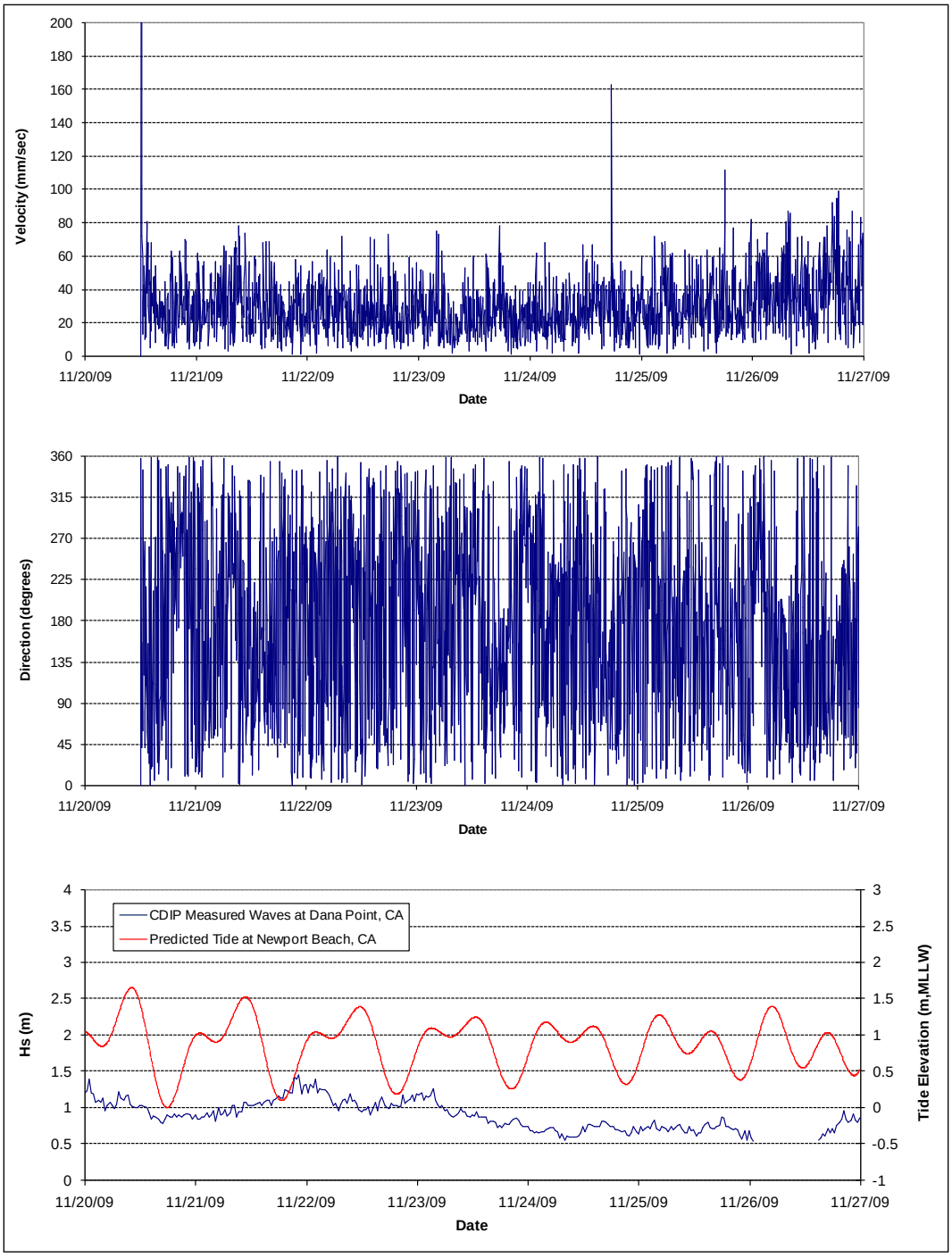

Figure 22. Week 1 – Bin 4 current measurements at Inside Gauge.

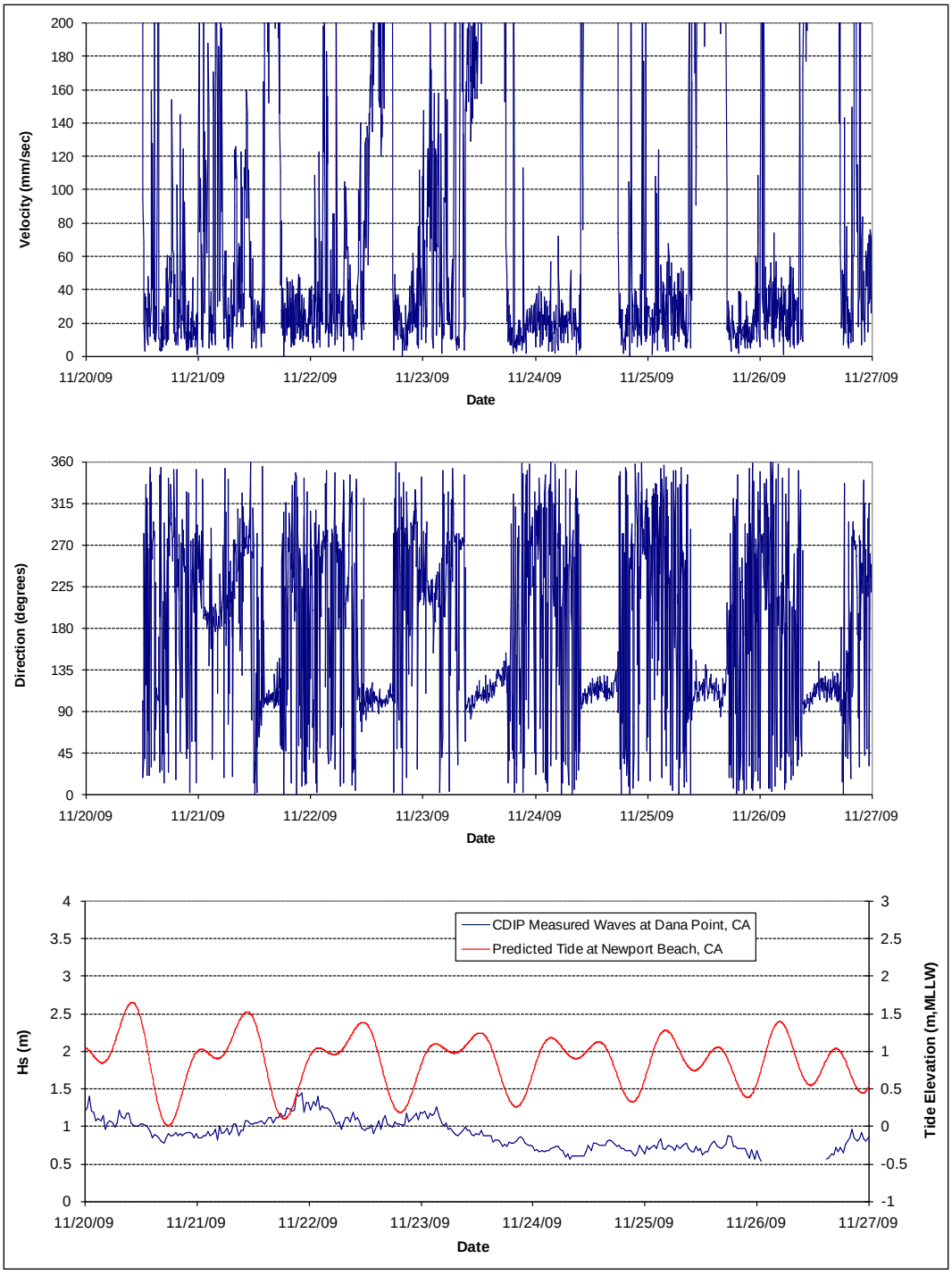

Figure 23. Week 1 – Bin 1 current measurements at Outside Gauge.

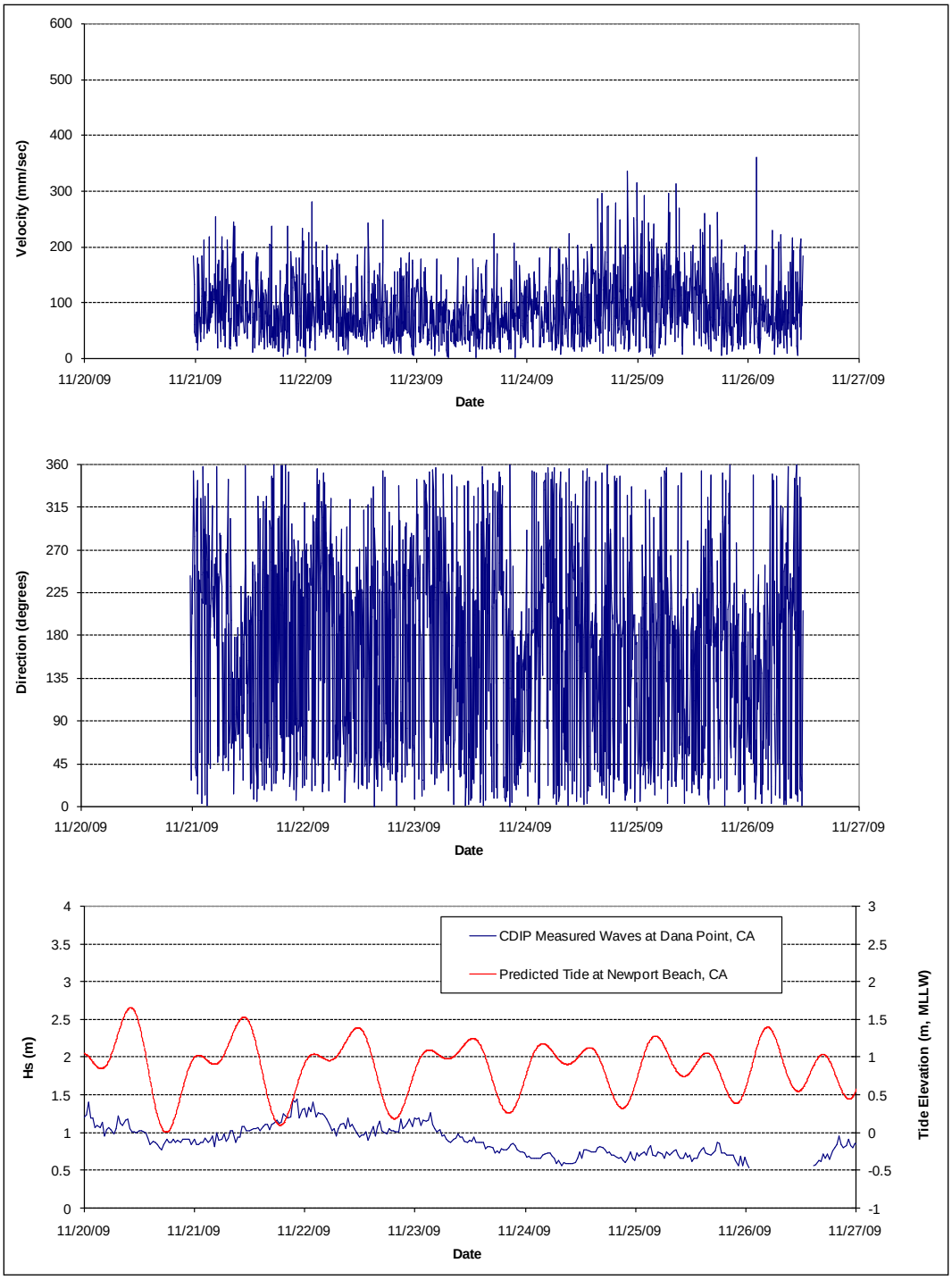

Figure 24. Week 1 – Bin 2 current measurements at Outside Gauge.

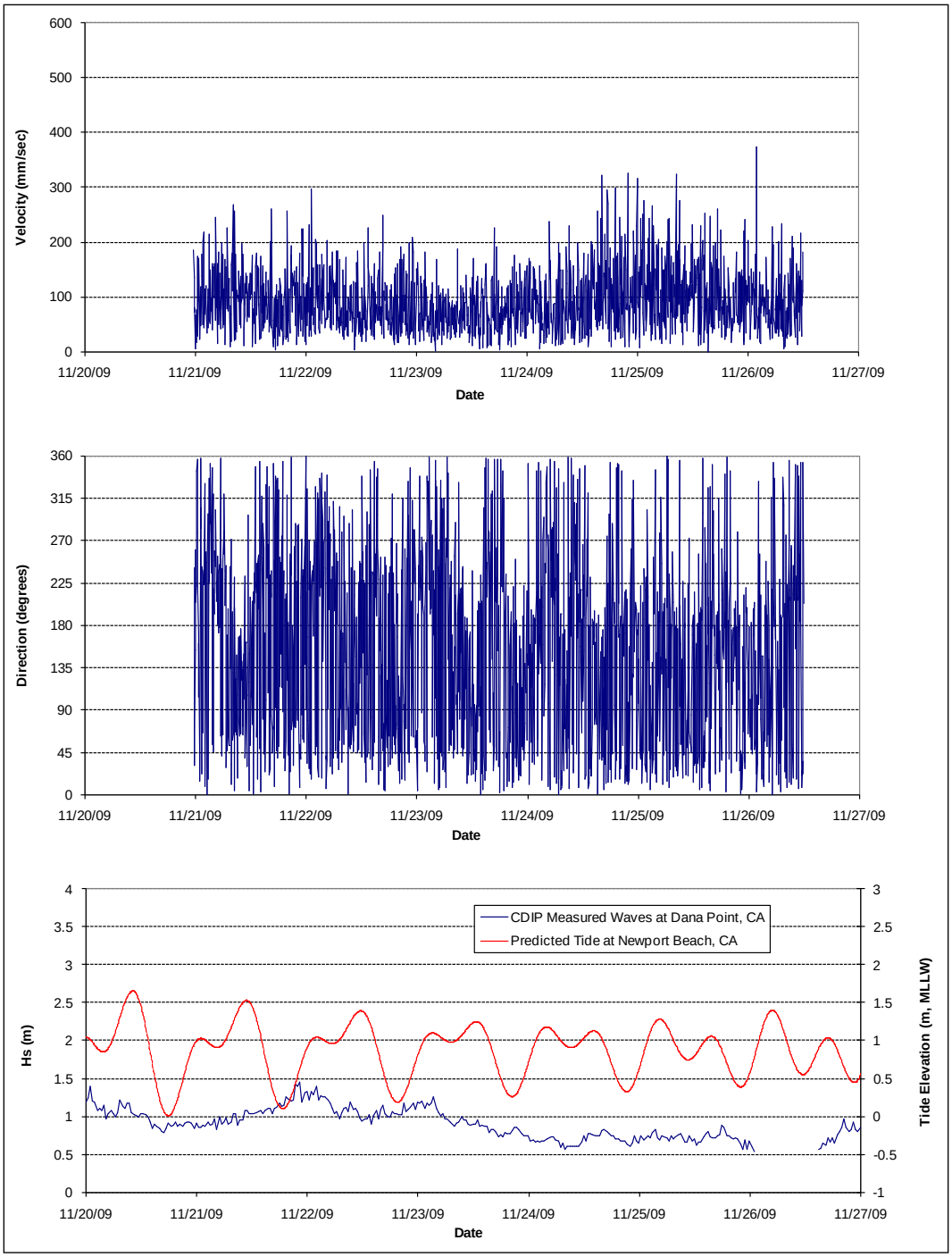

Figure 25. Week 1 – Bin 3 current measurements at Outside Gauge.

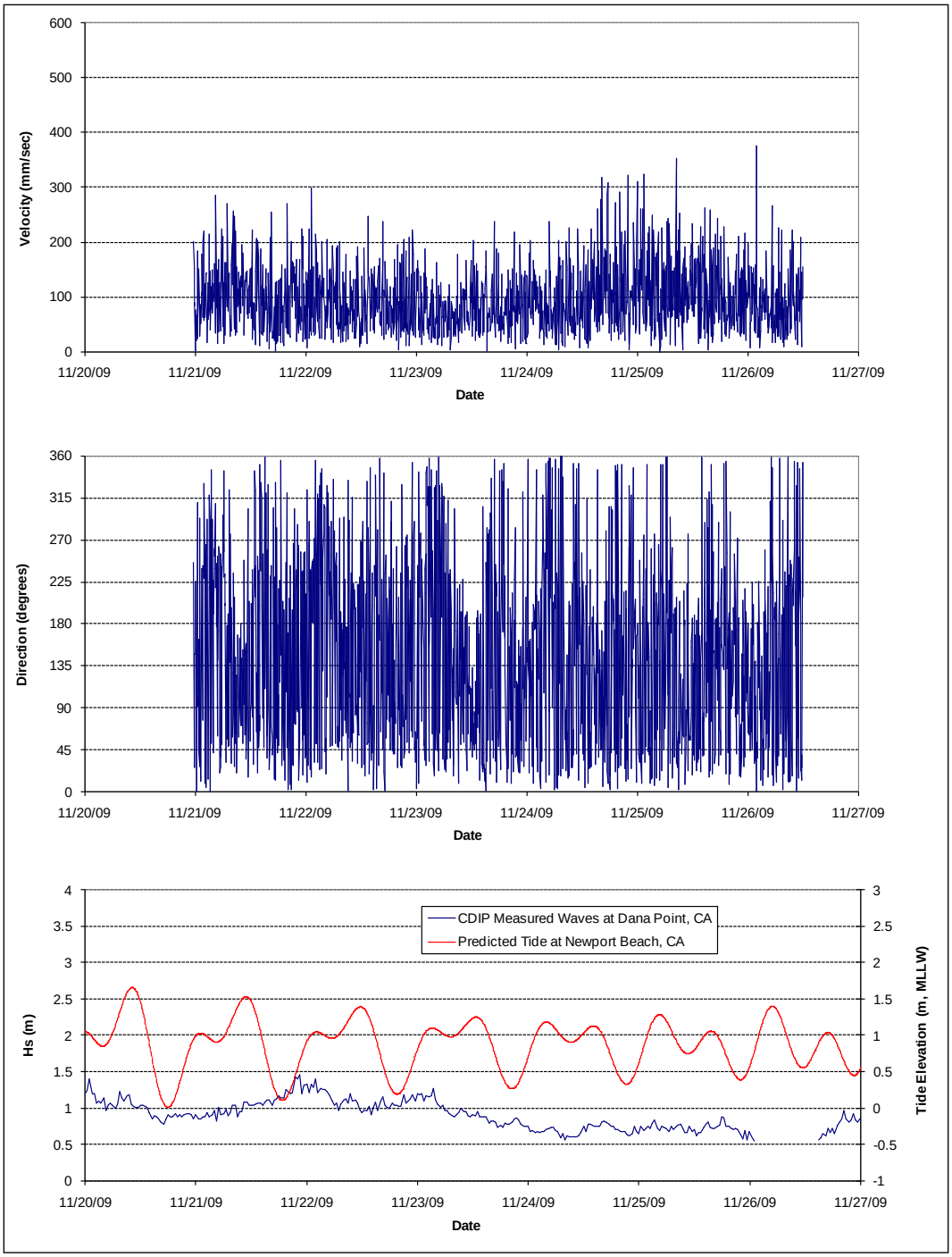

Figure 26. Week 1 – Bin 4 current measurements at Outside Gauge.

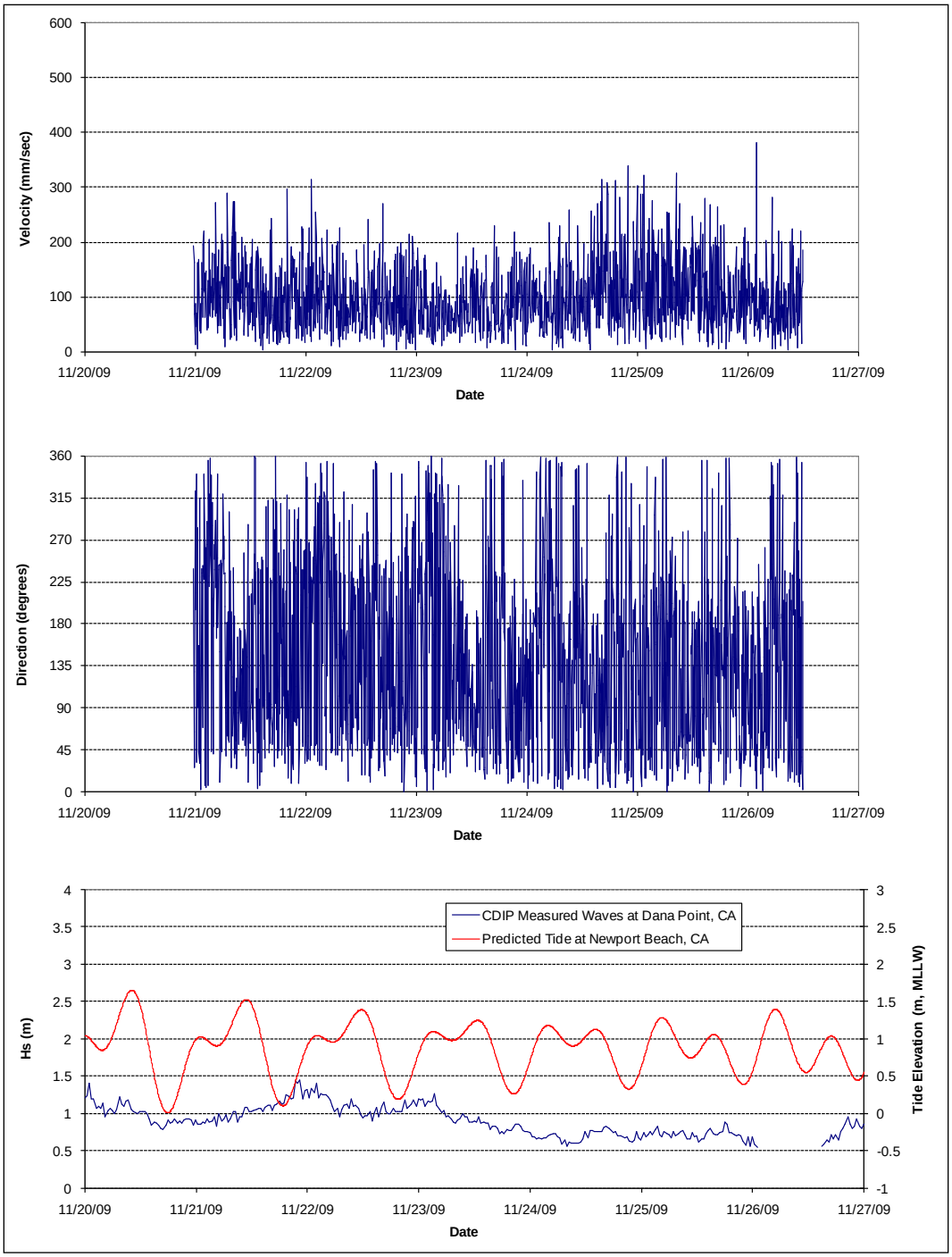

Figure 27. Week 1 – Bin 5 current measurements at Outside Gauge.

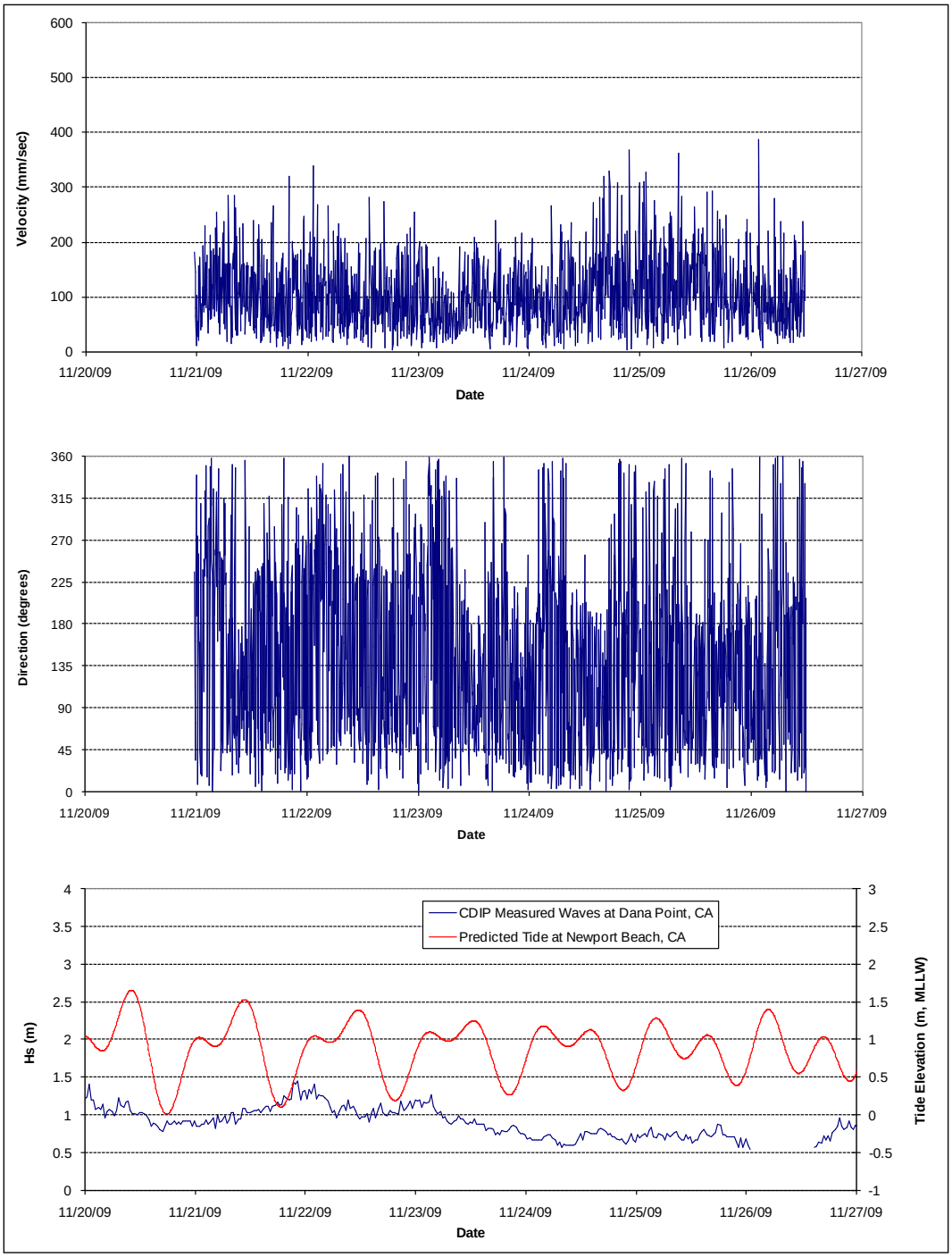

Figure 28. Week 1 – Bin 6 current measurements at Outside Gauge.

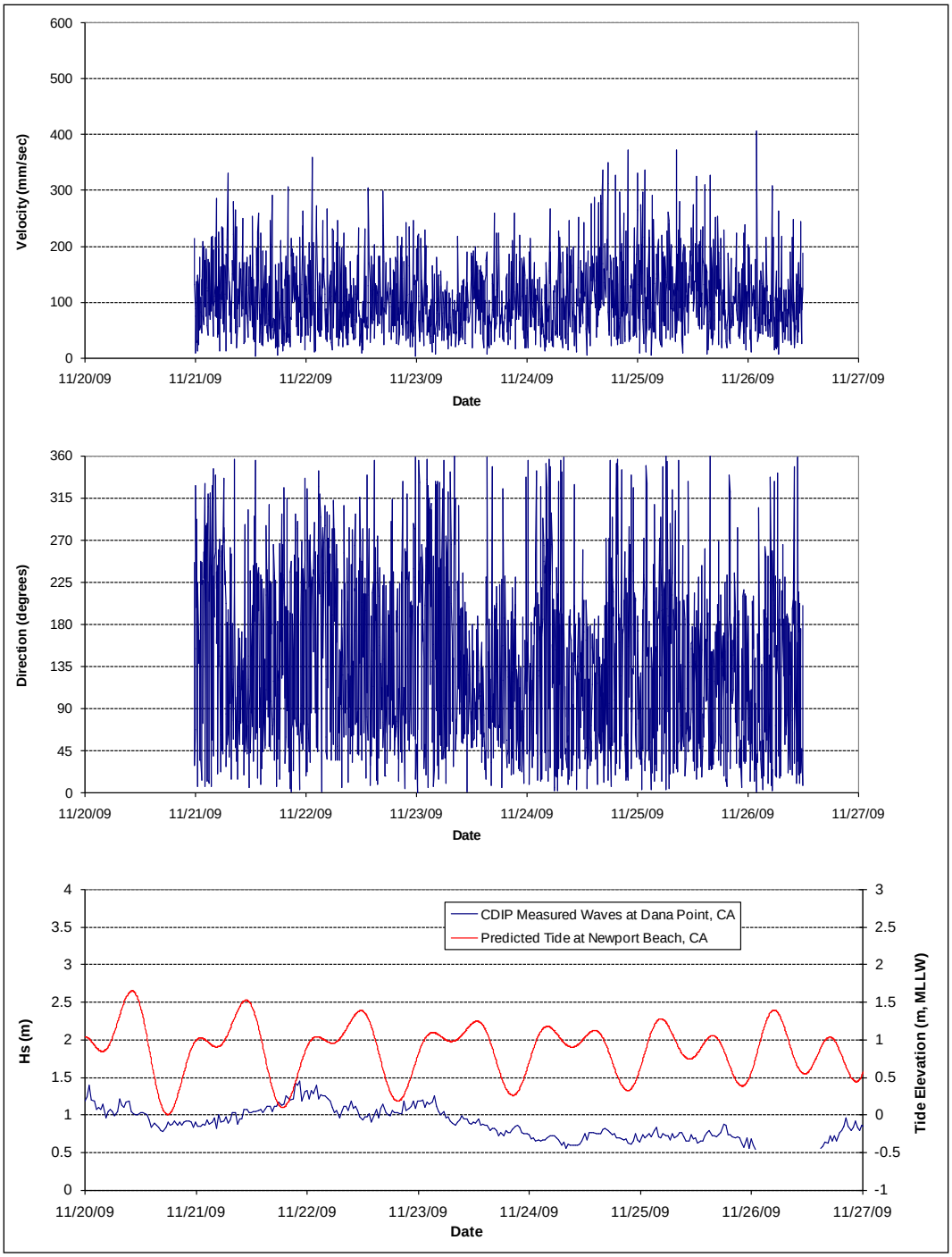

Figure 29. Week 1 – Bin 7 current measurements at Outside Gauge.

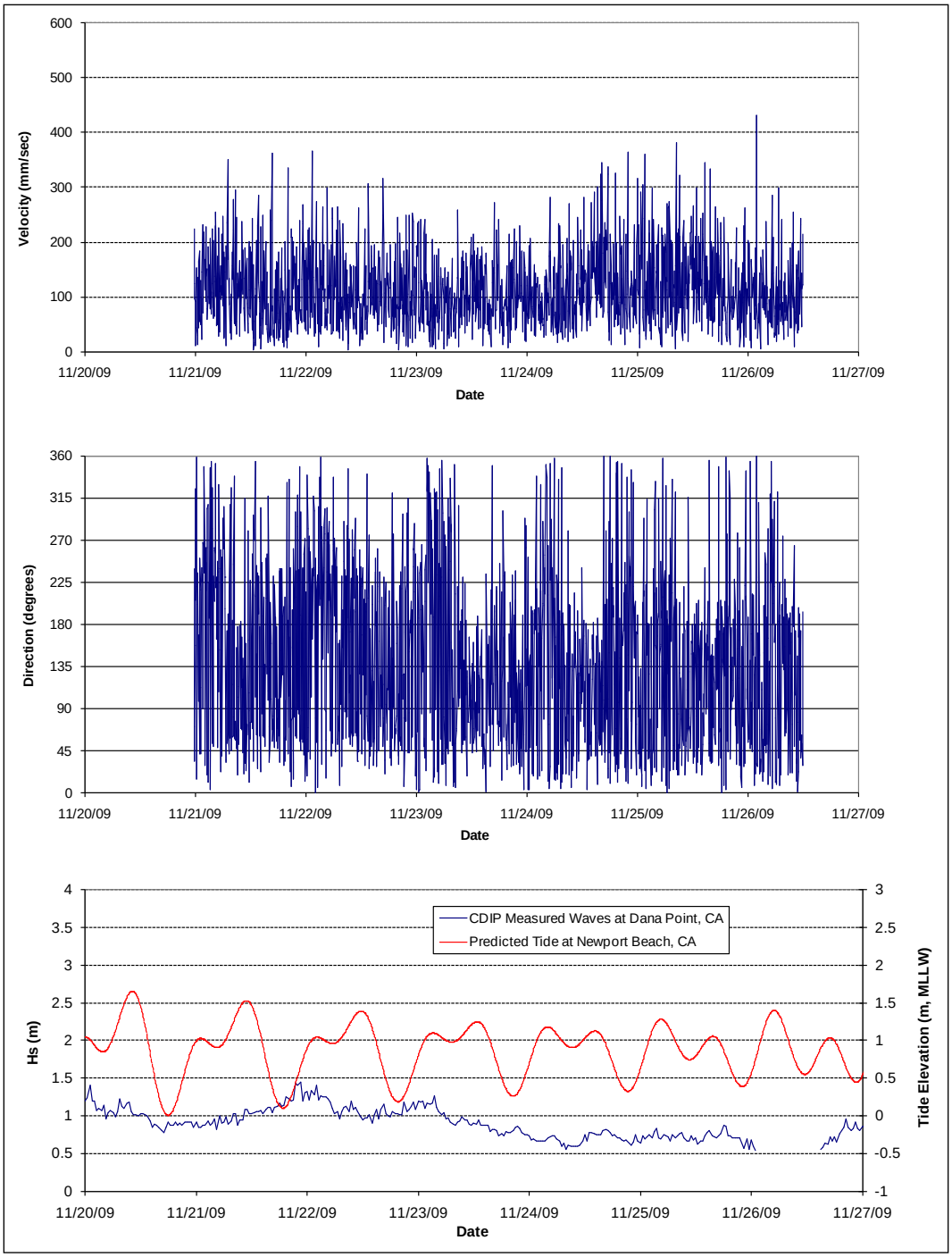

Figure 30. Current roses for Inside ADCP during ebb tide on 22 November 2009.

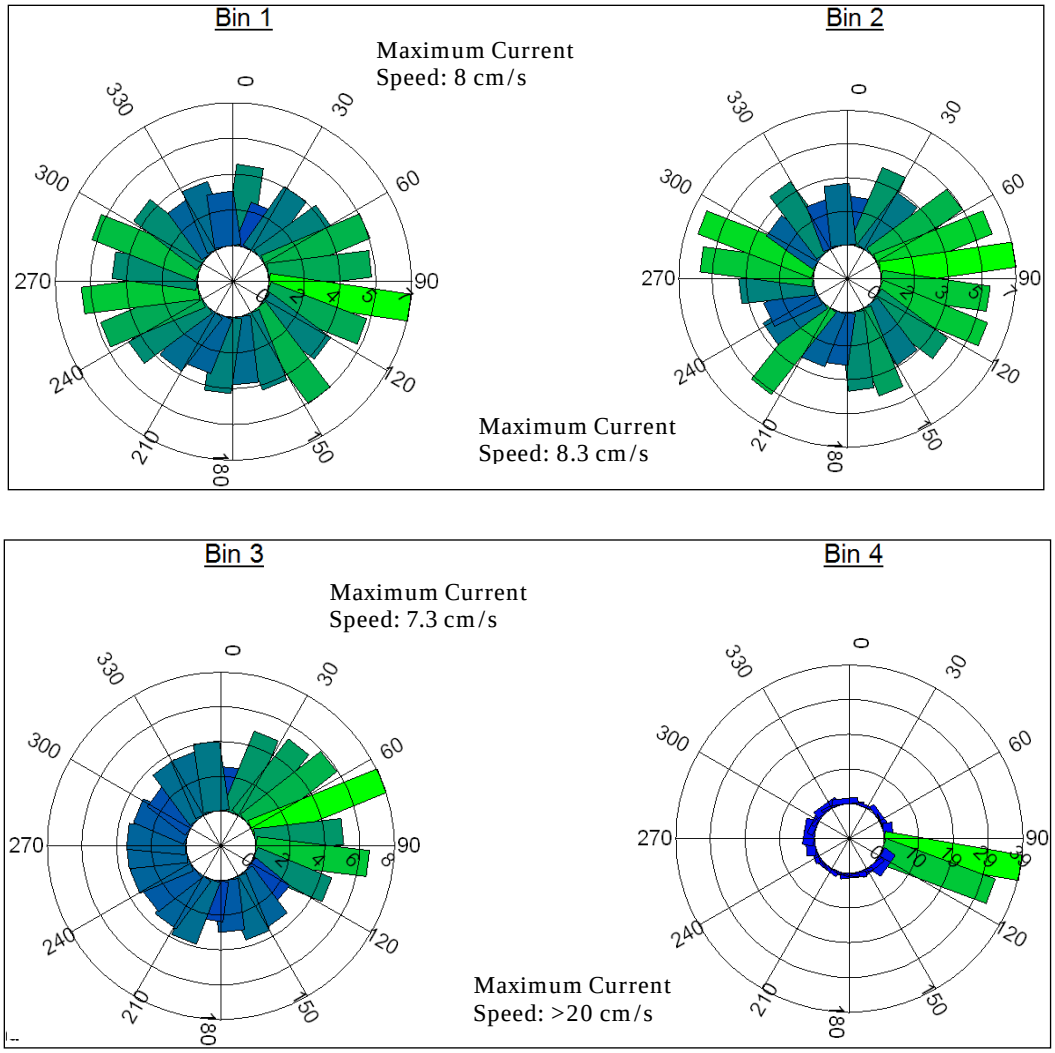

Notes: Duration from 12:00 pm to 7:30 pm, November 22, 2009

Tidal range =1.2 meters (3.9 feet)

90 deg indicates current flowing toward east

Figure 31. Current roses for Inside ADCP during flood tide on 22 November 2009.

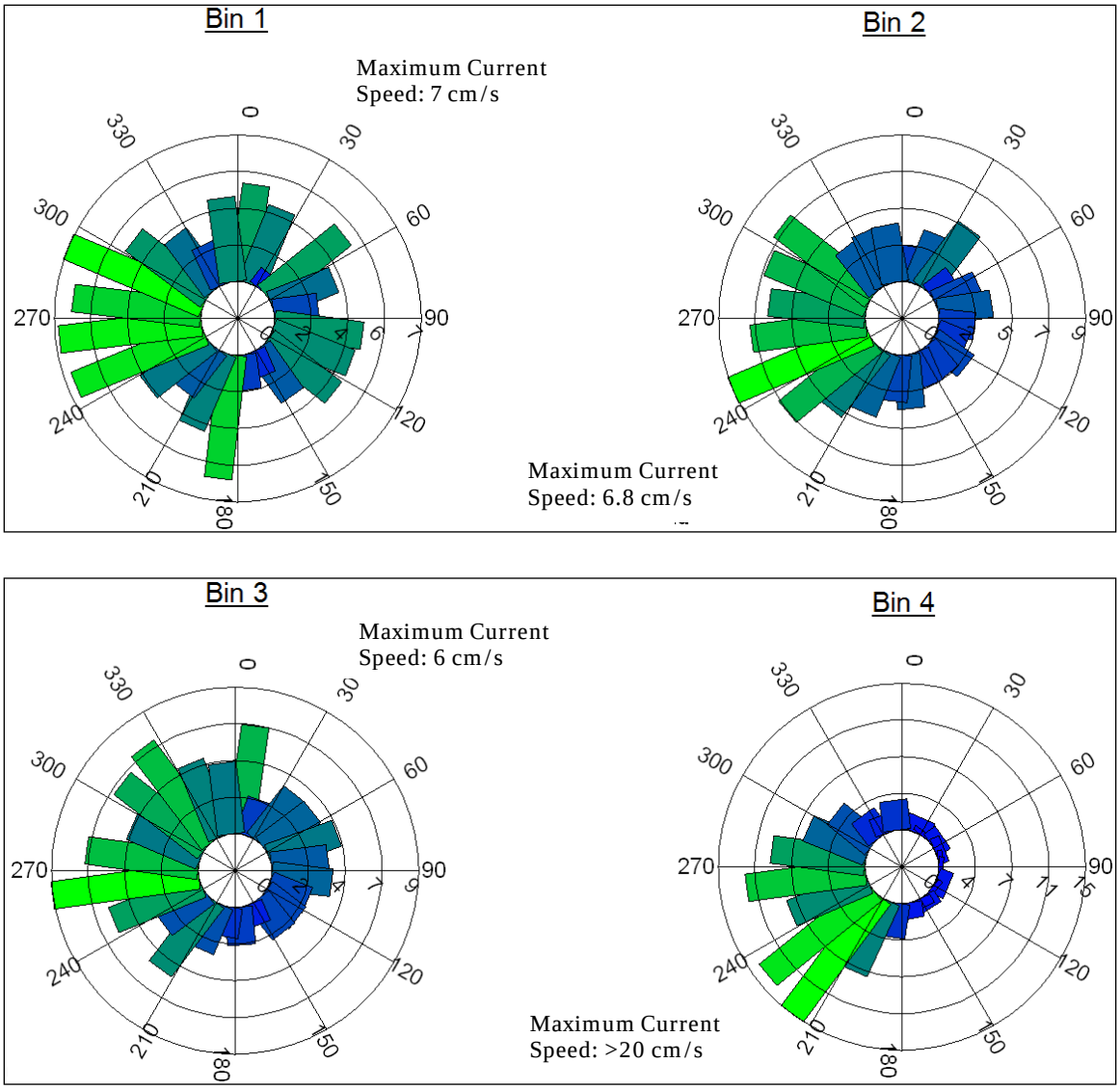

Notes: Duration from 7:35 pm, Nov. 22 to 2:55 am, Nov. 23, 2009

Tidal range =0.9 meters (3.0 feet)

90 deg indicates current flowing toward east

Figure 32. Current roses for Outside ADCP during ebb tide on 22 November 2009.

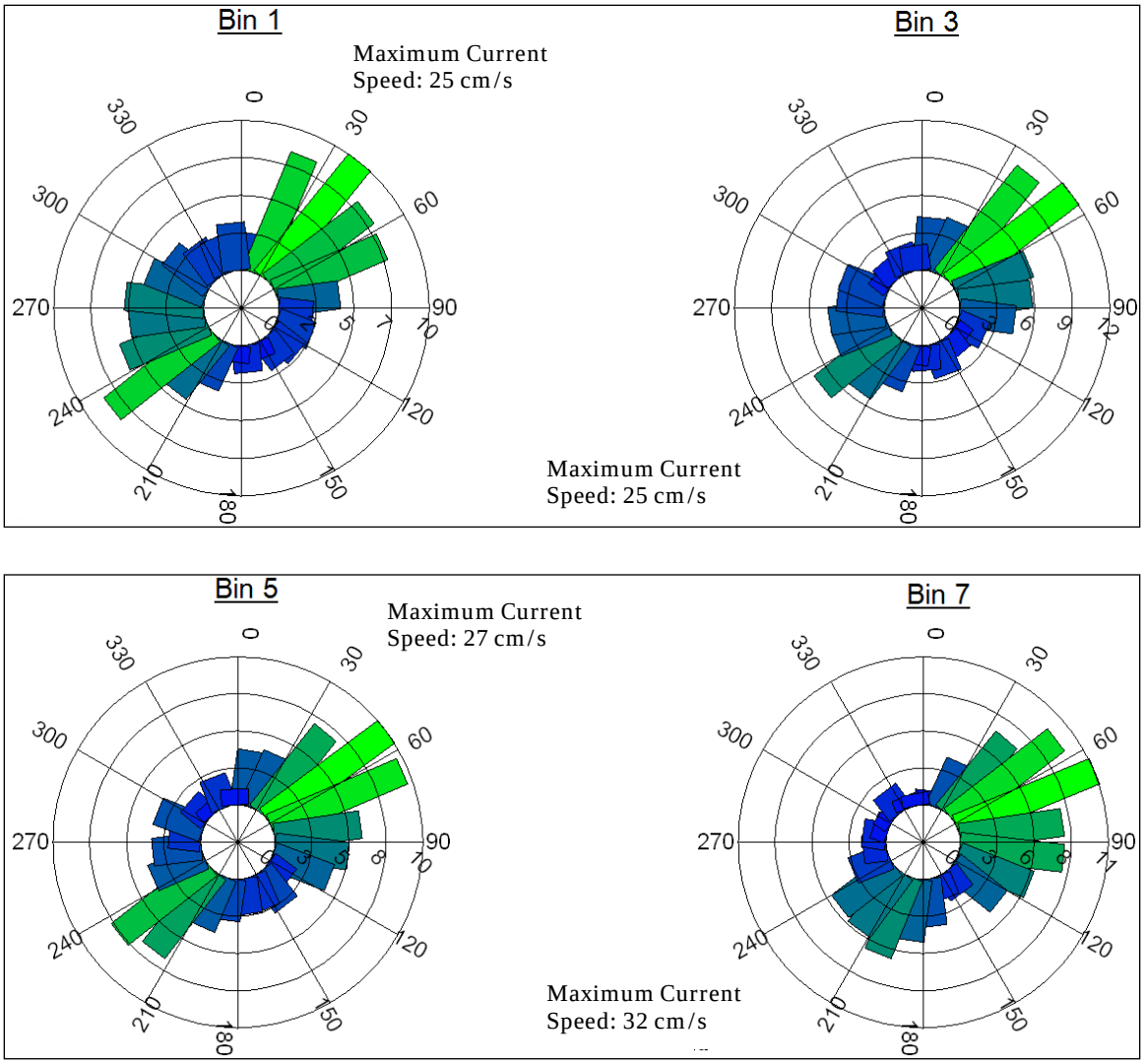

Notes: Duration from 12:00 pm to 7:30 pm, November 22, 2009

Tidal range =1.2 meters (3.9 feet)

90 deg indicates current flowing toward east

Figure 33. Current roses for Outside ADCP during flood tide on 22 November 2009.

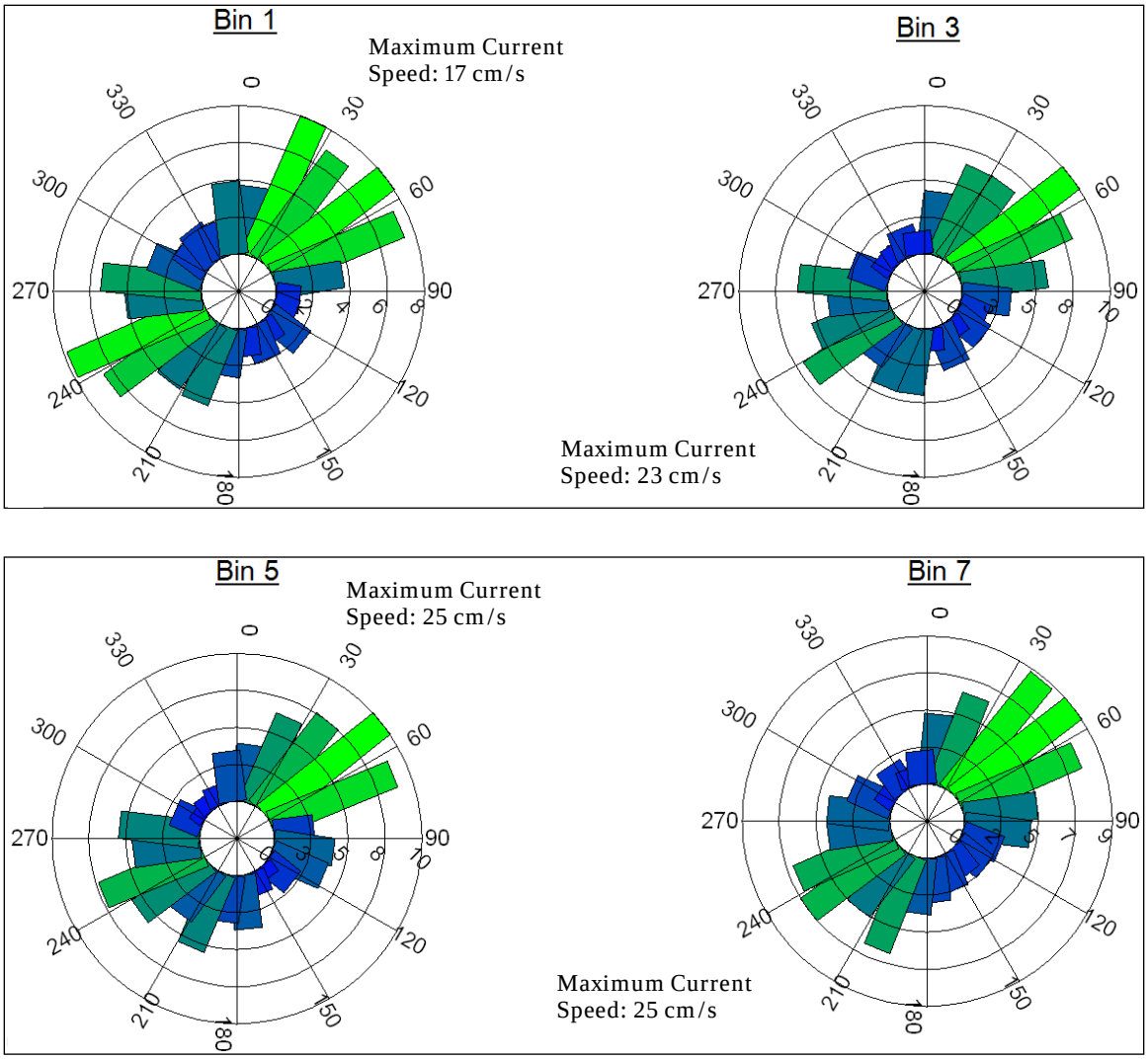

Notes: Duration from 7:35 pm, Nov. 22 to 2:55 am, Nov. 23, 2009

Tidal range =0.9 meters (3.0 feet)

90 deg indicates current flowing toward east

Measured instantaneous current velocities are typically smaller than 6 centimeters per second (cm/sec) (0.20 feet per second (ft/sec)) in the main channel and on the order of 10 to 20 cm/sec (0.33 to 0.66 ft/sec) in the seaside area of West Breakwater. It is evident that current flow through the rubble mound structure occurs throughout West Breakwater, consistent with the original design of a semipermeable rubble-mound structure. A wide range of current direction, likely resulting from current flow across West Breakwater, was observed in the lower water column in the navigational channel during both flood and ebb tides (current rose diagrams of Bins 1 to 3 in Figures 30 and 31). Influence of the through-breakwater currents appears to lessen near the water surface, as the measured currents with a narrower range of direction correspond well to the tide-driven flows, particularly during ebb tide (current rose diagram of Bin 4). The ranges of recorded direction are in the 90º to 120º sector for ebb tides and in the 210º to 270º sector during flood tides, respectively. The current measurements in different ebb and flood cycles exhibit a similar trend, as illustrated in Figures 34 and 35. For the flow field seaward of West Breakwater, the current patterns are relatively consistent throughout the vertical water column and differ only slightly for both ebb and flood tides (Figures 32 and 33).

Figure 34. Current roses for Inside ADCP during ebb tide on 5 January 2010.

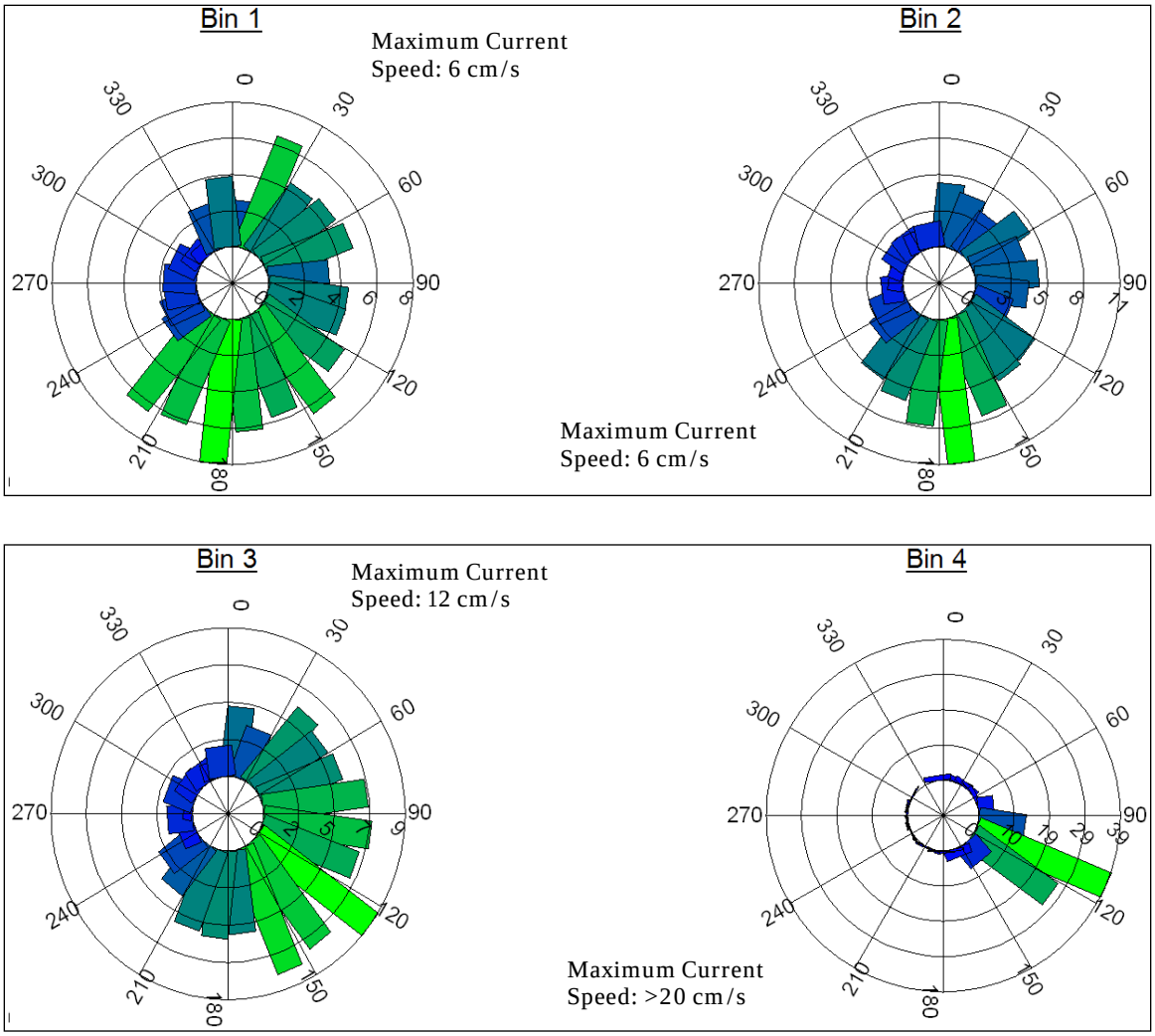

Notes: Duration from 12:30 pm to 6:45 pm, January 5, 2010

Tidal range =1.3 meters (4.3 feet)

90 deg indicates current flowing toward east

Figure 35. Current roses for Inside ADCP during flood tide on 5 January 2010.

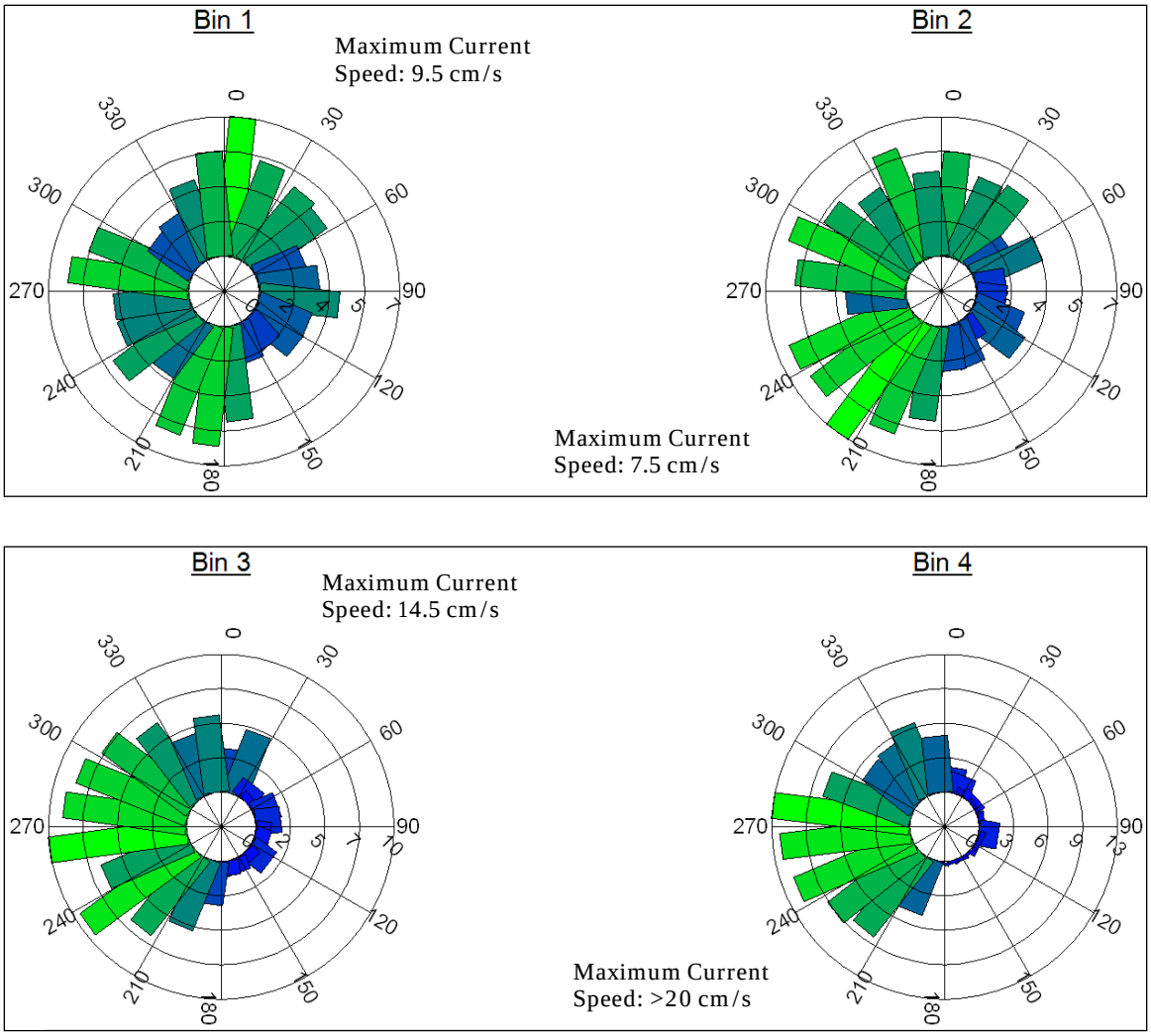

Notes: Duration from 7:00 pm Jan. 5 to 1:30 am, Jan. 6, 2010

Tidal range =1.4 meters (4.6 feet)

90 deg indicates current flowing toward east

3 CMS-Wave Model Simulations

The Coastal Modeling System (CMS) is a suite of major multidimensional numerical models integrated to simulate waves, currents, water levels, sediment transport and morphology change in coastal inlets, estuaries, and harbors. The CMS, developed by the U.S. Army Corps of Engineers Coastal and Hydraulics Laboratory, consists primarily of three modeling modules: CMS-Wave, CMS-Flow and Particle Tracking Model (PTM). Both CMS-Flow and CMS-Wave can be coupled and operated by a steering module within the Surface-water Modeling System (Zundel 2007) to dynamically simulate sediment transport and morphology change (Buttolph et al. 2006; Lin et al. 2008). PTM (Demirbilek et al. 2008) can be applied to compute the fate and pathways of sediment and other waterborne particles from the simulated wave environment, flow field, and water exchange via CMS-Wave and CMS-Flow.

3.1 CMS-Wave model description

CMS-Wave is a two-dimensional (2D) wave spectral transformation model implemented in the CMS. The model employs a forward-marching, finite-difference method to solve the wave action conservation equation. It is a phase-averaged model, which averages changes in the wave phase to calculate wave properties, and is based on the wave-action balance equation.

CMS-Wave has theoretically derived approximations for wave refraction, shoaling, diffraction, reflection, and wave-current interaction, and therefore is appropriate for conducting wave simulations at coastal inlets with jetties and in harbor entrances with breakwaters. It employs a forward-marching, finite-difference, steady-state (time-independent) Eulerian method to solve the wave action conservation equation. Wave diffraction is implemented by adding a diffraction term derived from the parabolic wave equation to the energy-balance equation (Mase et al. 2005). CMS-Wave can operate either on a coastal half-plane or full-plane with primary waves propagating from the seaward boundary toward the shore. Shoreward and seaward reflections are treated using a mirror reflection principle.

3.2 CMS-Wave model improvement

To improve the applicability for permeable rubble-mound breakwaters (e.g., West and East Breakwater at Dana Point Harbor) and allow for waves transmitting through the breakwaters, an additional component was included in the CMS-Wave to calculate the wave transmission coefficient K_t using d'Angremond et al. (1996) formula:

$$K_t = 0.64 \left[1 - \exp(-\frac{\xi}{2})\right](\frac{B}{H_i})^{-0.31} - 0.4\frac{h_c}{H_i} \quad , \text{ for } \quad B < 10\ H_i \qquad (1)$$

where:

B = the crest width
ξ = the Iribarren parameter that is defined as the fore-slope of the breakwater divided by the square-root of deepwater incident wave steepness and
h_c = the height between the still water surface and the crest of the breakwater.

3.3 CMS-Wave model calibration

To ensure the applicability of the specific physical process at the breakwaters, CMS-Wave was calibrated by comparing to the filtered directional wave data collected by the ADCP deployed outside (oceanside) West Breakwater. Figure 36 shows the CMS-Wave rectangular grid system that covers the entire harbor, the shoreline adjacent to the harbor, and the offshore region. The model domain extends approximately 5 km (3.1 miles) alongshore (expanding beyond the harbor boundary) and 4 km (2.5 miles) offshore. The offshore boundary of the model domain reaches as deep as 300 m (1,000 ft). The finite-difference grid consists of 130,473 (399 × 327) variable cells with the cell size ranging 5 m (15 ft) at the harbor and 200 m (600 ft) near the two seaward boundary corners. Both West and East Breakwater were specified as permeable structures that allow for waves transmission into the harbor.

The CMS-Wave calibration was performed using the collected wave data from 21 to 27 November 2009. The model input included measurements of wind, wave, and water level at selected coastal or ocean stations. The incident wave spectra were transformed from the CDIP Dana Point Buoy

Figure 36. CMS-Wave model domain and grid system.

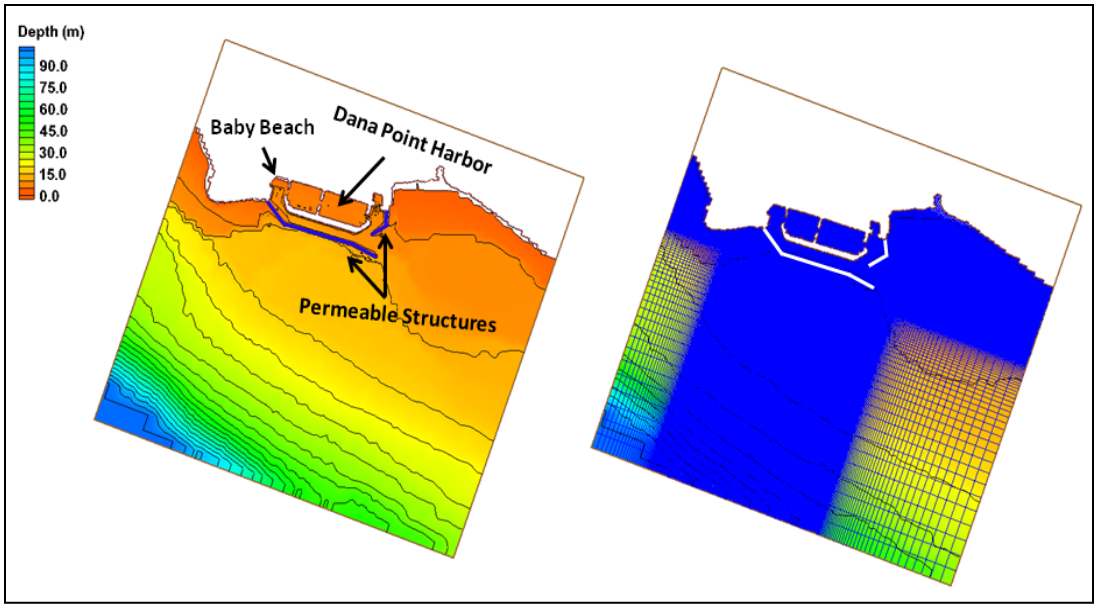

096 to the CMS-Wave grid offshore boundary using the linear wave theory with a simple assumption of shore-parallel depth contours. The measured water levels were extracted from National Oceanic Atmospheric Administration (NOAA) Coastal Station 9410660 at San Pedro, Los Angeles, Outer Harbor. The wind input information was acquired from the San Clemente Basin Buoy (Station 46086) of the National Data Buoy Center (NDBC). Figure 37 shows the time series of wave height and water level that were collected at CDIP 096 and NOAA Station 9410660 for the calibration period (i.e., 21 to 27 November 2009). The 6-day period represents a benign wave condition with a wave approach direction typically observed in November. Figure 38 illustrates the corresponding time series of wind speed and direction collected at NDBC Buoy 46086.

CMS-Wave was calibrated at a 3-hour (hr) interval with incident wave spectra and water levels specified at the sea boundary. Wind data from Buoy 46086 were used as atmospheric input applied to the entire model domain. The bottom friction is neglected in the calibration with fully reflected waves set at the breakwaters to account for the effect of rocky outcrop bottom along the perimeter of the harbor.

Figure 39 shows the comparison of wave parameters between the CMS-Wave-modeled results and field measurements at the outside ADCP. Table 4 presents the calibrated parameters that are pertinent to CMS-Wave. The calculated wave results show a good consistency with the

measured wave parameters. An underestimate of wave height during the beginning days could be related to the wind forcing as the wind input information was obtained from a NDBC offshore buoy. Strong wave refraction and reflection are evident from a comparison of the offshore (at the CDIP gauge) and near-breakwater wave directions.

Figure 37. CDIP 096 wave data and NOAA 9410660 water levels.

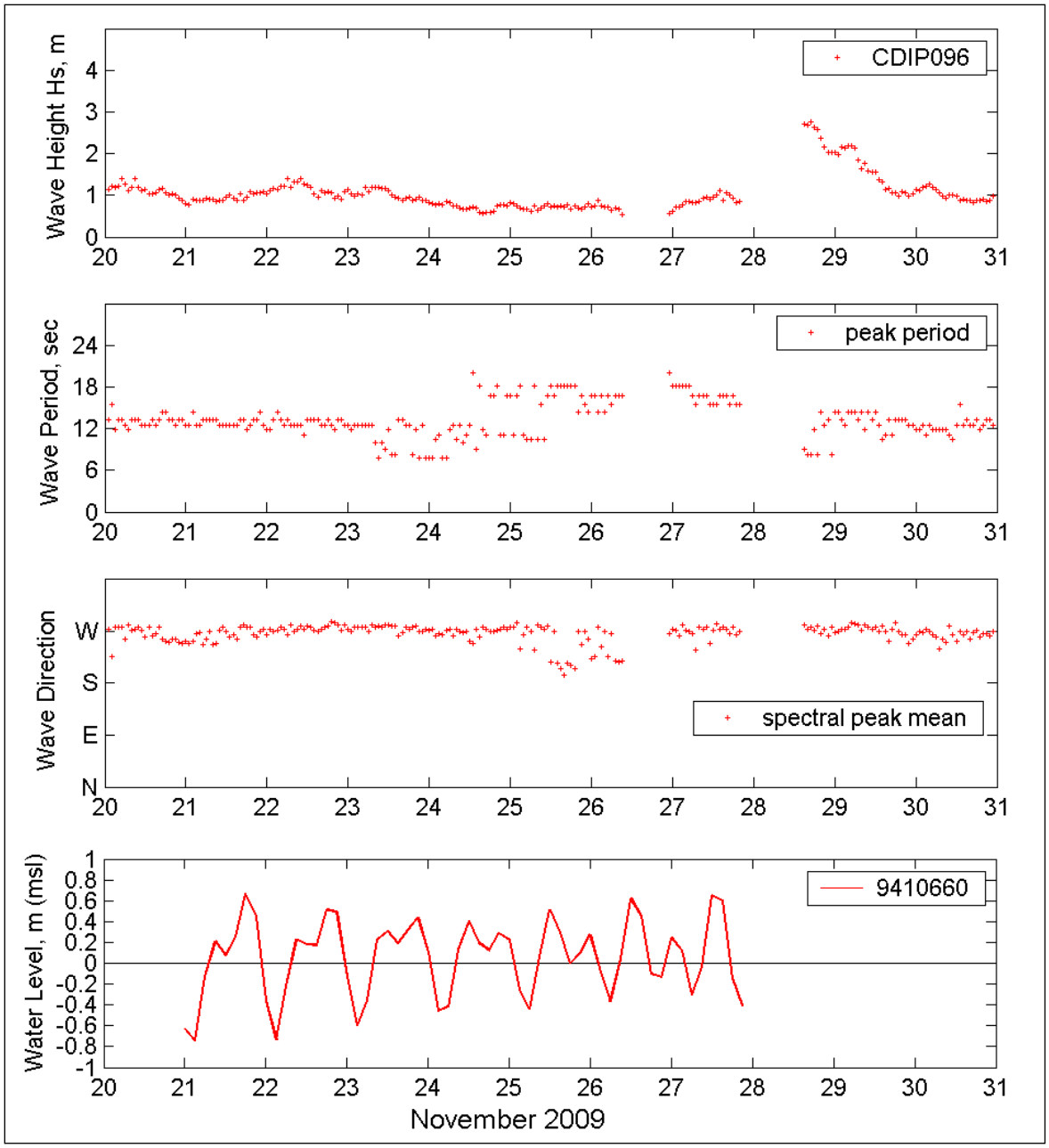

Figure 38. NDBC 46086 wind speed and direction data.

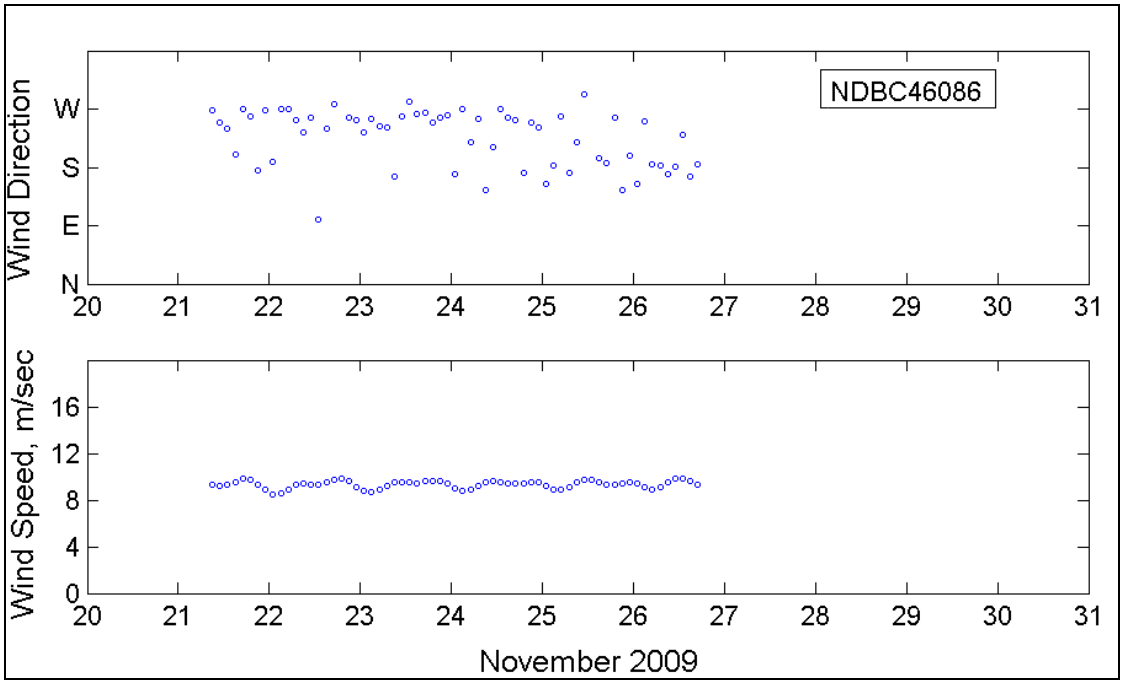

Figure 39. Comparison of calculated and measured wave parameters.

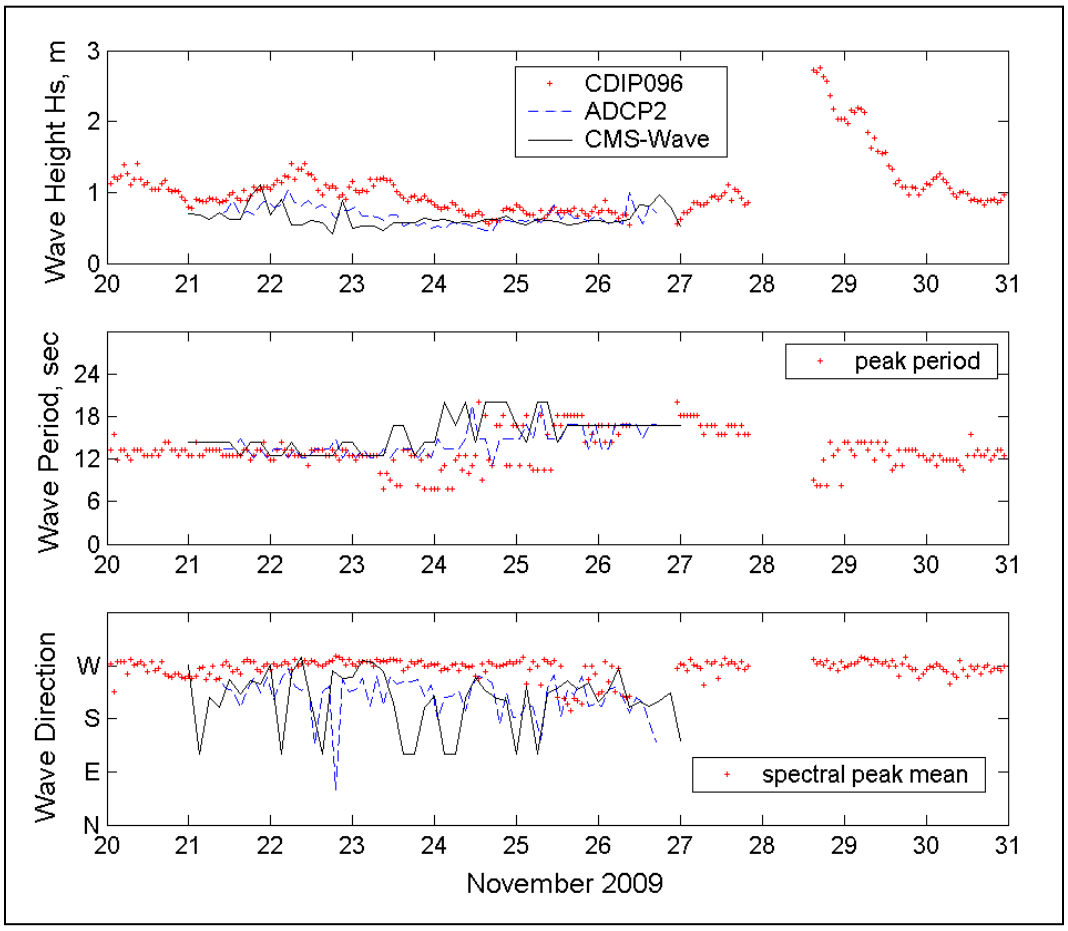

Table 4. Calibrated model parameters for CMS-Wave.

Model Parameter	Calibration
Wave Diffraction Intensity	4.0
Backward Reflection Coefficient	1.0
Bottom Friction Coefficient	0.0

Figure 40 shows the comparison of CMS-Wave simulations with and without wind input as well as without tides (i.e., without the input of water level variation as a result of daily tides). Table 5 presents the percent difference in model prediction compared to the oceanside ADCP measurements. The comparison indicates that the calculated wave height and direction with wind input and tides agree better with data than without the wind and water level (tide) forcing. The wave period calculation is not affected by the conditions with or without the wind and water level input. Exclusion of the wind and water level (tide) forcing in the simulations, CMS-Wave underpredicts the wave height by approximately 4% to 6% at the oceanside ADCP location.

Figure 41 shows the comparison of model results with and without wave reflection at breakwaters and bottom friction in the simulation. The CMS-Wave simulation with wave reflection at breakwaters agrees better with data than without the wave reflection calculation. Without invoking wave reflection of the breakwater, the model underprediction can be as high as 31% (Table 5). It is evident that wave reflection plays an important role in accurately predicting the incident wave height near the breakwaters. The effect of bottom friction, using a Mannings coefficient of 0.025, appears to be insignificant.

3.4 Design storm wave criteria at Dana Point Harbor

The aforecalibrated CMS-Wave was applied to establish the storm design criteria for the dual protective breakwaters at Dana Point Harbor. The storm wave criteria were derived based on the historical storm events. Peak wave heights at the dual breakwaters during individual storms were estimated by wave hindcast in deep water, wave transformation that accounts for offshore island sheltering, and the CMS-Wave simulations that include wave refraction, diffraction, shoaling and reflection.

Figure 40. Comparison of calculated waves with and without wind or water level input.

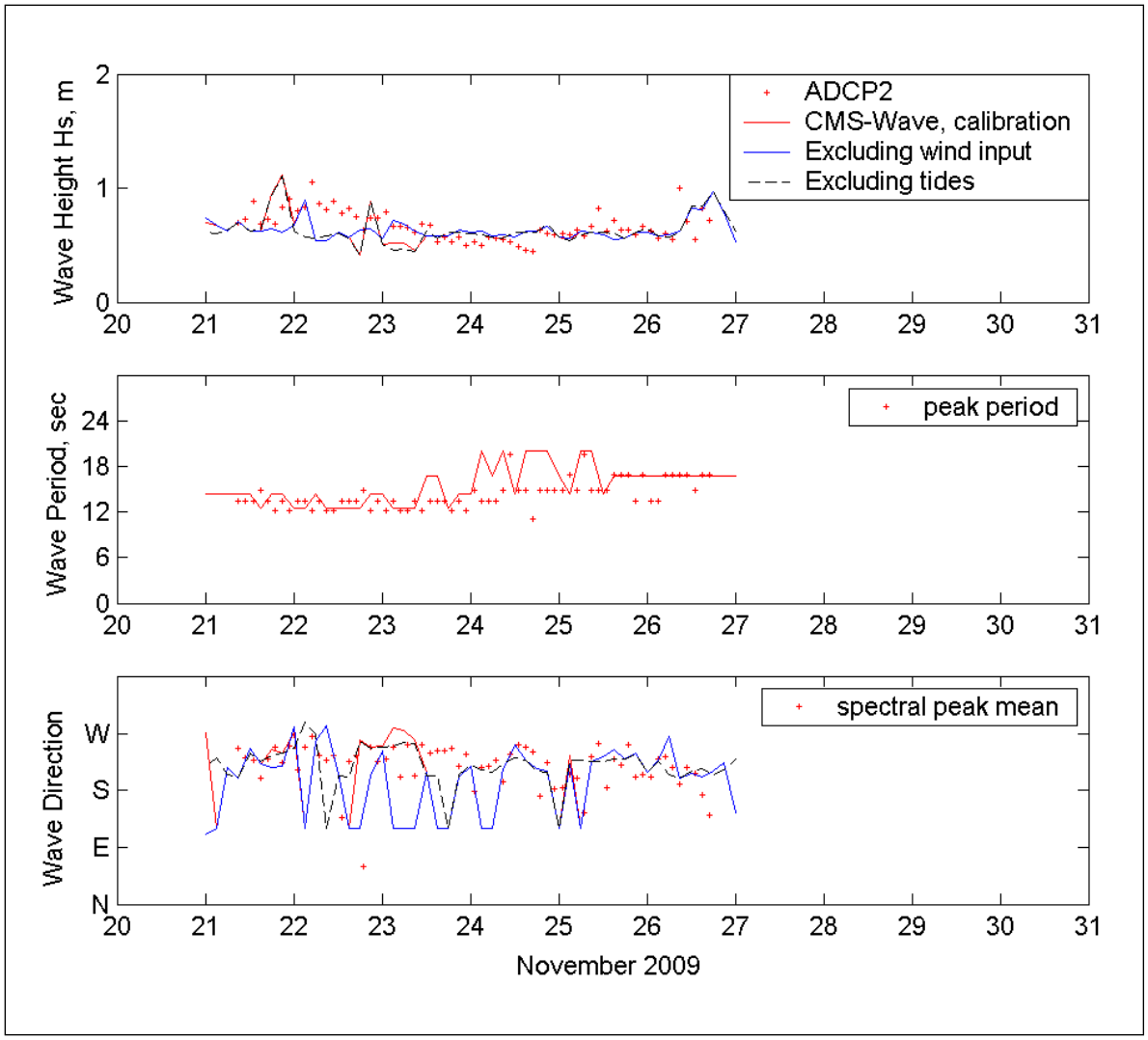

Table 5. Comparison of calculated significant wave height at Outside ADCP.

Data and Model Conditions	Average Hs (m)	Average Bias Hs (m)	Percent Difference (%)
ADCP Measurement	0.67	-	-
CMS-Wave Calibration	0.64	-0.03	4.5
Excluding Wind	0.64	-0.035	5.2
Excluding Tides	0.63	-0.04	6.0
With Bottom Friction	0.64	-0.03	4.5
Without Wave Reflection	0.46	-0.21	31.3

Figure 41. Comparison of calculated waves with and without wave reflection or bottom friction.

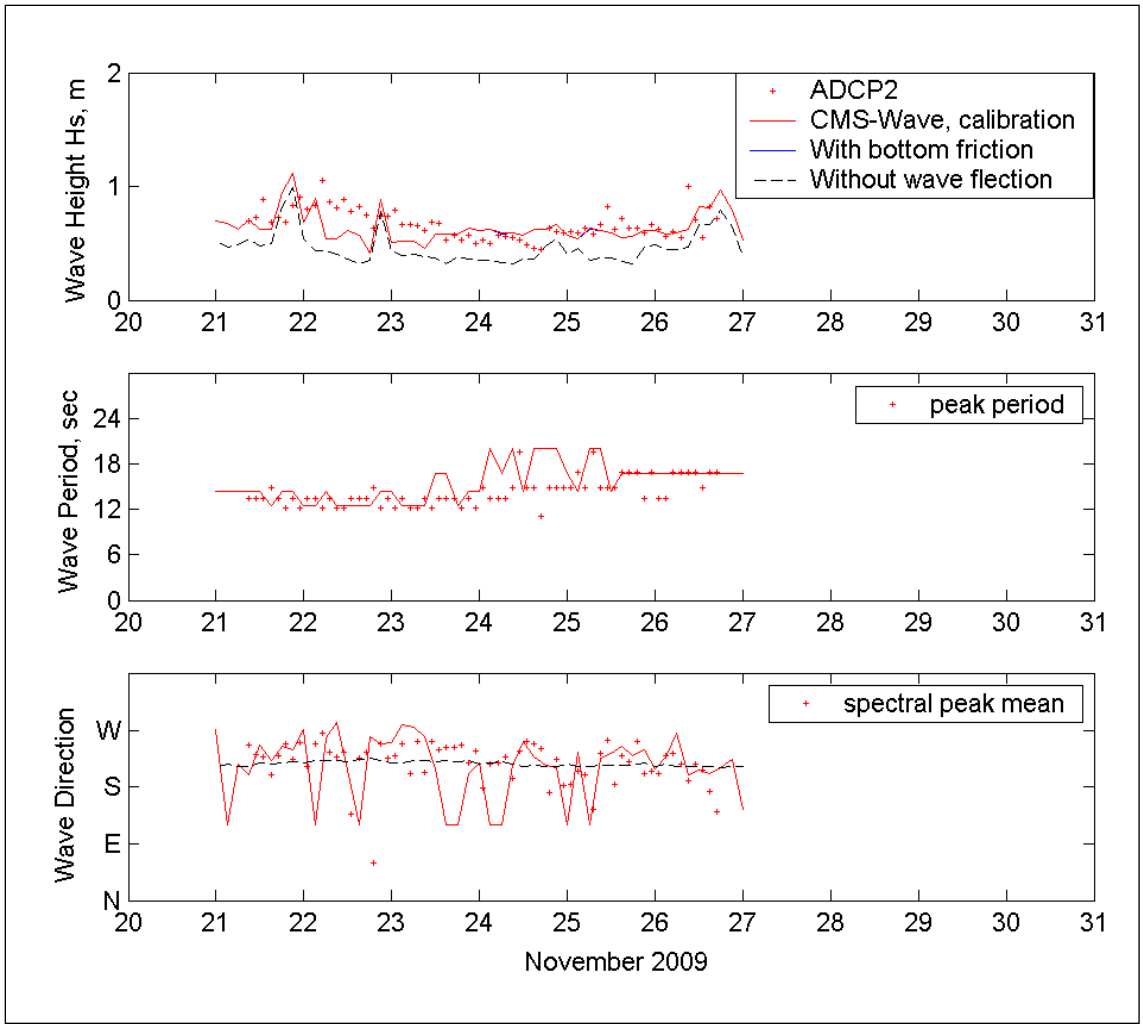

3.4.1 General wave climatic conditions

Wind generated waves and distant swells approaching Dana Point Harbor are produced by one of the following six meteorological patterns (USACE LAD 1996): 1) extratropical cyclone in the northern hemisphere; 2) north-west winds in the outer coastal waters; 3) west to northwest local sea; 4) prefrontal local sea; 5) tropical storm swell; and 6) extratropical cyclone in the southern hemisphere.

Extratropical cyclone in the northern hemisphere

Low-pressure centers which develop along the polar front are the source of the predominant wave action along the entire California coast during the winter season. Storm swells are typically generated at some distance from the Dana Point coastline in the North Pacific. Most commonly these storms

will traverse the mid-Pacific before turning northeastward toward the Gulf of Alaska with swells decaying on the average of 1,000 km (660 miles) to the coast of Southern California. However, under some meteorological conditions such as during the El Nino seasons, storms can develop in the low-latitude region west of the California coast and move in much closer to the coast. In a rare occasion, these storms may move directly across Southern California following a northeast, east, or southeast trajectory. The severe winter storm occurring in January 1988 is an example of the moving close-by storm which resulted in extremely high waves recorded along the Southern California coast.

Northwest winds in the outer coastal waters

The predominant wave action along the coast area within the south Orange County shoreline is due to the prevailing northwest winds. This is particularly true during the spring and summer months. Wave heights are usually low, less than 1 m, but on occasion, with superposition of a strong surface high and an upper level trough, the northwesterlies increase, becoming very strong from about Point Sal to San Nicolas Island. The inner waters of Southern California very often remain unaffected under the influence of the Catalina eddy circulation. Waves traveling at a variance to the mean wind direction reach the nearshore water with periods ranging from 6 to 10 sec. Moderate winds from the northwest will produce breaker heights of 1 to 2 m (3.3 to 6.6 ft), while strong events can generate heights of 2 to 3 m (6.6 to 10 ft).

West to northwest local sea

Local westerly winds can be divided into two types: 1) temperature-induced sea breezes and 2) gradient winds. The former exhibits a pronounced seasonal and diurnal variation. The strongest sea breezes occur during the late spring and summer months while the lightest winds are during December and January. The summer sea breezes averaging approximately 7.7 m/sec (15 knots) usually set in during the late morning and peak in the midafternoon. In winter months, sea breeze conditions are limited to a few hours during early afternoon with wind speeds on the order of 5.1 m/sec (10 knots). Gradient winds are confined largely to the months of November through May with the peak in March and early April. These typically occur following a frontal passage or with the development of a cold low-pressure area over the southwestern United States.

Prefrontal local sea

The coastal zone within the south Orange County area is vulnerable under extratropical winter storm conditions (a counterclockwise wind motion) prior to frontal passage winds blowing strongly from the southeast along the coast but turning toward the south-southeast to south a short distance offshore. Wind waves, with the peak period averaging between 6 and 8 sec, reach the shore with minimal loss. Significant wave heights are generally in the range of 1 to 2.5 m (3.3 to 8.3 ft). Extreme wave heights are rare because the fetch to the shoreline is generally limited, and the duration of the event is typically short. An example of this rare case is the storm of 4 January 1995, which generated southerly seas of 3 m (10 ft).

Tropical storm swell

Tropical cyclones form regularly along the intertropical convergence zone west of Mexico from early July to early October. On the average, 15 to 20 of them are to be expected each year. Most of the tropical cyclones travel on a westerly track. Swells generated by these storms have little or no effect on Southern California. A few of them can take a northwest track and lengthen the effective fetch over which swells will travel toward south Orange County.

Extratropical cyclone in the southern hemisphere

From the months of April through October, and to a lesser extent the remainder of the year, large South Pacific storm systems traversing the ocean between 40^0 and 60^0 south from Australia to South America send swells northward to the west coast of Central and North America. The great circle approaching directions to Southern California range from approximately 215^0 for storms near New Zealand to 170^0 for South American storm systems, respectively. The decay distance ranges from approximately 7,200 to 11,200 km (4,750 to 7,400 miles). Wave heights in deep water are usually low, on the order of less than 1 m. As these waves are nearly monochromatic, their capacity for shoaling is greatly enhanced. Breakers of 2 to 3 m (6.6 to 10 ft) in the south Orange County coastal region are not uncommon.

3.4.2 Deep-water wave climate

Because long-term measurements of waves and currents are not available in the study area, it is necessary to use the wave hindcast information. The Global Reanalysis of Ocean Waves (GROW, http://www.oceanweather.com/metocean/grow/) data for 1970–2008 was selected to investigate the long-term wave climate along the Dana Point coast. The GROW hindcast is based on historical data consisting of background wind fields, tropical storm archives, and ocean buoy data for the validation purposes. It has a global grid spacing of 0.625° in latitude by 1.25° in longitude and uses the Pierson-Moskowitz fully developed sea condition. The hindcasted sea and swell were derived from a 2D spectral wind-wave generation model. Figure 42 shows the GROW deepwater hindcast Station 38190 located west of San Nicholas Island at 33.125°N and 120.0°W in a water depth of 1,000 m (3,300 ft). The 39 yr GROW data (1970-2008) were used to establish a database of offshore deepwater wave climate.

Figure 42. Wave data station locations.

3.4.3 Wave transformation

To determine wave characteristics at the offshore boundary for the CMS simulations, the GROW data were transformed via the O'Reilly spectral back-refraction model (O'Reilly and Guza 1991) to account for the island sheltering effect, wave refraction, and wave shoaling. The O'Reilly spectral back-refraction model performs a linear refraction transformation in which the transferred spectrum is established from the incident wave spectrum by

back-refracting rays from the target site. Unlike more traditional forward ray refraction methods, the O'Reilly model back-refracts wave rays from the site of interest, therefore eliminating caustics which plague forward ray tracing schemes. This transformation model has been extensively validated in the field throughout the Southern California coast.

The two locations (CMS_1 and CMS_2) (Figure 43) that were selected for the Dana Point study area are situated in water depths of 35 m (115 ft) and 300 meters (984 ft), respectively. The 39 yr GROW hindcast wave data in the deep water were converted to 2D wave spectra and transformed to these two locations. It is noted that the wave parameters of the GROW data include separate estimates of sea and swell energy, peak periods, and mean directions.

Figure 43. Transformed wave data station locations.

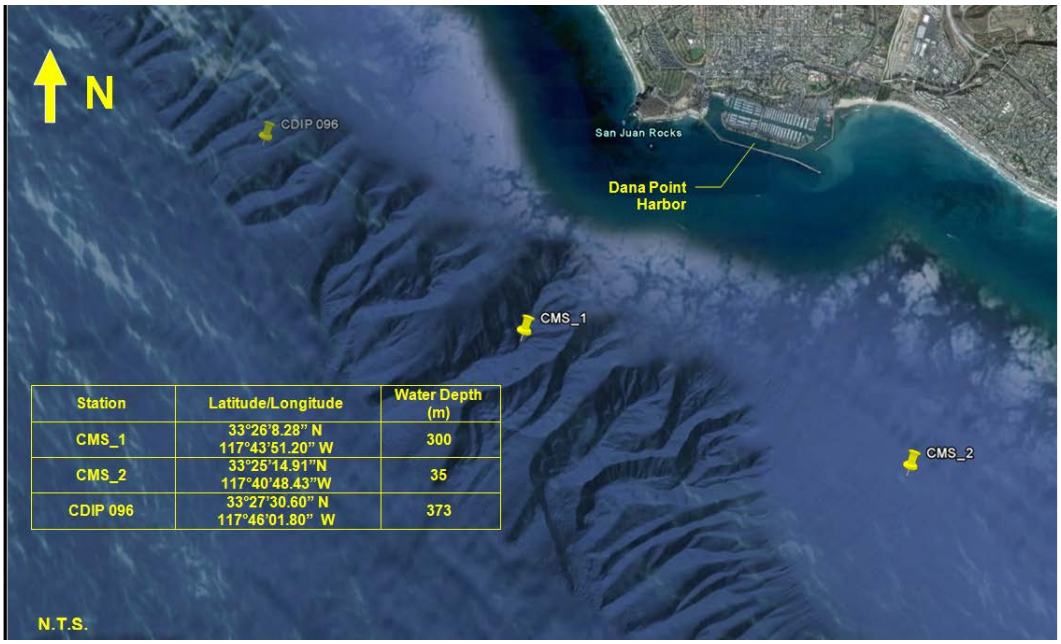

Station	Latitude/Longitude	Water Depth (m)
CMS_1	33°26'8.28" N 117°43'51.20" W	300
CMS_2	33°25'14.91"N 117°40'48.43"W	35
CDIP 096	33°27'30.60" N 117°46'01.80" W	373

The 39 yr (1970–2008) time series of GROW deep-water sea and swell wave parameters were transformed and propagated through the Southern California Islands to the Dana Point coast by first converting the deep-water wave parameters to a 2D JONSWAP (http://www.igi-global.com/dictionary/jonswap-spectrum/16030)-Mitsuyasu spectrum after Goda (1985). The JONSWAP-Mitsuyasu 2D wave spectra are characterized by a spectral peak enhancement factor, Gamma, and a directional spreading parameter (S_{max}) to describe the distribution of wave energy around the peak period (T_p) and peak wave direction (D_p). Based on the observed frequency and directional

spreading at the San Nicolas Island wave buoy, the following values were respectively assigned to Gamma and S_{max} for different peak periods:

- Gamma = 3 for $T_p \leq 6$ sec
- Gamma = $T_p/2$ for $T_p > 6$ sec
- $S_{max} = 50$ for both sea and swell.

The sea and swell spectra were estimated separately and then combined to form the final deep-water 2D spectrum prior to its transformation to the nearshore water region. The spectral refraction wave transformation yields five spectral wave parameters that are measured by directional wave buoys: the wave energy content in a frequency bin, and the first four directional Fourier coefficients (*a1*, *b1*, *a2*, and *b2*), as a function of the corresponding wave frequency (Kuik et al. 1988). The directional coefficients were used with a directional estimator, based on Maximum Entropy Method to estimate the 2D wave spectra time series at CMS_1 and CMS_2 (Lygre and Krogstad 1986).

3.4.4 Hindcast validation

Extreme winter wave events were of the greatest concern in this study, and these waves reach the Dana Point through relatively narrow directional windows on either side of Santa Catalina Island (Figure 42). As a result, wave conditions near Dana Point are considerably smaller than offshore wave conditions on average. Wave hindcast in this region can be sensitive to small directional bias in the incident wave spectra, which can result in too much or too little wave energy passing around the islands.

To fine tune and validate the transformation of GROW data to the Dana Point region, the transformed wave heights were compared to measured waves at the CDIP Dana Point Buoy 096 (Figure 3-7) from 2000 to 2008. Figure 44 shows the result of the 8 yr validation. A direct wave height time series comparison of buoy and transformed GROW data show a modest but consistent overprediction of larger winter wave events. However, by rotating the offshore swell directional spectra 5^{o} northward, a good overall peak wave height agreement between the Dana Point buoy and the transformed GROW hindcast was obtained.

The offshore GROW hindcast wave heights (GROW, green line) are significantly greater than those measured at Dana Point Buoy 096 in the

lee of islands (Dana Buoy, red line). The GROW spectra were rotated 5º and transformed to the Dana Point Buoy 096 location using the spectral refraction model (GROW ADJ, blue line). Figure 44 illustrates that the transformation captures the overall reduction in wave heights (red and blue time series fluctuate at the same level) as well as the extreme conditions (max red and blue heights are of the same magnitude).

Figure 44. Comparison of significant wave heights from 2000 to 2008.

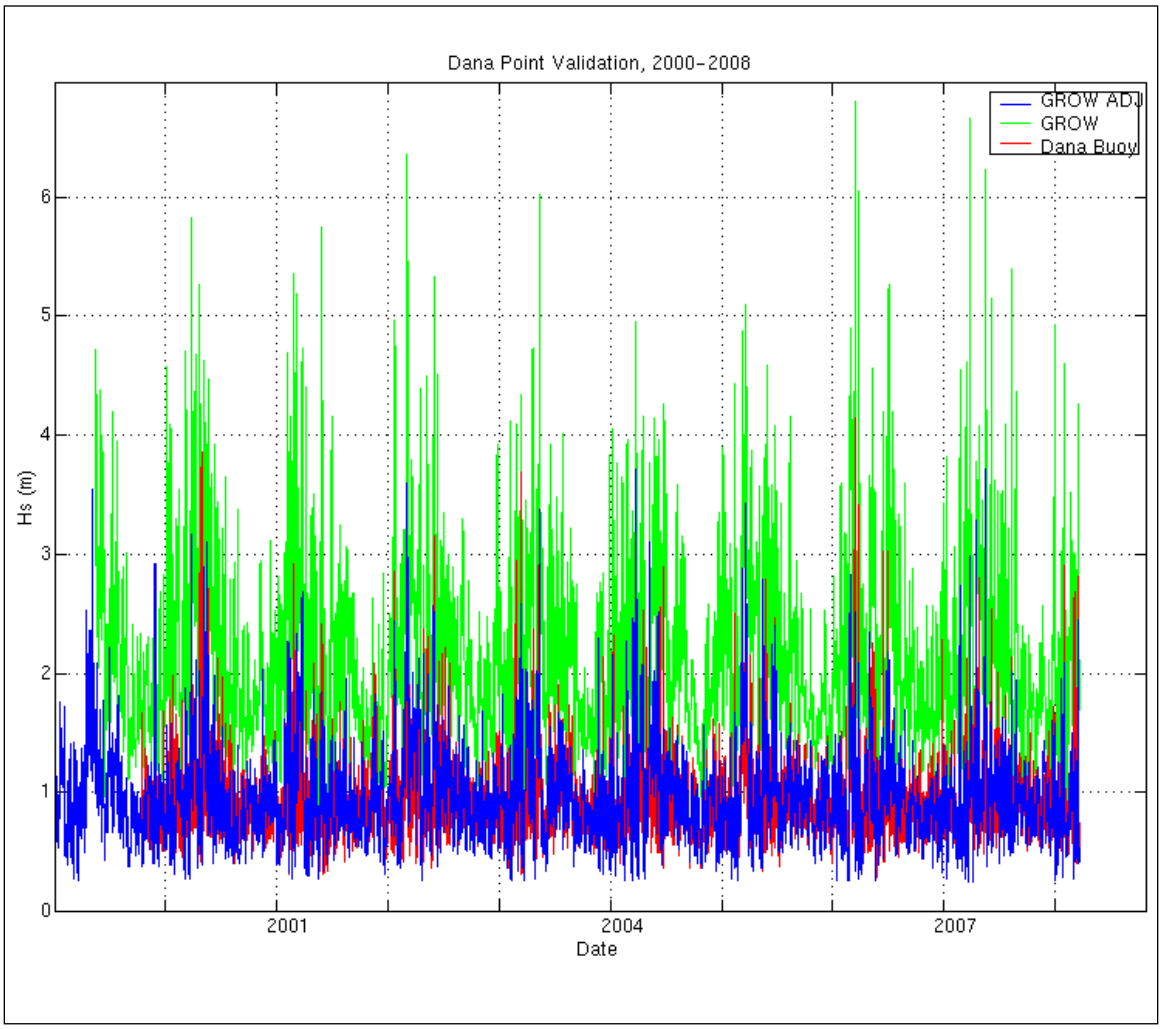

Note: The green line represents the offshore GROW hindcast significant wave heights.

The red line represents observed significant wave heights at the Dana Point buoy.

The blue line represents the significant wave heights of the transformed GROW hindcast waves at the Dana Point buoy location using a spectral refraction model.

Figure 45 shows the transformed GROW wave heights versus the buoy observations. While there is considerable scatter, the transformed GROW spectra yield relatively unbiased estimates of larger wave events. The transformed GROW waves tend to underpredict the height during low wave conditions that are a minor concern in less energetic wave situation. The calculated correlation coefficient is 0.78, and average bias (hindcast – buoy wave height) is –0.24 m.

Figure 45. Scatter plot of observed CDIP and hindcast significant wave heights.

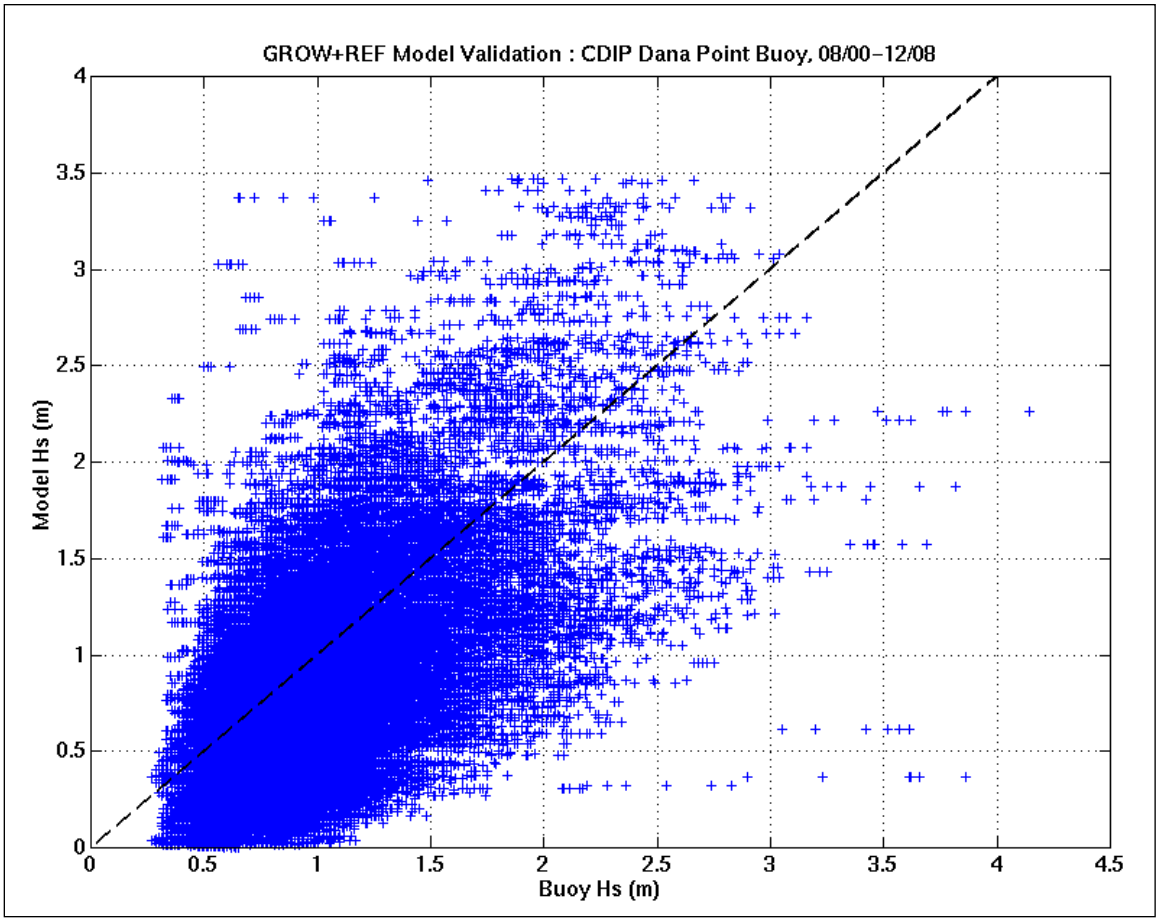

Note: Scatter plot compares observed significant wave heights at the CDIP Dana Point buoy to the transformed hindcast significant wave heights, which is based on the spectral transformation of the GROW offshore hindcast spectra to the Dana Point buoy location.

Some scatter at larger wave heights can be attributed to small-storm timing errors between the hindcast and actual wave arrivals. Figure 46 shows, as an example, the January 2008 comparison. During this particular time period, several large wave heights were underpredicted by the transformed hindcast (blue line). The hindcast is good for the last storm (circled) of the

sequence. A timing offset appears in the scatter plot. In the present study, a hindcast that reflects the proper frequency of occurrence and size of winter storm wave conditions, in a general statistical sense, is most critical. Accordingly, the 5º rotation of GROW offshore swell directions was applied to the entire 39 yr dataset for transforming the hindcasts to the two selected nearshore locations (CMS_1 and CMS_2), which were used in the CMS simulations.

Figure 46. Comparison of significant wave heights for January 2008.

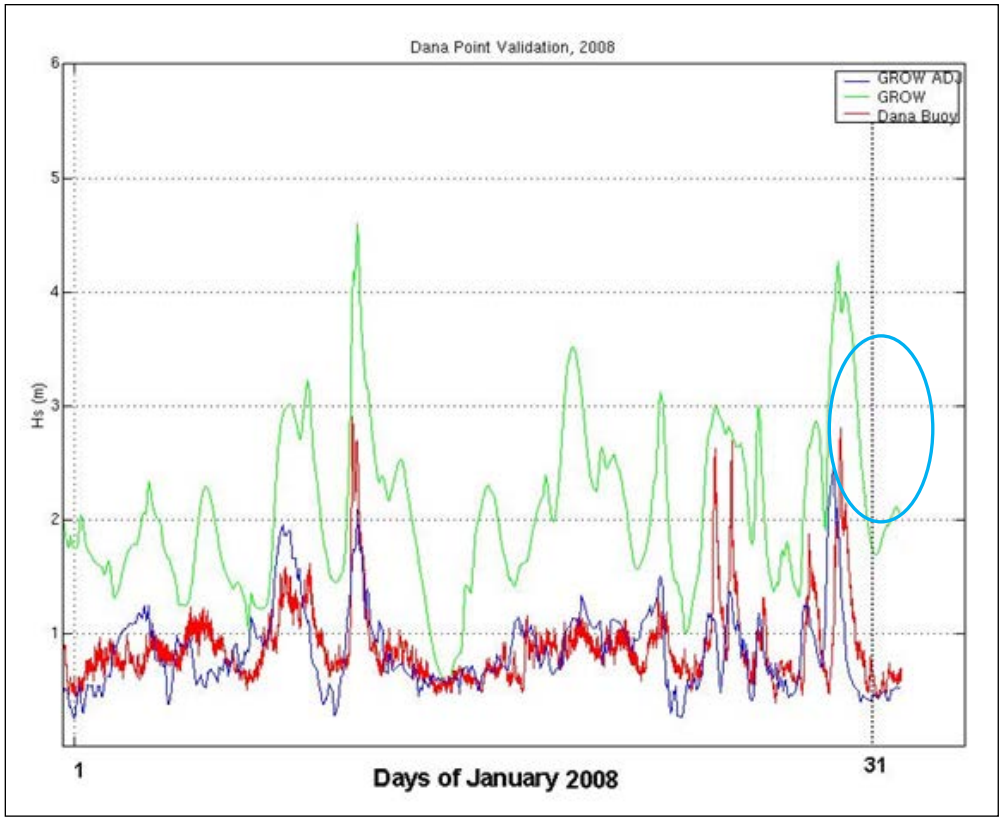

Note: The red line represents observed significant wave heights at the Dana Point buoy.

The green line represents the offshore GROW hindcast significant wave heights.

The blue line represents the significant wave heights of the transformed GROW

3.4.5 Historical storm events

Historical storm events between 1970 and 2008 were selected based on the defined threshold criteria of wave height at CMS_1 as well as previously documented historical storm events. The 39 yr wave data were sorted to satisfy the following criteria:

1. Wave height greater than a specified threshold value.
2. Only one peak wave height is allowed for each storm event (i.e., over the 3-day interval), as it is typical for a storm event occurring in Southern California to have a duration of approximately 3 days.

In addition, previously known historical storm events were referenced to assist in determining each storm episode. In total, 42 individual historic storm events with the information of peak significant wave height, wave period and approach direction were selected at the transformed offshore CMS_1 location, as listed in Table 6. To ensure that the wave characteristics during an entire storm event were captured, 5 days of wave data for each selected event were extracted at CMS_1 and CMS_2 as the offshore boundary input for the CMS simulations.

Table 6. Selected historical storm wave events.

	Deepwater Wave Characteristics at CMS_1		
Date of Storm	Peak Hs m (ft)	Tp (sec)	Dir (deg)
Jan 18, 1973	2.6 (8.5)	7.1	201.4
Dec 28, 1974	2.3 (7.5)	12.5	278.8
Jan 16, 1978	2.8 (9.2)	12.5	277.4
Mar 5, 1978	2.9 (9.5)	7.7	206.5
Dec 24, 1979	3.5 (11.5)	8.3	188.2
Feb 17, 1980	3.7 (12.1)	12.5	248.1
Jan 23, 1981	3.1 (10.2)	14.3	277.2
Jan 28, 1981	3.3 (10.8)	12.5	277.4
Dec 1, 1982	2.8 (9.2)	10.0	265.8
Jan 27, 1983	3.5 (11.5)	16.7	277.8
Feb 13, 1983	2.9 (9.5)	14.3	277.2
Mar 2, 1983	4.9 (16.1)	16.7	267.7
Mar 18, 1983	3.0 (9.8)	14.3	277.2
Dec 4, 1983	2.0 (6.6)	8.3	264.4
Dec 3, 1985	2.8 (9.2)	14.3	277.2
Feb 1, 1986	3.1 (10.2)	14.3	278.1
Feb 15, 1986	4.4 (14.4)	14.3	249.5
Mar 11, 1986	3.3 (10.8)	16.7	276.6
Mar 16, 1986	3.1 (10.2)	14.3	278.1
Dec 8, 1987	2.1 (6.9)	16.7	279.0
Dec 17, 1987	3.7 (12.1)	14.3	252.9

Date of Storm	Deepwater Wave Characteristics at CMS_1		
	Peak Hs m (ft)	Tp (sec)	Dir (deg)
Jan 18, 1988	4.4 (14.4)	11.1	263.7
Mar 1, 1991	3.0 (9.8)	11.1	277.5
Jan 18, 1993	3.1 (10.2)	11.1	249.8
Jan 5, 1995	3.5 (11.5)	9.1	244.3
Jan 11, 1995	3.8 (12.5)	12.5	275.2
Mar 12, 1995	3.1 (10.2)	12.5	269.7
Dec 13, 1995	3.0 (9.8)	14.3	277.2
Nov 27, 1997	2.8 (9.2)	11.1	275.3
Feb 3, 1998	4.6 (15.1)	8.3	190.9
Feb 7, 1998	4.3 (14.1)	12.5	248.1
Feb 17, 1998	3.0 (9.8)	16.7	277.8
Feb 24, 1998	2.6 (8.5)	14.3	278.1
Feb 21, 2000	3.2 (10.5)	12.5	275.2
Jan 11, 2001	2.8 (9.2)	14.3	278.1
Dec 17, 2002	3.2 (10.5)	14.3	278.1
Feb 26, 2004	3.1 (10.2)	14.3	278.1
Jan 7, 2005	3.6 (12.0)	8.3	205.5
Jan 2, 2006	3.2 (10.5)	8.3	208.9
Dec 28, 2006	2.3 (7.5)	11.1	271.0
Jan 5, 2008	2.7 (8.9)	16.7	278.5
Feb 25, 2008	3.4 (11.2)	14.3	277.2

3.4.6 Storm wave characteristics at Dana Point Harbor

In the CMS-Wave simulation, nearshore storm wave characteristics were deduced at six observation locations immediately offshore of both East and West Breakwater (Figure 47). A total of eighteen monitoring cells in the CMS-Wave grid were chosen to represent the six observation locations near breakwaters. Three clustered monitoring cells were selected for each observation location. The model results include a time series of significant wave height, wave period, and wave direction at each monitoring cell. Figures 48 and 49 show the deduced maximum significant wave heights at six observation locations for each modeled storm event. The large wave heights observed at Observation Location 4 depict the wave conditions at the head of West Breakwater while the reduced wave heights at Location 5 describe sheltered wave conditions at the head of East Breakwater.

Figure 47. Observation locations of CMS model results.

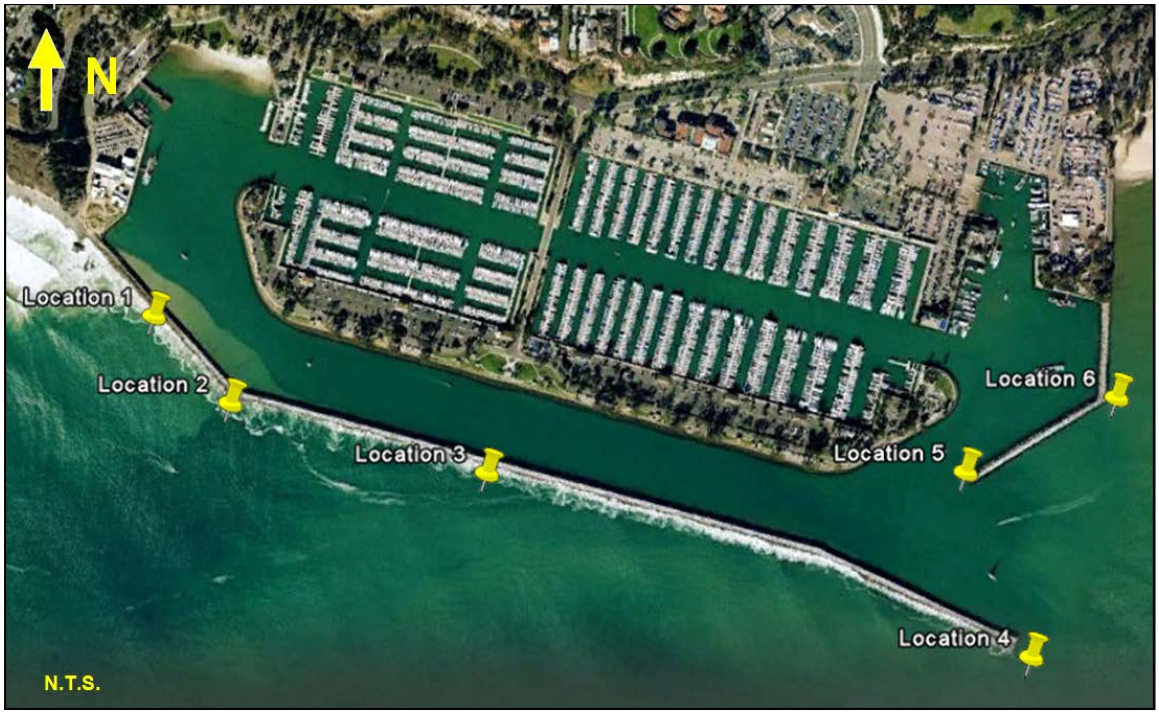

Source: Google Earth (31 December 2005)

The transformed nearshore wave conditions over a 39 yr time period (1970–2008) at the selected eighteen grid cells were analyzed to determine the extreme recurrence intervals using the probability distribution method provided by the Corps of Engineers (Leenknecht et al. 1992). The maximum computed significant wave heights (refer to Figures 48 and 49) were fitted to a Fisher-Tippet Type I (FT-I) or Weibull probability distribution approximation. These curve fittings were performed through the Automated Coastal Engineering System (ACES), which was developed by the Corps of Engineers (USACE 1991). It was observed that the data could be best described by a FT-I probability distribution function. Subsequently, the significant wave heights associated with various return periods were estimated for each selected breakwater location by selecting the maximum computed return wave height among the three grid cells. Table 7 lists the deduced wave heights for the 5, 10, 25, 50, and 100 yr return intervals at individual locations. The graphic representation of the data fitting for each respective station is displayed in Figures 50 to 55.

Figure 48. Maximum significant wave heights during storm events at Locations 1, 2, and 3.

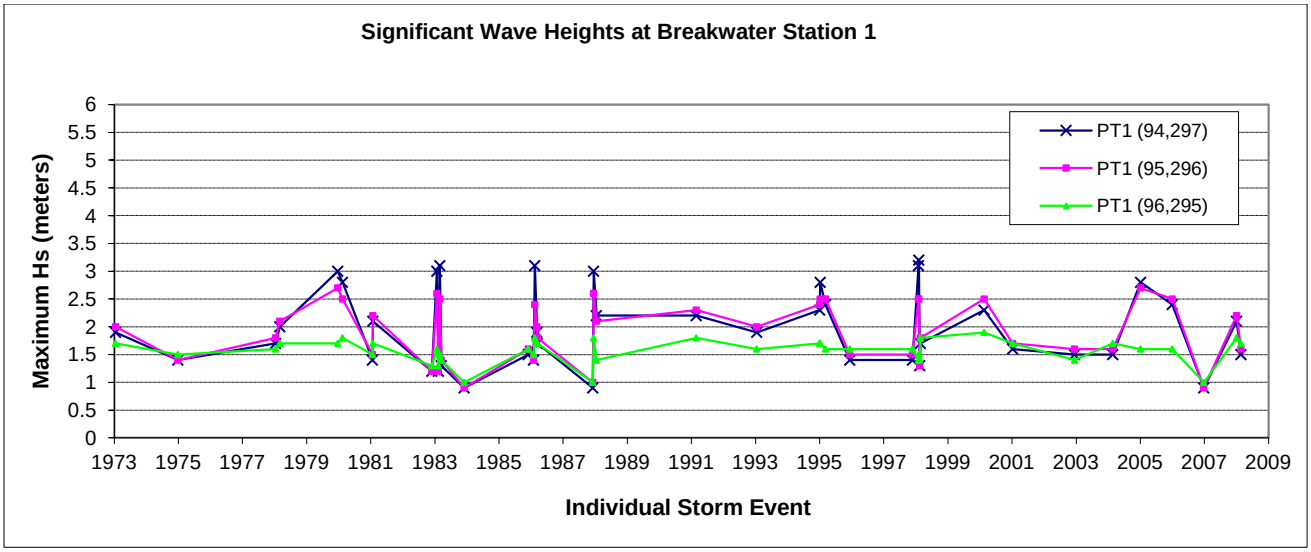

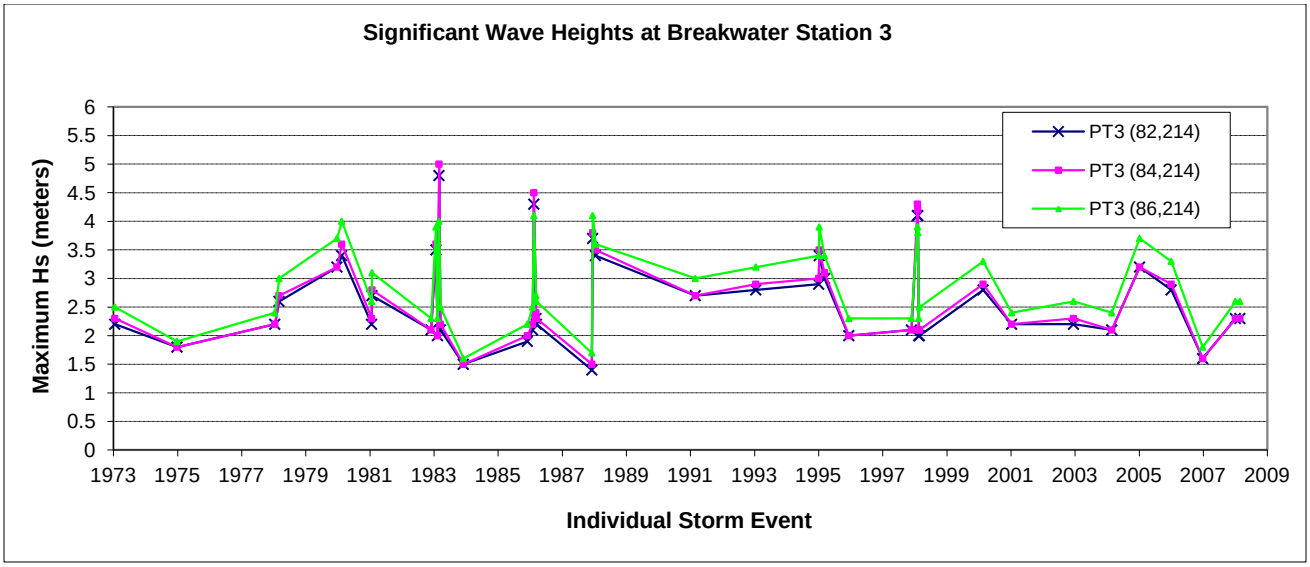

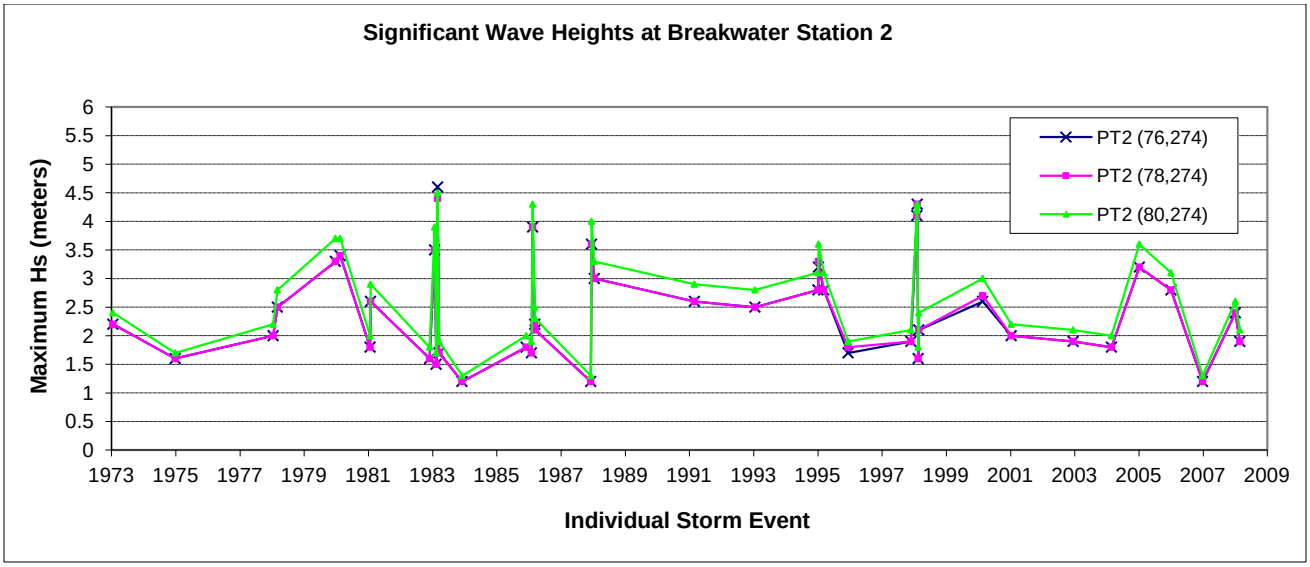

Figure 49. Maximum significant wave heights during storm events at Locations 4, 5, and 6.

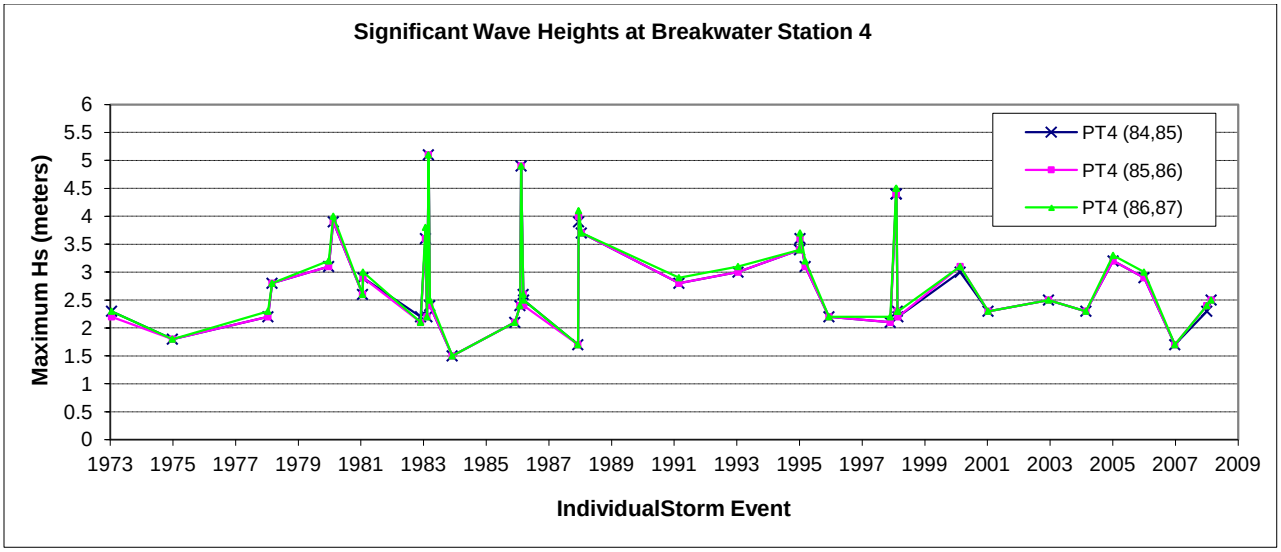

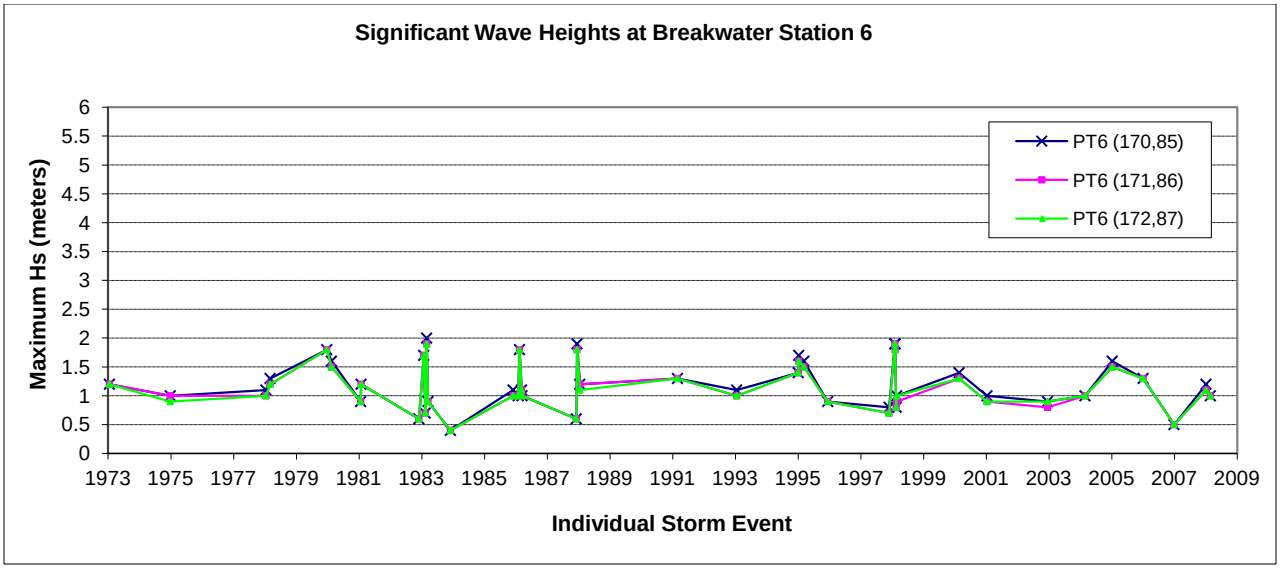

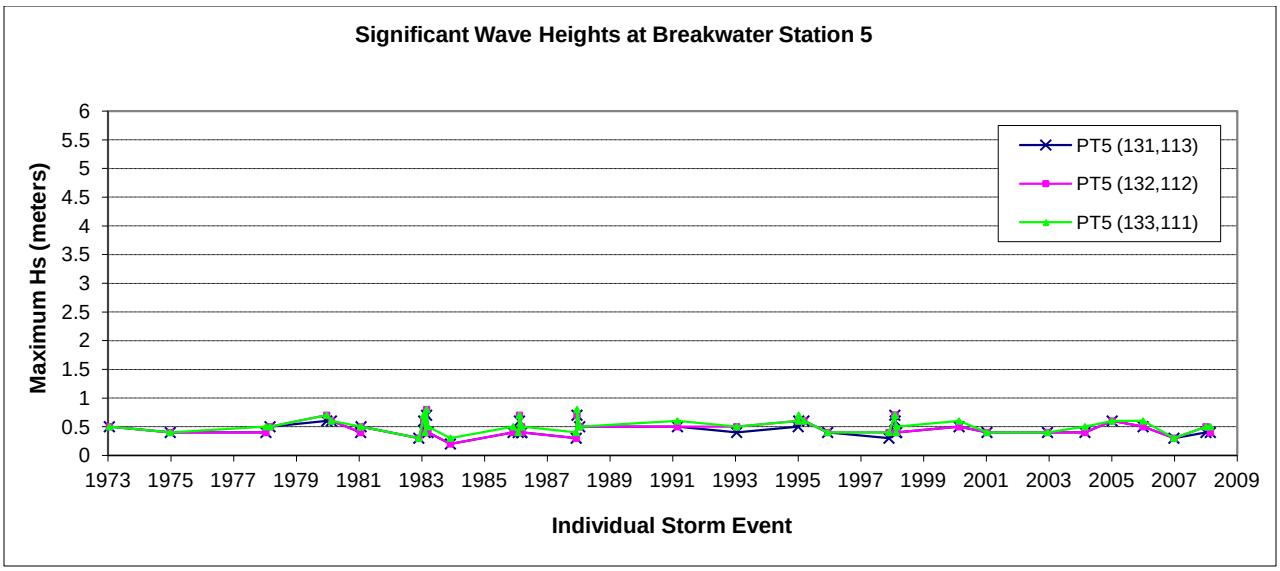

Table 7. Estimated extreme return wave heights.

Breakwater Location		Return Wave Heights m (ft)				
		5 yr	10 yr	25 yr	50 yr	100 yr
West Breakwater	Location 1	2.5 (8.2)	2.9 (9.5)	3.5 (11.5)	3.8 (12.5)	4.2 (13.8)
	Location 2	3.4 (11.2)	3.9 (12.8)	4.6 (15.1)	5.1 (16.7)	5.7 (18.7)
	Location 3	3.4 (11.2)	3.9 (12.8)	4.5 (14.8)	5.0 (16.4)	5.5 (18.0)
	Location 4	3.6 (11.8)	4.1 (13.5)	4.8 (15.7)	5.3 (17.4)	5.8 (19.0)
East Breakwater	Location 5	0.6 (2.0)	0.7 (2.3)	0.8 (2.6)	0.9 (3.0)	0.9 (3.0)
	Location 6	1.5 (4.9)	1.8 (5.9)	2.1 (6.9)	2.3 (7.5)	2.6 (8.5)

Figure 50. Deduced extreme wave height distribution at Location 1.

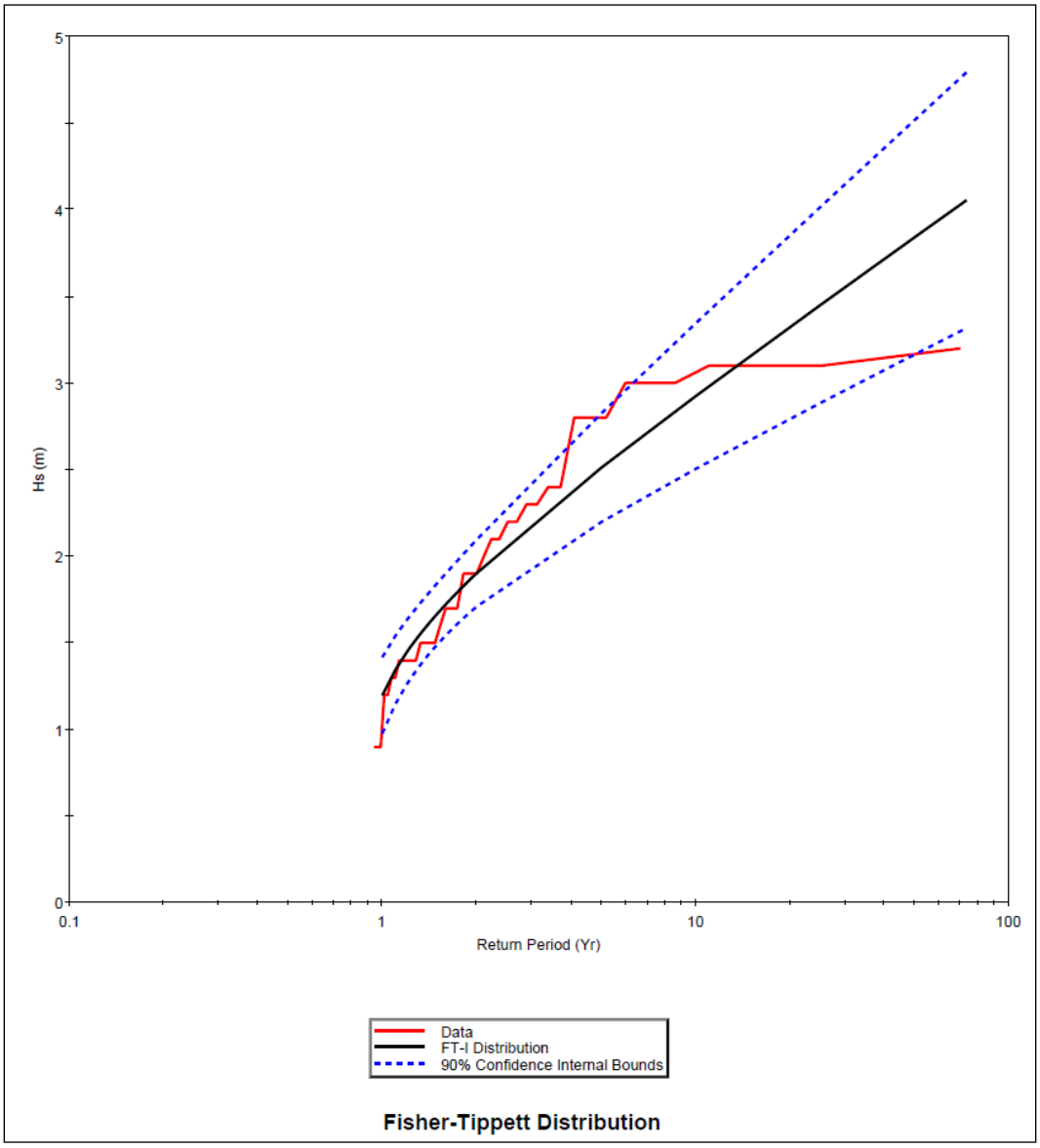

Note: Extreme waves estimated at breakwater observation point PT1 (94,297)

Figure 51. Deduced extreme wave height distribution at Location 2.

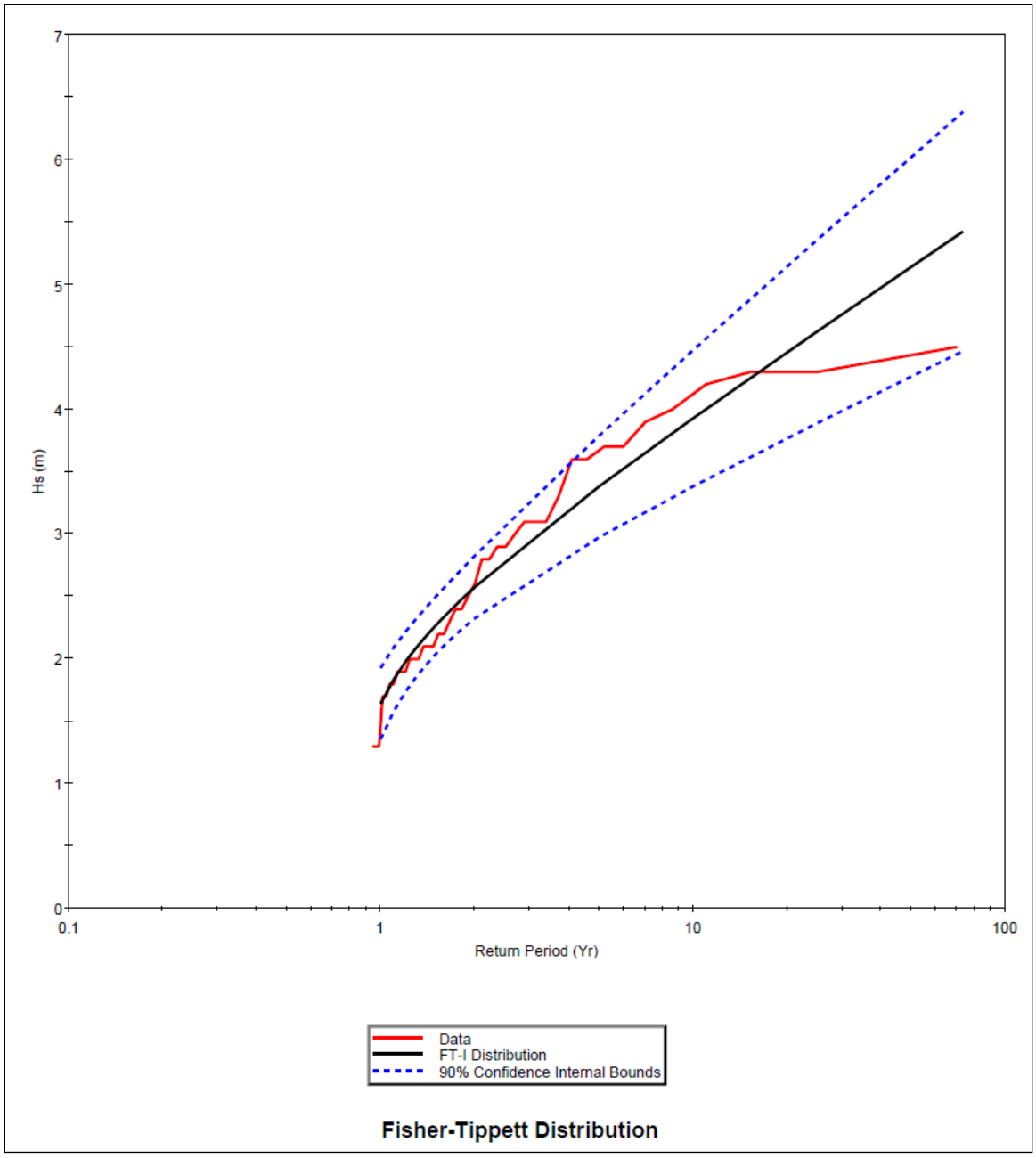

Note: Extreme waves estimated at breakwater observation point PT2 (80,274)

Figure 52. Deduced extreme wave height distribution at Location 3.

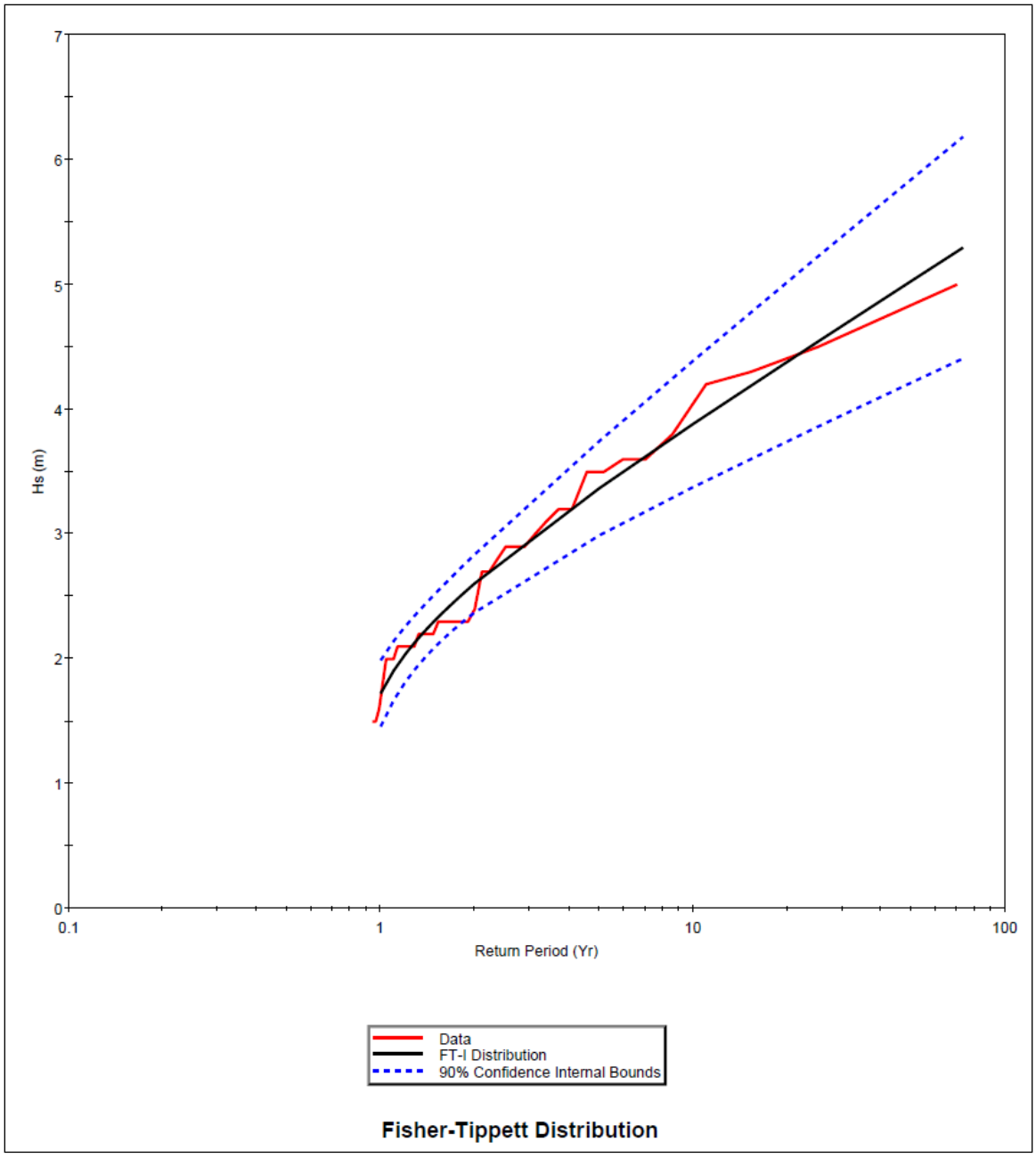

Note: Extreme waves estimated at breakwater observation point PT3 (84,214)

Figure 53. Deduced extreme wave height distribution at Location 4.

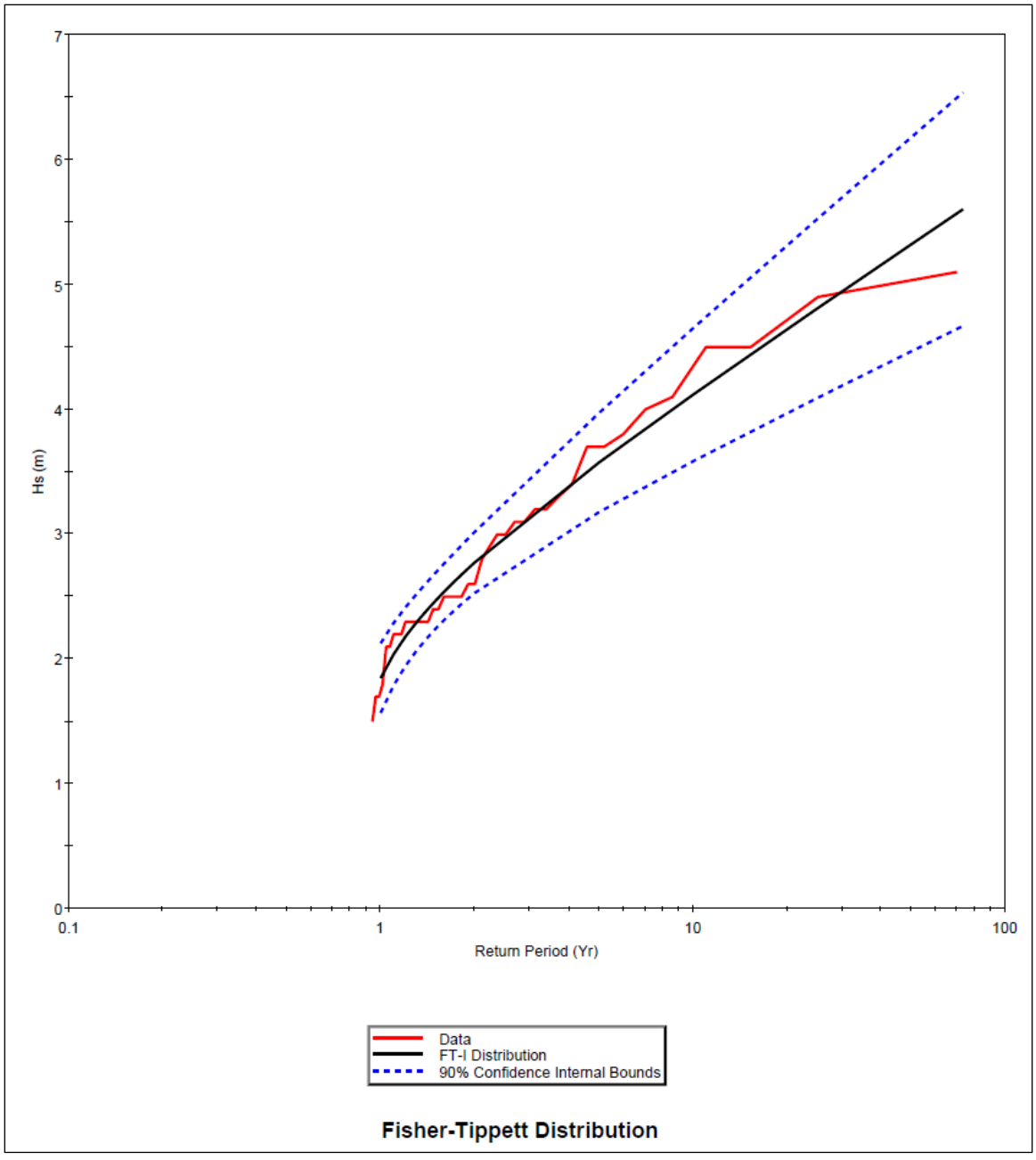

Note: Extreme waves estimated at breakwater observation point PT4 (86,87)

Figure 54. Deduced extreme wave height distribution at Location 5.

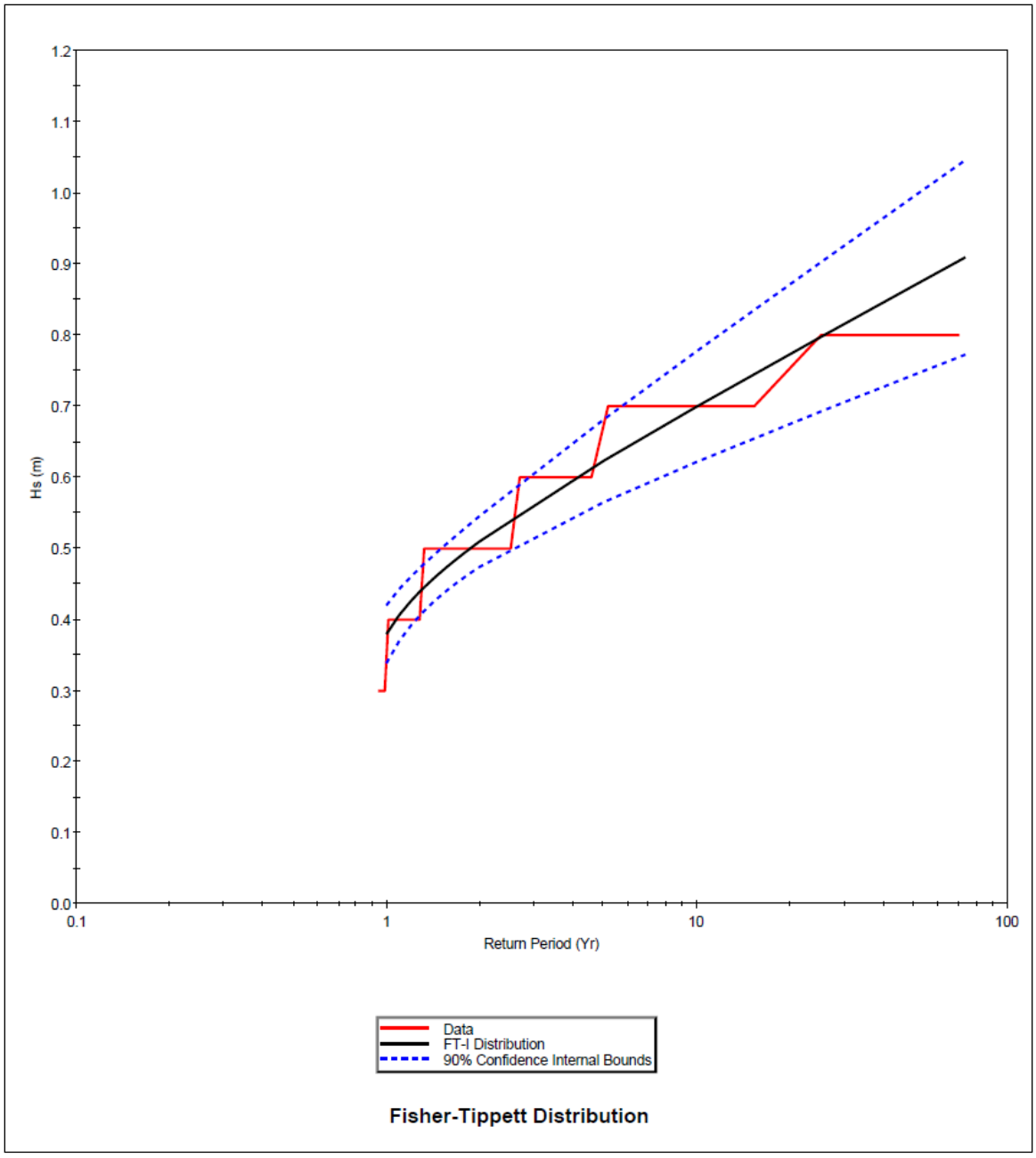

Note: Extreme waves estimated at breakwater observation point PT5 (133,111)

Figure 55. Deduced extreme wave height distribution at Location 6.

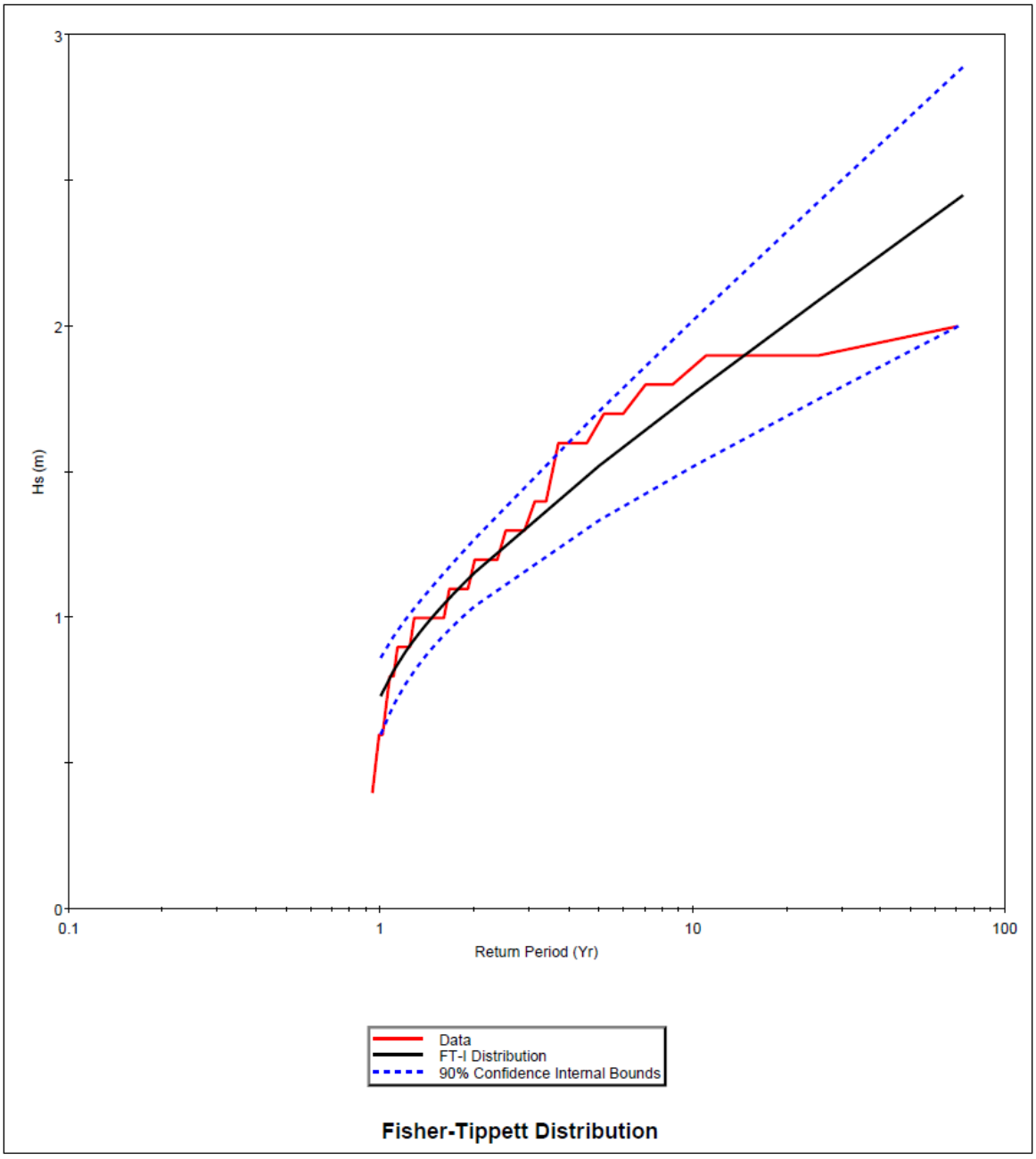

Note: Extreme waves estimated at breakwater observation point PT6 (170,85)

The deduced wave characteristics for severe extratropical storms during the 39 yr time period (1970–2008) are comparable to peak storm wave heights that were previously computed for the general design of Dana Point Harbor (USACE LAD 1965). The peak wave heights at West Breakwater for three referred historic extratropical storm events prior to 1965, which were listed in the Design Memorandum, are 4.9 m (16.1 ft) for the March 1904 storm; 4.9 m (16.1 ft) for the January 1915; and 4.3 m (14.1 ft) for the January 1943

storm, respectively. The maximum storm wave height simulated by CMS-Wave is 5 m (16.4 ft) during 28 February 1983. The 1965 Design Memorandum called for 6 to 20 tons of riprap stones to construct the outer layers of West Breakwater from Stations 0+91 to 16+76 (Sta 3+00 to 55+00 in ft).

It is noted that a recent study was performed by the California Climate Change Center (Cayan et al. 2009) to assess likely winter wave height changes along the California coast under various scenarios of greenhouse gas emission (i.e., sea level rise) in the future. It was concluded that the intensity of future winter storms is expected to follow a slightly negative trend within southern California as the mean cyclone track with a warmer climate tends to move farther north. Therefore, the return wave heights deduced from the 1970–2008 period should still be applicable in the future if any alteration or maintenance of the breakwaters is required.

4 CMS-Flow Simulations

The flow field is numerically simulated by CMS-Flow (Buttolph et al. 2006), an integrated current and sedimentation model under CMS for modeling coastal current and sediment transport processes (Demirbilek and Rosati 2011). The numerical modeling is focused on the wind- and wave-induced circulation and sediment transport at harbor and through permeable breakwaters. The CMS-Flow simulations provide technical information necessary for investigation of the existing harbor sedimentation condition and remedial solutions to the circulation near Baby Beach inside the harbor.

4.1 Model description

CMS-Flow is a 3D, finite-volume model that solves the mass conservation and shallow-water momentum equations of water motion on a nonuniform Cartesian grid. The model simulates currents, water level, and sediment transport to characterize the water circulation pattern and morphologic change in the coastal zone. The model can be executed in a 2D mode based on the depth-integrated continuity equation, which was applied in the present study. The 2D depth-integrated continuity and momentum governing equations are

$$\frac{\partial(h+\eta)}{\partial t}+\frac{\partial q_x}{\partial x}+\frac{\partial q_y}{\partial y}=0 \tag{2}$$

$$\begin{aligned}\frac{\partial q_x}{\partial t}+\frac{\partial u q_x}{\partial x}+\frac{\partial v q_x}{\partial y}+\frac{1}{2}g\frac{\partial(h+\eta)^2}{\partial x}=\frac{\partial}{\partial x}(D_x\frac{\partial q_x}{\partial x})+\frac{\partial}{\partial y}(D_y\frac{\partial q_x}{\partial y})\\ +f\,q_y-\tau_{bx}+\tau_{wx}+\tau_{sx}\end{aligned} \tag{3}$$

$$\begin{aligned}\frac{\partial q_y}{\partial t}+\frac{\partial u q_y}{\partial x}+\frac{\partial v q_y}{\partial y}+\frac{1}{2}g\frac{\partial(h+\eta)^2}{\partial y}=\frac{\partial}{\partial x}(D_x\frac{\partial q_y}{\partial x})+\frac{\partial}{\partial y}(D_y\frac{\partial q_y}{\partial y})\\ +f\,q_x-\tau_{by}+\tau_{wy}+\tau_{sy}\end{aligned} \tag{4}$$

where q_x and q_y are mass fluxes parallel to the x and y axes, respectively;

g = the gravitational acceleration
η = the water surface elevation from the still water level
h = and t are the still water level and time, respectively
u and v = are depth-average current velocities parallel to the x and y axes
D_x and D_y = are diffusion coefficients
f = the Coriolis parameter
τ_{bx} and τ_{by} = are bottom stress parallel to the x and y axes
τ_{wx} and τ_{wy} = are surface stress parallel to the x and y axes
τ_{sx} and τ_{sy} = are wave stress parallel to the x and y axes.

The wave radiation stress and wave information entering flow and sediment transport formulas are supplied to CMS-Flow through coupling with CMS-Wave. Calculated currents and water level changes from CMS-Flow in turn provide an update flow field and water surface conditions to the wave model to increase the accuracy of the wave transformation prediction (Buttolph et al. 2006).

4.2 CMS-Flow model improvement

As described in Section 3.3, both West and East Breakwater were specified in CMS as permeable structures that allow for wave transmission, flow penetration, and sediment seepage. Figure 56 shows the sketch of wave transmission and flow penetration through a permeable structure. Based on the Forchheimer equation (Forchheimer 1901) with unidirectional flow (u), through a permeable structure in the x-direction, the momentum equation is

$$g(h+\eta)\frac{\partial(h+\eta)}{\partial x} = ag(h+\eta)u + bg(h+\eta)u^2 \tag{5}$$

where a and b are resistance coefficients.

The left-hand side of Eq.5 is the hydraulic gradient, and the linear term on the right-hand side corresponds to the laminar and the nonlinear term to the turbulent component of flow resistance. The resistance coefficients a and b are a function of structure permeability and the kinematic viscosity of the fluid (Sidiropoulou et al. 2007). The values of coefficients a and b depend on the rock diameter and the hydraulic conductivity through the

Figure 56. Sketch of wave transmission and flow penetration through a permeable structure.

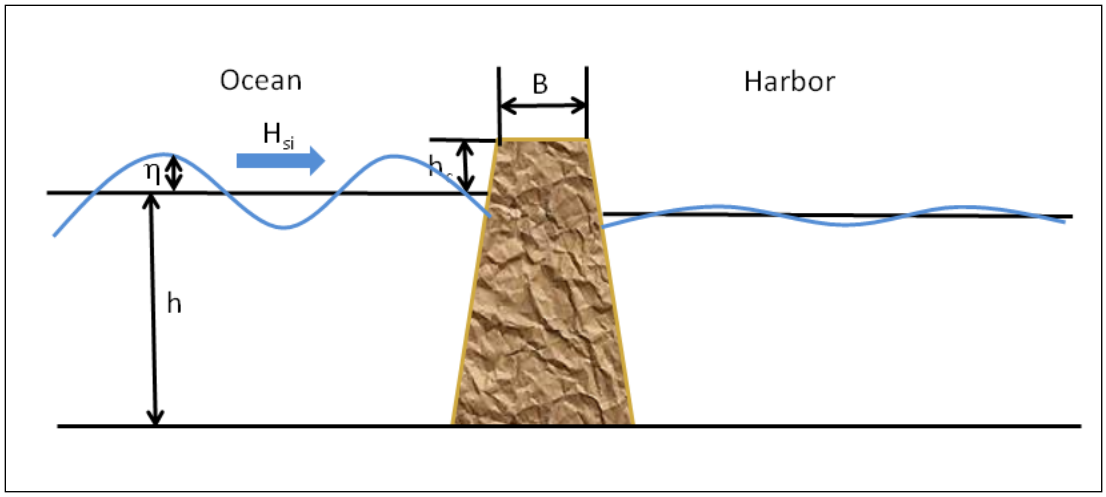

permeable structure. Higher values of coefficients *a* and *b* imply less flow passing through the structure, which results in less sedimentation in the lee of West Breakwater. The implementation of a permeable structure in the CMS requires modifications of the conservation of mass equation by introducing the structure void factor (*n'*). The revised equation of change of η to time *t* is

$$\frac{\partial \eta}{\partial t} = \frac{1}{n'}\left[\frac{\partial q_x}{\partial x} + \frac{\partial q_y}{\partial y}\right] \tag{6}$$

where *n'* is the structure void factor.

In the morphologic simulation, the similar equation for the change in bed elevation is revised to account for the structure void factor:

$$\frac{\partial \varsigma}{\partial t} = \frac{1}{n'}\left[\frac{\partial q_{sx}}{\partial x} + \frac{\partial q_{sy}}{\partial y} - E + D\right] \tag{7}$$

where ζ is the bed elevation

q_{sx} and q_{sy} = are the bedload fluxes in the *x* and *y* directions, respectively

E = the erosion flux

D = is the deposition flux.

4.3 CMS-Flow calibration and sensitivity analysis

CMS-Flow was calibrated and validated against the water level and current measurements. The hydrodynamic calibration was performed for a 10-day period from 18 to 27 November 2009, and followed by a 30-day validation period from 18 November to 17 December 2009. Inside ADCP current measurements were available during the calibration and validation periods; however, water surface elevation and wave measurements were only available from 21 to 26 November 2009, for the outside ADCP (i.e., the ocean side of the West Breakwater).

Figure 57 shows the comparison of calculated and measured water surface elevations (WSE) at the outside ADCP location from 18 to 27 November 2009. During this neap tidal period, the CMS predicts water levels at the ADCP outside of the West Breakwater well. The goodness-of-fit parameters indicate an agreement between model and data by a correlation coefficient of 0.99, a root mean square error (RMSE) of 5.3 cm/sec (0.17 ft/sec), and a relative RMSE of 4.0%.

Figure 57. Comparison of calculated and measured water levels at Outside ADCP station.

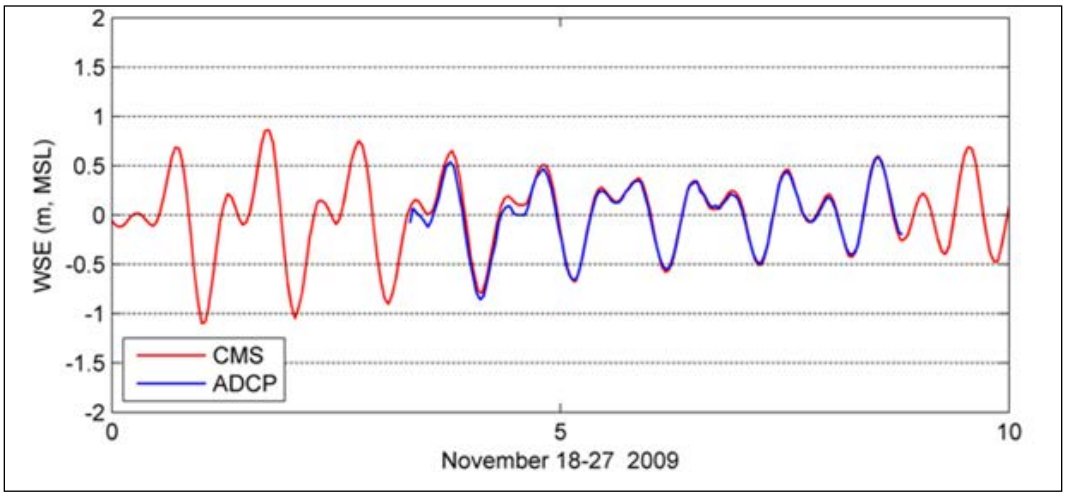

Around the West Breakwater, wave- and tide-induced current generally flows parallel to the structure. To compare the calculated current with the measurements and examine the flow pattern, principal flow axes were identified for the calculated results and the measured data. Current components (east-west and north-south) were projected to the principal axes for calculated and measured current comparison.

Figure 58 shows the calculated currents and measurements at the inside ADCP location and the calculated currents at the outside ADCP location for the 1-month simulation from 18 November through 17 December 2009. Positive direction corresponds to east-southeast flow parallel to the breakwater and the ebb current direction at the inside gage. Different flow patterns were exhibited at the two locations.

Figure 58. Comparison of calculated and measured currents at the Inside ADCP station (top) and calculated currents at the outside ADCP station (bottom).

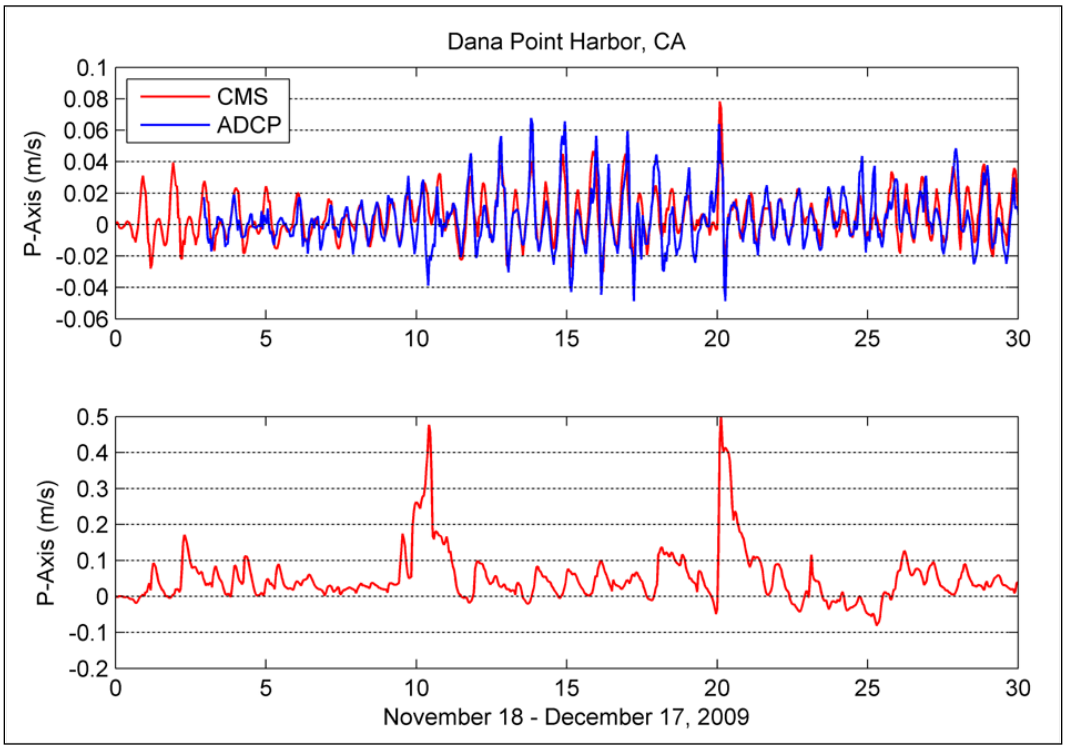

Inside the breakwater, the current generally has a speed of less than 4 cm/sec (0.13 ft/sec) and shows a clear, strong flood and ebb-tidal current signal. A larger current spike up to 8 cm/sec (0.26 ft/sec) occurred around 7-8 December 2009, as a response to a winter storm. The current speed at the outside ADCP location had a magnitude of 5 to 10 cm/sec (o.16 to 0.33 ft/sec) with a dominant current direction from west northwest (i.e., traveling along the west breakwater) toward southeast under both flood and ebb conditions. Two northwest winter storms occurring between 27-28 November and 7-8 December 2009, caused high currents outside the harbor and current speeds at the outside gage were close to 50 cm/sec (1.6 ft/sec). Besides wave and wind forcing, tide is also responsible for current changes, which is clearly demonstrated by the spring/neap pattern at the inside gage.

Comparing to the ADCP data, the CMS well reproduced the tide- and storm-induced currents at the inside ADCP location. The goodness-of-fit parameters indicate an agreement between model and data by a correlation coefficient of 0.73, an RMSE of 1.1 cm/sec (0.04 ft/sec), and a relative RMSE of 9.2%.

Snapshots of depth-averaged water circulation field surrounding the Dana Point Harbor at two instantaneous times were retrieved from the CMS simulations. Figure 59 shows the flow fields at 05:00 GMT and 22:00 GMT, 19 November 2009, during the flood and ebb tide cycles, respectively. During the flood tide, strong tidal currents occur outside the harbor along the shoreline and follow the alignments of the West and East Breakwaters. The current magnitude can be greater than 50 cm/sec (1.64 ft/sec) at the northwest end of the West Breakwater and ranges between 15 and 30 cm/sec (0.49 and 0.98 ft/sec) outside (ocean side) the East Breakwater. Within the harbor, the maximum current speed ranges from 6 to 8 cm/sec (0.20 to 0.26 ft/sec). Under the ebb tide condition, the alongshore current outside the harbor is weaker, decreasing from 50 cm/sec (1.64 ft/sec) to less than 10 cm/sec (0.33 ft/sec).

At the ocean side of the breakwaters, currents move predominantly east-southeastward parallel to the West Breakwater in accordance with the approaching wave direction. Inside the harbor, the current pattern is closely associated with tide and is sensitive to wind while sheltered by breakwaters from wave impingement.

Figure 59 shows the simulated flow fields at 05:00 GMT and 22:00 GMT, 19 November 2009, during the flood and ebb tide cycles, respectively. During the flood tide, strong tidal currents occur outside the harbor along the shoreline and follow the alignments of West and East Breakwater. The current speed can be greater than 50 cm/sec (1.64 ft/sec). Within the harbor, the maximum current speed ranges from 6 to 8 cm/sec (0.20 to 0.26 ft/sec). Under the ebb tide condition, the alongshore current outside the harbor is weaker. The current magnitude at the northwest end of West Breakwater and the outside (ocean side) of East Breakwater is between 15 and 30 cm/sec (0.49 and o.98 ft/sec). The maximum current speed along the entrance channel inside the harbor is approximately 5 cm/sec (0.16 ft/sec).

Figure 59. Calculated depth-averaged current fields.

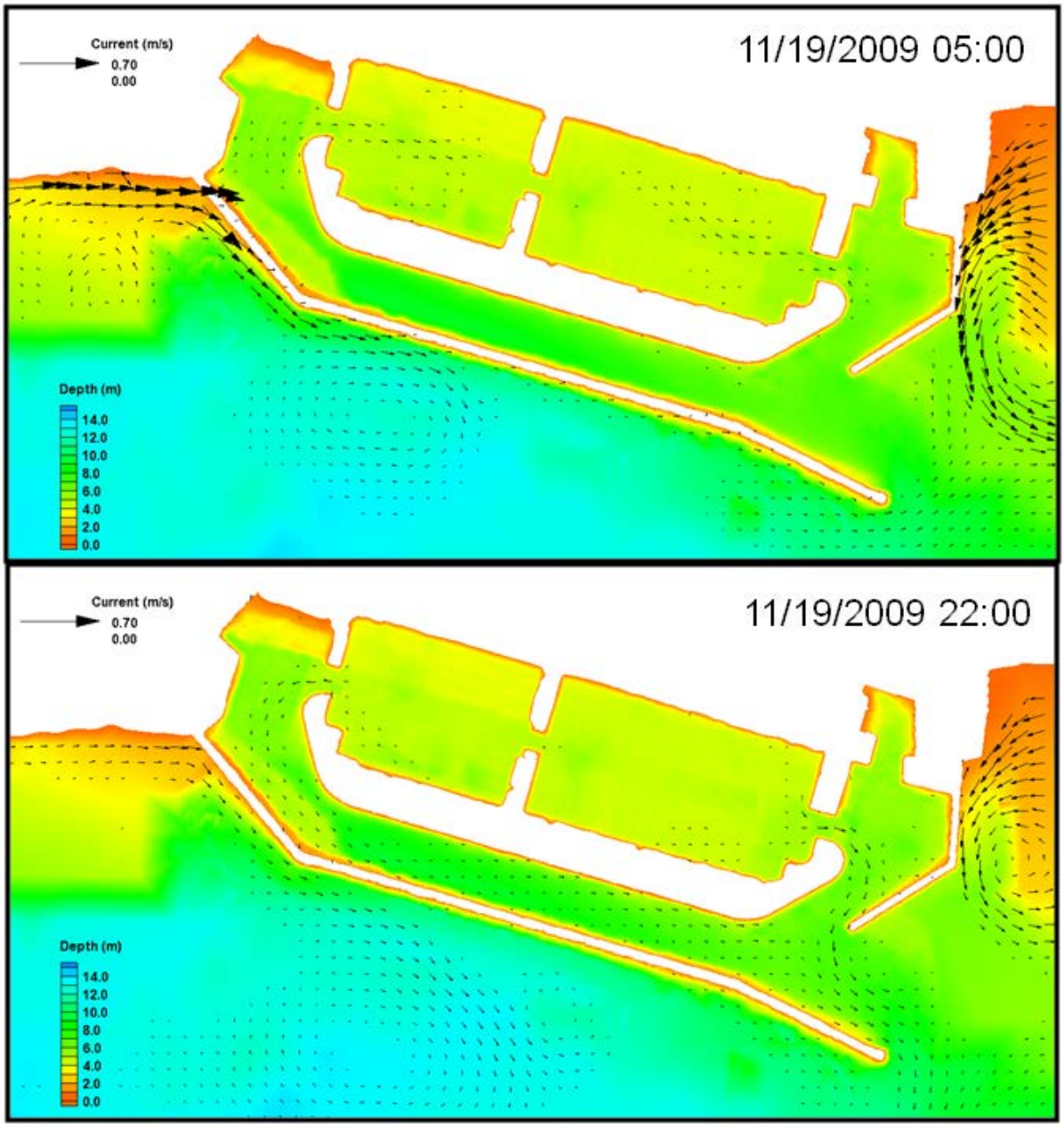

Within the nearshore wave-dominated environment oceanside of the breakwaters, currents move predominantly east-southeastward parallel to West Breakwater in accordance with the approaching wave direction. The ADCP measurements show the same trend as the observed current patterns in ebb and flood cycles. Inside the harbor, the current pattern is closely associated with tide and is sensitive to wind while sheltered by breakwaters from wave impingement.

A sensitivity analysis was performed to examine CMS results in response to the different forcing parameters, the permeability of the West Breakwater, and harbor shoaling. This includes applying three different sets of wind data collected at offshore NDBC Buoy 46047, the Ocean Institute in the Dana Point Harbor, and at the NOAA La Jolla Pier for the model simulations. Figure 60 shows the comparison of wind data collected from 18 to 27 November 2009. Wind conditions typically vary between the offshore region and coastal zone. Because the wind is generally stronger at the offshore buoy than along the coast, the buoy wind is less representative for the harbor condition. At La Jolla Pier, the wind direction is characterized by the diurnal cycle of sea breeze while the NOAA buoy wind is dominated by the northwest-northeasterly wind offshore Dana Point. Figure 61 shows that wind collected at the offshore buoy and the Ocean Institute induced greater current in east-southeast direction. The CMS simulation with the wind data at La Jolla yields a more accurate model flow field (Figure 58) comparing to those with the buoy wind, which yields a correlation coefficient of 0.69, an RMSE of 1.3 cm/sec (0.04 ft/sec) and a relative RMSE of 10.8% between the model and data. A previous field study at Dana Point Harbor (SAIC 2003a) showed the evidence of flow passing through the West Breakwater and its impact on the current pattern in the navigational channel. A permeable breakwater acts as a wave/current energy damper, and it could allow for more water flow through the structure and absorb more energy with an increase in length of the permeable segment. In the present model study, both the West and East Breakwaters were specified as permeable structures. To examine current responses to the changes in permeable length, two other scenarios with partial segment permeability of the West Breakwater were simulated. As shown in Figure 62, the permeable portion has a length of 230 and 760 m (755 and 2494 ft), respectively, for these two cases. The calculated results clearly show the increase in current speeds at the inside and outside breakwater with the decrease in length of permeable portion of the breakwater.

Additional analysis includes the flow conditions for nonpermeable breakwaters and a shoaling scenario in the harbor. Figure 63 shows the same depth-averaged current snapshots as in Figure 59 to illustrate the simulation with nonpermeable breakwaters. The eddy formed outside the East Breakwater indicates a slight increase of current speed in the harbor for the nonpermeable breakwaters.

Figure 60. Wind speed and direction at various locations.

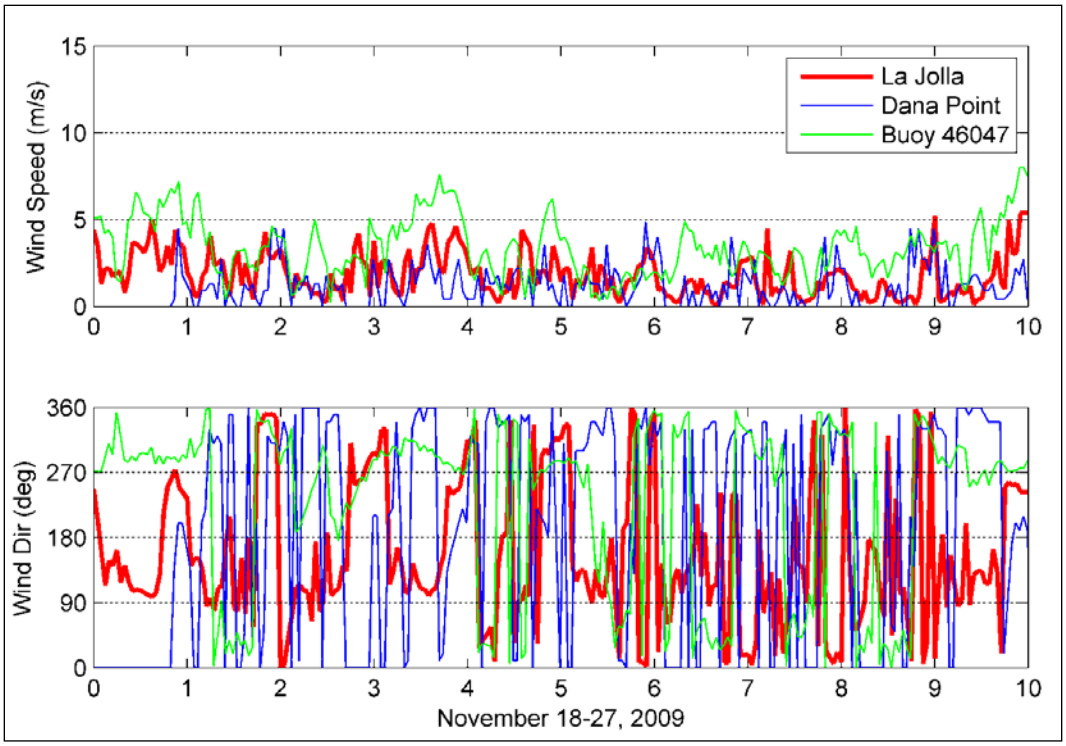

Note: The gauge locations are at NOAA La Jolla Station (9419230), Dana Point Harbor (Ocean Institute), and NDBC buoy (46047); 18–27 November 2009.

Figure 61. Comparison of calculated currents at Inside (top) and Outside (bottom) ADCP stations with the La Jolla, the Dana Point, and the offshore buoy wind, respectively.

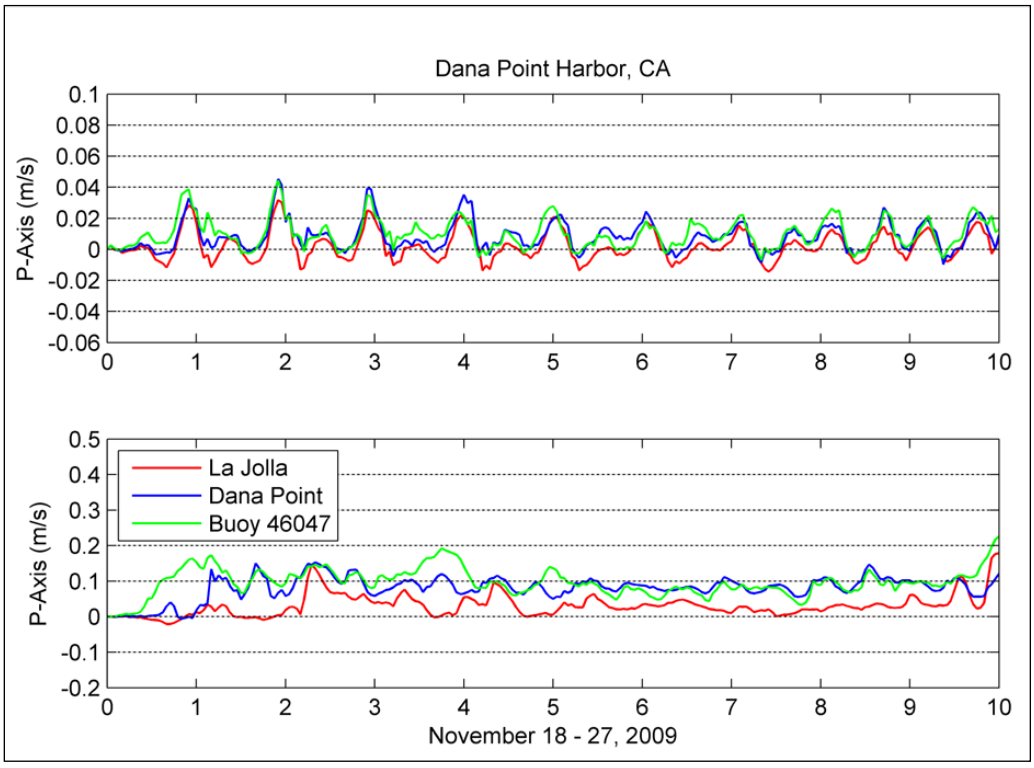

Figure 62. Comparison of calculated currents at Inside (top) and Outside (bottom) ADCP stations with different lengths of permeable breakwater segment.

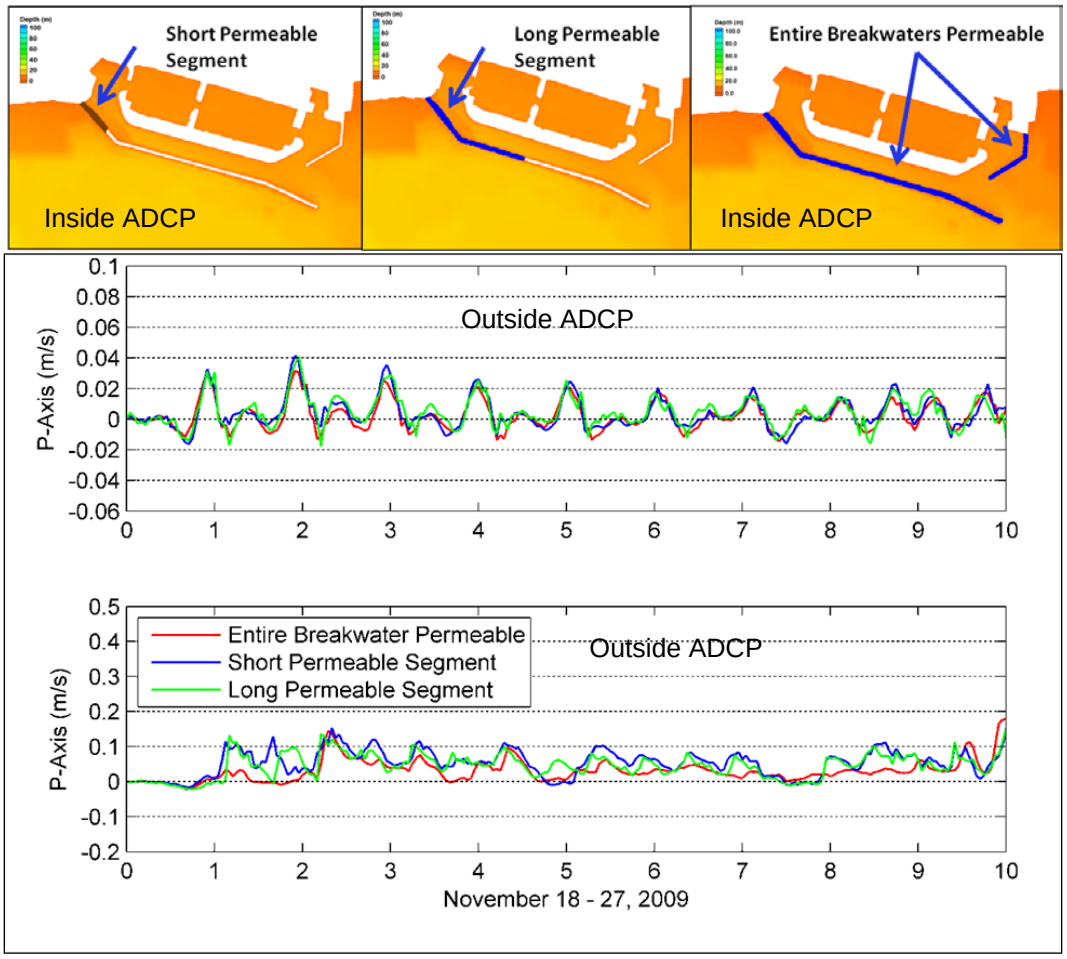

Figure 63. Calculated depth-averaged current fields for non-permeable breakwaters.

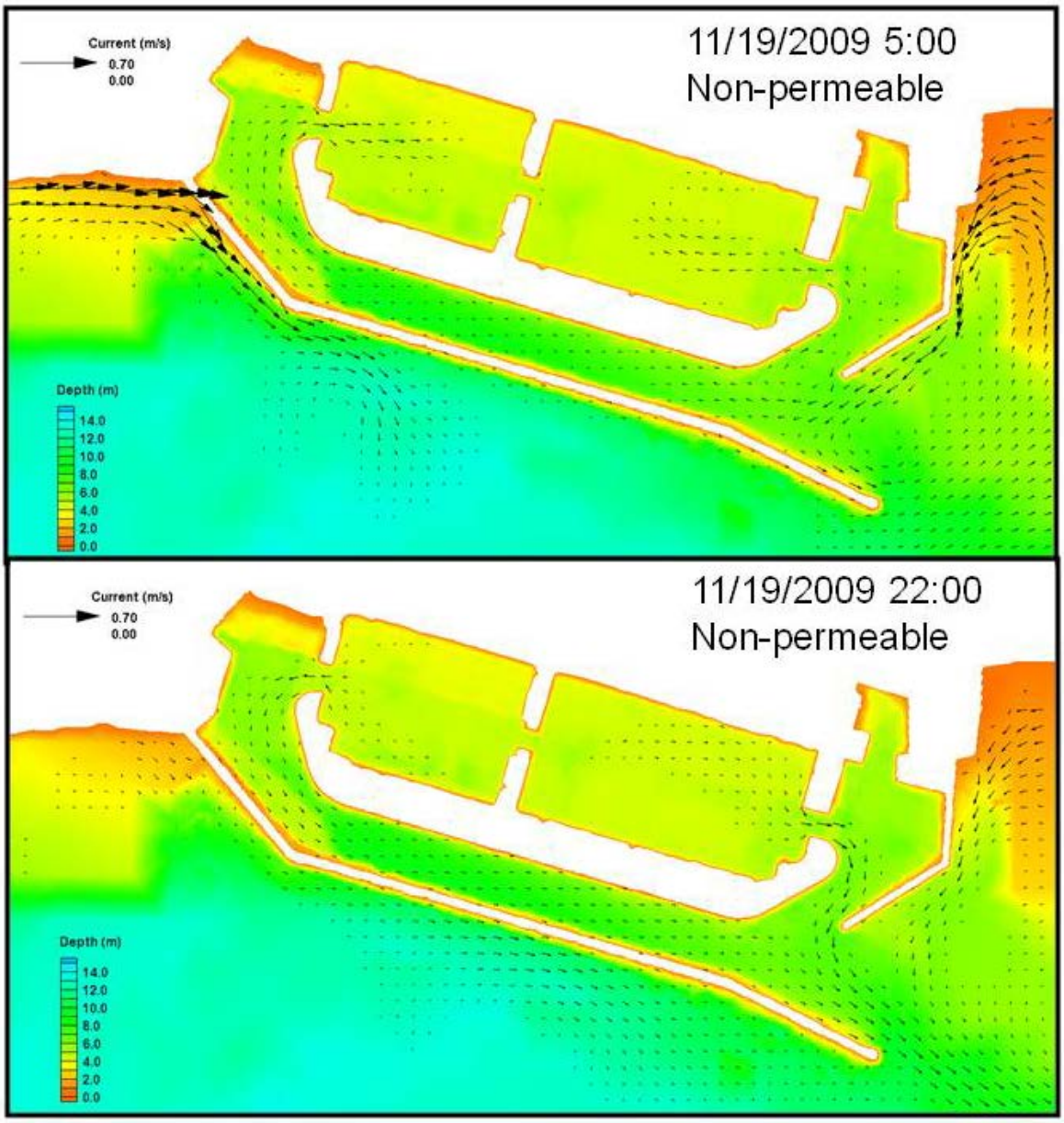

Notes: Current fields correspond to a flood tide and an ebb tide, respectively, on 19 November 2009 at 05:00 GMT and 22:00 GMT. Both breakwaters are non-permeable.

The shoaling is due to the sediment seepage and accumulation in the harbor, which greatly reduces the water depth and narrows the navigational channel near the northwest end of the West Breakwater (Figure 64). Corresponding to this scenario, changes in the flood and ebb currents were not significant inside the harbor, while an anticipated stronger depth-averaged current was calculated in the shoaling area.

Figure 64. Calculated depth-averaged current fields with a developed shoal.

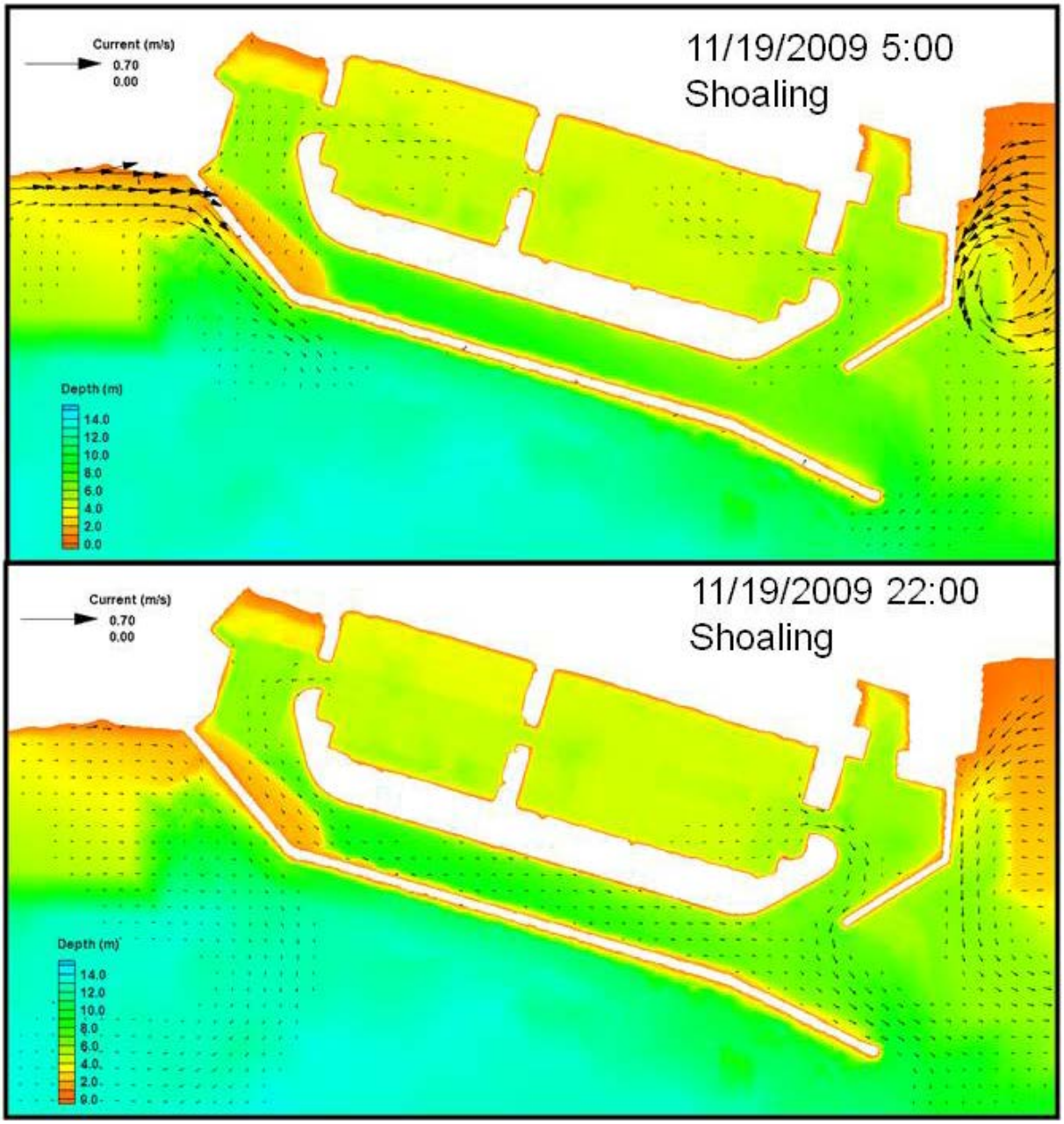

Notes: Current fields correspond to a flood tide and an ebb tide, respectively, on 19 November 2009 at 05:00 GMT and 22:00 GMT. Both breakwaters are permeable with a shoal developed on the West Breakwater

4.4 Historical maintenance dredging

Maintenance dredging at Dana Point Harbor primarily focuses in the lee area of the West Breakwater as a consequence of sediment seeping through the breakwater. The shoaling area is located primarily in the area between

Sta 0+60 and Sta 4+80 (see Figure 4), which results in impacts on recreational activity such as stand-up paddle surfing within the harbor. A total of three maintenance dredging operations, averaging approximately 10 yr per cycle, have occurred since the harbor was constructed in the 1960s. Relatively small quantity of fine material that was discharged through the drainage system was also dredged in navigation channels and berthing basins. The dredge quantities listed in Table 8 reflect only the sediment volume that was removed along the harbor-side of the West Breakwater. This particular accumulation zone, which is exemplified in Figure 1, accounts for the majority of the maintenance dredging requirements.

Table 8. Dredging quantities for West Breakwater sediment deposition.

Year	Quantity of Dredged Material (cubic yard (cy))
1990	23,500
2000	35,500
2009	54,100

Comparisons of sequential bathymetric surveys that were conducted by the U.S. Army Corps of Engineers (USACE) reveal the general shoaling pattern that occurs along the harbor side of West Breakwater. Figures 65 and 66 show the isopachs of the shoal formation between two consecutive years from 2000 to 2004, respectively. The polygon shown on each plot identifies the typical sediment deposition zone that has been observed in the past. An absence of color (the white area in the polygon) on the isopach maps denotes the areas where survey data were unavailable. Between 2000 and 2001 (Figure 65), a significant shoal was developed immediately following the maintenance dredging operation that was conducted in the spring of 2000. The sediment deposition during this postdredging period was limited to areas immediately on the lee of the breakwater as sediment quickly settled and deposited on the dredged channel bottom. Over time, the rising shoal formation started to expand into the main navigational channel as shown in the subsequent isopach maps.

Figure 65. Isopach of shoal formation from 2000 to 2002.

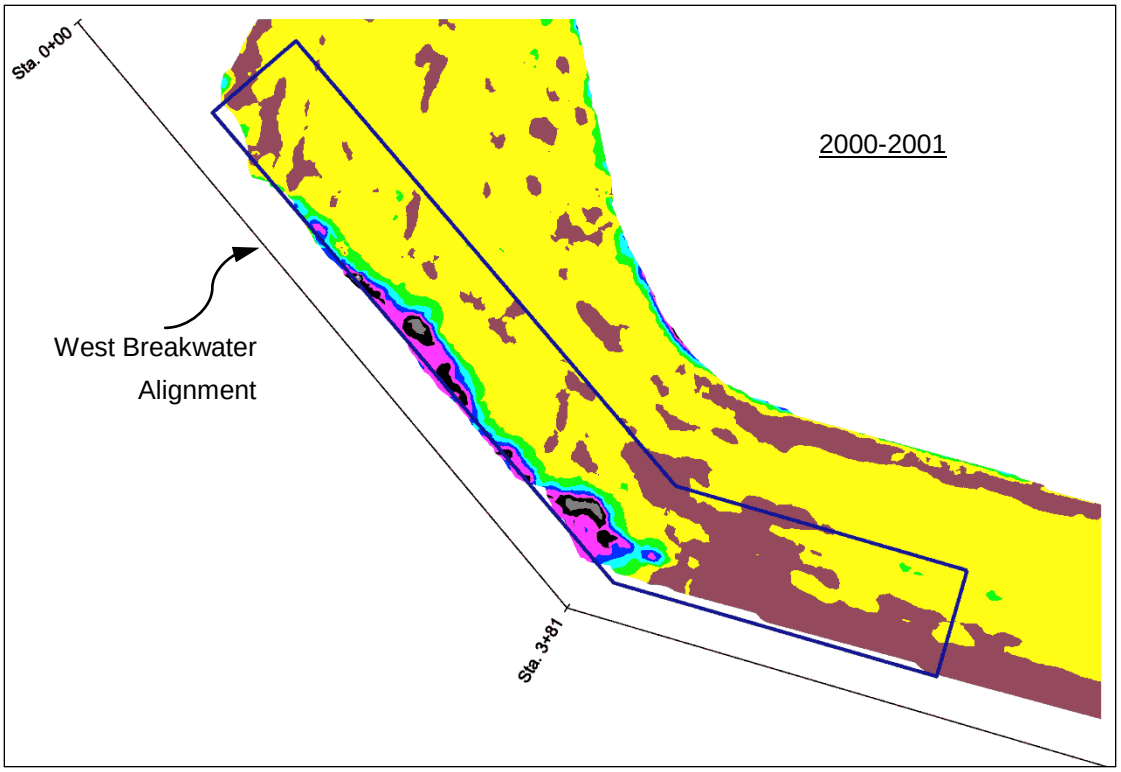

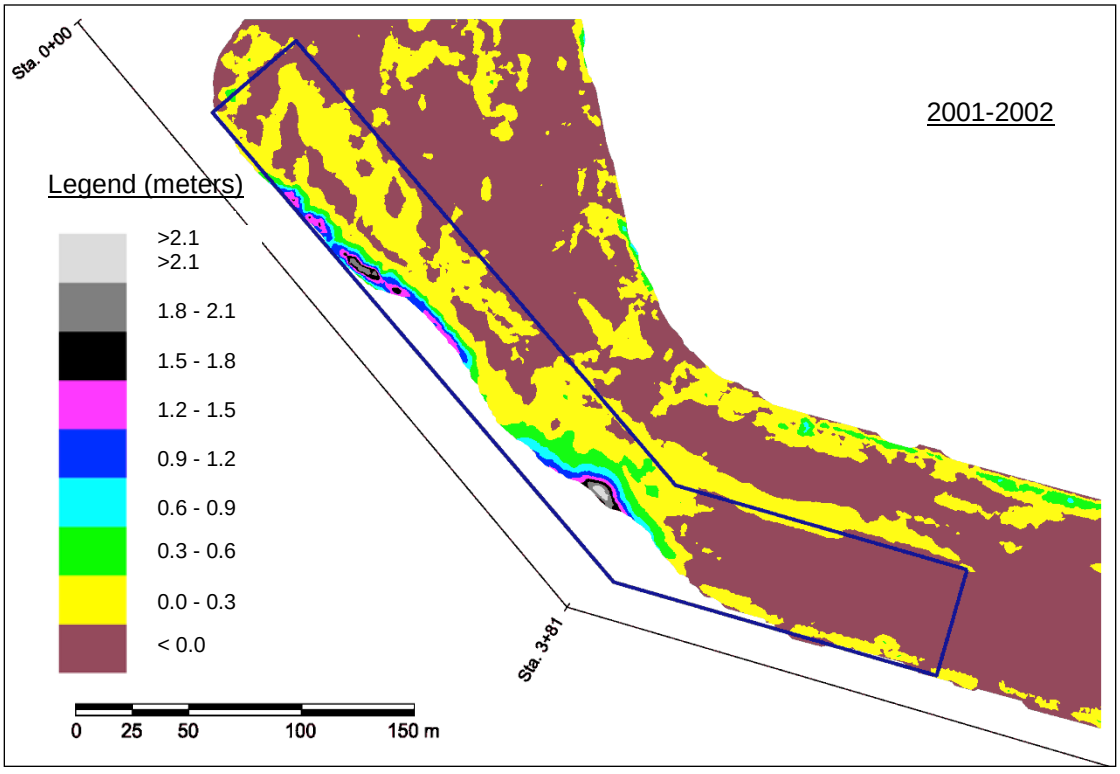

Figure 66. Isopach of shoal formation from 2002 to 2004.

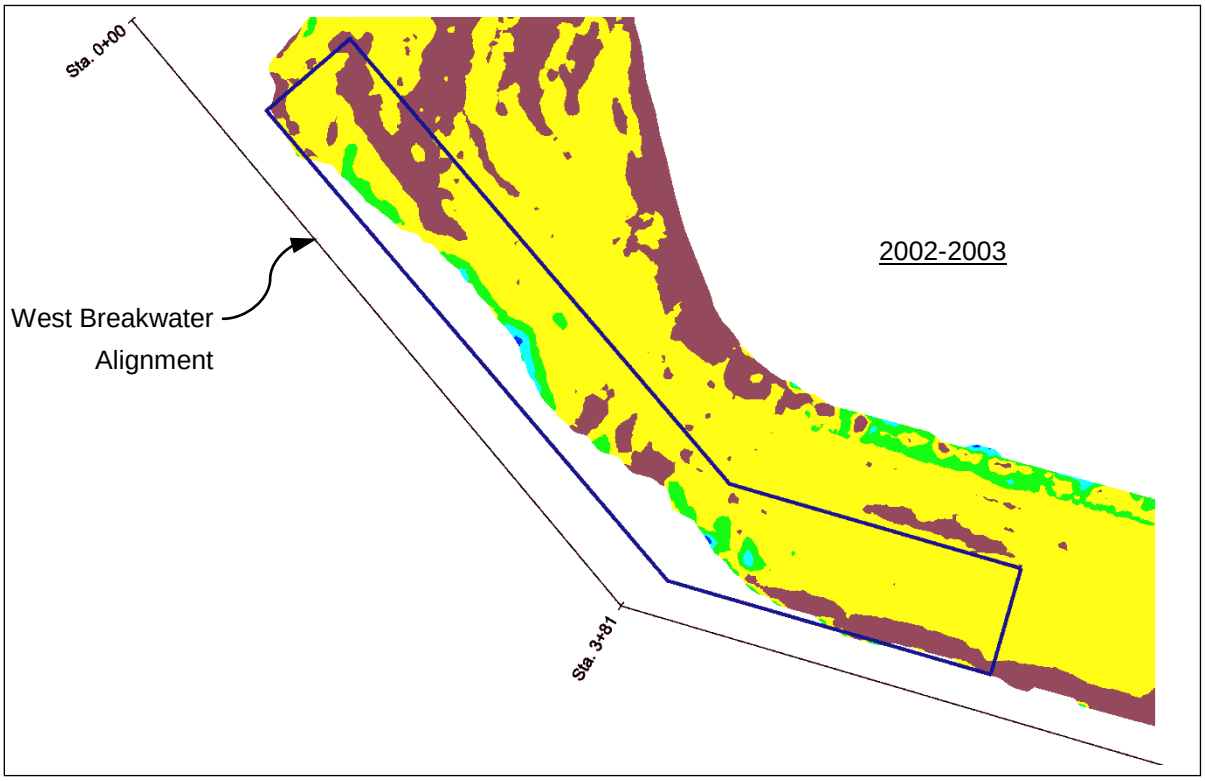

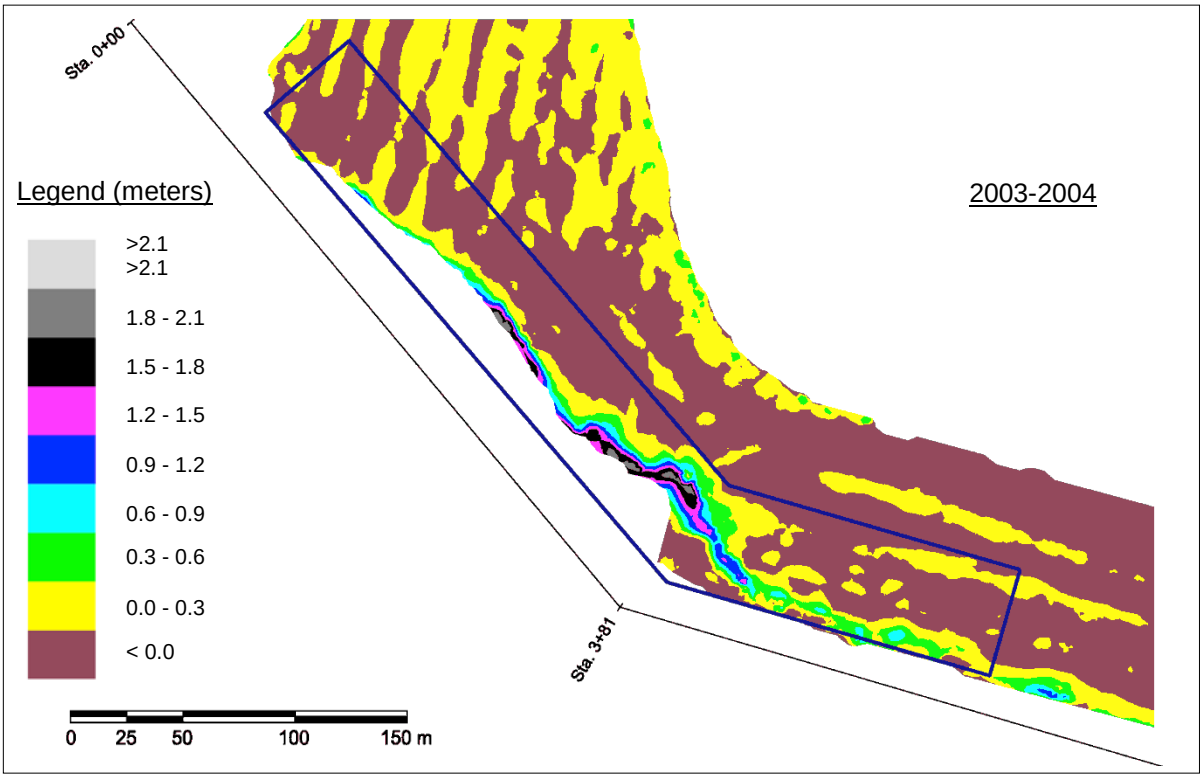

4.5 Simulation of morphologic change

The aerial photograph of Google Earth taken in 2005 (Figure 1) shows sand seepage through the breakwater and a shoal formation developed inside West Breakwater after the previous dredging cycle in 2000. The observed average annual sand deposition rate is approximately 3,500 and 6,000 cy/yr based on the maintenance dredging record in 2000 and the latest dredging event conducted in early 2009 (Table 8).

To estimate the volume of sediment seeping through the permeable West Breakwater, sediment transport through the breakwater and the morphologic change inside the breakwater were modeled by coupling of CMS-Flow and CMS-Wave. The simulations of sediment seepage were conducted for 1 yr from 18 November 2009 to 17 November 2010. The structure permeability was specified by adjusting the resistance parameters in the Forchheimer equation and the structure void factor in the conservation of mass equation (Li et al. 2013). Table 9 presents the pertinent model parameters and coefficients that were specified for flow and sediment seepage through the breakwaters; the hydraulic resistance coefficients *a* and *b* were determined by using a void factor of 0.2 and a rock size of 1.5 m (4.9 ft), which is approximately equivalent to a 6-ton riprap stone.

Table 9. Calibrated structure parameters and coefficients for CMS-Flow.

Structure Parameter	Value
Void Factor (Porosity) *n'*	0.2
Resistance Coefficient *a*	0.0016
Resistance Coefficient *b*	0.7304

Figure 67 shows the morphologic change adjacent to the West Breakwater at the end of the 1 yr simulation. Sand transport within structure cells is greatly reduced by weaker flow, lower wave energy, and subsequent smaller bottom stresses. As a result, the majority of deposition occurs within the breakwater as show in Figure 67. The calculated morphology changes indicate 0.7 to 0.8 m (2.3 to 2.6 ft) of sediment accumulation inside the harbor along the West Breakwater.

The morphology and total sediment volume changes were calculated at the end of the simulation within a polygon area north of the West Breakwater inside the harbor (Figure 67). The CMS results show an annual sediment deposition rate of 3,400 cy/yr in the lee of the West Breakwater, which is quantitatively comparable to the average annual volume dredged in 2000 but significantly less than that dredged in 2009.

Figure 67. Morphology change at the end of the 1 yr simulation. The blue line denotes the area where bed volume change was estimated, and the red dot is the location where time series of depth change was plotted.

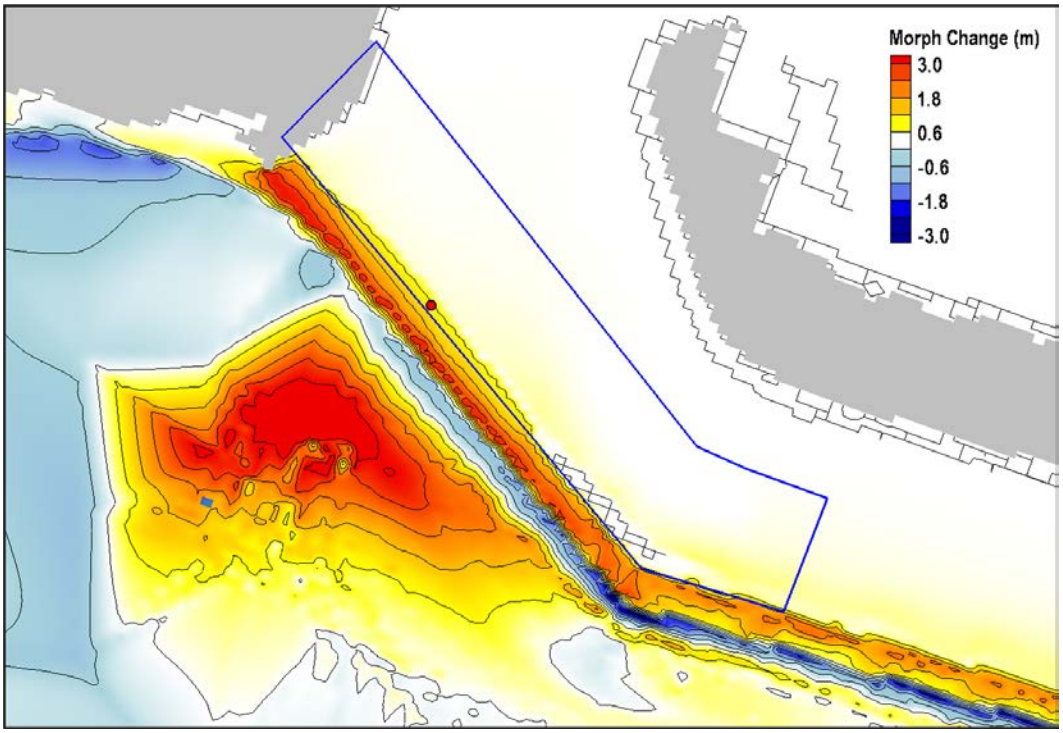

A sensitivity test was conducted by adjusting rock size and void factor for sediment seepage through the breakwater and sedimentation in the navigational channel. The test includes a 10-day simulation (18–27 November 2007) to examine changes in sediment seepage through structures in response to breakwater parameter changes. Table 10 presents the comparison of the computed 10-day sedimentation for varying rock sizes and void factor values. The results indicate that proper representation of structure porosity in the simulations can reproduce the correct amount of sediment seepage through a structure.

Table 10. Comparison of computed 10-day sedimentation.

Porosity	Size of Riprap Stones (m)	
	1.5	2.0
0.2	166 cy	187 cy
0.4	168 cy	193 cy

Based on the above sensitivity results, the 1 yr simulation was rerun with larger rock size. However, the annual seepage rate did not show any improvement. Temporal changes of depth at a location inside the harbor (Figure 68) indicate that sediment has a rapid accumulation rate in the

first 2 months and reaches the equilibrium state after 5 months of the simulation. For a longer term simulation, the sediment seepage rate through a structure would not change significantly in response to the change in porosity parameters if an equilibrium state between sediment seepage and structure storage capacity has been reached.

Figure 68. Depth change at the location inside the West Breakwater.

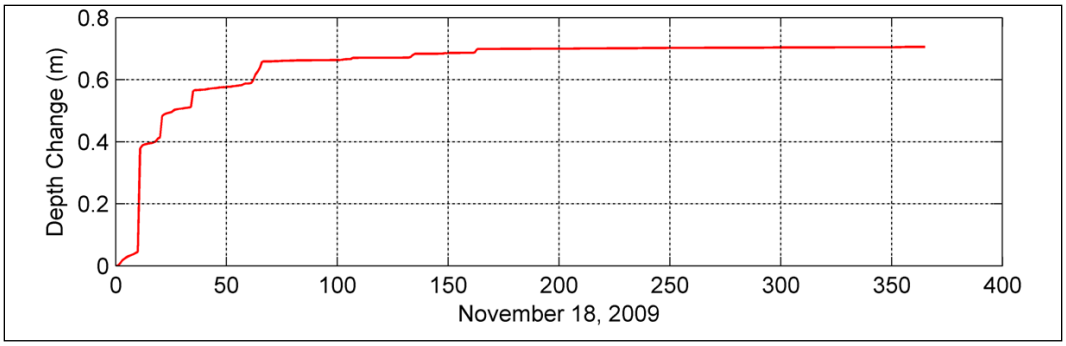

The difference in sediment accumulation between the dredging volumes and model results can be caused by the following reasons: 1) structure porosity properties are not properly represented in the transport equations, 2) lack of the more detailed dredge information, for example, covered areas of dredging operations may not overlap with the polygon area in Figure 67, and 3) lack of information on fine material brought into the navigation channel by the drainage system.

As part of the sensitivity analysis, the impact of the shoaling on sediment seepage through the breakwater was examined using the bathymetric information prior to the 2009 dredging cycle (Figure 64). For the 10-day simulation, the amount of sediment deposition in the lee of the West Breakwater was computed to be approximately 140 cy. It is a 15% decrease comparing to the model results with the immediate postdredging bathymetry in Table 10, which indicates that the predredging period corresponds to a lower sediment seepage rate through the West Breakwater.

5 Particle Tracking Modeling

The CMS calculates water levels, currents, and waves through the coupling of CMS-Flow and CMS-Wave. CMS-Flow is driven by time-dependent water surface elevation at the offshore open boundaries and wind forcing over the surface boundary. Directional wave input spectra are specified at the seaward boundaries for CMS-Wave. Figure 69 illustrates the calculated water circulation patterns in the harbor and adjacent areas during the flood and ebb cycles.

Using CMS-Flow and CMS-Wave simulation outputs, a PTM can be applied to track neutrally buoyant or sediment particle movements to assess water circulation, sediment transport, and water-quality related issues. The periodically precalculated hydrodynamic and wave field from a CMS simulation allows for simultaneous executions of PTM.

5.1 PTM description

The PTM is a Lagrangian-based particle transport model and designed to determine the fate and pathways of sediments and other waterborne particulates, chemicals, debris, biota, etc., for dredging operations and coastal engineering applications. In a complex hydrodynamic and wave environment, particles are released from local sources such as dredging and placement sites, outfalls, and propeller wash (MacDonald et al. 2006; Demirbilek et al. 2008).

In the PTM, particle movements are represented by the following equation:

$$\frac{dX}{dt} = U_A + U_D \tag{8}$$

where X, U_A, *and* U_D are vectors; X defines the position in three dimensions, x, y, and z, of a particle; U_A and U_D are the advection and diffusion velocities, respectively. The estimate of the turbulent diffusion coefficient in U_D is also used to drive a random walk model.

Figure 69. Water circulation patterns.

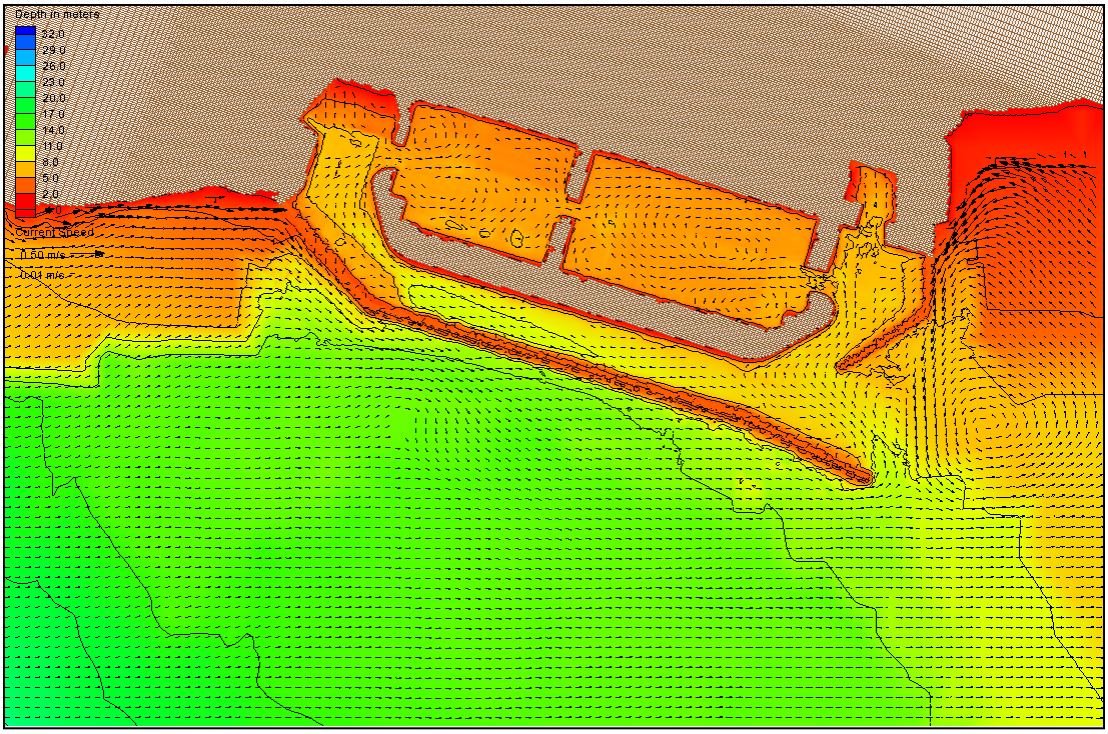

Flood-Tide Condition

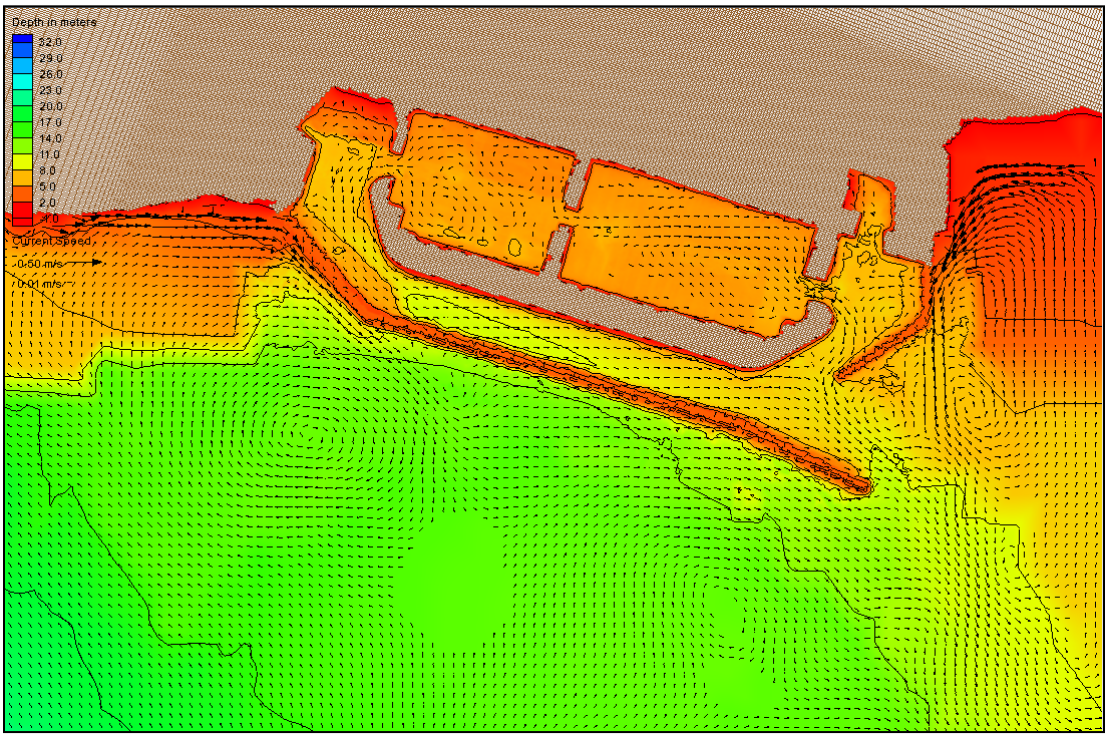

Ebb-Tide Condition

A particle position at time $t + dt$ is solved using a second-order predictor-corrector technique which is implemented in two stages. Taking the x component in Eq.8 as an example, the first stage is to predict the particle position one-half time-step ($n + 1/2$) into the future, $x_{n+1/2}$, based on the particle position at the present (x_n):

$$x_{n+1/2} = x_n + \frac{1}{2}(u_{Ax}dt + u_{Dx}dt) \tag{9}$$

where u_{Ax} and u_{Dx} are the x-direction advection and diffusion velocities at the present location x_n, respectively. The second stage is to obtain the particle position at the full time-step (x_{n+1}):

$$x_{n+1} = x_n + u_{Ax,n+1/2}dt + u_{Dx,n+1/2}dt \tag{10}$$

where $u_{Ax,n+1/2}$ and $u_{Dx,n+1/2}$ are the x-direction advection and diffusion velocities at time-step n+1 and n+1/2, respectively.

The PTM includes processes vital to sediment particle transport such as settling, deposition, resuspension, and hiding and exposure function. Similar to CMS-Wave and CMS-Flow, PTM was operated in the Surface-water Modeling System (SMS), which provides a robust, user-friendly interface for model setup, model execution, data analysis, and postprocessing.

5.2 PTM simulations

The PTM simulations were performed using the flow field obtained from the CMS-Flow simulation during the same calibration period (i.e., 19–27 November 2009). A total of 1080 neutrally buoyant particles were released for each simulation inside the Dana Point Harbor. Because a particle pathway depends strongly on tidal conditions (flood or ebb) after its release, the hourly release lasted for 12 hr to cover the semidiurnal tidal period. To optimize the evaluation of water quality issue at Baby Beach and the particle movement within the harbor, three local particle sources where the particles were released were selected. Two are located at Baby Beach (in the east and west areas) and the third one is in the main navigation channel. Figure 70 illustrates the three locations where the particles were released in the PTM simulations.

Figure 70. Local sources of particle release in Dana Point Harbor.

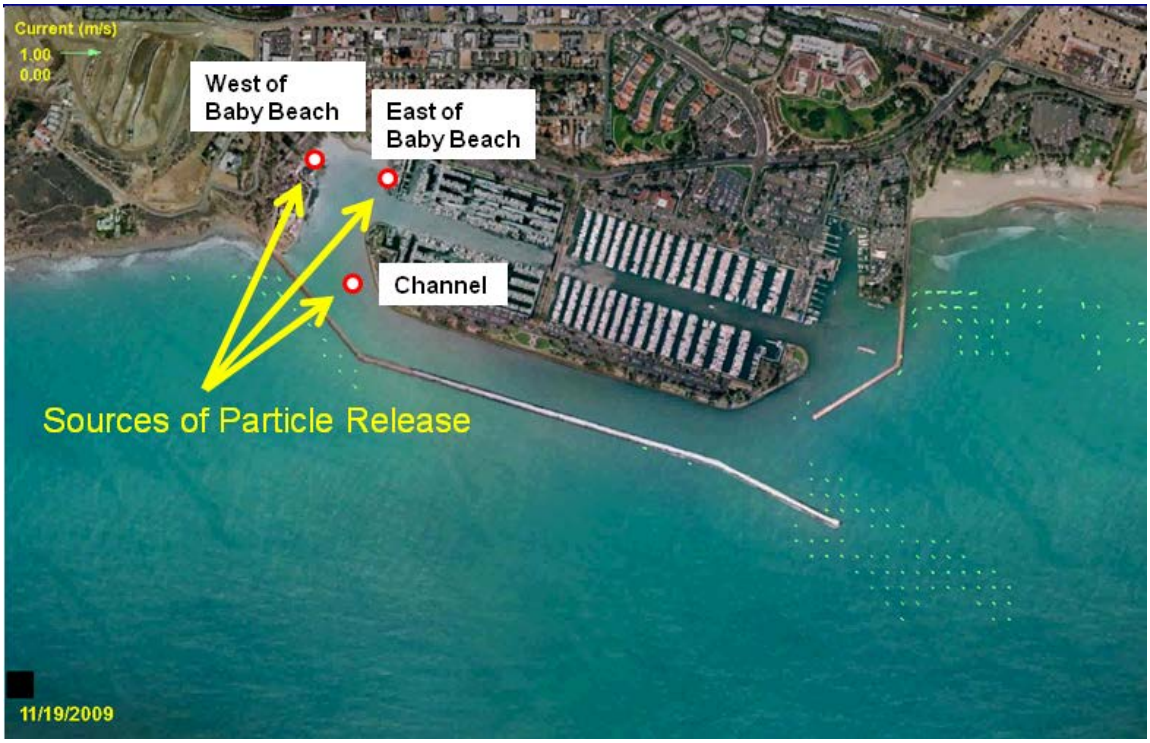

Particle pathways and fate were compared after their release at three aforementioned locations. Figures 71 to 73 show the particle distributions at the Dana Point Harbor 2 days after particles were released at west, east Baby Beach and in the navigation channel, respectively. Figure 71 shows that most of the released particles at west Baby Beach are still residing inside the harbor while a small percentage of particles is moved out of the harbor and into the open water. A cluster of particles can still be detected at Baby Beach. The flood tides bring in water/particles that subsequently are trapped in the beach area, as the previous wet cells consequently become isolated drying cells during ebb tides. Released from east Baby Beach, most of the particles are also staying inside the harbor (Figure 72) although the particle distribution pattern appears to be slightly different. More particles are found in the West Basin instead of the East Basin for the releasing location at east Baby Beach. Among the three release scenarios, the channel release shows that the harbor was retaining the fewest number of particles after 2 days.

Figure 71. Snapshot of particle distribution in Dana Point Harbor 2 days after the particle release at the west Baby Beach.

Figure 72. Snapshot of particle distribution in Dana Point Harbor 2 days after the particle release at the east Baby Beach.

Figure 73. Snapshot of particle distribution in Dana Point Harbor 2 days after the particle release in the Main Channel.

5.3 Residence times

After the 9-day simulations, the particles released from three local sources were tracked, and the residence times of particles were estimated, as presented in Table 11. The residence time is defined as the duration required for 67.7% of particles being moved out from the harbor into the open water. It is a common criterion used to measure the relatively tidal flushing capability within a subject harbor. For the two release locations at Baby Beach, more than 60% of particles are still in the harbor at the end of the 9-day simulations. In other words, the residence time of particles released at Baby Beach would be much longer than 9 days. The residence time of particles released at the channel location is approximately 5 days. The calculated flow field in the harbor indicates relatively stronger tidal currents at this location. As a result, a much shorter residence time is expected.

Table 11. Number of particles leaving Dana Point Harbor after release at Baby Beach.

Release Location	West of Baby Beach				East of Baby Beach				Navigational Channel			
Day after Release	Particle	Accu. Particle	%	Accu. %	Particle	Accu. Particle	%	Accu. %	Particle	Accu. Particle	%	Accu. %
1	99	99	9.2	9.2	88	88	8.1	8.1	662	662	61.3	61.3
2	120	219	11.1	20.3	84	172	7.8	15.9	33	695	3.1	64.4
3	51	270	4.7	25.0	43	215	4.0	19.9	5	700	0.5	64.9
4	50	320	4.6	29.6	41	256	3.8	23.7	18	718	1.7	66.6
5	25	345	2.3	31.9	34	290	3.1	26.8	11	729	1.0	67.6
6	27	372	2.5	34.4	35	325	3.2	30.0	7	736	0.6	68.2
7	19	391	1.8	36.2	27	352	2.5	32.5	3	739	0.3	68.5
8	5	396	0.5	36.7	10	362	0.9	33.4	3	742	0.3	68.8

Note: total released particles =1080

6 Summary and Conclusions

A comprehensive condition survey was conducted for the dual breakwaters at Dana Point Harbor, CA, to assess the present-day structure conditions and their protective functionality against storm wave attack. In addition, a concurrent effort was performed to evaluate wave dynamics at the breakwaters, tidal hydrodyanmics and water circulation within the harbor, and sedimentation along the lee of West Breakwater via numerical simulations. Both numerical models CMS-Wave and CMS-Flow were improved to enhance the model capability in characterizing the permeability of the breakwaters.

A bathymetric and 3D LiDAR survey was conducted on 20–24 October 2009 to collect basic physical data including nearshore and in-harbor bathymetry and 3D images of breakwaters, revetments, Baby Beach, and other pertinent features in the harbor. The survey utilized the swath bathymetry system for the underwater portion and the laser scanning system for elevations above the water line.

Oceanographic data collection, including current speed and direction as well as wave height, was conducted by deploying two ADCPs at both sides of West Breakwater from 20 November 2009 to 15 January 2010. Improvement of CMS-Wave and CMS-Flow was achieved to allow breakwaters to act as permeable structures through which the capability of incident wave transmission, flow movement, and sediment seepage was incorporated in the model. Based upon the comprehensive condition survey, oceanographic data collection, and CMS numerical simulations, several findings are summarized in the following sections.

6.1 Conditions of breakwaters

The present-day structure conditions of the dual breakwaters were examined via the combination of reviewing the processed 3D LiDAR images and bathymetry and visual confirmation above the water line.

At West Breakwater, dislodged stones on the harbor side near Sta 00+97 and Sta 02+13 are detected below the water surface (Figure 6). In addition, displaced stones above the MSL are observed at Sta 15+54 and near the

head of West Breakwater (Figures 7 and 8). Nevertheless, the structure appears to function as originally designed for sheltering harbor facilities from west to northwest winter storm waves.

At East Breakwater, the structure remains intact and functions as a protective device for the normal operation of harbor activities. Some armor stones located below the water surface on the harbor side appear to be dislodged from their original positions (Figures 10 and 11).

6.2 Flow field conditions

Current data at various depths were collected from two ADCPs that were deployed at both sides of West Breakwater for a period of 8 weeks. Measured instantaneous current velocities are typically less than 6 cm/sec (0.20 ft/sec) in the main navigational channel (Figures 19–22) and on the order of 10 to 20 cm/sec (0.33 to 0.66 ft/sec) in the oceanside area of West Breakwater (Figures 23–29).

It is evident that currents moving through the rubble-mound structure occur throughout the West Breakwater, consistent with the original design of a semipermeable rubble-mound structure. A wide range of current direction, likely resulting from current flow across West Breakwater, was observed in the lower water column of the navigational channel during both flood and ebb tides (Figures 30 and 31). Influence of the through-breakwater currents appears weaker near the water surface. The ranges of recorded direction near water surface (Bin 4) are in the 90° to 120° sector for ebb tides (Figures 30 and 34) and primarily in the 210° to 270° sector during flood tides (Figures 31 and 35), respectively. For the flow field in the ocean side of West Breakwater, the currents that generally move toward southwest along the breakwater are relatively consistent throughout the vertical water column and differ slightly for both ebb and flood cycles (Figures 32 and 33).

6.3 Improvement of CMS models

The enhanced Coastal Modeling System was applied to evaluate circulation and wave conditions surrounding the Dana Point Harbor and to assess the wave transmission, flow penetration, and sediment seepage through the permeable breakwaters.

The capability of CMS-Wave was improved by allowing wave transmission through the breakwaters. Several model parameters such as forcing wind and tidal fluctuation were examined to assess their impact to the model simulations. The model performance marginally improves with the forcing of the offshore wind condition and temporal water levels. Inclusion of the wave reflection at the breakwaters substantially increases the model accuracy of wave height prediction seaward of the breakwaters (Table 5). In order to predict morphologic change and sedimentation in the main navigational channel, the capability of CMS-Flow was enhanced to account for flow penetration through the permeable breakwaters.

6.4 Storm wave characteristics

Storm wave conditions at the breakwaters were characterized based on the deepwater GROW wave hindcast data, spanning 39 yr (1970–2008), via wave transformation through offshore islands by a back-refraction spectral model and subsequently nearshore wave propagation using CMS-Wave.

The deduced wave characteristics for severe extratropical storms from 1970 to 2008 are comparable to peak storm wave heights that were previously used in the 1965 General Design Memorandum of Dana Point Harbor. The deduced extratropical peak wave heights at West Breakwater for three referred historic extratropical storms range from 4.3 to 4.9 m (14.1 to 16.1 ft). The maximum storm wave height simulated by CMS-Wave is 5 m (16.4 ft) during the 28 February 1983 storm event.

A recent study to assess likely winter wave height changes along the Southern California coast under various scenarios of future greenhouse gas emission, resulting in varying degrees of sea level rise, concluded that the intensity of future storms is expected to follow a slightly negative trend within the region as the winter cyclone track with a warmer climate tends to move farther north. Therefore, the extratropical storm wave characteristics deduced from the 1970–2008 period will be applicable in the future if any alteration or maintenance of the breakwaters is required.

6.5 Sedimentation and water circulation patterns

The CMS was validated by the measured waves, currents, and water surface elevations. The implementation of the algorithms for flow penetration and sediment seepage through the permeable breakwater was verified by the historical dredging information. In the 10-day model validation during a

neap tide period between 18 and 27 November 2009, the average current speed is in the range of 2 to 10 cm/sec (0.07 to 0.33 ft/sec) in the main navigational channel.

By applying and adjusting the parameters of the breakwater void factor and flow resistance, the cumulative morphologic change due to sediment transport through the permeable West Breakwater was estimated at the end of the 10-day simulation. An annual sediment deposition rate of 6,060 cy/yr was predicted from the linear extrapolation of the CMS results. This sediment transport rate is comparable to the volumes obtained from the 2009 maintenance dredging activity at Dana Point Harbor.

Sensitivity analysis was conducted by examining model forcing, structure permeability, and harbor shoaling. The CMS results indicate that the harbor is well protected by waves with a tide-dominated environment within the harbor and a wave-dominated environment in the open ocean. The permeability of West and East Breakwater may slightly change the current speed inside the harbor (Figures 59 and 63), but the circulation pattern is not affected by different specifications of the breakwater permeability. In other words, wave transmission through West Breakwater alters the circulation pattern slightly in the main navigational channel, but the effect is localized and inconsequential in the inner harbor (e.g., Baby Beach). The permeability of West Breakwater results in only little improvement of tidal flushing in the Baby Beach area.

The presence of a shoal in the lee of West Breakwater reduces the annual sedimentation rate by approximately 15% as compared to the sand deposition during the immediate postdredging period. The formed shoal results in relatively larger depth-averaged currents in the adjacent area. The overall harbor circulation pattern is not altered (Figures 59 and 64). The residence time in the harbor was estimated by a PTM. Depending on the particle release locations, the estimated residence time varies. For the two release locations at Baby Beach (i.e., the west and east ends), more than 60% of particles remain in the harbor at the end of a 9-day simulation. Therefore, any constituents situated in the Baby Beach area require much longer time than 9 days to flush approximately 67% (the residence time) out into the ocean. Conversely, the residence time of particles released in the main navigational channel is fewer than 5 days owing to better tidal flushing in the channel.

References

Buttolph, A. M., C. W. Reed, N. C. Kraus, N. Ono, M. Larson, B. Camenen, H. Hanson, T. Wamsley, and A. K. Zundel. 2006. *Two-dimensional depth-averaged circulation model CMS-M2D: Version 3.0, Report 2, sediment transport and morphology change*. ERDC/CHL-TR-06-7. Vicksburg, MS: U.S. Army Engineer Research and Development Center.

Cayan, D., M. Tyree, M. Dettinger, H. Hidalgo, T. Das, E. Maurer, P. Bromirski, N. Graham, and R. Flick. 2009. *Climate change scenarios and sea level rise estimates for the California 2009*. CA Water Plan Update 2009, Vol. 4 Reference Guide CEC-500-2009-014-F. Final Paper. California Climate Change Center.

County of Orange Parks. 2011. http://www.ocparks.com/danapointharbor/default.asp?Show=History

d'Angremond, K., J. W. Van der Meer, and R. J. de Jong. 1996. Wave transmission at low-crested structures. In *Proceedings, 25th International Conference on Coastal Engineering*, Orlando, FL. USA, ASCE, 2418–2427.

Demirbilek, Z., K. J. Connell, N. J. MacDonald, and A. K. Zundel. 2008. *Particle tracking model in the SMS10: IV. Link to Coastal Modeling System*. ERDC/CHL CHETN-IV-71. Vicksburg, MS: U.S. Army Engineer Research and Development Center. http://chl.erdc.usace.army.mil/chetn.

Demirbilek, Z., and J. Rosati. 2011. *Verification and validation of the Coastal Modeling System, report 1: Summary report*. ERDC/CHL TR-11-10.Vicksburg, MS: U.S. Army Corps of Engineers Research and Development Center.

Everest International Consultants. 2006. *Circulation improvement pilot project at Baby Beach, Dana Point, final report*. January 2006.

Forchheimer, P. H. 1901. Wasserbewegung durch Boden. *Zeitschrift des Vereines Deutscher Ingenieure* 50, 1781–1788.

Fugro West Inc. 2010. *USACE Dana Point Harbor breakwater comprehensive condition survey, field operation report*. May 2010.

Goda, Y. 1985. *Random seas and the design of maritime structures*. Hongo, Bunkyo, Tokyo: University of Tokyo Press.

Kuik, A. J., G. Ph. van Vledder, and L. H. Holthuijsen. 1988. A method for routine analysis of pitch-and-roll buoy data. *Journal of Physical Oceanography* 18: 1020–1034.

Leenknecht, D. A., A. Szuwalski, and A. R. Sherlock. 1992. *Automated coastal engineering system: User guide and technical reference, version 1.07*. Vicksburg, MS: U.S. Army Engineer Waterways Experiment Station.

Li, H., A. Sanchez, W. Wu, and C. W. Reed. 2013. *Implementation of structures in the CMS: Part I, rubble mound*. ERDC/CHL CHETN-IV-93. Vicksburg, MS: U.S. Army Engineer Research and Development Center.

Lin, L., Z. Demirbilek, H. Mase, J. Zheng, and F. Yamada. 2008. *CMS-Wave: A nearshore spectral wave processes model for coastal inlets and navigation projects*. ERDC/CHL-TR-08-13. Vicksburg, MS: U.S. Army Engineer Research and Development Center.

Lygre, A., and H. E. Krogstad. 1986. Maximum entropy estimation of the directional distribution of ocean wave spectra. *Journal of Physical Oceanography* 16(12): 1986.

MacDonald, N. J., M. H. Davies, A. K. Zundel, J. D. Howlett, T. C. Lackey, Z. Demirbilek, and J. Z. Gailani. 2006. *PTM: Particle Tracking Model; Report 1: Model theory, implementation, and example applications*. ERDC/CHL-TR-06-20. Vicksburg, MS: U.S. Army Engineer Research and Development Center.

Mase, H., H. Amamori, and T. Takayama. 2005. Wave prediction model in wave-current coexisting field. In *Proceedings, 12th Canadian Coastal Conference* (CD-ROM).

Orange County Resources and Development Management Department (OC RDMD). 2006. *Baby Beach in Dana Point Harbor, Orange County, final report, CBI grant nos. 19 and 260*. March 2006.

O'Reilly, W. C., and R. T. Guza. 1991. *Modeling surface gravity waves in the Southern California bight*. SIO Reference Series No. 19-25, September 1991.

O'Reilly W. C., and R. T. Guza. 1993. A comparison of spectral wave models in the Southern California Bight. *Coastal Engineering* 19(3): 263–282.

Science Application International Corporation (SAIC) and County of Orange Public Facilities and Resources Department. 2002. *Baby Beach circulation study sampling and analysis plan (SAP)*. September 2002.

SAIC. 2003a. *Data mining task for state of the beach report: Evaluation of bacteriological data and associated parameters for Baby Beach*. January 2003.

———. *2003b. Baby Beach circulation study final report*. March 2003.

———. *2003c. Baby Beach bacteriological special studies report*. June 2003.

———. *2003d. State of the beach report Baby Beach region, Dana Point Harbor*. June 2003.

Sidiropoulou, M. G., K .N. Moutsopoulos, and V. A. Tsihrintzis. 2007. Determination of coefficients a and b of the Forchheimer equation. *Hydrological Processes* 21 (4): 534–554.

Teledyne. 2006. *Acoustic Doppler Current Profile, principle of operation, a practical primer*. P/N 951-6069-00, November 2006.

USACE LAD. 1965. *Design Memorandum No. 1, General Design for Dana Point Harbor, Dana Point, California*. September 1965.

———. 1991. *Comprehensive condition survey, Dana Point Harbor*. Final Report, December 1991.

———. 1996. *Nearshore hydrodynamic factors and wave study of the Orange County coast, coast of California storm and tidal wave study South Coast Region, Orange County, Final Report No. 96-3*.

Weston Solutions, Inc. 2006. *Regional harbor monitoring program pilot project 2005-06 final report.* Prepared for the City of Dana Point.

Zundel, A. K. 2007. *Surface-water modeling system reference manual, Version 10.0*. Provo, UT: Brigham Young University Environmental Modeling Research Laboratory. http://www.ems-i.com/SMS/SMS_Overview/sms_overview.html.

Appendix A: ADCP Measurements

Figure A1. Week 2 – Bin 1 current measurements at Inside Gauge.

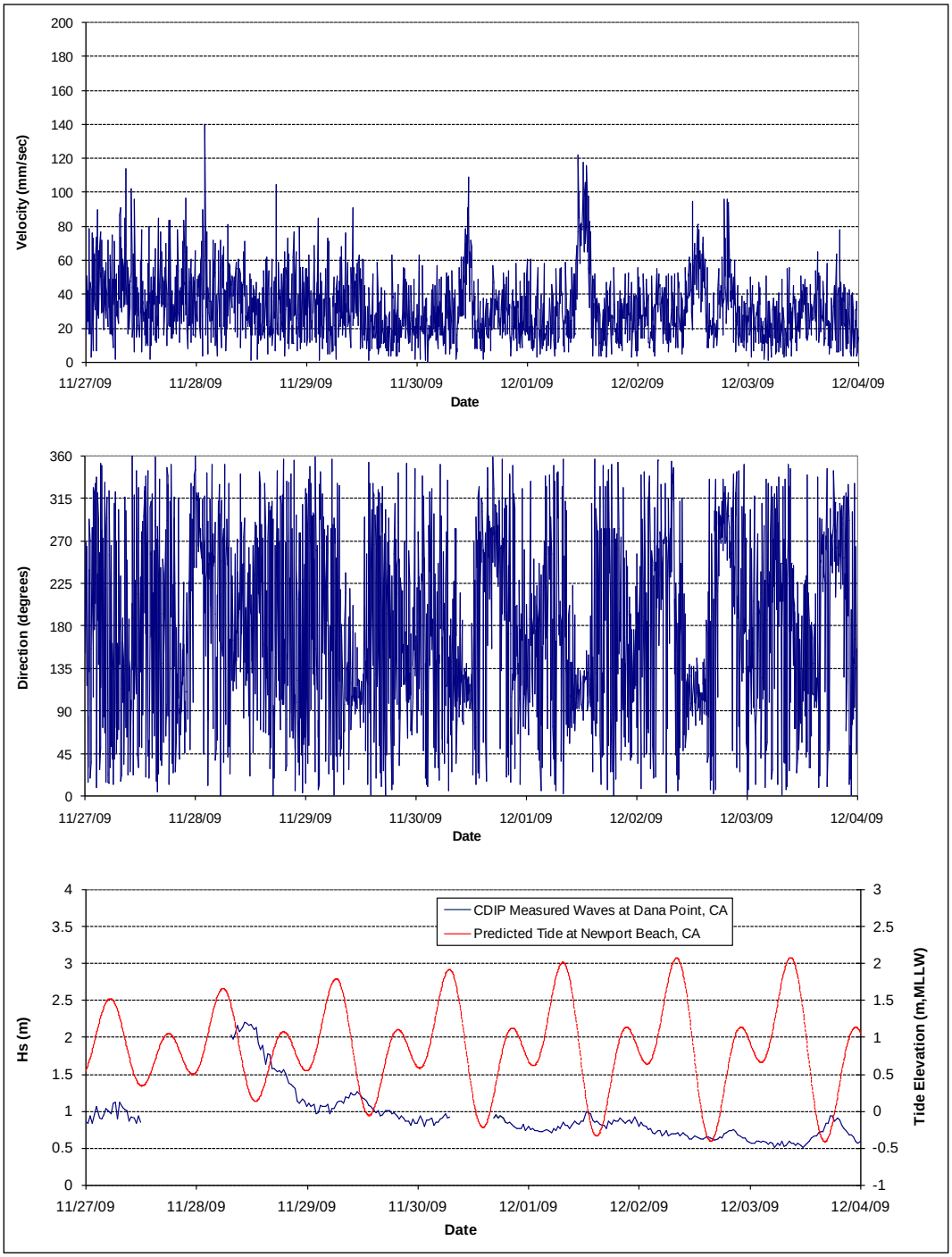

Figure A2. Week 2 – Bin 2 current measurements at Inside Gauge.

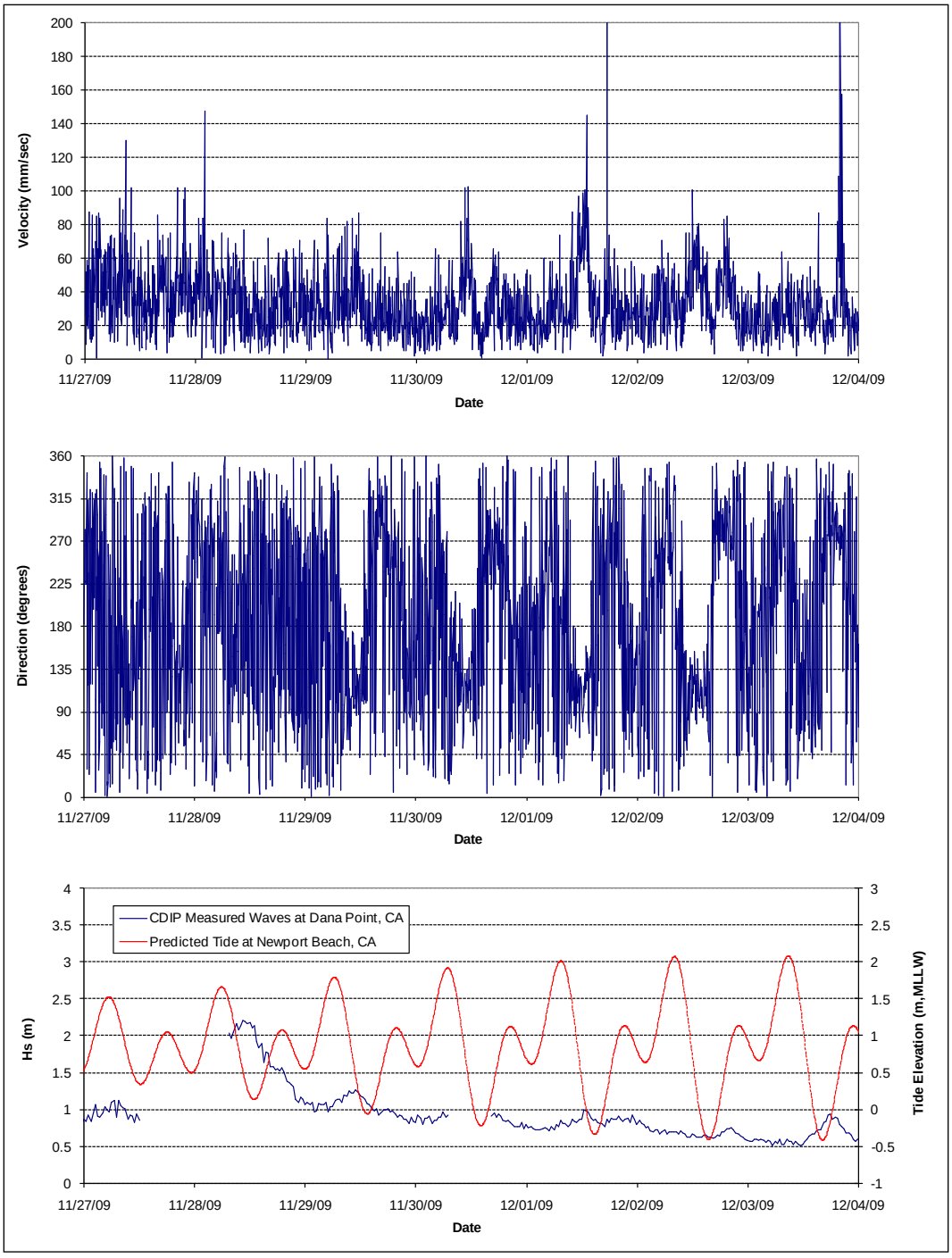

Figure A3. Week 2 – Bin 3 current measurements at Inside Gauge.

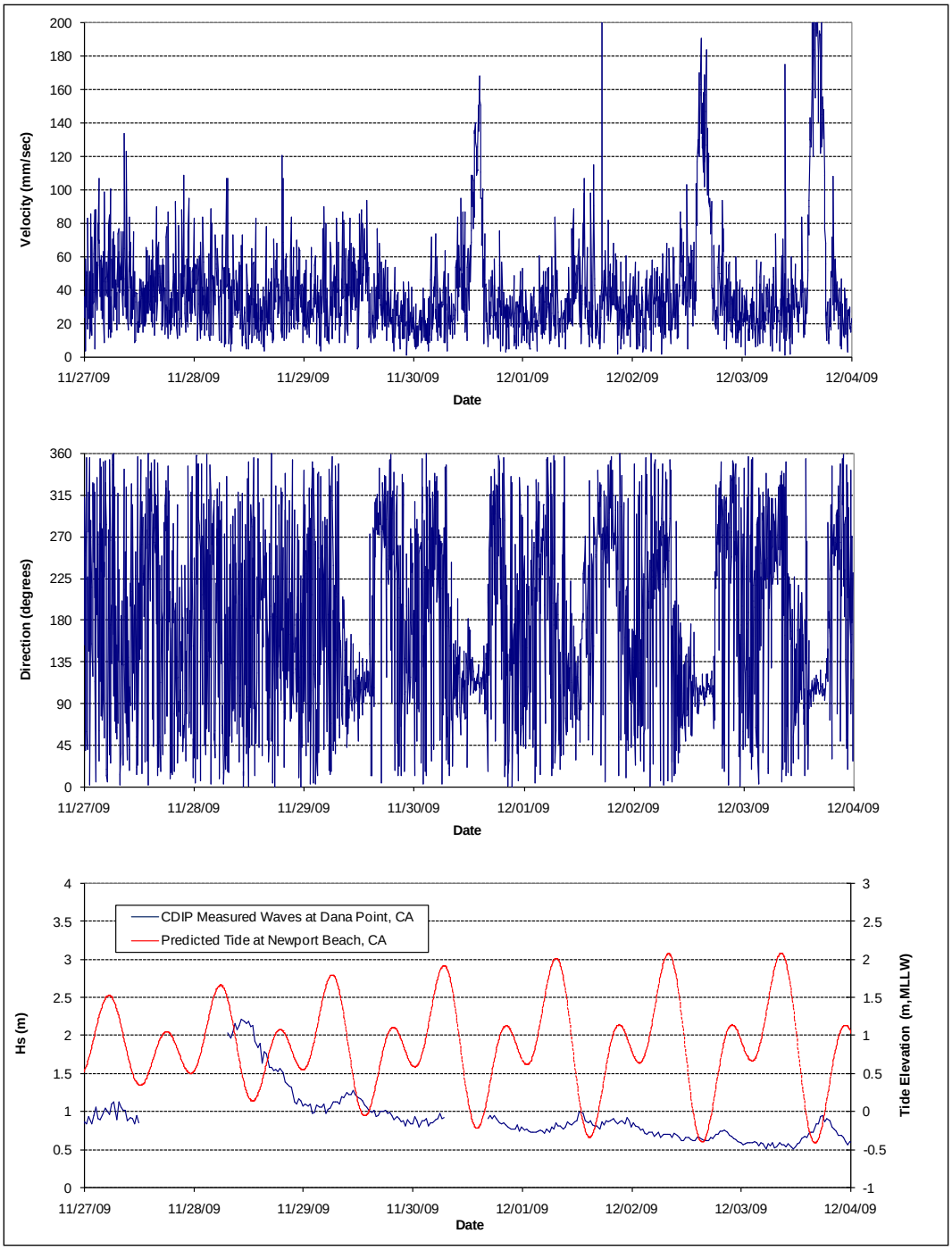

Figure A4. Week 2 – Bin 4 current measurements at Inside Gauge.

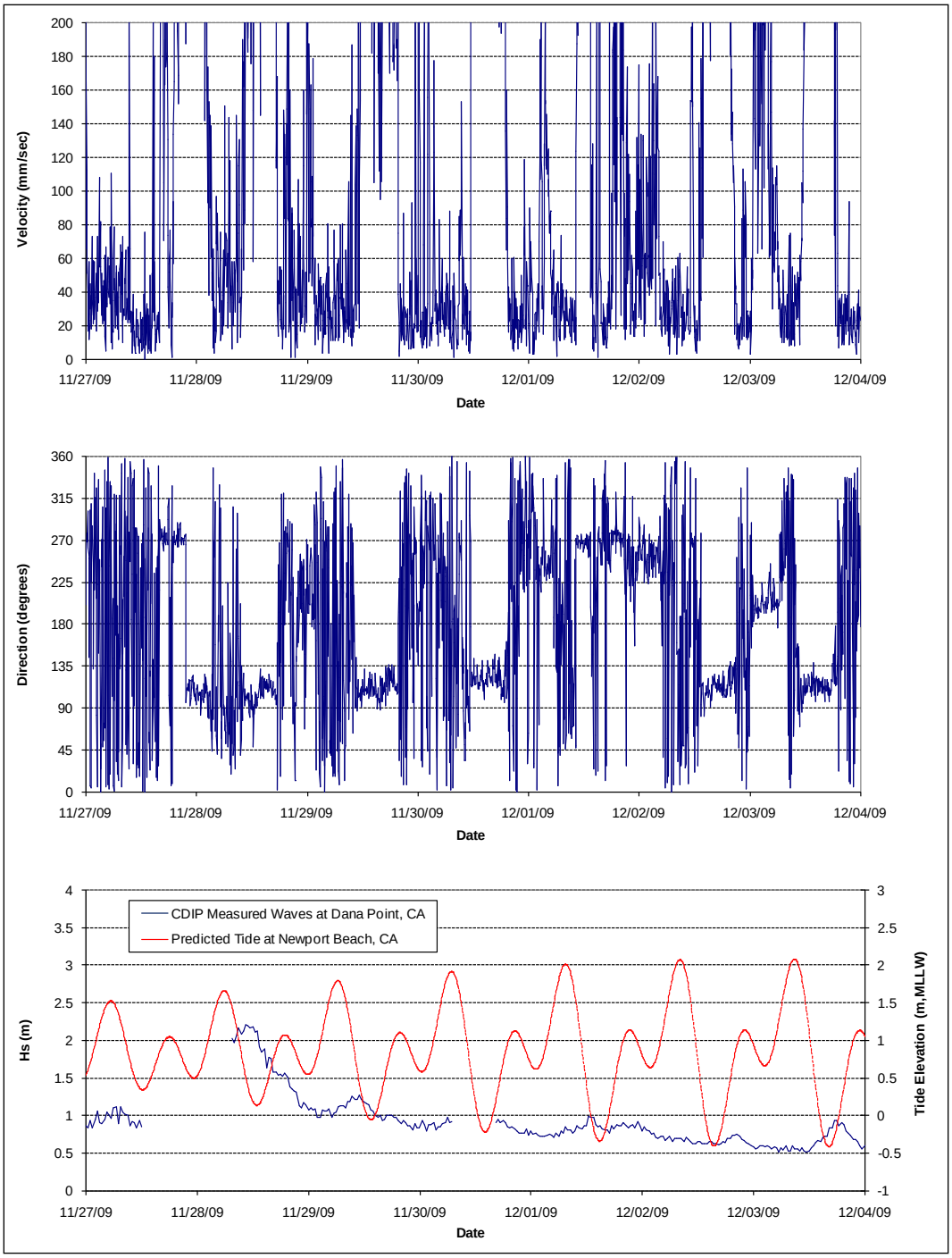

Figure A5. Week 3 – Bin 1 current measurements at Inside Gauge.

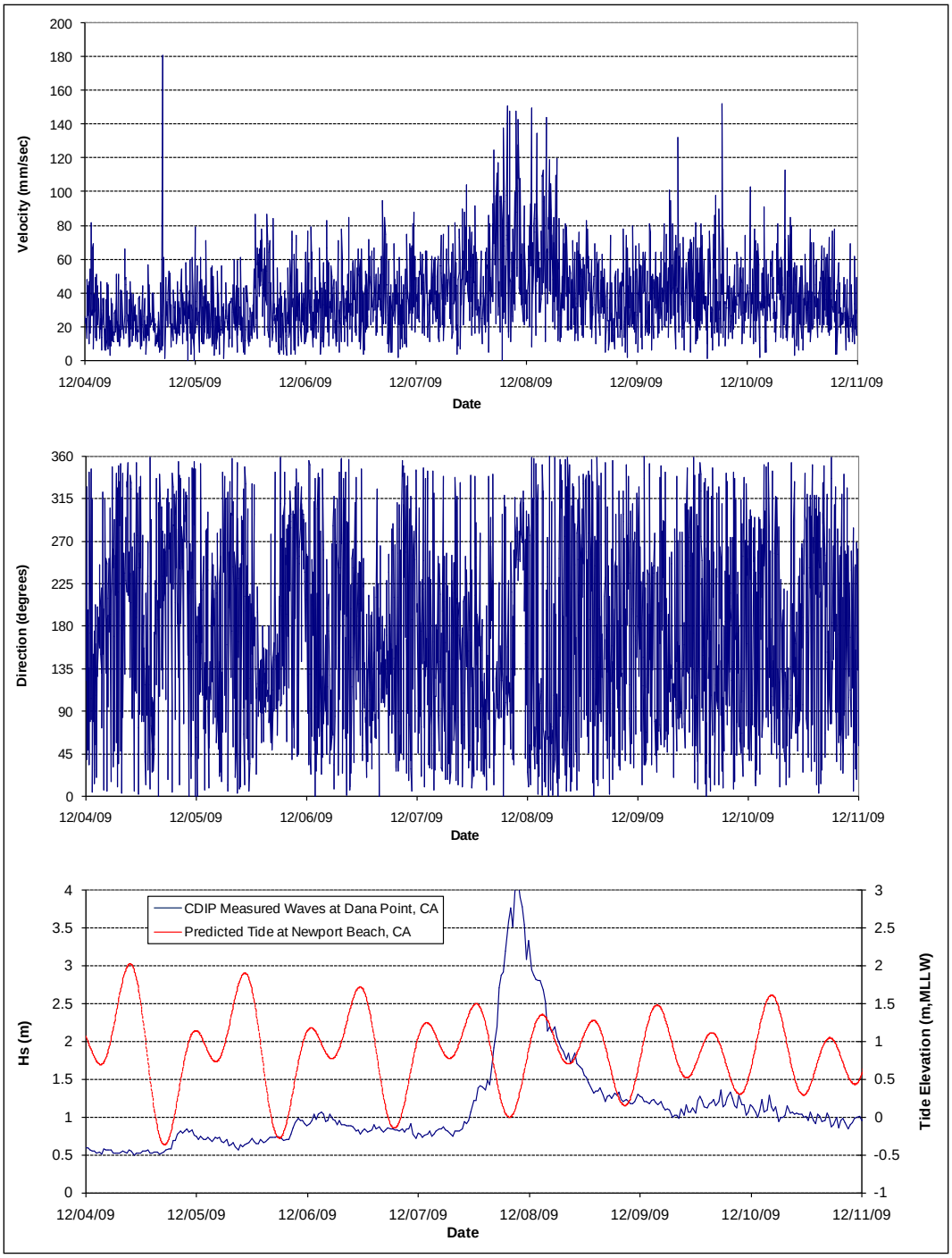

Figure A6. Week 3 – Bin 2 current measurements at Inside Gauge.

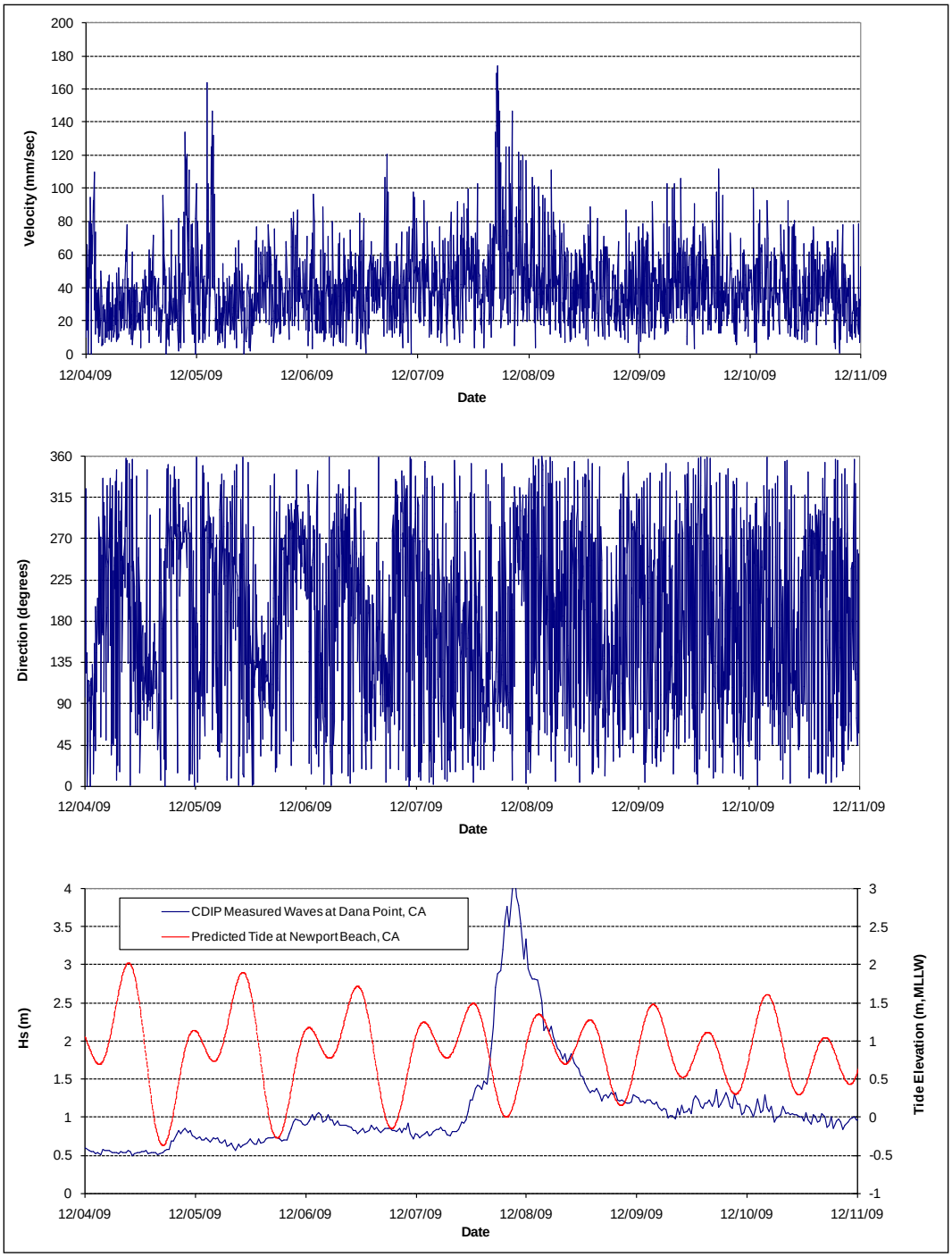

Figure A7. Week 3 – Bin 3 current measurements at Inside Gauge.

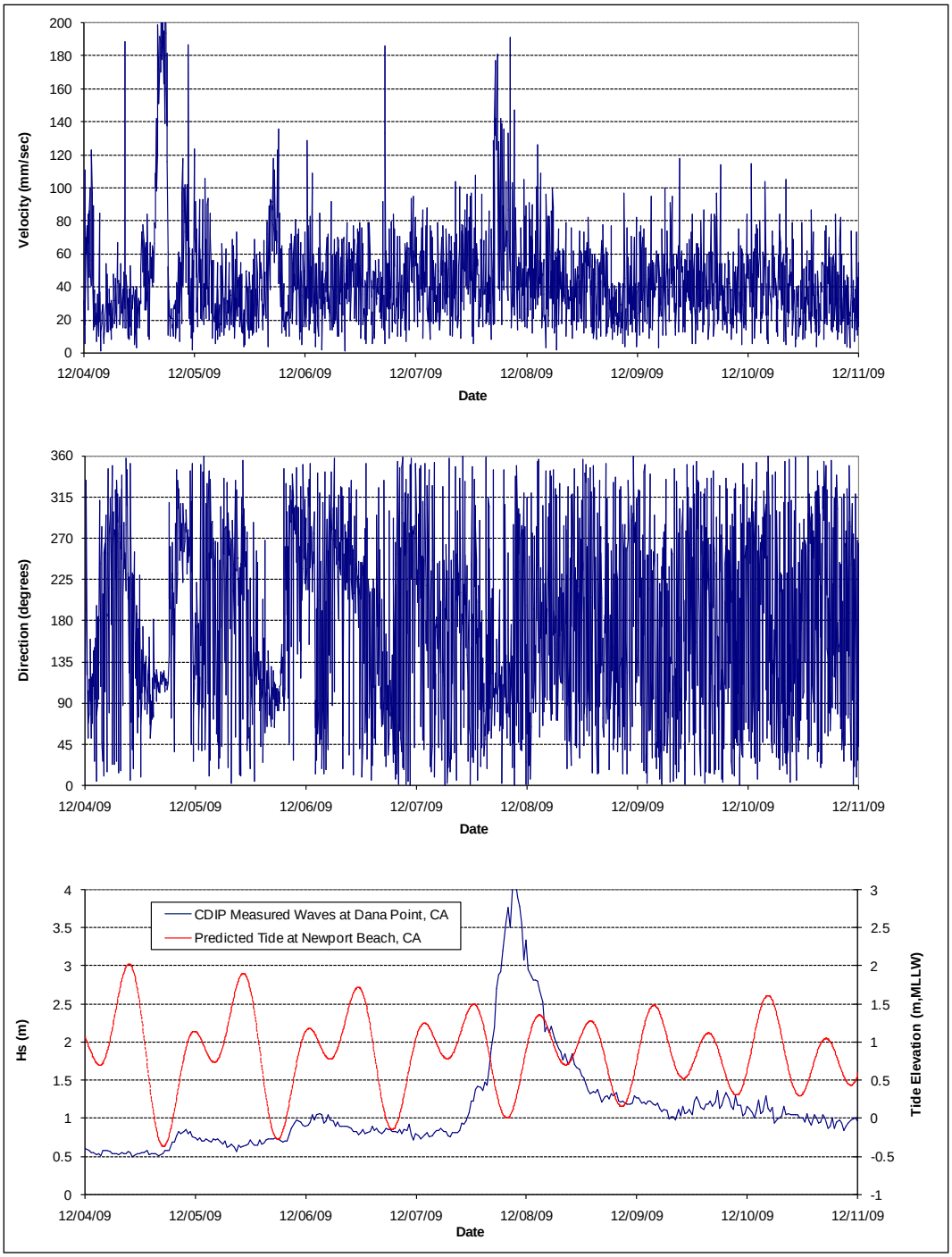

Figure A8. Week 3 – Bin 4 current measurements at Inside Gauge.

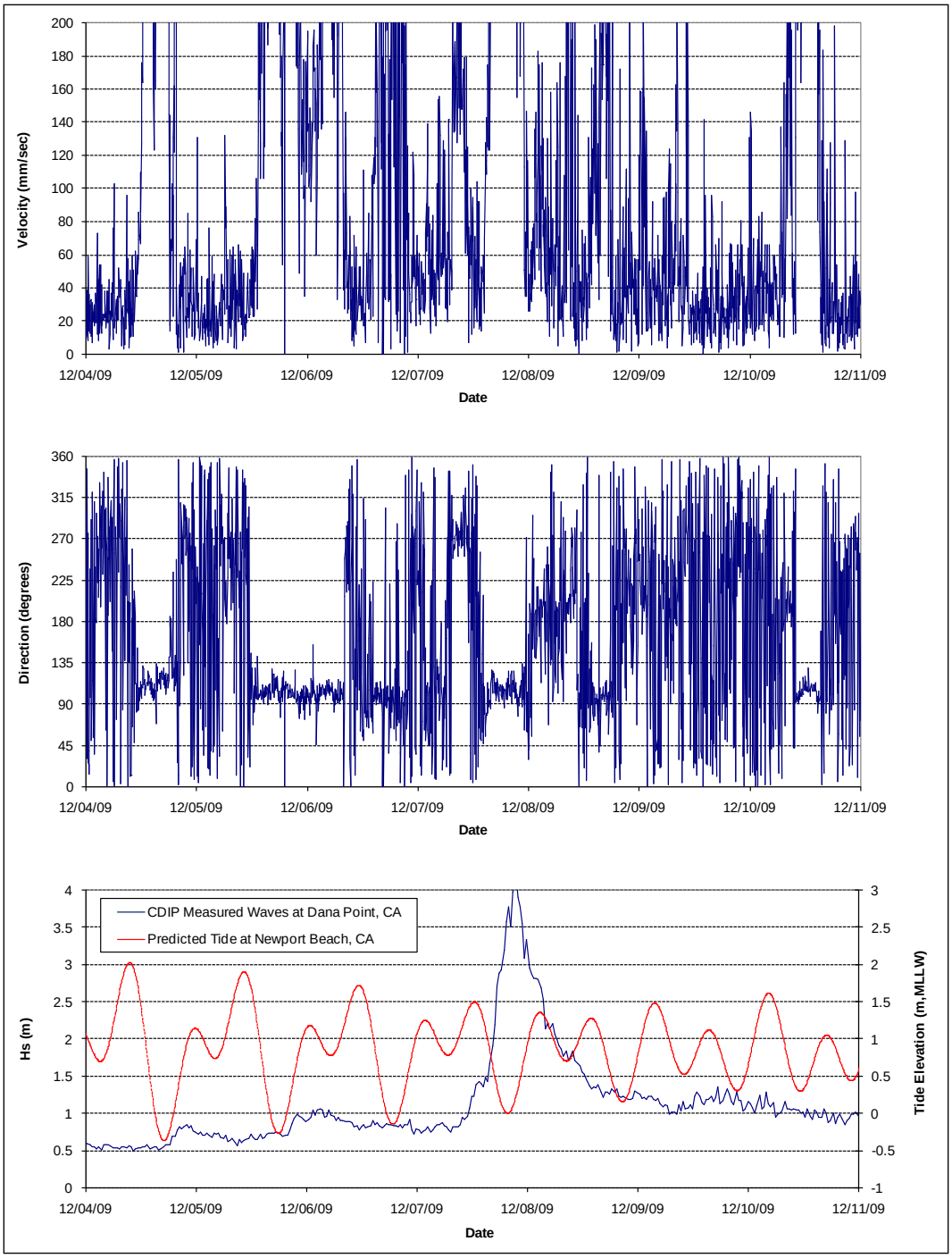

Figure A9. Week 4 – Bin 1 current measurements at Inside Gauge.

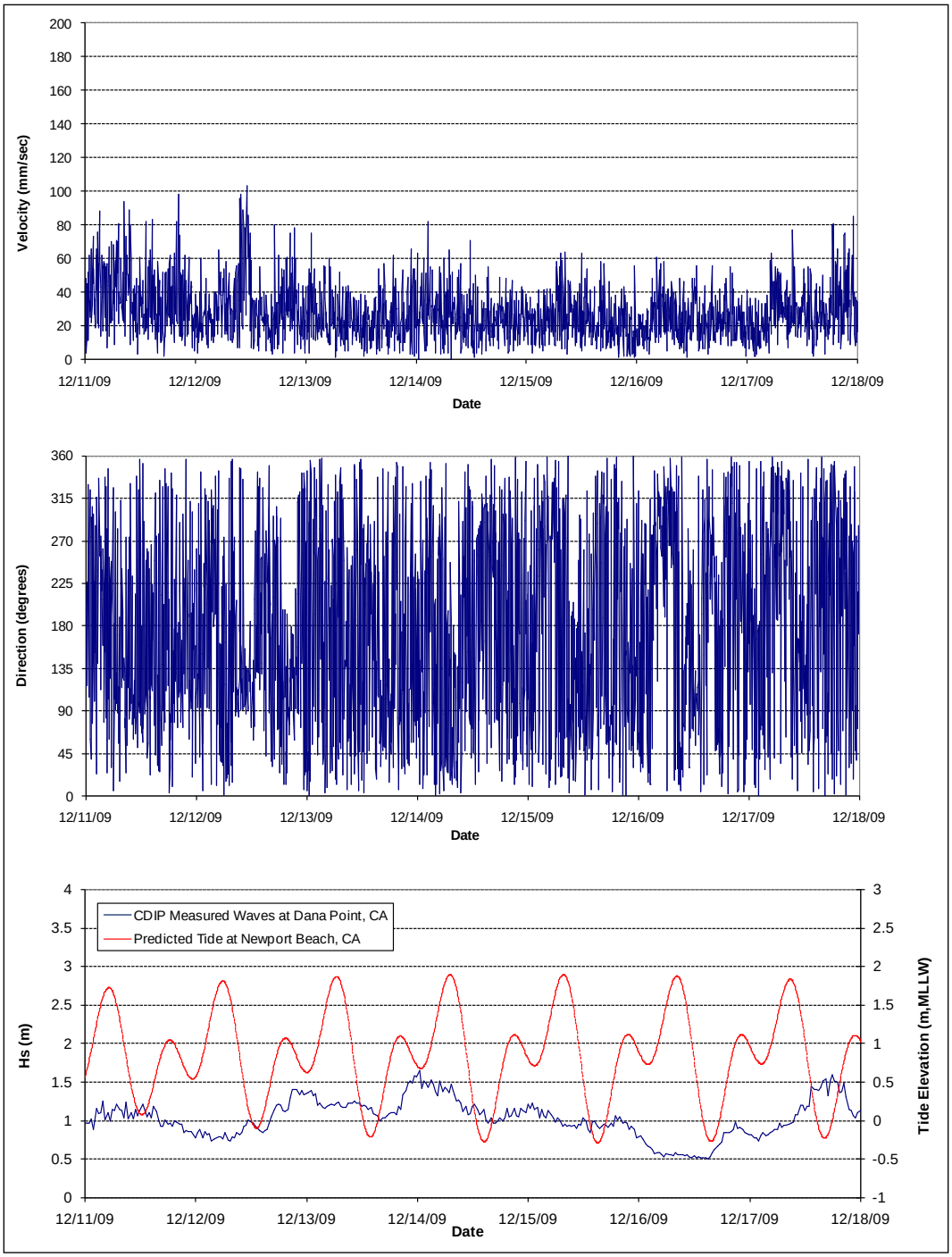

Figure A10. Week 4 – Bin 2 current measurements at Inside Gauge.

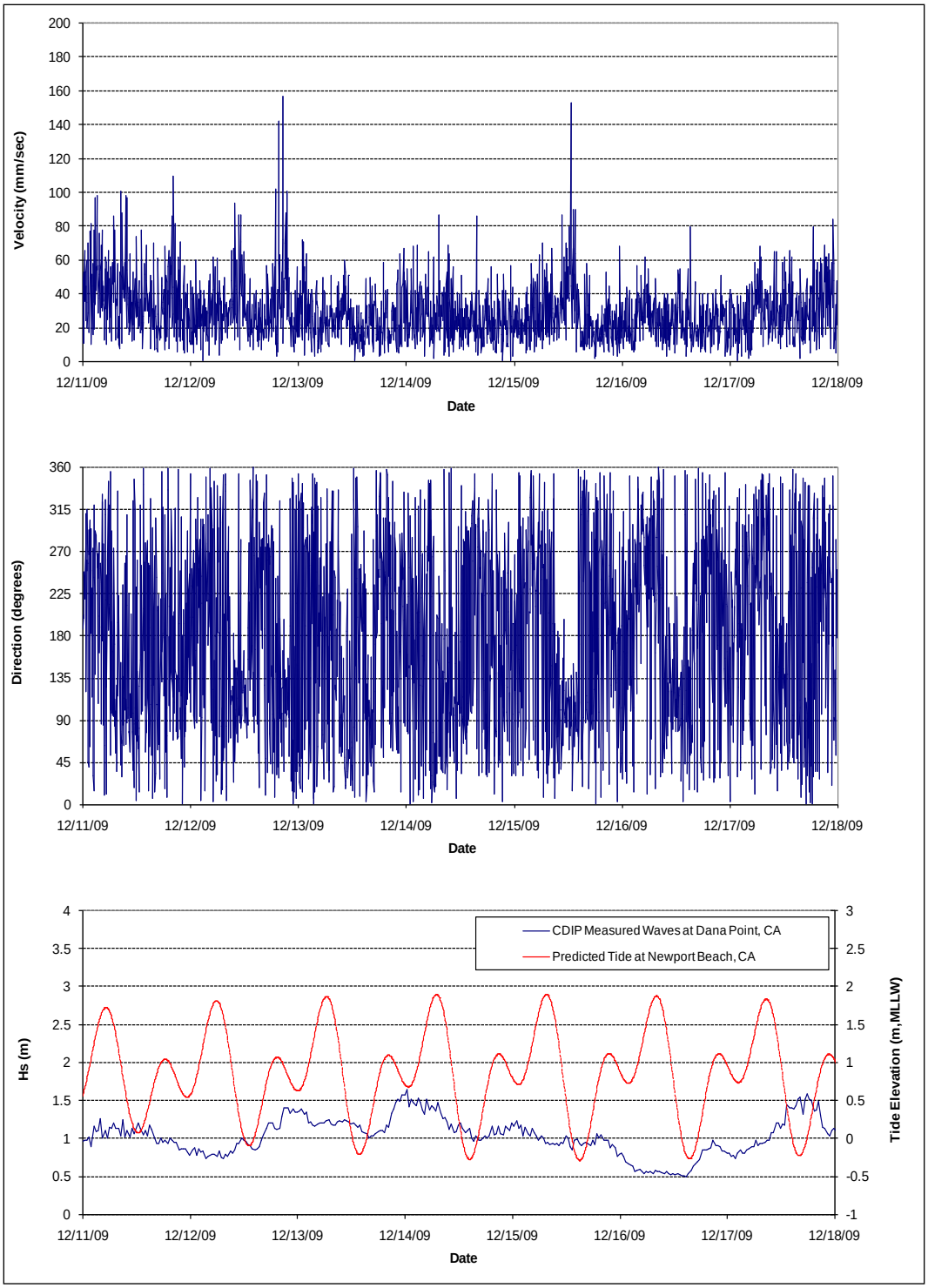

Figure A11. Week 4 – Bin 3 current measurements at Inside Gauge.

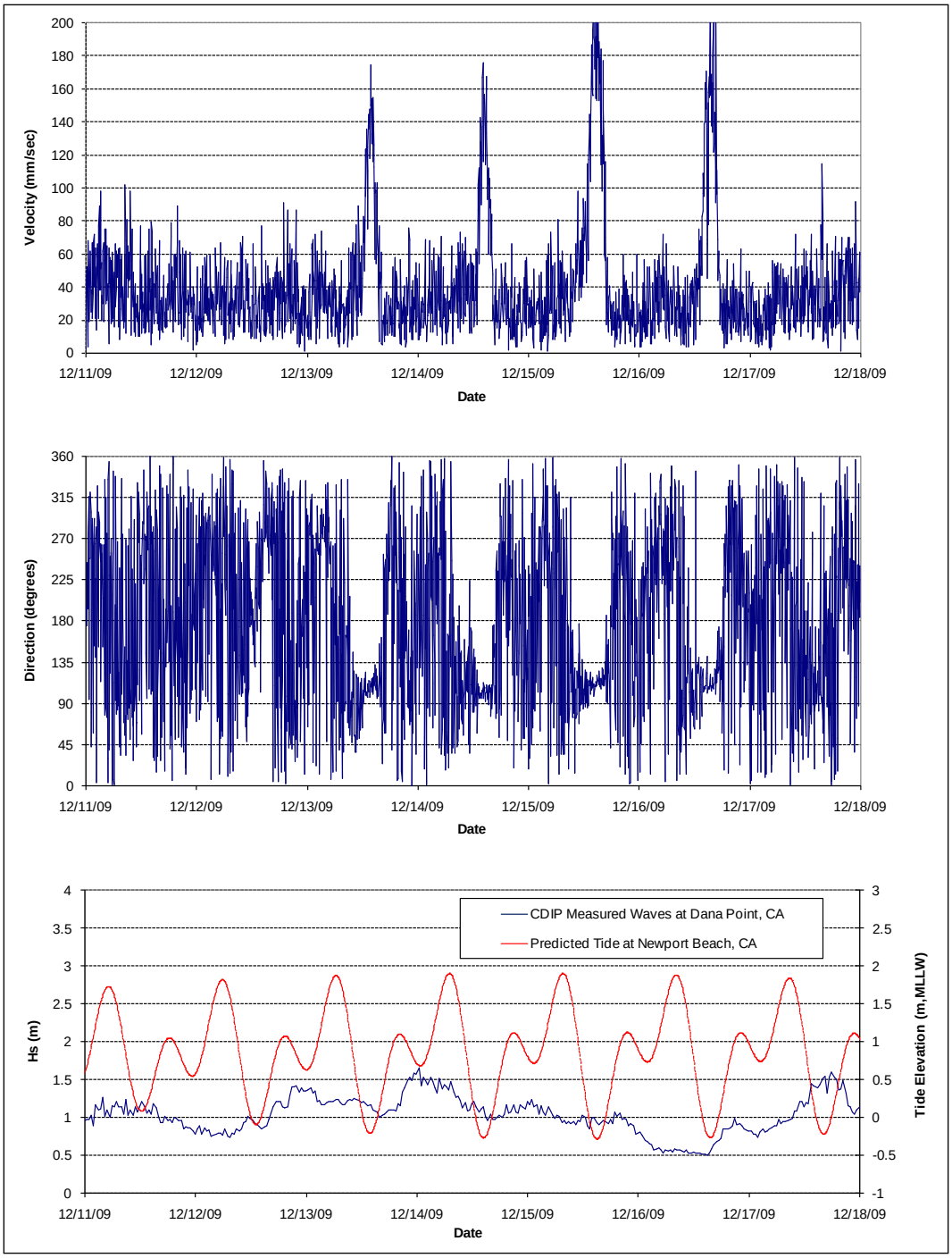

Figure A12. Week 4 – Bin 4 current measurements at Inside Gauge.

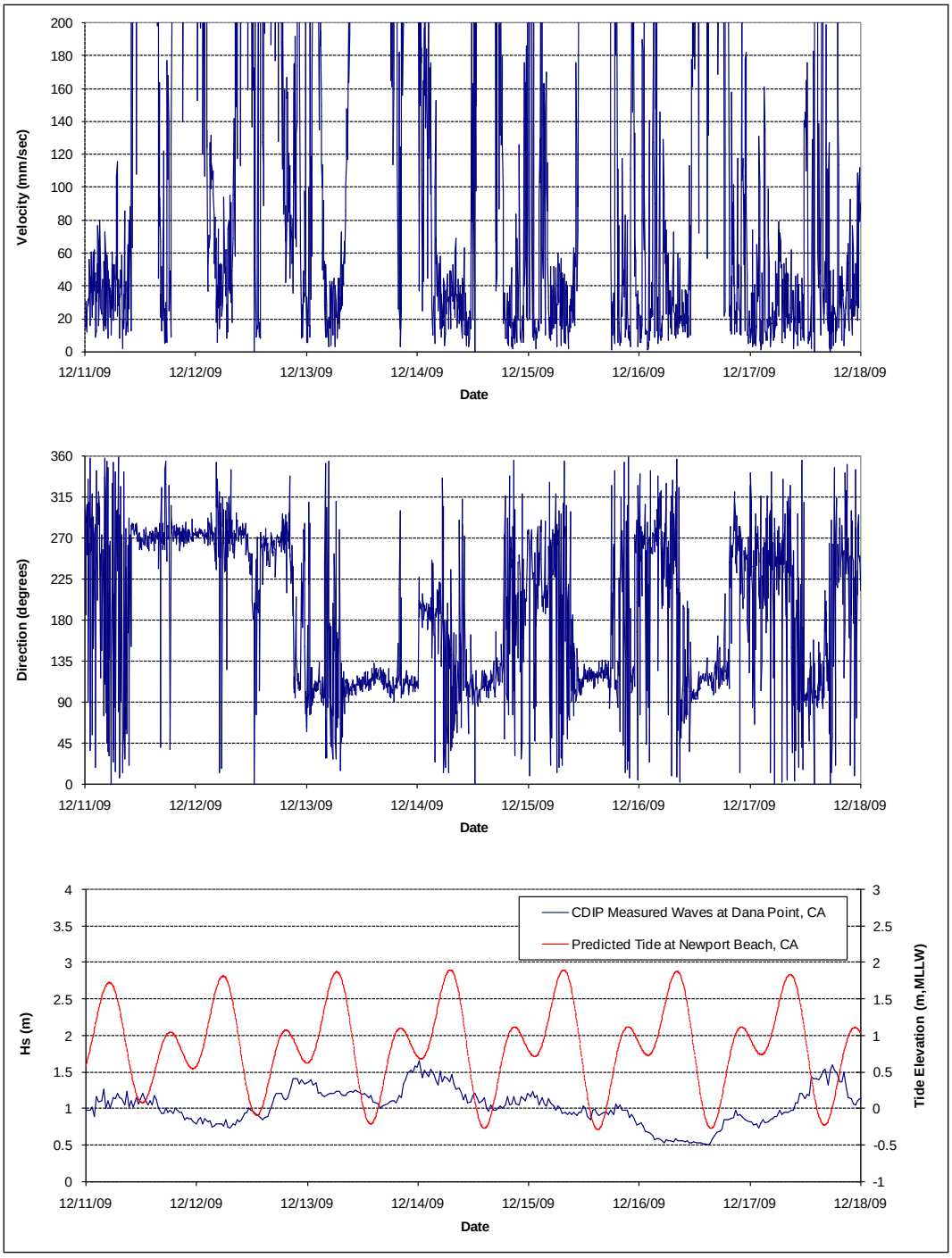

Figure A13. Week 5 – Bin 1 current measurements at Inside Gauge.

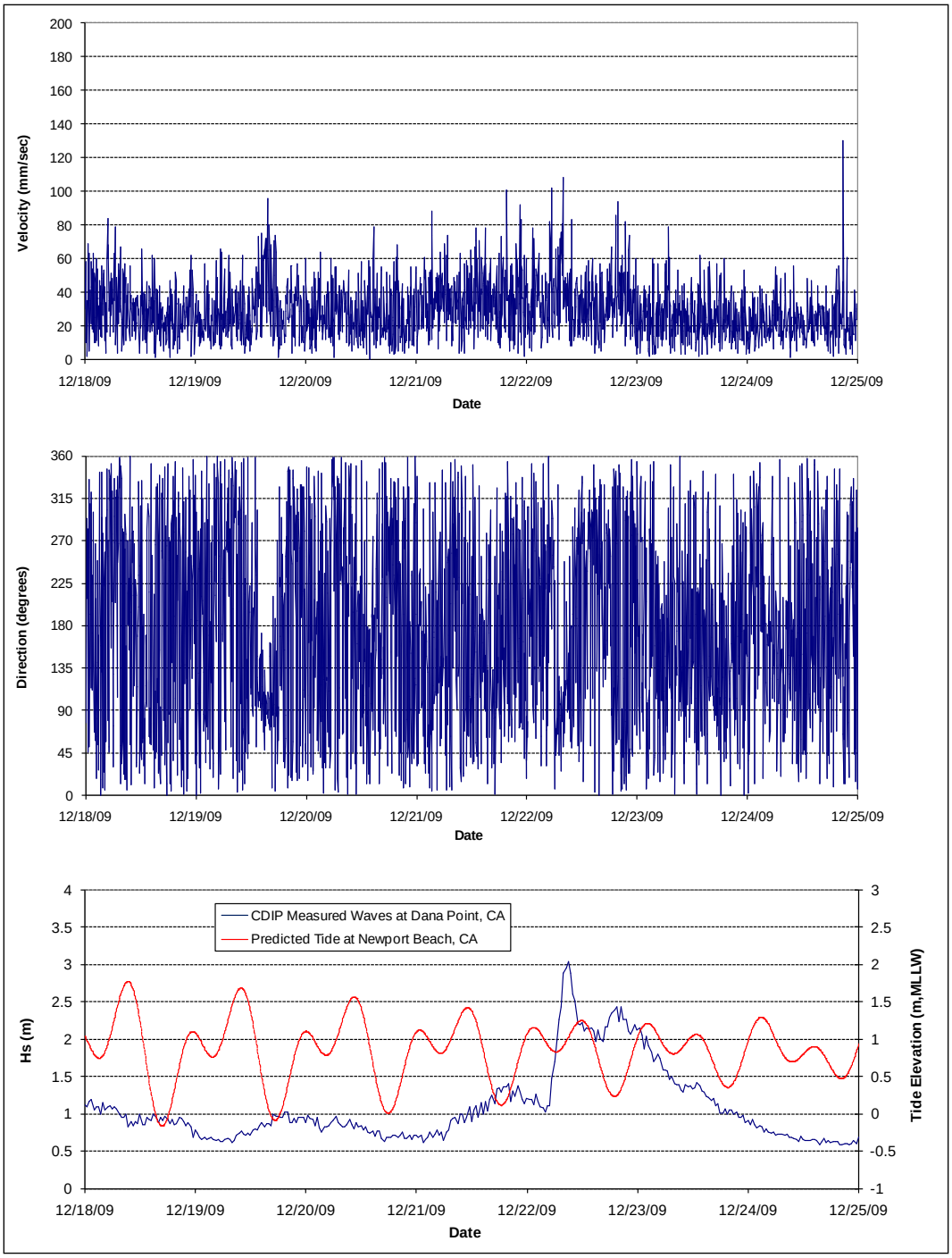

Figure A14. Week 5 – Bin 2 current measurements at Inside Gauge.

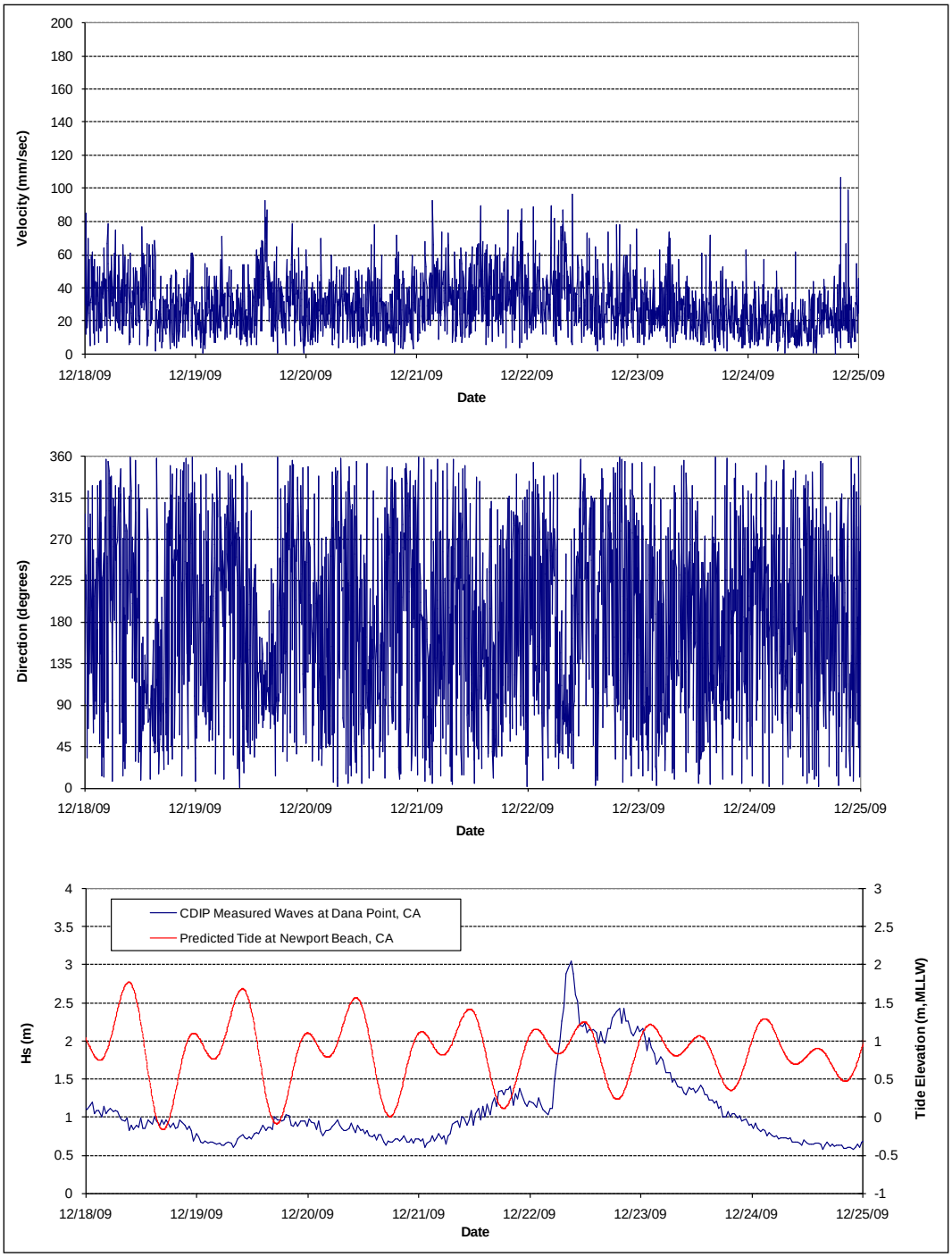

Figure A15. Week 5 – Bin 3 current measurements at Inside Gauge.

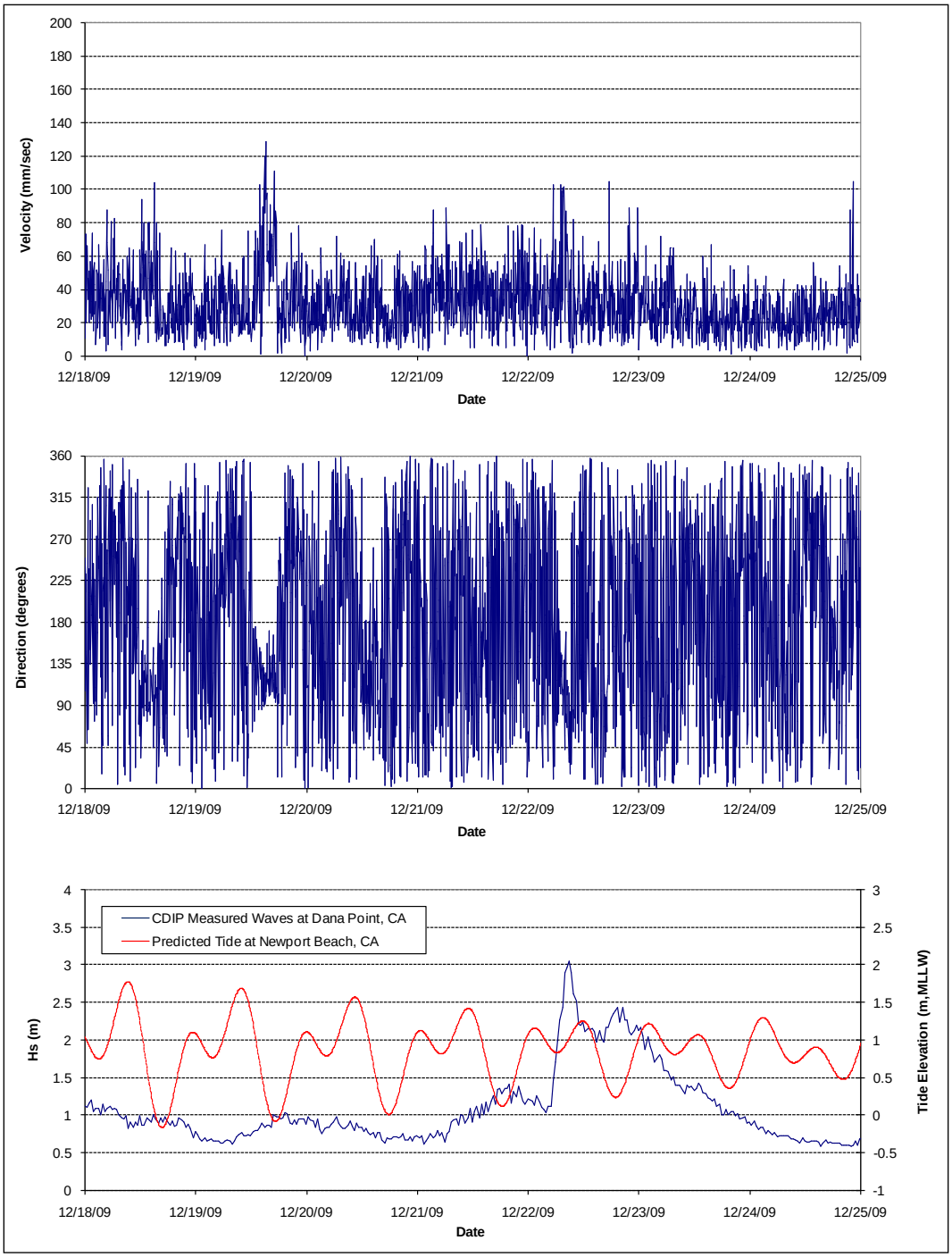

Figure A16. Week 5 – Bin 4 current measurements at Inside Gauge.

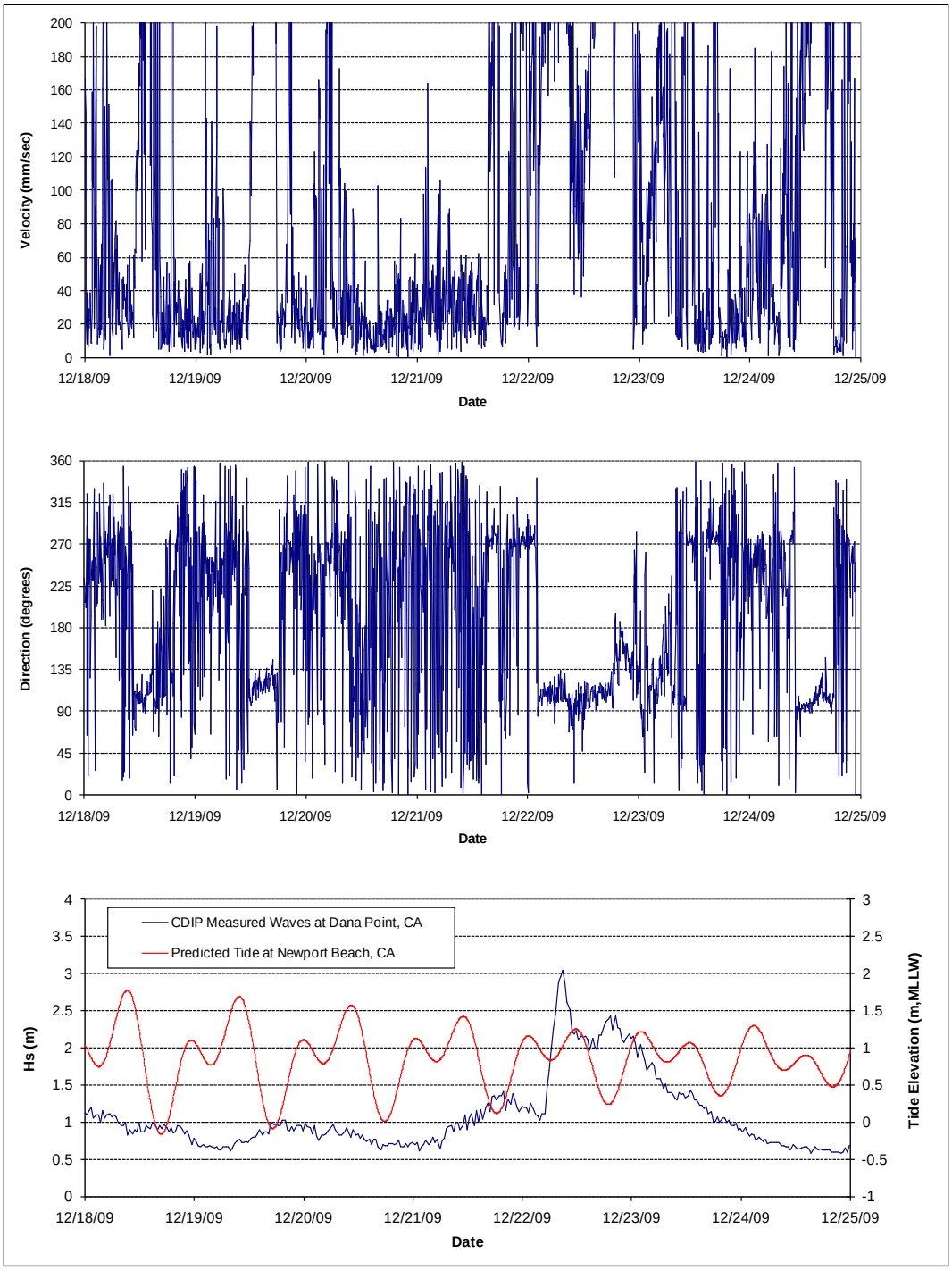

Figure A17. Week 6 – Bin 1 current measurements at Inside Gauge.

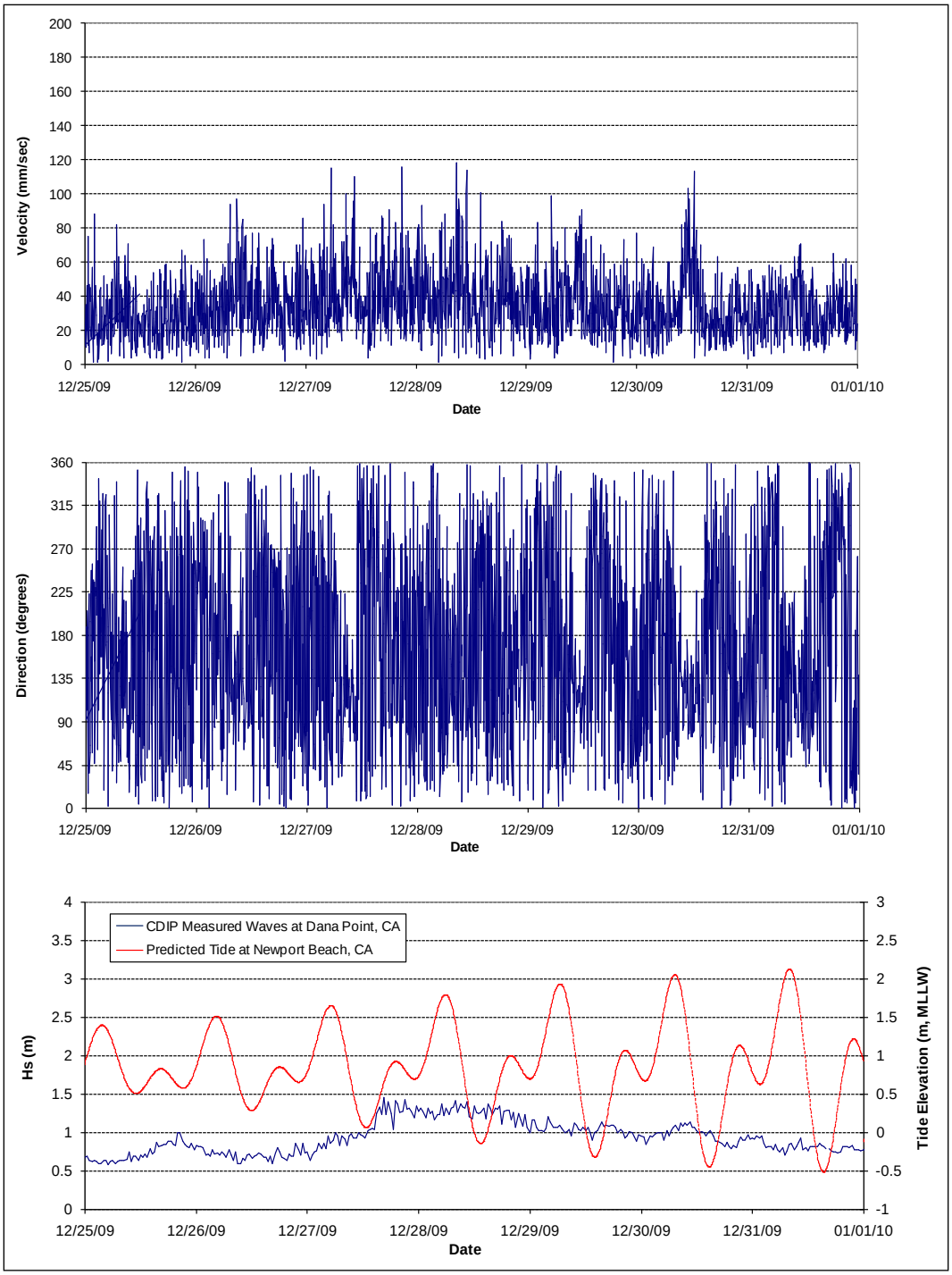

Figure A18. Week 6 – Bin 2 current measurements at Inside Gauge.

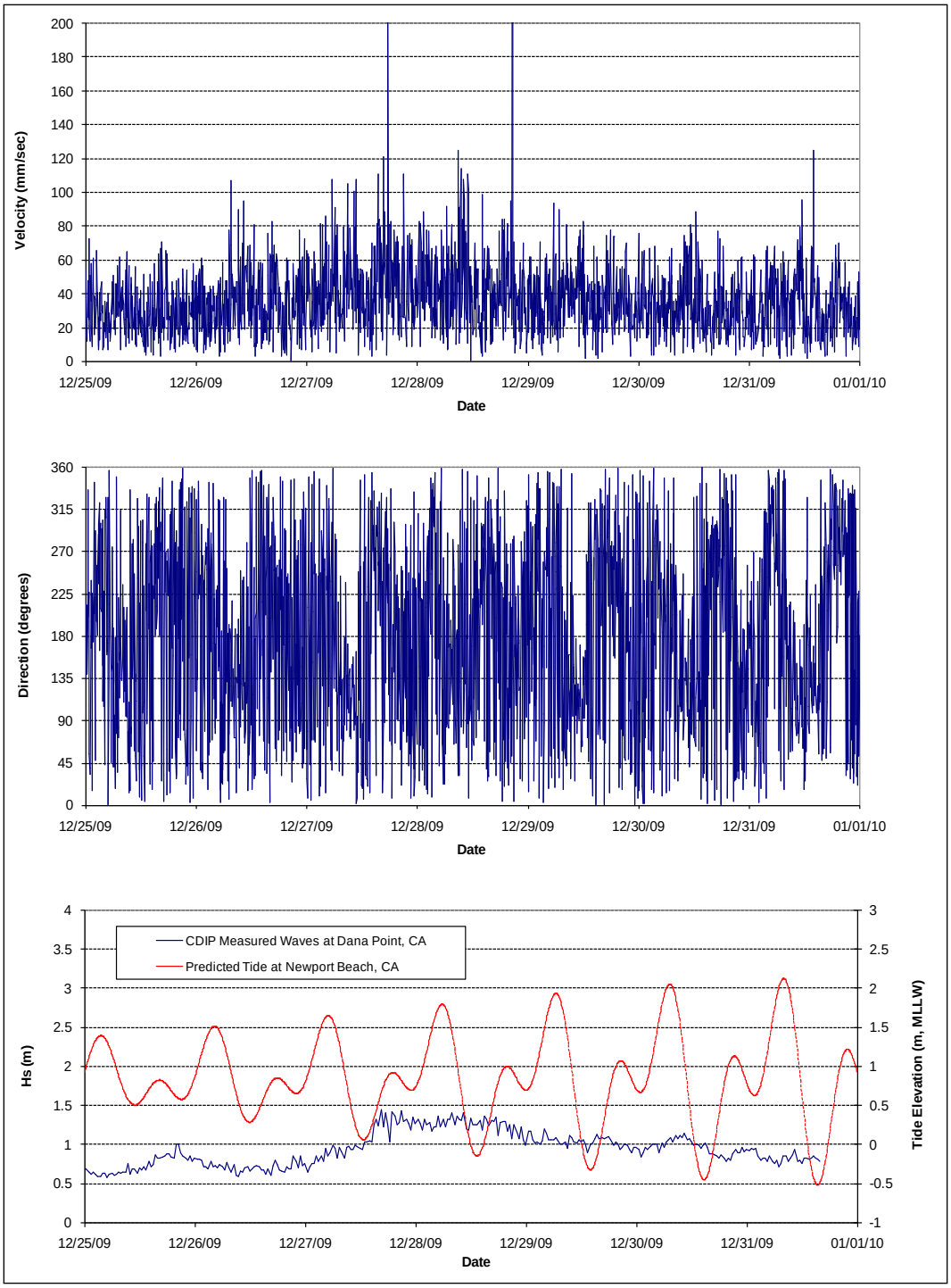

Figure A19. Week 6 – Bin 3 current measurements at Inside Gauge.

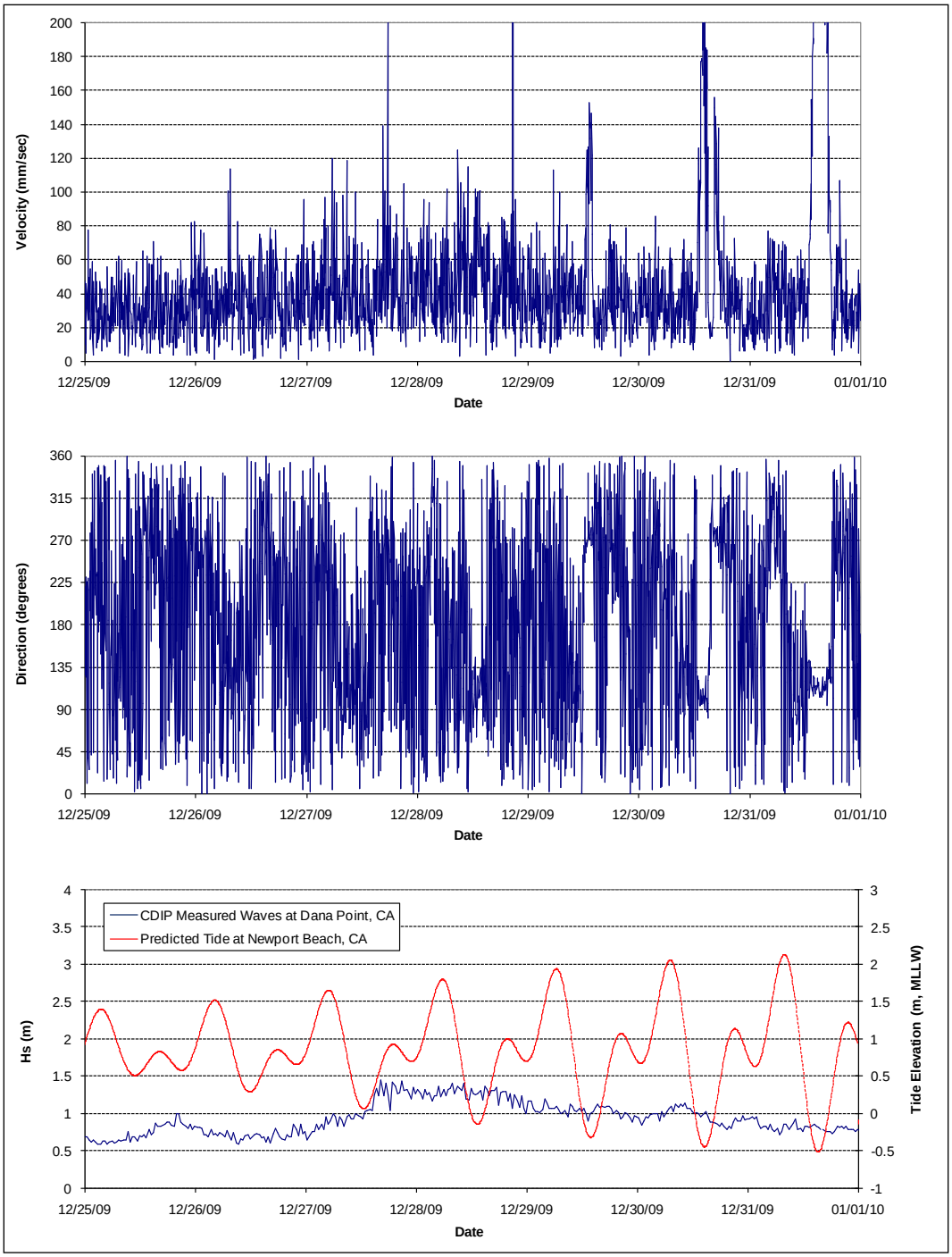

Figure A20. Week 6 – Bin 4 current measurements at Inside Gauge.

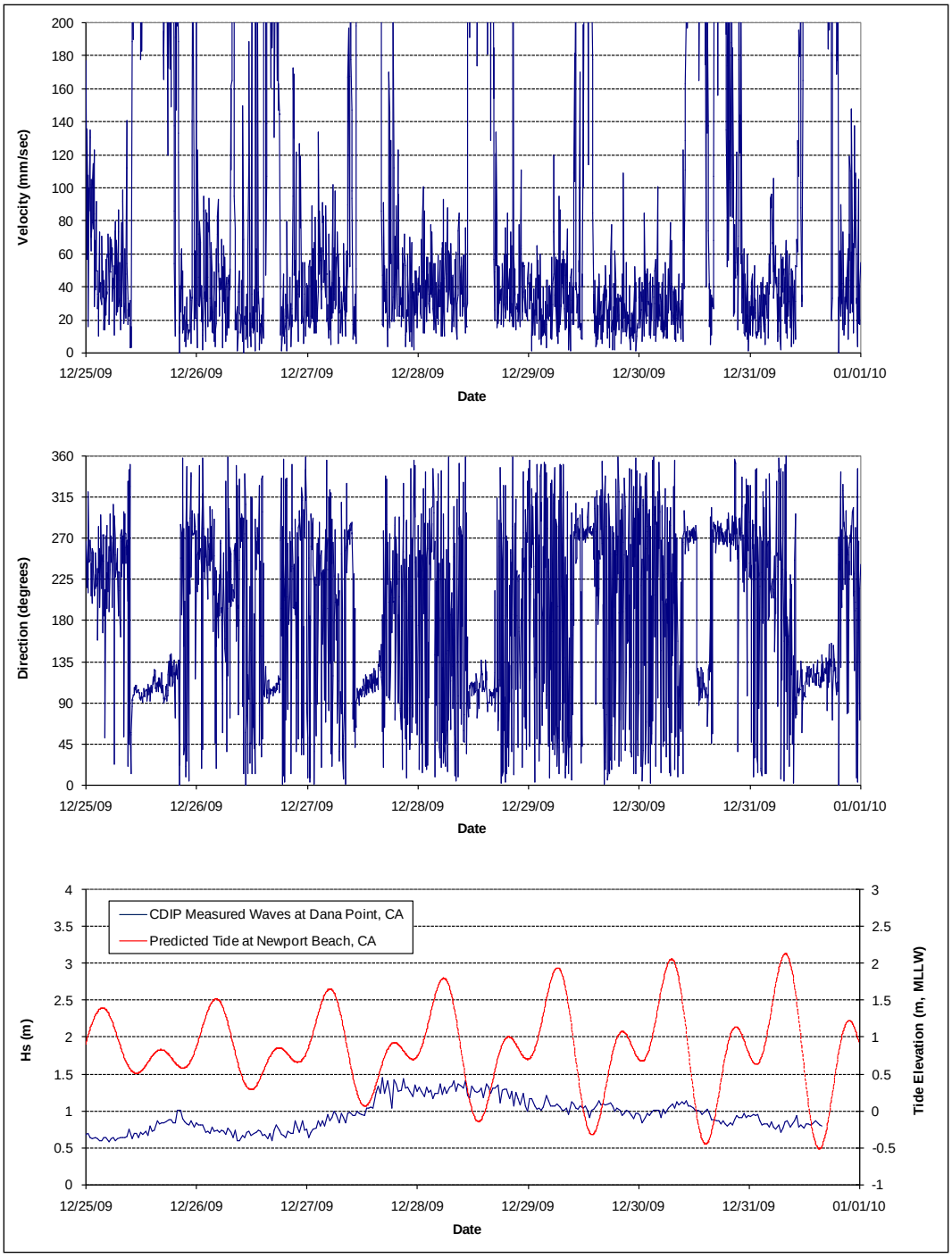

Figure A21. Week 7 – Bin 1 current measurements at Inside Gauge.

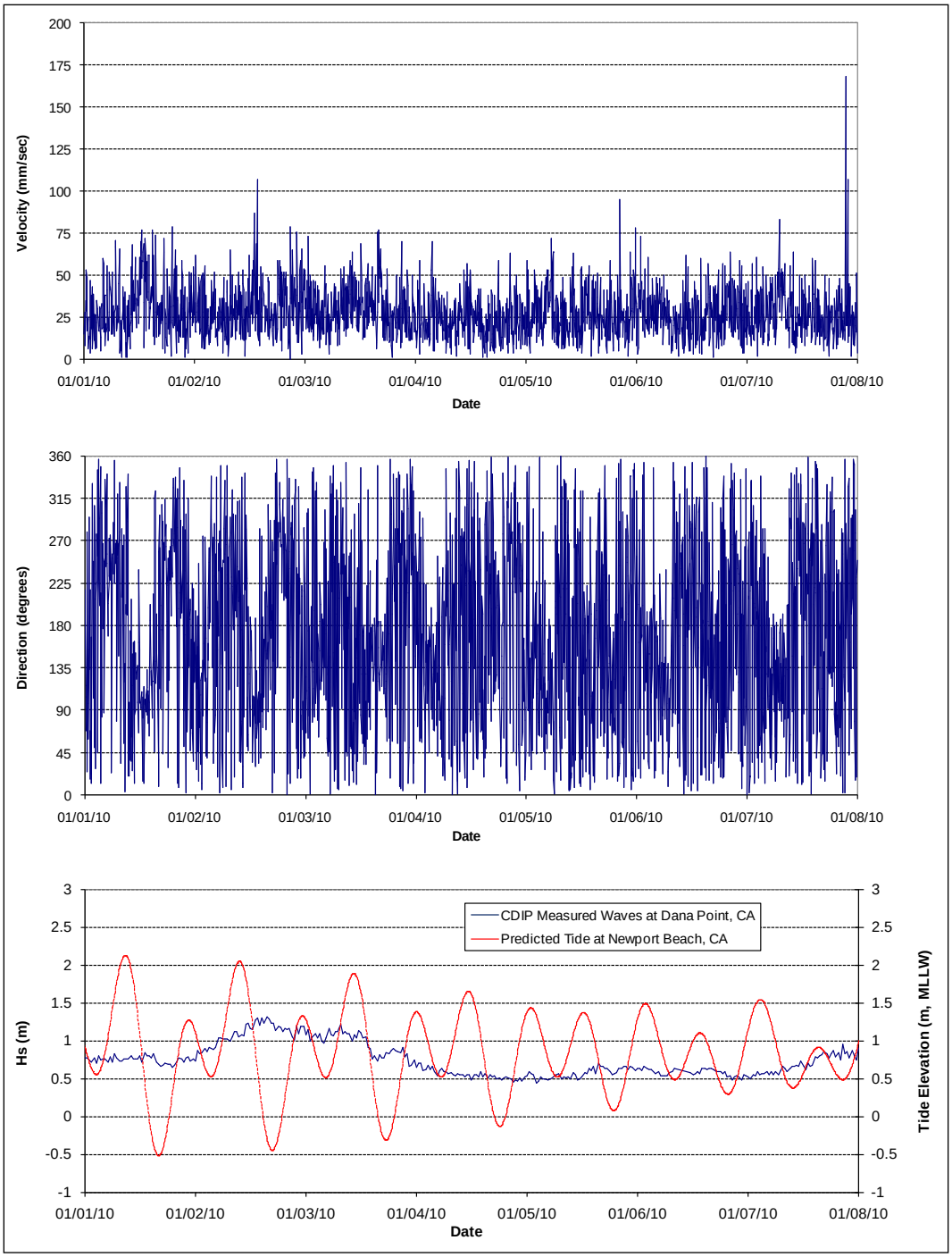

Figure A22. Week 7 – Bin 2 current measurements at Inside Gauge.

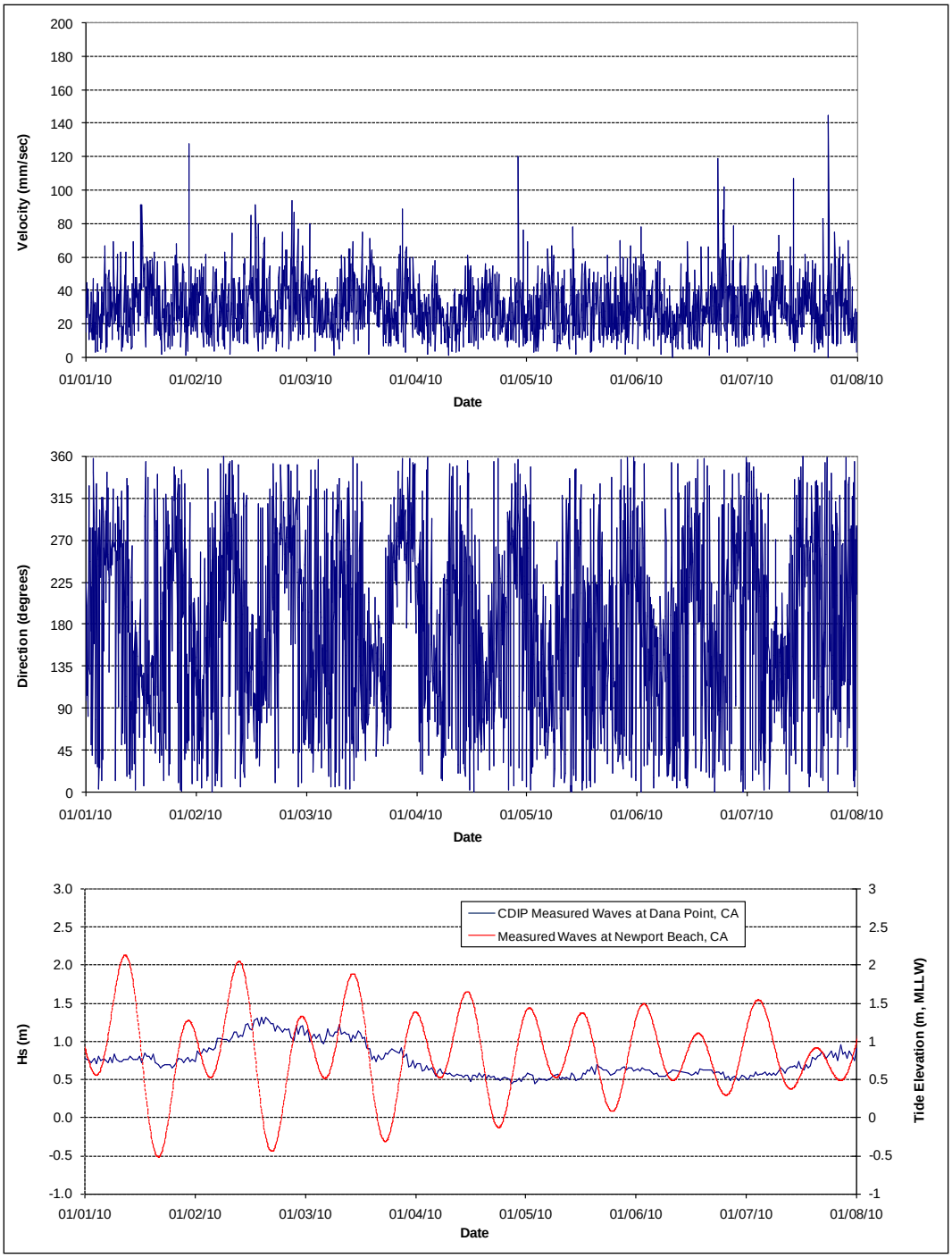

Figure A23. Week 7 – Bin 3 current measurements at Inside Gauge.

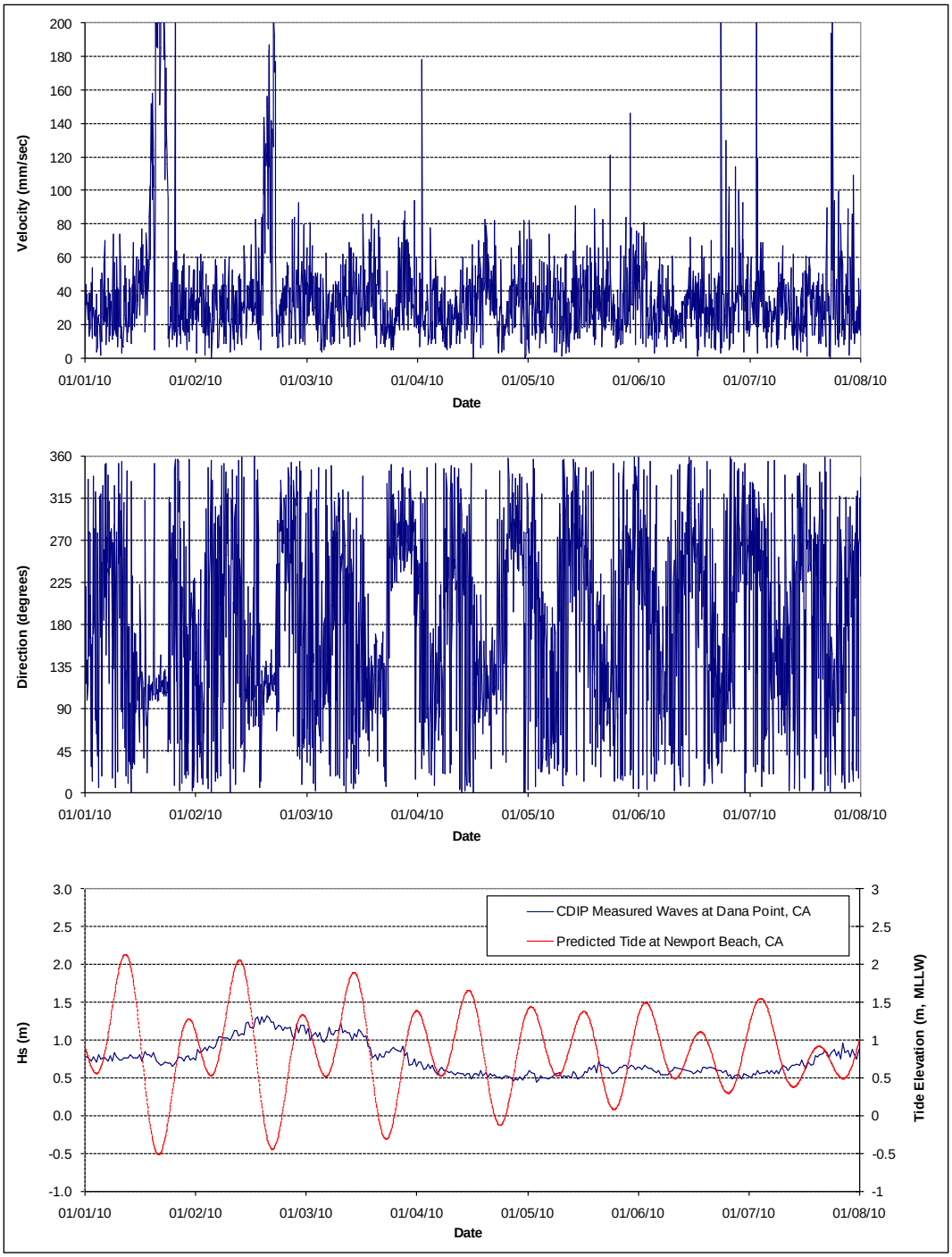

Figure A24. Week 7 – Bin 4 current measurements at Inside Gauge.

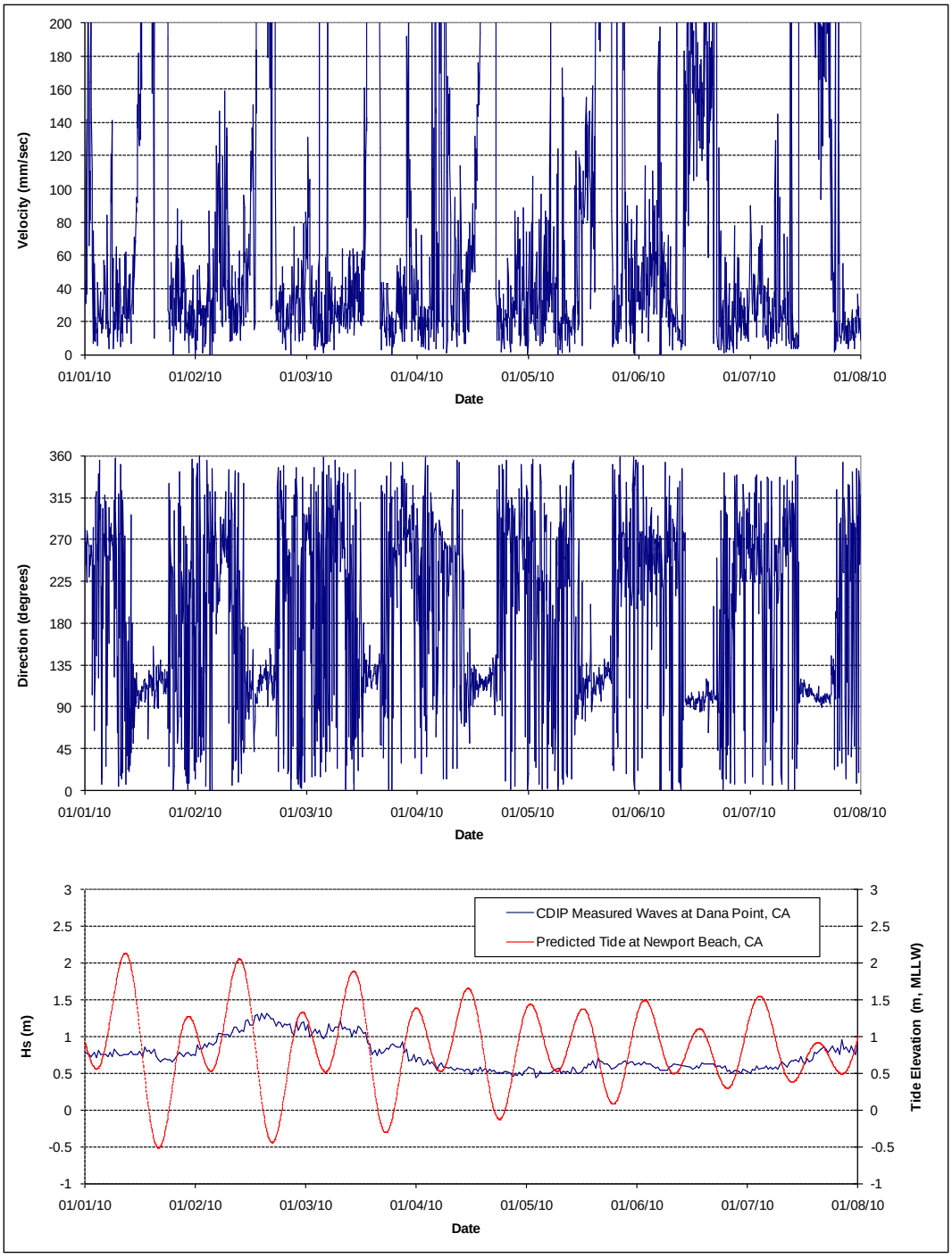

Figure A25. Week 8 – Bin 1 current measurements at Inside Gauge.

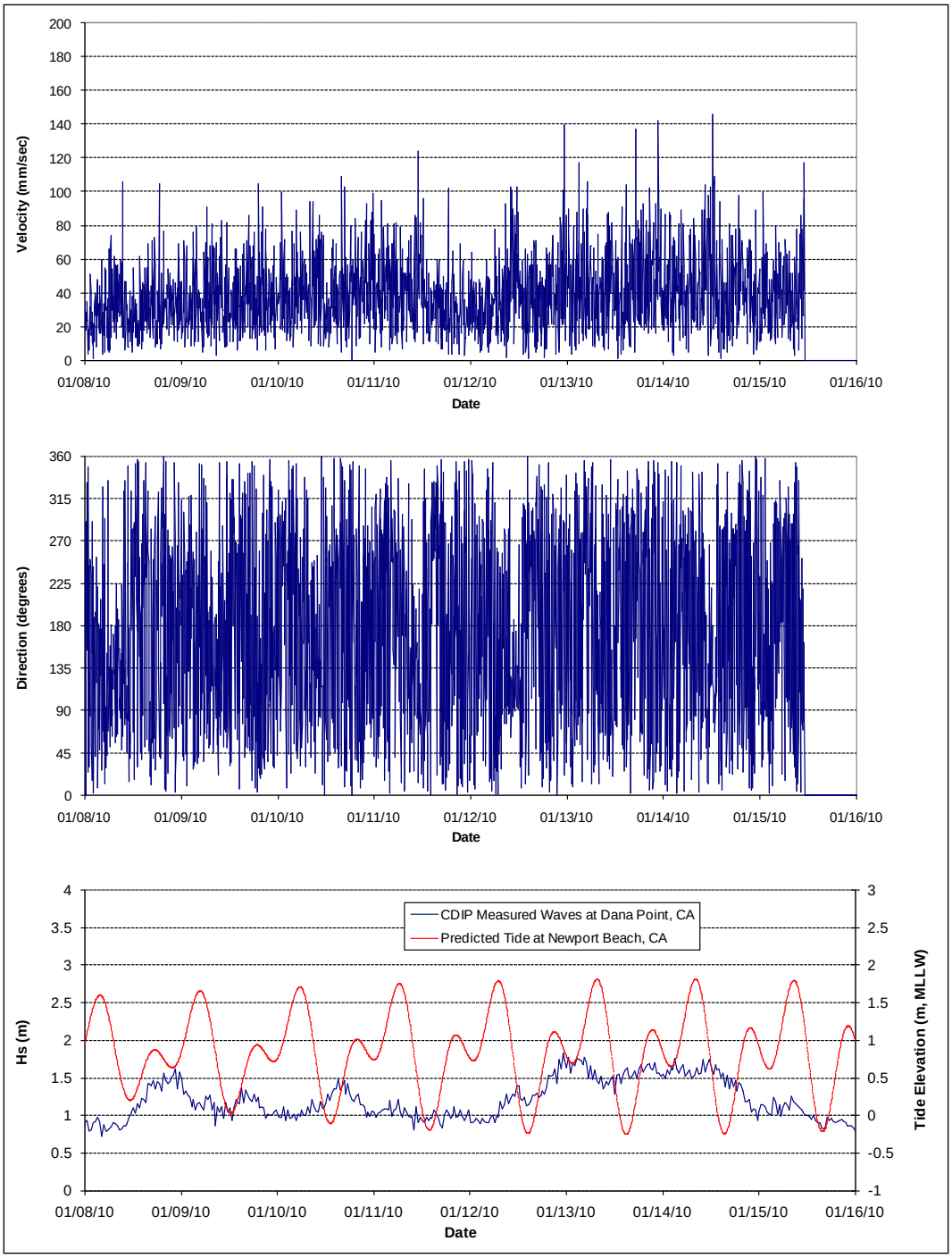

Figure A26. Week 8 – Bin 2 current measurements at Inside Gauge.

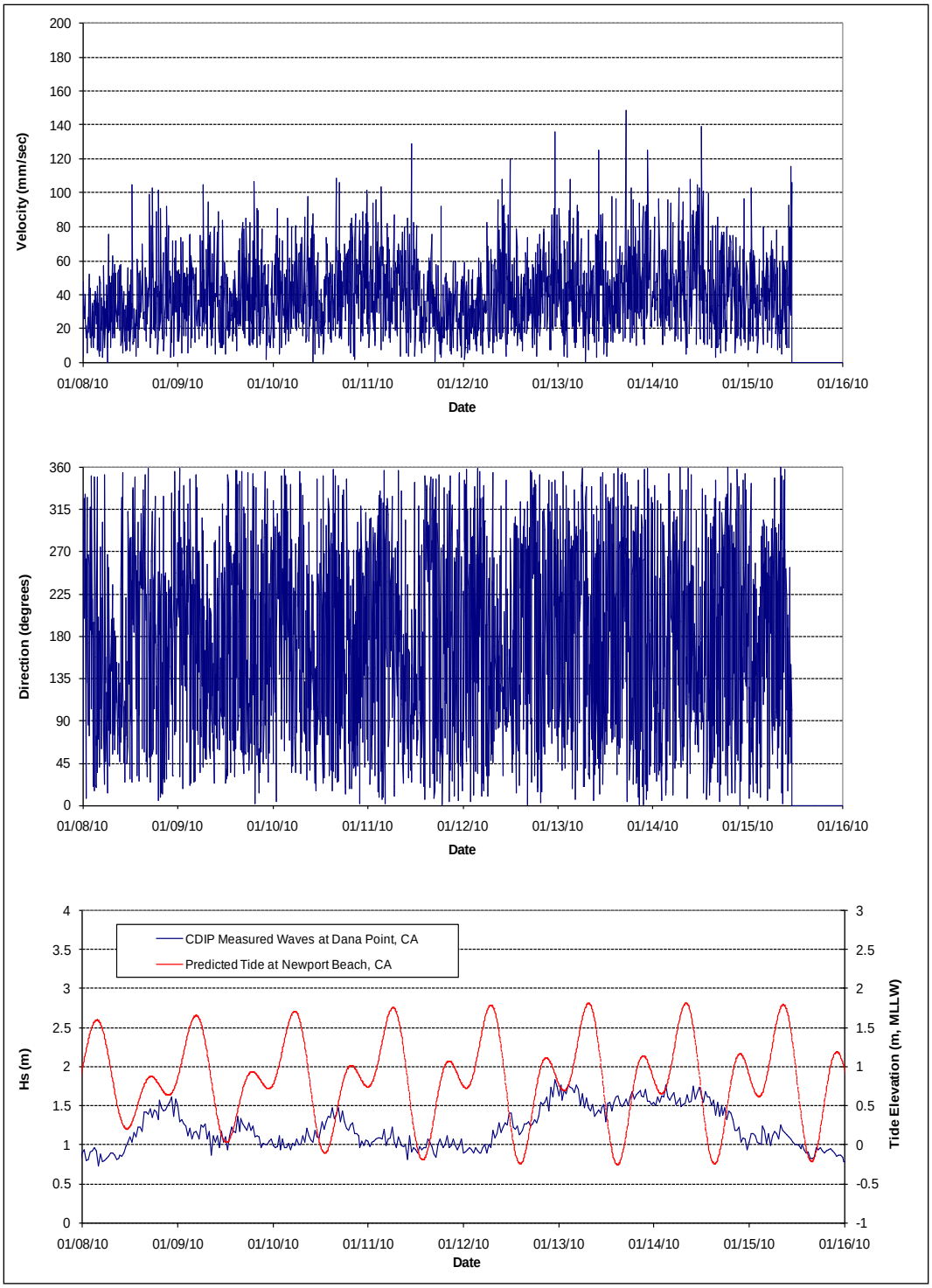

Figure A27. Week 8 – Bin 3 current measurements at Inside Gauge.

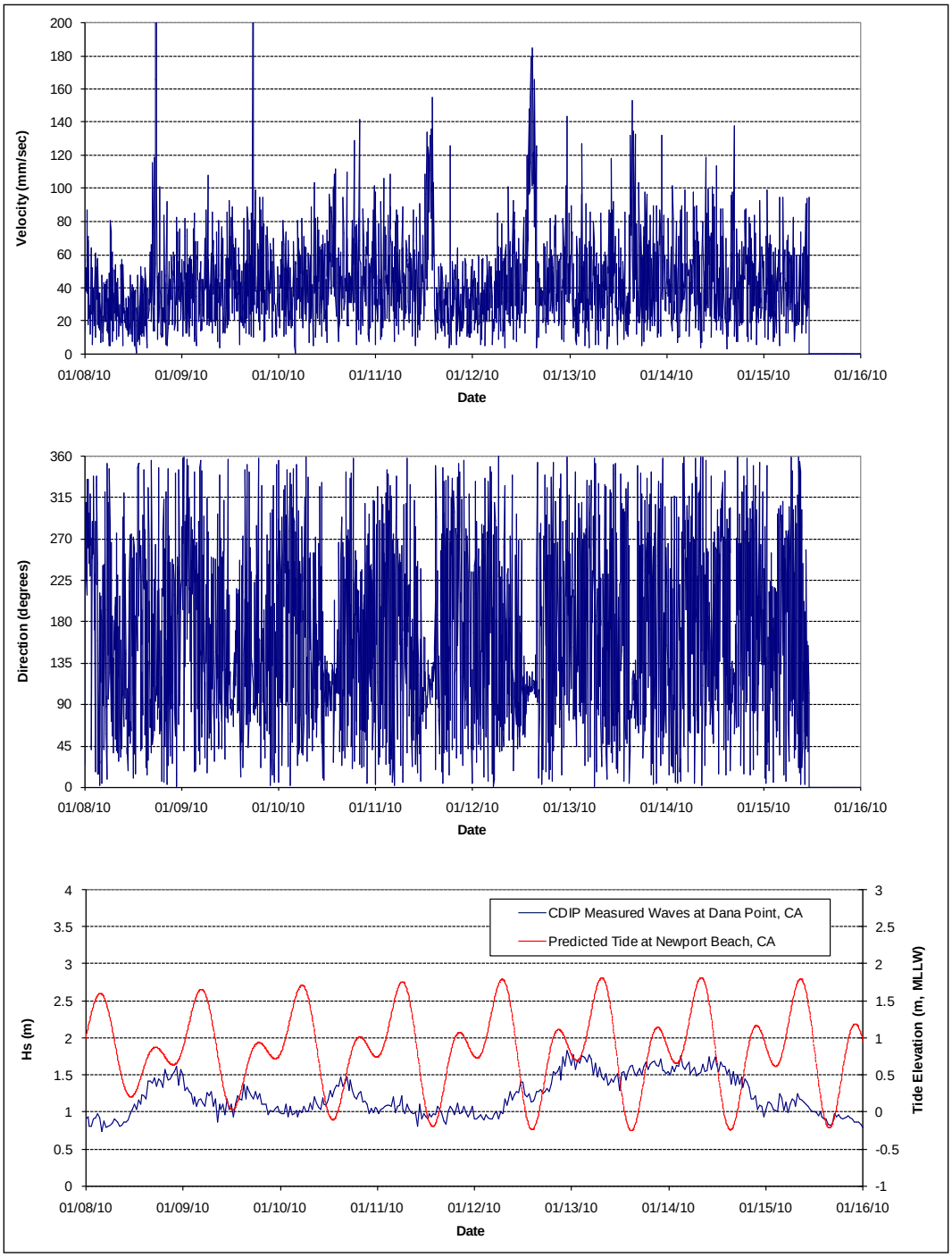

Figure A28. Week 8 – Bin 4 current measurements at Inside Gauge.

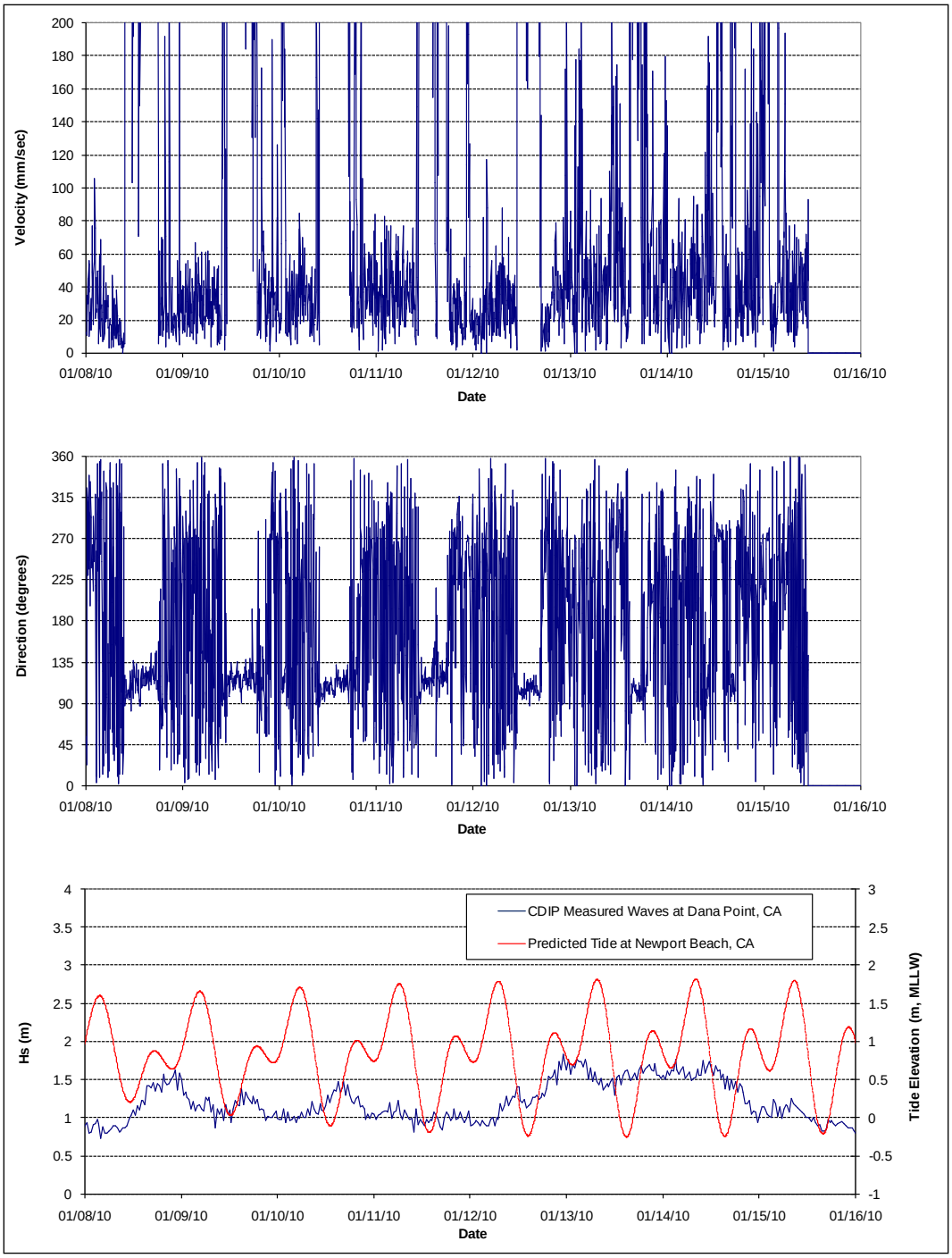

Figure A29. Week 1 – Bin 1-3 water level measurements at Inside Gauge.

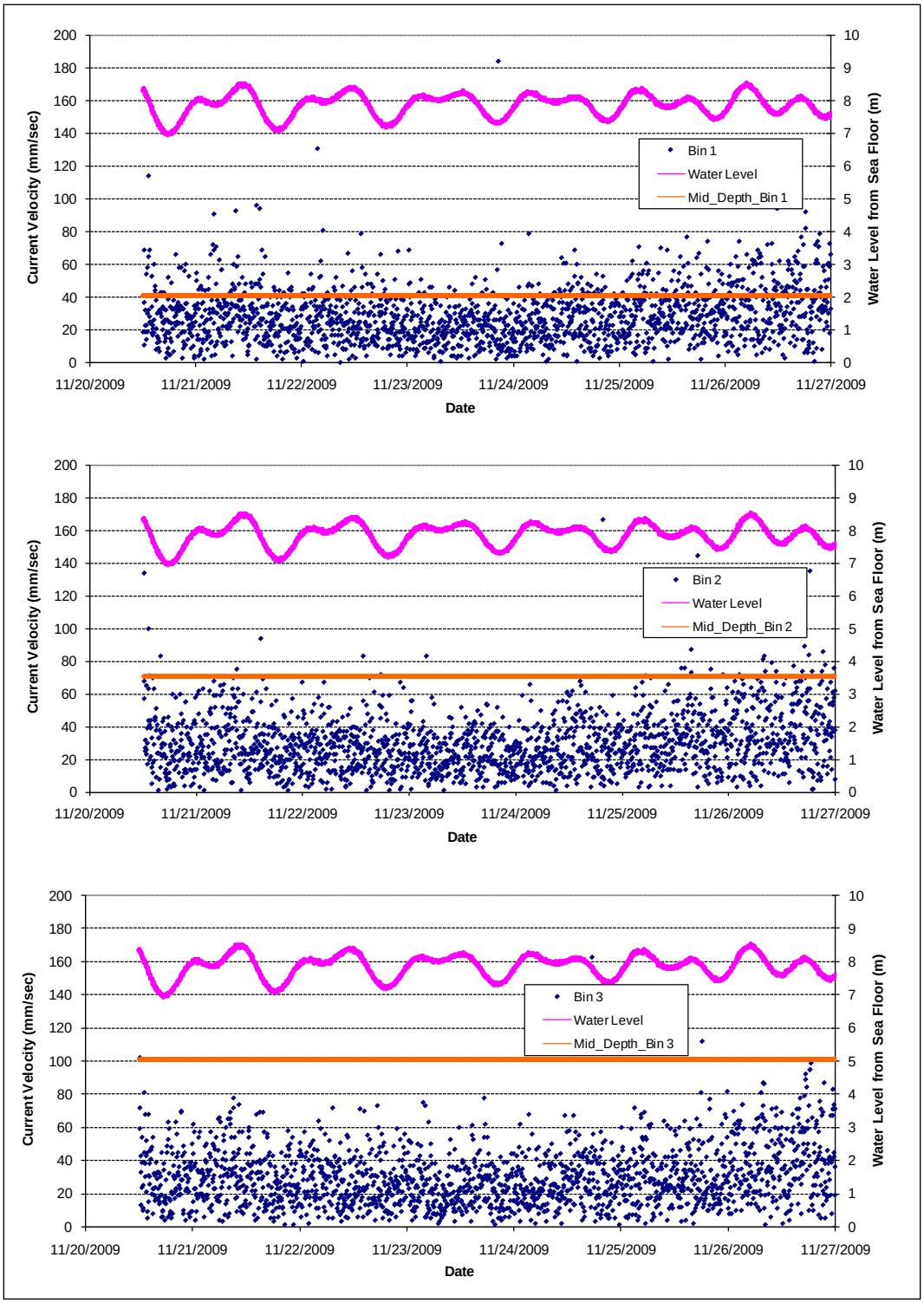

Figure A30. Week 1 – Bin 4 water level measurements at Inside Gauge.

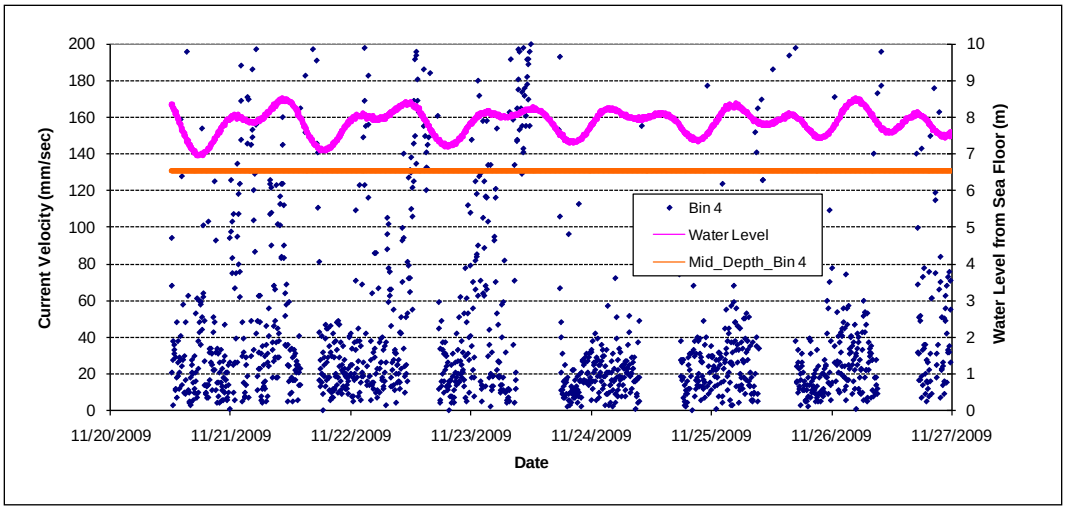

Figure A31. Week 2 – Bin 1-3 water level measurements at Inside Gauge.

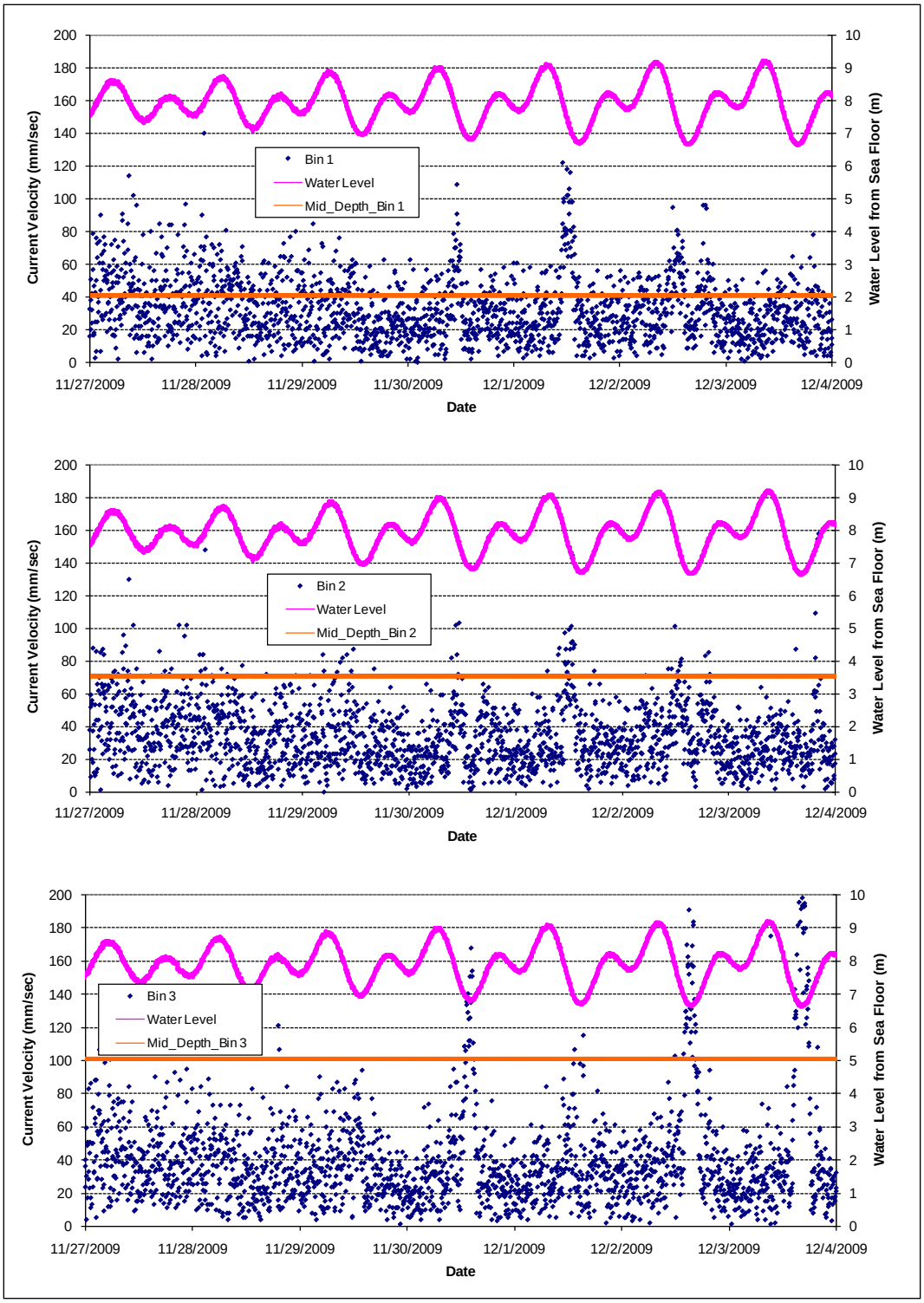

Figure A32. Week 2 – Bin 4 water level measurements at Inside Gauge.

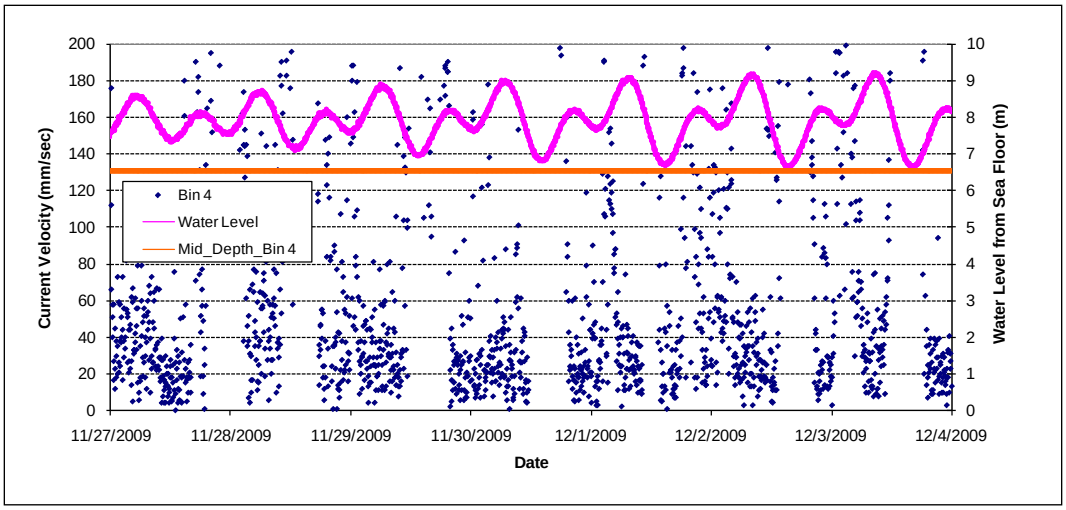

Figure A33. Week 3 – Bin 1-3 water level measurements at Inside Gauge.

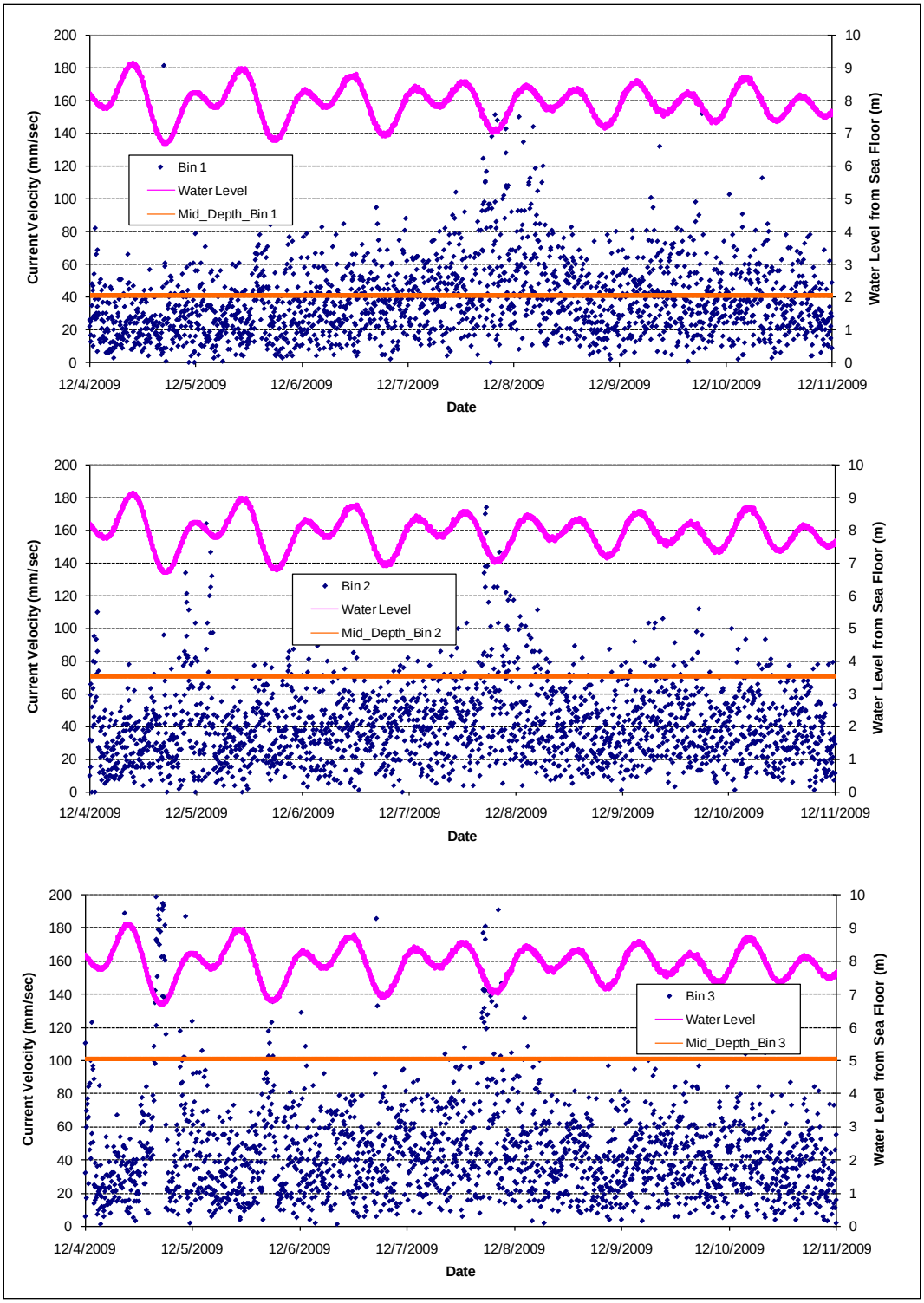

Figure A34. Week 3 – Bin 4 water level measurements at Inside Gauge.

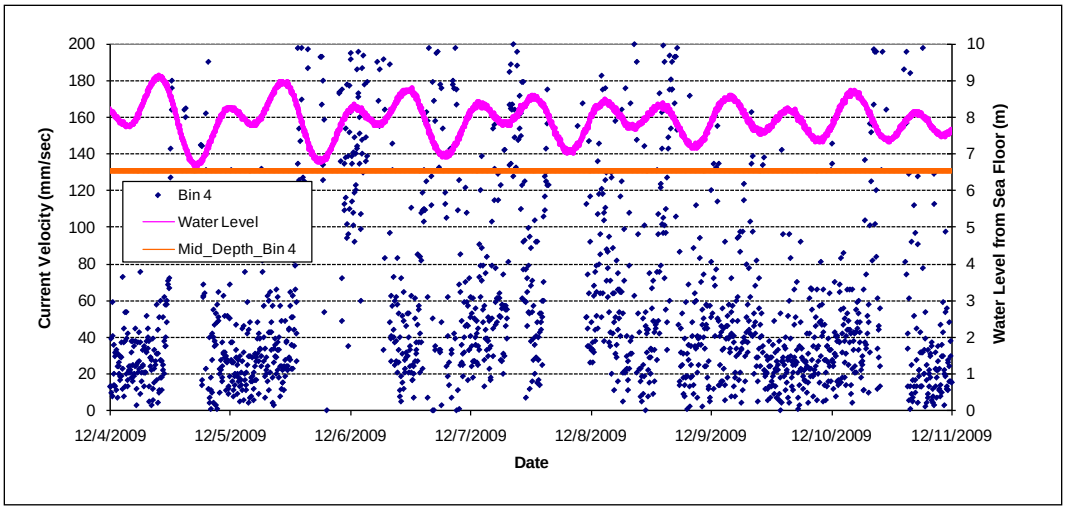

Figure A35. Week 4 – Bin 1-3 water level measurements at Inside Gauge.

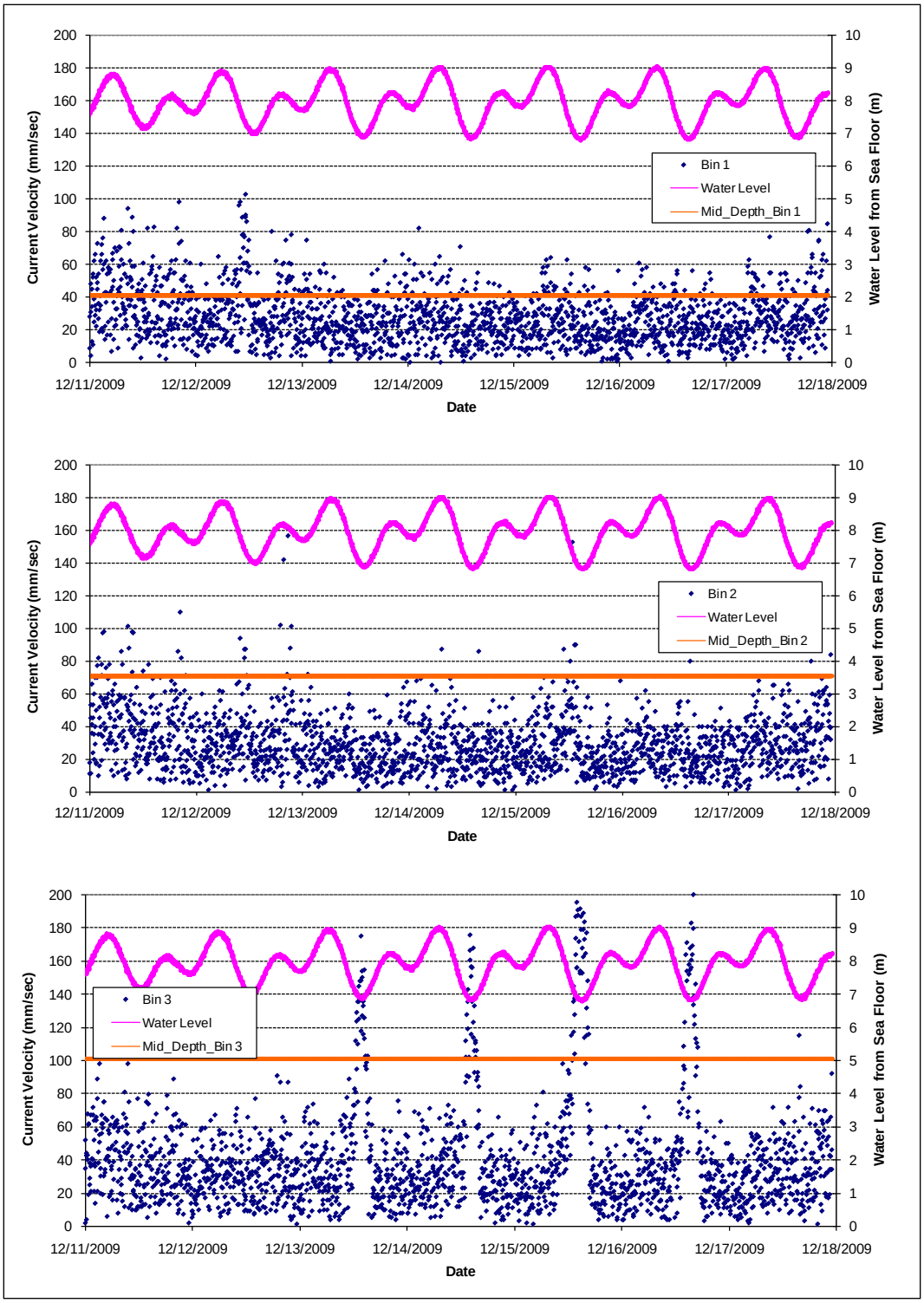

Figure A36. Week 4 – Bin 4 water level measurements at Inside Gauge.

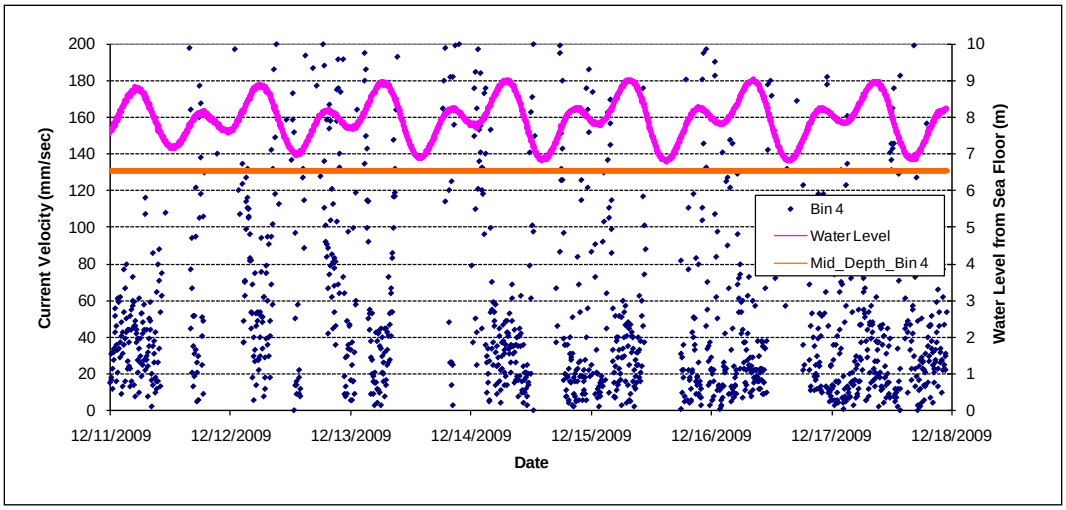

Figure A37. Week 5 – Bin 1-3 water level measurements at Inside Gauge.

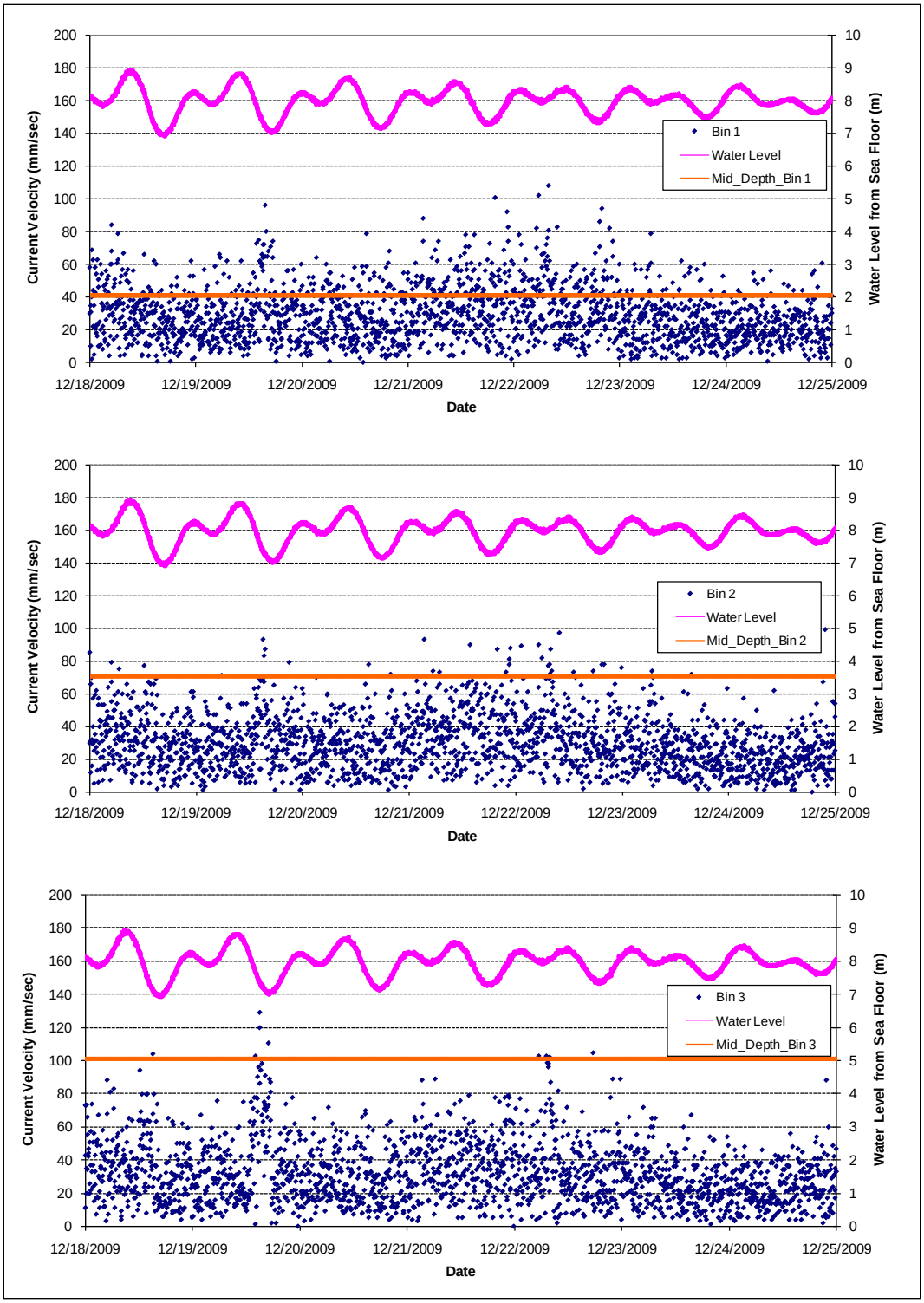

Figure A38. Week 5 – Bin 4 water level measurements at Inside Gauge.

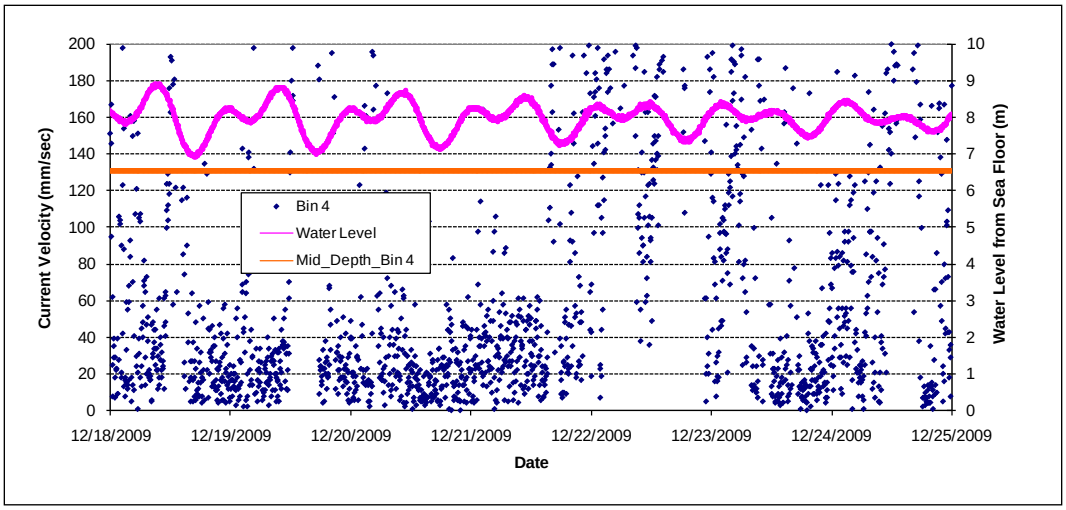

Figure A39. Week 6 – Bin 1-3 water level measurements at Inside Gauge.

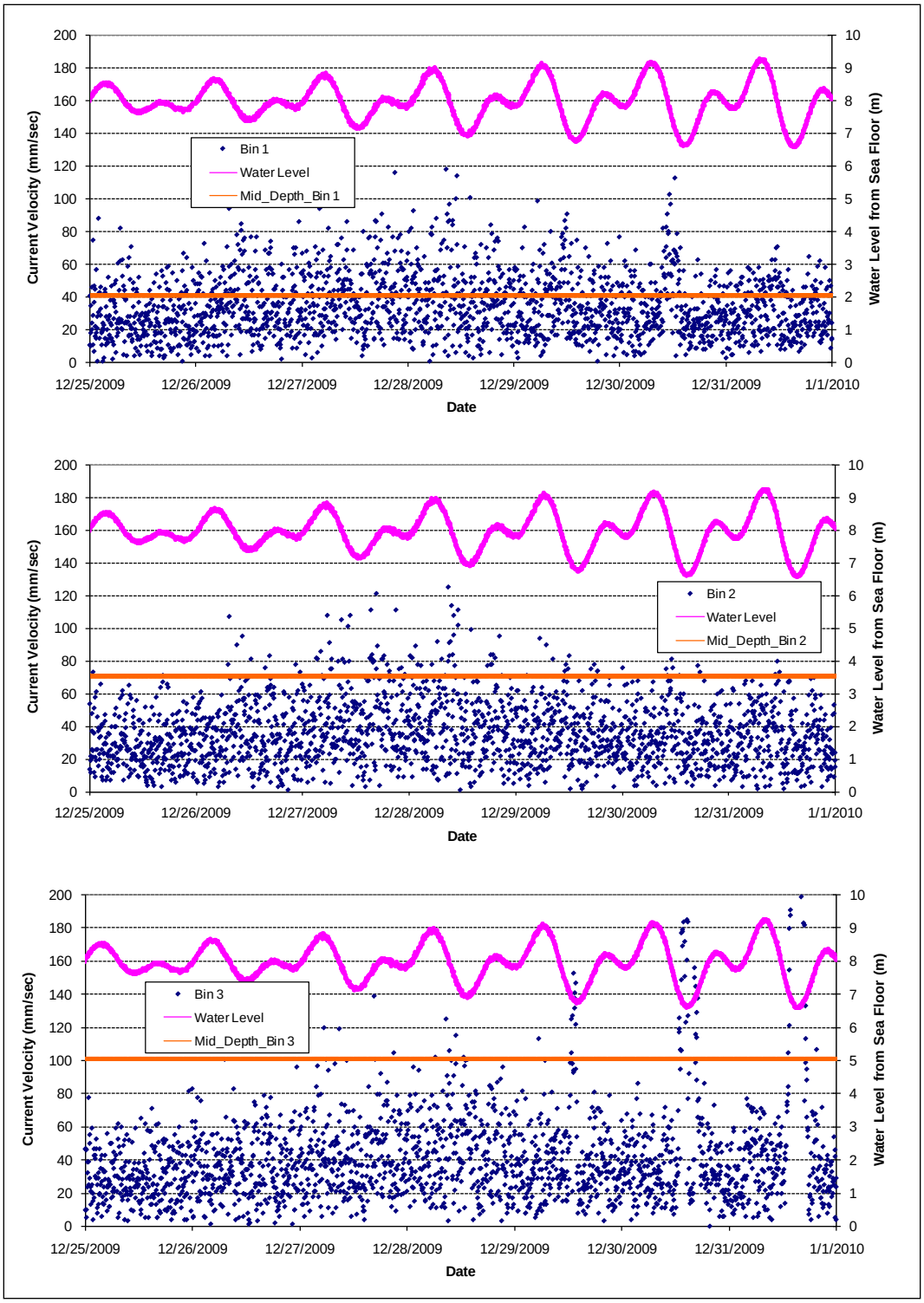

Figure A40. Week 6 – Bin 4 water level measurements at Inside Gauge.

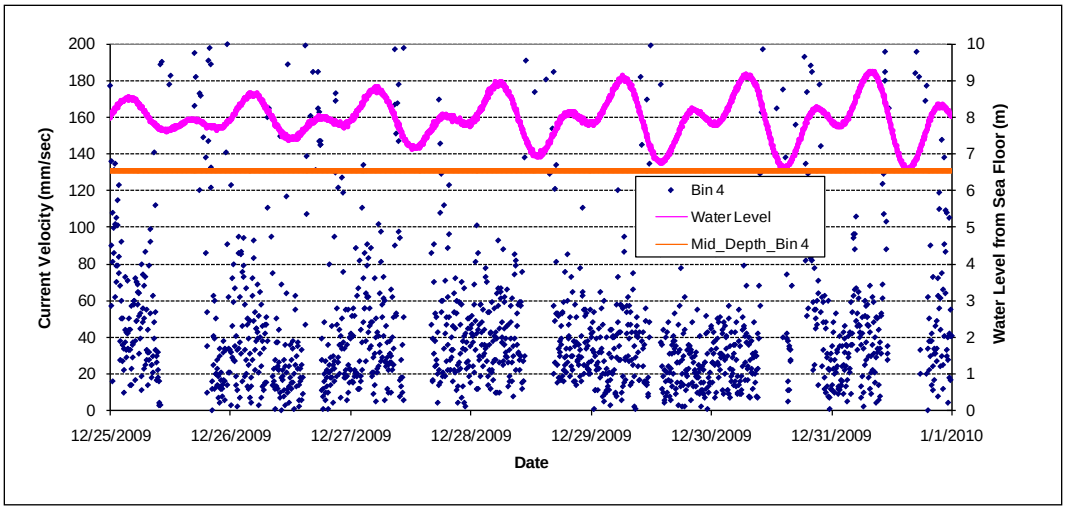

Figure A41. Week 7 – Bin 1-3 water level measurements at Inside Gauge.

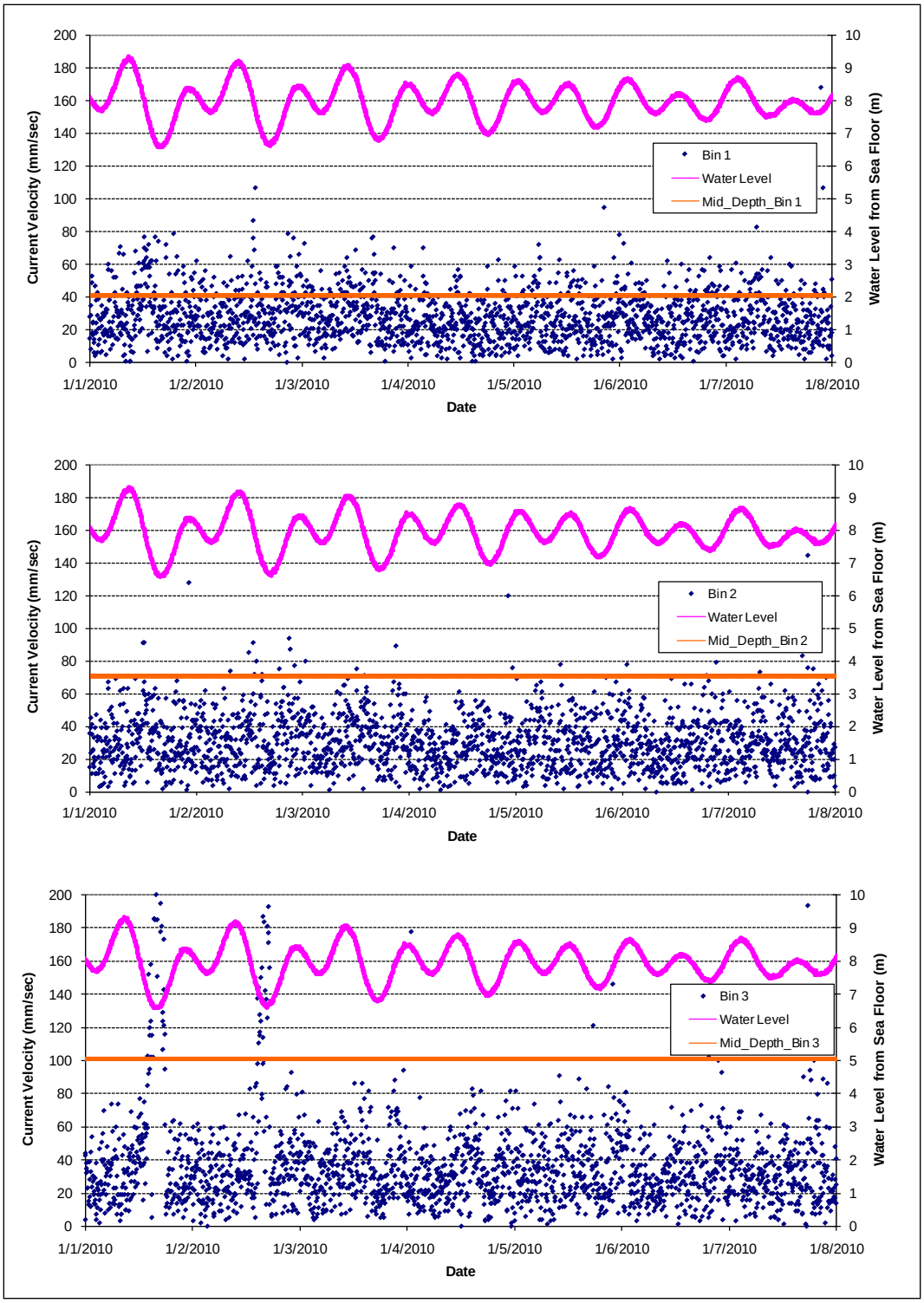

Figure A42. Week 7 – Bin 4 water level measurements at Inside Gauge.

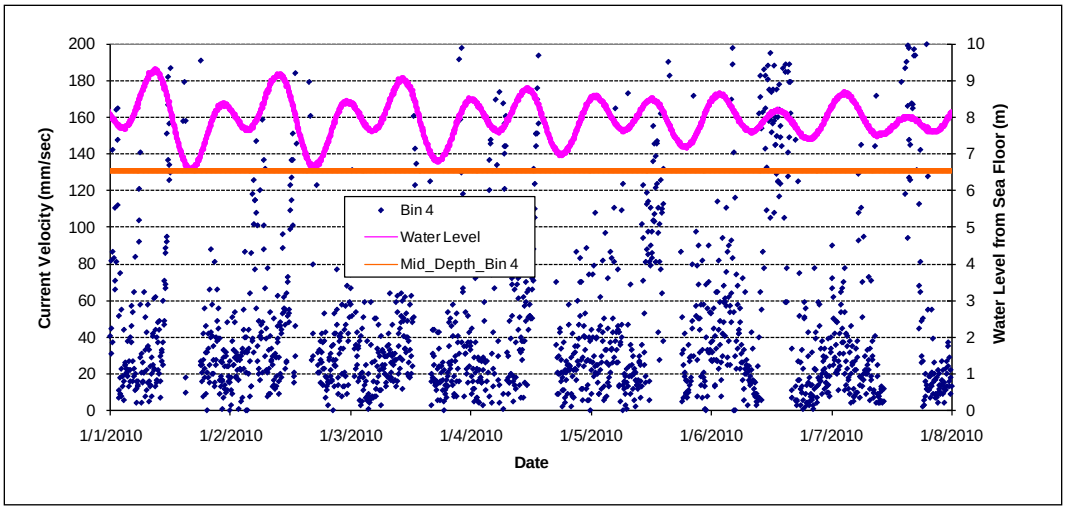

Figure A43. Week 8 – Bin 1-3 water level measurements at Inside Gauge.

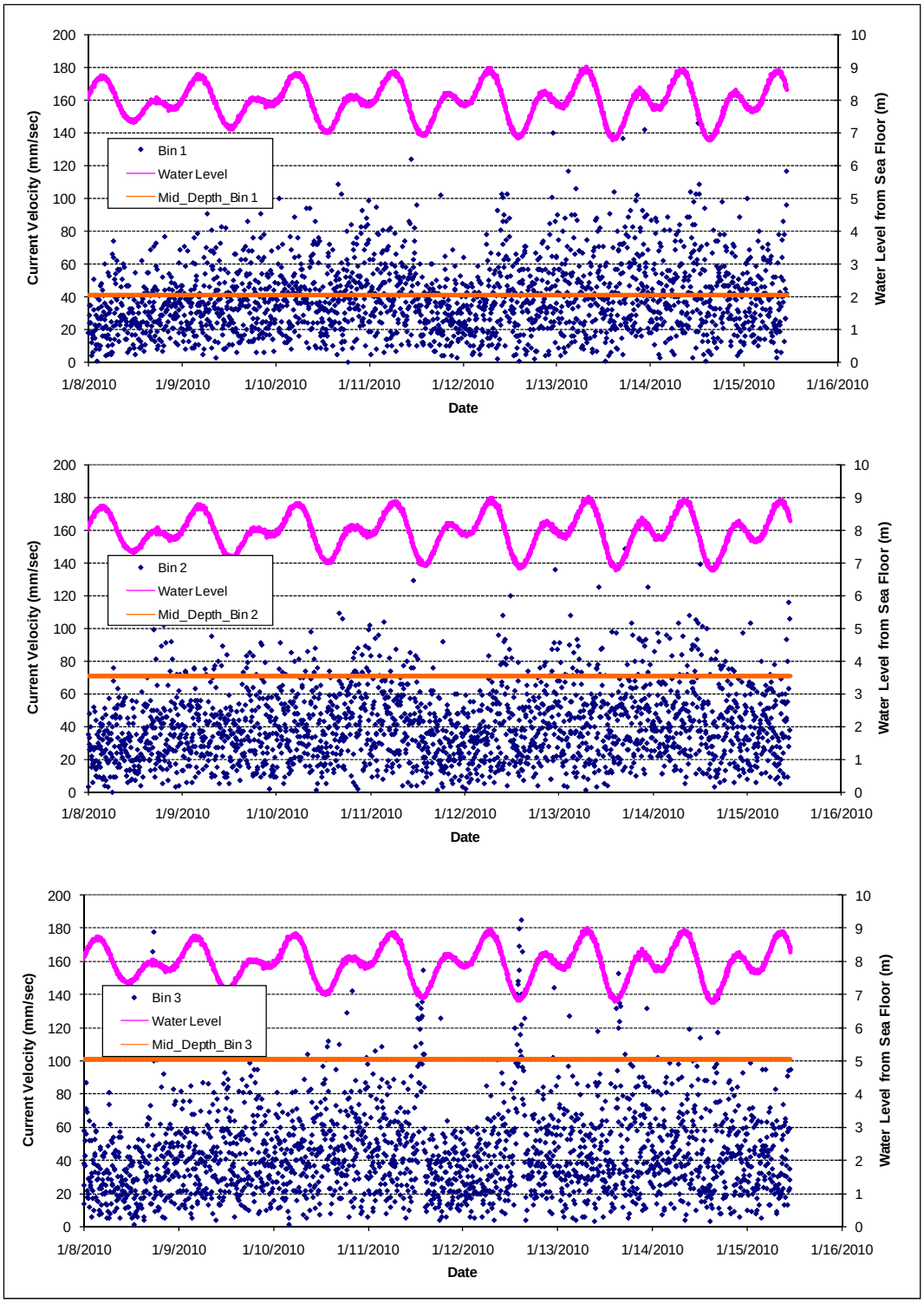

Figure A44. Week 8 – Bin 4 water level measurements at Inside Gauge.

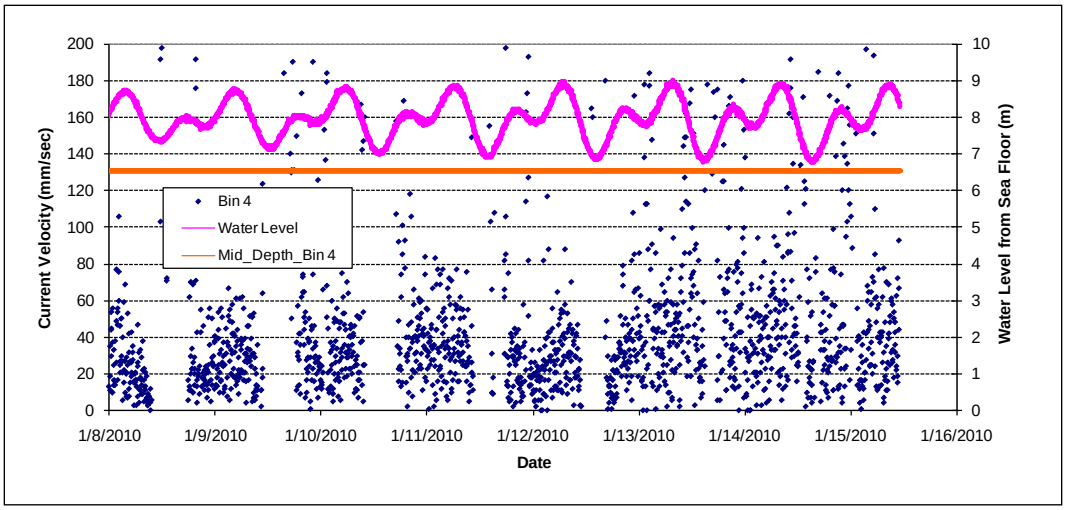

Figure A45. Week 1 – Bin 1-3 water level measurements at Outside Gauge.

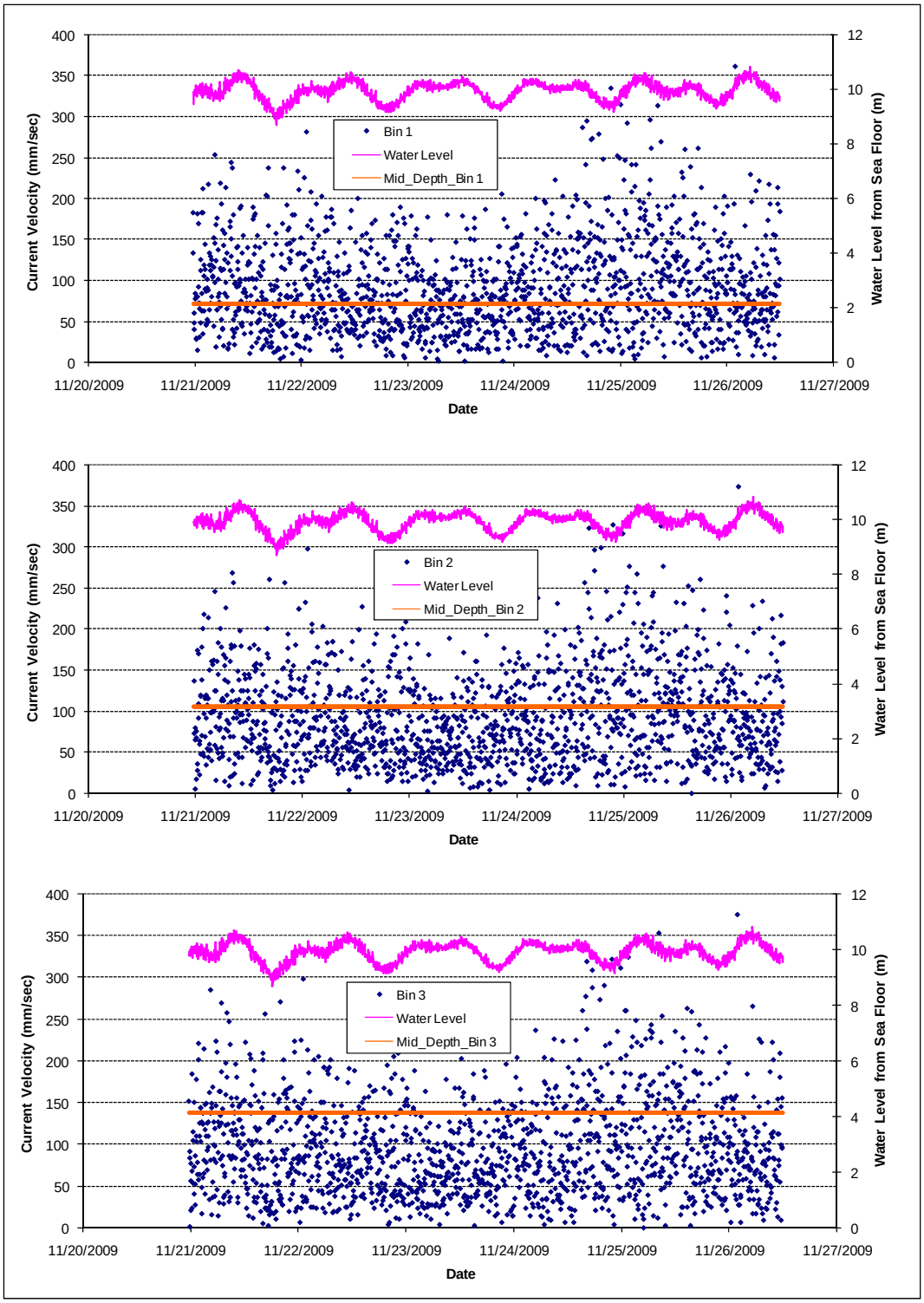

Figure A46. Week 1 – Bin 4-6 water level measurements at Outside Gauge.

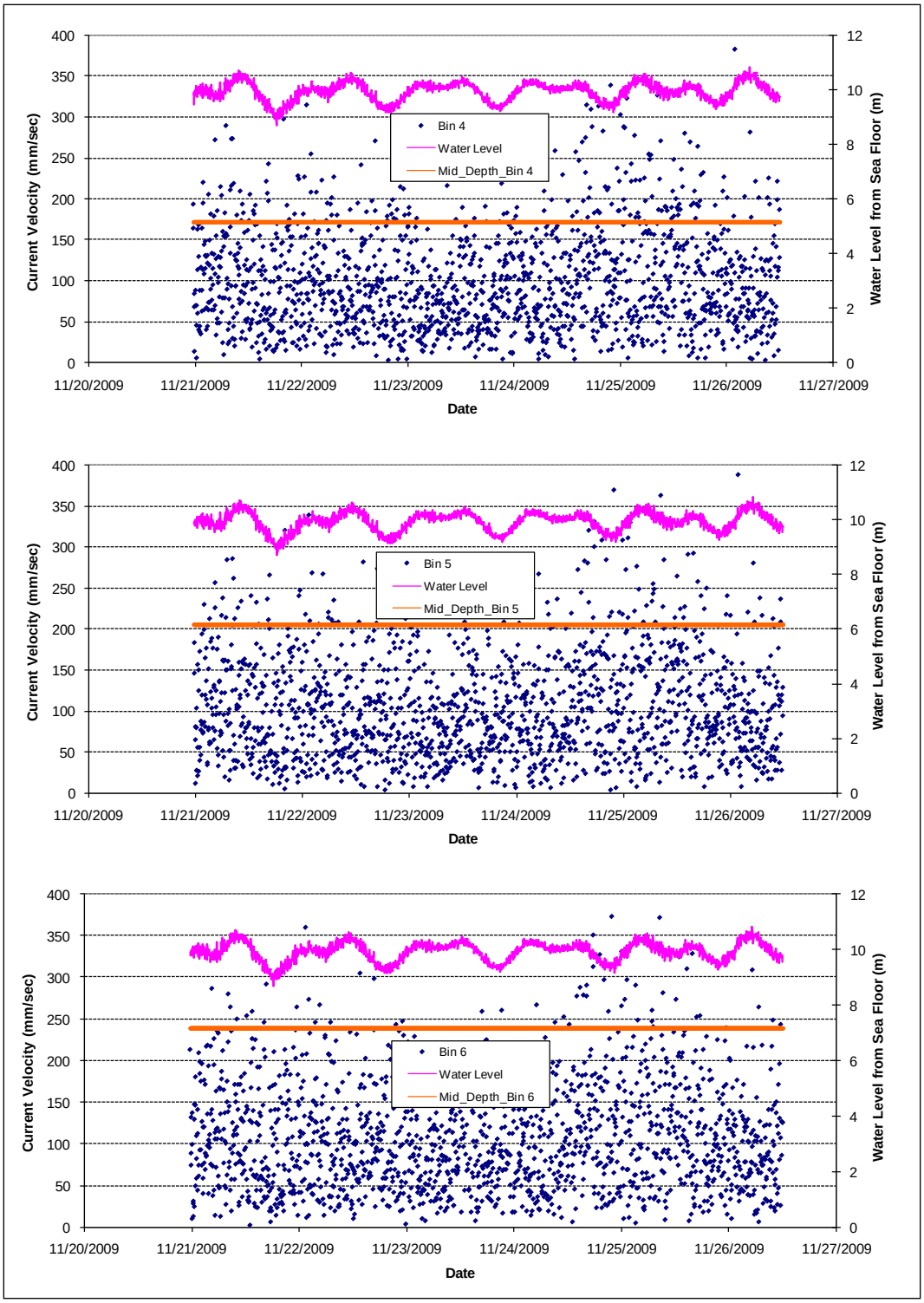

Figure A47. Week 1 – Bin 7 water level measurements at Outside Gauge.

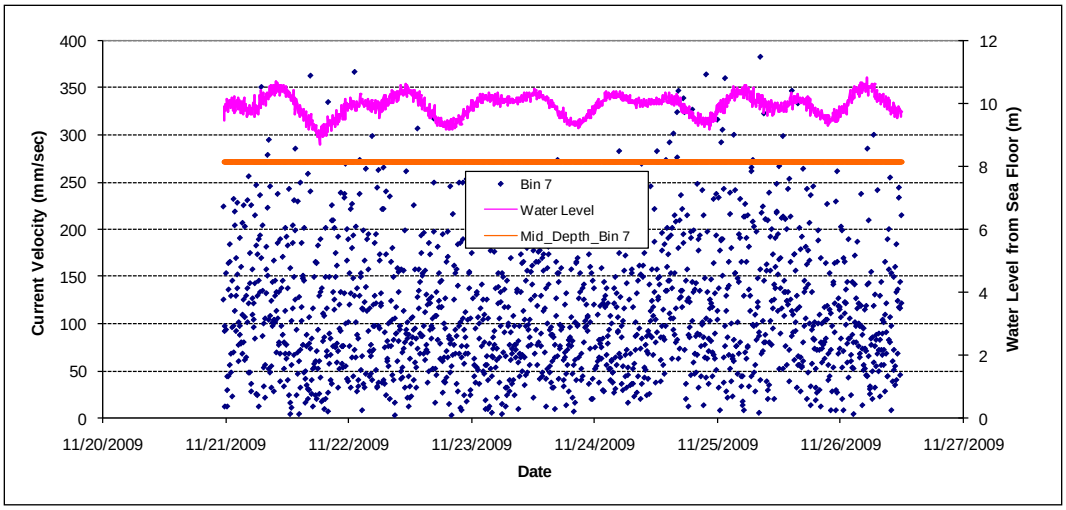

REPORT DOCUMENTATION PAGE

Form Approved
OMB No. 0704-0188

1. REPORT DATE *(DD-MM-YYYY)*	**2. REPORT TYPE**	**3. DATES COVERED** *(From - To)*
December 2014	Final Report	

4. TITLE AND SUBTITLE
Comprehensive condition survey and Storm Waves, Circulation, and Sedimentation Study, Dana Point Harbor, CA

5a. CONTRACT NUMBER

5b. GRANT NUMBER

5c. PROGRAM ELEMENT NUMBER

6. AUTHOR(S)

Chia-Chi Lu, Arthur Shak, Honghai Li, Lihwa Lin

5d. PROJECT NUMBER

5e. TASK NUMBER

5f. WORK UNIT NUMBER

7. PERFORMING ORGANIZATION NAME(S) AND ADDRESS(ES)

U.S. Army Corps of Engineers, Engineer Research and Development Center
3909 Halls Ferry Road, Vicksburg, MS 39180

8. PERFORMING ORGANIZATION REPORT NUMBER

ERDC/CHL TR-14-13

9. SPONSORING / MONITORING AGENCY NAME(S) AND ADDRESS(ES)

U.S. Army Engineer District, Los Angeles District
915 Wilshire Blvd, Los Angeles, CA 90017

10. SPONSOR/MONITOR'S ACRONYM(S)

11. SPONSOR/MONITOR'S REPORT NUMBER(S)

12. DISTRIBUTION / AVAILABILITY STATEMENT

Approved for public release; distribution is unlimited.

13. SUPPLEMENTARY NOTES

14. ABSTRACT

The U.S. Army Engineer District, Los Angeles and the Coastal Inlets Research Program have conducted a comprehensive study to investigate wave, flow, sediment transport, and permeable breakwaters with rocky outcrop bottom at Dana Point Harbor, as a part of the harbor revitalization project, on the southern Orange County coast, CA. The 5,500-ft shore-parallel West Breakwater and 2,250-ft shore-normal East Breakwater to protect the harbor are the main interest in the study of the structural integrity and functionality. The field data collection includes 2009 survey of breakwaters, marinas, harbor entrance and surrounding at the harbor, and installation of a pair of ADCPs to measure water levels, waves, and currents inside and outside West Breakwater. The numerical models were used to calculate wave transmission, current and sediment seepage through permeable breakwaters and circulation in the harbor. Permeable breakwaters are simulated by models under wind forcing, tides, bottom friction, and wave reflection. The oceanographic design criteria established previously for the Harbor were updated based on historical storm waves and the present model simulations for 50-yr and 100-yr return periods. The data analysis and model results together provide information to ascertain the action to repair breakwaters and structural alternatives to improve the navigation channel maintenance and tidal flushing in the harbor.

15. SUBJECT TERMS

Coastal modeling system
Laser sonar scan system
Particle tracking model
Permeable breakwater
Sediment seepage
Tidal flushing
Wave transmission

16. SECURITY CLASSIFICATION OF: None			**17. LIMITATION OF ABSTRACT**	**18. NUMBER OF PAGES**	**19a. NAME OF RESPONSIBLE PERSON Lihwa Lin**
a. REPORT	**b. ABSTRACT**	**c. THIS PAGE**			**19b. TELEPHONE NUMBER** *(include area code)*
UNCLASSIFIED	UNCLASSIFIED	UNCLASSIFIED		165	601-634-2704